Mathematical models of light acclimation mechanisms in higher plants and green algae

Inaugural-Dissertation

zur Erlangung des Doktorgrades

der Mathematisch-Naturwissenschaftlichen Fakultät
der Heinrich-Heine-Universität Düsseldorf

vorgelegt von
Anna Barbara Matuszyńska
aus Gdynia, Polen

Düsseldorf, September 2016

Erklärung

Ich versichere an Eides statt, dass die Dissertation von mir selbstständig und ohne unzuläassige fremde Hilfe unter Beachtung der "Grundsätze zur Sicherung guter wissenschaftlicher Praxis an der Heinrich-Heine Universität Düsseldorf" erstellt worden ist. Die Dissertation habe ich in dieser oder in ähnlicher Form noch bei keiner anderen Institution eingereicht. Ich habe bisher keine erfolglosen oder erfolgreichen Promotionsversuche unternommen.

Düsseldorf, den 24. September 2016

Anna Matuszyńska

Mojej rodzinie,
tej, w której miałam zaszczyt się urodzić i tej, którą razem tworzymy

Mamo, Tato, dziękuję za wyposażenie mnie w system wartości, dzięki któremu mogę się stawać lepszym człowiekiem, za pokazanie co to miłość i stworzenie rodziny, z której czerpię siłę każdego dnia, nie ważne ile kilometrów nas dzieli. **Beato, Piotrze**, dziękuję za to, że zawsze mogę na Was polegać i za tę nić zrozumienia, którą można dzielić tylko z rodzeństwem. **Babciu, Dziadku**, dziękuję za modlitwę i odwieczny doping. **Ciociu**, za nasze bezcenne wtorki. I przede wszystkim dziękuję Tobie **Kacprze**. Za cierpliwość, wsparcie i wiarę w moje umiejętności. Za bycie moim pierwszym recenzentem przez ostatnie trzy lata. Za to, że z dala od tego co nam znane, stworzyłeś ze mną dom pełen miłości i wzajemnego zrozumienia, opierający się na zasadach partnerstwa.

Abstract

Mathematical models have become an increasingly accepted and widely used tool in biology. Their power lies in detecting common underlying principles behind broad classes of phenomena. Throughout this work, a modelling approach was used to study photosynthesis and provide a better understanding of the role and regulation of several short-term acclimation mechanisms in plants and green algae, collectively termed as non-photochemical quenching (NPQ).

In the process of photosynthesis, solar energy is harvested by chlorophyll pigments and converted into chemical energy by a series of redox reactions. High light intensities may severely impair the photosynthetic apparatus and damage the reaction centres, where charge separation occurs. In order to protect themselves against photodamage, plants and other photosynthetic organisms are capable of switching from a photosynthetic, light-harvesting state to a protective one, in which excess absorbed radiant energy is dissipated as heat. Through the re-organisation of light harvesting complexes various photosynthetic organisms gain the ability to dynamically react to external stimuli and to keep the redox balance within the thylakoid membrane. However, what is a desired and even an essential mechanism in natural, fluctuating environments, becomes an unwanted feature in industrial cultivation, where one aims at utilising the applied light energy with the highest possible efficiency.

A developed modular, mathematical model of light acclimation processes of the photosynthetic electron transport chain translates our current knowledge gained from years of experimental work, into more general, mathematical statements. With that, a more thorough understanding of the molecular signalling mechanisms guiding acclimation responses is possible. The model sets a framework for assessing the role of photoprotective mechanisms in improving fitness of the organisms and helps to answer open questions on the molecular mechanisms of key components of the signalling pathways of acclimation. Thanks to its simplicity and modularisation, it can be used to test various hypotheses regarding photoprotective behaviour of plants under specific conditions. The model was successfully applied to quantify the contribution of several acclimation components on short-term light memory, to analyse possible mechanisms of state transitions and to predict the response of organisms responses while exposed to monochromatic light. It is envisaged that the detailed understanding of non-photochemical quenching shall contribute to developing optimal strategies for a sustainable biotechnological exploitation of plants and microalgae.

Zusammenfassung

Mathematische Modelle sind ein zunehmend anerkanntes und weit verbreitetes Hilfsmittel in der Biologie. Ihre Stärke liegt in der Erforschung der zugrunde liegenden Prinzipien hinter einer breiten Klassen von Phänomenen. In dieser Arbeit wurde ein Modellierungsansatz verwendet um Photosynthese zu untersuchen und ein besseres Verständnis für die Rolle und Regulierung von mehreren kurzfristigen, photoprotektiven Mechanismen in Pflanzen und Grünalgen zu liefern, die zusammen als Nicht-photochemische Löschung bzw. Quenching (NPQ) bezeichnet werden.

In der Photosynthese wird Sonnenenergie durch Chlorophyllpigmente absorbiert und durch eine Reihe von Redoxreaktionen in chemische Energie umgewandelt. Hohe Lichtintensitäten können den Photosyntheseapparat stark beeinträchtigen und die Reaktionszentren beschädigen, in denen die Ladungstrennung stattfindet. Um sich gegen Lichtschäden zu schützen, sind Pflanzen und andere photosynthetische Organismen in der Lage, aus einem photosynthetisch- lichtspeichernden in einen geschützten Zustand zu wechseln, bei dem überschüssige Strahlungsenergie absorbiert und als Wärme abgeführt wird. Durch die Neuorganisation der Lichtsammelkomplexe gewinnen verschiedene photosynthetische Organismen die Fähigkeit, auf äußere Reize dynamisch zu reagieren und das Redoxgleichgewicht in der Thylakoidmembran zu erhalten. Doch was ein erwünschter und wesentlicher Mechanismus in natürlichen, dynamischen Umgebungen ist, wird zu einer unerwünschten Eigenschaft in der industriellen Kultivierung, die darauf abzielt die verwendete Lichtenergie mit der höchstmöglichen Effizienz zu nutzen.

Das entwickelte modulare, mathematische Modell für Lichtakklimatisierungsprozesse der photosynthetischen Elektronentransportkette übersetzt unser aktuelles, aus jahrelanger experimenteller Arbeit gewonnenes Wissen, in allgemeingültige, mathematische Aussagen. Dadurch wird ein besseres Verständnis der molekularen Signalmechanismen, die die Akklimatisierungsreaktionen begleiten, möglich. Das Modell bildet einen Rahmen für die Beurteilung der Rolle der Lichtschutzmechanismen für die Verbesserung der Fitness von Organismen und trägt dazu bei, offene Fragen bezüglich molekularer Mechanismen von Schlüsselkomponenten der Signalwege der Akklimatisierung zu beantworten. Dank seiner Funktionalität und Modularität kann es verwendet werden, um verschiedene Hypothesen in Bezug auf pflanzenphotoprotektives Verhalten unter bestimmten Bedingungen zu testen. Das Modell wurde erfolgreich angewendet, um die Komponenten, die zu einer „Erinnerung" an vorherige Lichtperioden beitragen, zu quantifizieren, die möglichen Mechanismen der Zustandsübergänge zu analysieren und das Verhalten von Organismen, die monochromatischem Licht ausgesetzt wurden, vorherzusagen. Es ist zu erwarten, dass das detaillierte Verständnis über Nicht-photochemische Löschung bzw. Quenching dazu beitragen kann, optimale Strategien für eine nachhaltige biotechnologische Nutzung von Pflanzen und Mikroalgen zu entwickeln.

Contents

I	Part One

II   Part Two

Abbreviations

ATP Adenosine triphosphate

CEF Cyclic Electron Flow

FCCP Carbonyl cyanide-4-(trifluoromethoxy) phenylhydrazone

Fd Ferredoxin

FNR Ferredoxin-NADP Reductase

LEF Linear Electron Flow

LHC Ligth Harvesting Complexes

LHCSR3 Light-Harvesting Complex Stress-Related protein

NADP$^+$ Nicotinamide Adenine Dinucleotide Phosphate

NADPH reduced form of NADP$^+$

NIBB National Institute for Basic Biology

NPQ Non-Photochemical Quenching of chlorophyll a fluorescence

ODE Ordinary Differential Equations

PAM Pulse Amplitude Modulation

PAR Photosynthetically Active Radiation

PC Plastocyanin

Pmax maximum photosynthesis rate

pmf proton motive force

PQ Plastoquinone

PSI Photosystem I

PSII Photosystem II

PsbS Photosystem II subunit S

PSs Photosystems

PTOX Plastoquinol Terminal Oxidase (or Plastid Terminal Oxidase)

qE Energy dependent quenching

qI Photoinhibition quenching

qT State transitions

qZ Zeaxanthin dependent quenching

TP Glyceraldehyde 3-phosphate

VDE Violaxanthin De-epoxidase Enzyme

Vx Violaxanthin

Zx Zeaxanthin

Preface

„I am among those who think that science has great beauty. A scientist in his laboratory is not only a technician: he is also a child placed before natural phenomena which impress him like a fairy tale.”

- ***Maria Skłodowska-Curie***, *double Nobel Prize winner*
Madame Curie: A Biography, by Eve Curie Labouisse (1937)

Almost all life on Earth depends directly or indirectly on energy derived from the Sun. Exceptionally, there is only one biological process, named photosynthesis, that can harvest photons and convert them into chemical energy in the form of ATP and reducing power, NADPH. Plants, algae and some bacteria are capable of using light energy to assimilate carbon dioxide to synthesise carbohydrates (saccharides), the energy storage molecules. This energy is then used to drive plants cellular processes and ultimately provides us food. Moreover, in most cases, oxygen is produced as a waste product of the photosynthetic process[1] providing the critical element for any eukaryotic form of life on Earth[2]. For these reasons, photosynthesis may already be seen as arguably the single most important biological process on Earth and, therefore, explain why over the decades people had worked so passionately on deciphering its mechanism.

In light of the United Nation Global Issues, the motivation behind understanding how plants perform this marvellous process gained new and broader perspective. With the expanding global population, aging society and increasing energy demand, the interest lies now more on optimising photosynthetic efficiency to reach manifold benefits ranging from higher world food production rates, finding alternative sources of energy (such as biogas, hydrogen or ethanol from microalgae), optimising production of nutraceuticals and other materials. For decades, scientists have been working on understanding photosynthesis and are employing multiple strategies to solve the agriculture problems. They range from fundamental research on understanding the molecular mechanisms of biochemical processes leading to the transduction of light

---

[1] Some types of bacteria carry out anoxygenic photosynthesis where light energy is captured and converted to ATP, without the production of oxygen.

[2] Although there are some species of bacteria, that can grow in darkness and gain their energy from chemical reactions (so called chemoautotrophic bacteria), all us, eukaryotes, we strive on the oxygen!

energy into biomass, to searches for more resistant and optimal species and strains that can grow under non-optimal conditions, or genetic engineering with the aim of for instance, 'upgrading' C_3 plants to C_4.

An interesting feature studied by many is plants' capability of dynamic adjustment to changes in their environment. In order to maintain their optimal functionality under varying conditions, the photosynthetic apparatus acquired several mechanisms that allow **acclimation** to such changes, that may vary from changes in the intensity and wavelength of radiant light, to temperature, irrigation or nutrients availability. Among the most commonly studied mechanisms responsible for a short-term **photo**acclimation are high-energy dependent quenching, state transitions and photoinhibition, collectively termed as non-photochemical quenching of fluorescence (NPQ). On a time scale of seconds to minutes, due to those mechanisms, photosynthetic organisms are defending themselves against photodamage, adjusting their photosynthetic activity and balancing the excitation of photosystems.

This thesis is the result of a collaborative effort of several European Institutions working together on increasing our understanding of various photoacclimation processes. Within the Marie Curie Initial Training Network **AccliPhot**, a multidisciplinary and international project funded by the European Commission, we investigated short-term acclimation mechanisms to changes in light conditions. In order to establish a systems-wide understanding of such acclimation processes, we investigated not only the photosynthetic metabolism and growth of algae and higher plants, but also followed signalling pathways that respond to environmental changes. Considering theoretical approaches as powerful tools to discover organisational principles governing the design of biological systems I developed a modular, mathematical model of the photosynthetic electron transport chain to study the dynamics of NPQ under various light intensities and wavelengths.

The goal of my doctoral research was to convert our current understanding of these processes into more general, mathematical terms. Numerous mathematical models were developed over the years to describe and predict the relation between photosynthetic rate and irradiance, but most of them excluded the dynamic aspects of light acclimation. For that, I have developed a mathematical model of photosynthesis that includes various short-term photoprotective mechanisms mentioned above. The design of the model allows for an easy adaptation to various species and strains. Here it is demonstrated using a thale cress *Arabidopsis thaliana*, a green alga *Chlamydomonas reinhardtii* and an ornament plant *Epipremnum aureum*. The model can be effortlessly reduced to its minimal form that links light absorption with ATP production, as well as can be expanded to include other reactions and processes, and therefore should serve as a tool to study numerous questions related to the dynamics of photosynthesis.

The interdisciplinarity of this research requires understanding of several disciplines, therefore I divided my dissertation into two parts. In **Part One** I first lay the foundation for this work by providing a brief introduction to photosynthesis, that includes a short history of photosynthetic research. The section on photosynthetic acclimation is an extract from the review written together by all AccliPhot collaborators, edited by Dr Moejes and myself[3]. Next, I explain the main principles of fluorescence experiments widely used while studying the dynamics of photosynthesis. Finally, I explain how modelling can contribute to our understanding of short-term acclimation and argue why the differential equations' based model is the most appropriate mathematical description to study self regulation in plants and algae. This Chapter is based on the mini-review I co-authored with my supervisor[4].

My scientific results are presented in **Part Two** of this thesis. First two Chapters focus on models constructed to increase our understanding of the molecular mechanisms of photoacclimation. I start with a model of

---

[3]A. Matuszyńska, F. Moejes *et al.*, (2016) A systems-wide understanding of the photosynthetic acclimation in algae and higher plants - retrospection and perspectives, *Journal of Experimental Botany*

[4]A. Matuszyńska and O. Ebenhöh, (2015) A reductionist approach to model photosynthetic self-regulation in eukaryotes in response to light, *Biochemical Society Transactions*, vol. 43, no. 6. doi: 10.1042/BST20150136.

a high-energy dependent quenching in plants, significantly reduced in its complexity, designed to answer questions regarding NPQ in a context of plant memory (Chapter 4). Work presented here is a result of a collaboration with Dr Sommayeh Heidari from Ferdowsi University of Masshad, Iran and Prof. Peter Jahns from Heinrich-Heine University Düsseldorf, Germany, and was summarised in the joint manuscript[5]. Next, building on the previous work of my collaborators, I present a model of two other mechanisms: state transitions and photoinhibition, crafted for a green alga *Chlamydomonas reinhardtii* (Chapter 5). The presented results are an effect of a work performed during my scientific stays in the group of Prof. Michel Goldschmidt-Clermont at the University of Geneva, Switzerland and in the group of Dr Giovanni Finazzi at Commissariat à l'énergie atomique et aux énergies alternatives (CEA), Grenoble, France. In Chapter 6 the two modules were combined together to provide a framework to study the impact of changes in the light colour on the photosynthetic performance. I provide a proof of concept that the model can be used to simulate the photosynthetic dynamics depending on the light colour and present a partial, unpublished results of an ongoing collaborative project between the group of Dr Finazzi in Grenoble, France, and group of Prof. Jun Minagawa at the National Institute for Basic Biology in Okazaki, Japan. Noticed discrepancies suggested a need for a more realistic depiction of cell's energy demand and therefore in the Summary and Outlook I discuss possible further directions of the development of this models, provide the broader context to my research and try to highlight potential applications of this work.

Finally, the source code that was used to produce computational results in this Thesis is available to the public under my github account and everyone is encouraged to use it. With the detailed description of the model and its modules provided in this work, it should be a rather straightforward exercise to utilise this work to answer various other photosynthetic questions. Therefore the real usefulness of my work will depend on the engagement of its users.

Düsseldorf, September 2016

---

[5]A. Matuszyńska, S. Heidari, P. Jahns and O. Ebenhöh, (2016) A mathematical model of non-photochemical quenching to study short-term light memory in plants, *Biochemica et Biophysica Acta Bioenergetics*. doi: 10.1016/j.bbabio.2016.09.003

Part One

1. Photosynthesis and short-term acclimation

„We cannot cheat on DNA. We cannot get round photosynthesis. We cannot say I am not going to give a damn about phytoplankton. All these tiny mechanisms provide the preconditions of our planetary life. To say we do not care is to say in the most literal sense that 'we choose death'."

*- **Barbara Ward**, economist and writer*

Only One Earth (1972)

Photosynthesis is arguably the most fascinating and important biochemical process on Earth. Through this process, organisms are capable of absorbing energy from light and by series of reactions convert it into the stable high-energy molecules, named saccharides. Photosynthesis itself is a remarkable example of the process for which complete understanding we need a multidisciplinary knowledge from various disciplines. It took hundred years of research to establish the final chemical equation of photosynthesis:

$$\underset{\text{Carbon dioxide}}{CO_2} + \underset{\text{Water}}{H_2O} \longrightarrow \underset{\text{Carbohydrate}}{(CH_2O)_n} + \underset{\text{Oxygen}}{O_2} \tag{1.0.1}$$
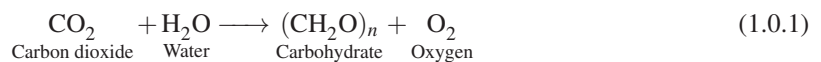
and to reach today's level of understanding of the complexity of the whole process. But yet, there is still so much we can learn. In this Chapter I will provide an introduction to photosynthesis, inspired by a great book by Blankenship [1]. I start with a little historical background to highlight the diversity of research conducted over the years and acknowledge the most critical discoveries. I introduce the basic principles that underline oxygenic photosynthesis and provide the necessary vocabulary and definitions used widely in the field. I provide an introduction to the short-term acclimation of photosynthesis and finally, I outline the remaining questions regarding photosynthetic acclimation, justifying the need for my research.

1.1   A brief history of early photosynthetic discoveries

The term photosynthesis was coined by **Charles Barnes** in 1893 [2]. With the knowledge on a production of higher carbohydrates from CO_2 and H_2O, in the presence of chlorophyll and radiant energy, he proposed to call the '*process of formation of complex carbon compounds out of simple ones under the influence of light*' 'photosyntax' or 'photosynthesis' [3]. And although it is hard to decide on first or most important discovery in the research of photosynthesis, there are several names worth mentioning, as results of their work and experiments contributed to its today's understanding. A subjective selection of relevant early discoveries presented here is based on the excellent reviews of the discoveries in photosynthesis by Huzisige and Ke [4] and Govindjee and Krogmann [5].

1.1.1   Recognising photosynthesis

Following the discovery timeline provided by Huzisige and Ke [4], the seventeenth-century Flemish scientist, **Jan Baptist Van Helmont**, can be placed at the very beginning of the photosynthetic journey, although it is challenged by some that the idea behind his famous experiment is believed to originate from Nicolaus of Cusa (see [6]). Van Helmont's aim was to determine where plants are getting their mass from, for what he launched a five years long experiment where he planted a willow tree in a tub of soil. He continued to measure the weight of the soil, leaves that fell off each autumn and water he added. At the end of the experiment he weighted all the compartments separately and by noticing that the weight of the soil is almost the same, he concluded in his work *Ortus medicinae* that plant's mass is formed solely from the water he added, rejecting the Aristotelian dogma that plants derive nourishment from the soil [4]. Although it was incorrect, as today we know that plants' mass derives not only from water, the first product of the photosynthetic equation (Eq. 1.0.1) was identified.

Nearly 80 years later, it was recognised that plants can obtain their nourishment also from the atmosphere. In 1727 an English clergyman **Stephen Hales** published his studies on plant physiology where he concluded that '*Plants very probably drawing thro' their leaves some part of their nourishment from the air*' [7]. He was also most likely the first one to report the unidirectional way of flow of water from soil to the the transpiring leaves [8, 9].

Another remarkable discovery belongs to **Joseph Priestley**. In 1771, he indirectly discovered production of oxygen by plants (firstly named by him as '*dephlogisticated air*'), by observing that candle burned in a closed vessel can be lit again after few days from when he put a sprig of mint under the chamber [10]. It gave rise to exiting discoveries conducted in next 30 years by **Jan Ingenhousz**, **Jean Senebier** and **Nicolas de Saussure**, that all lead to establishing unbalanced chemical equation of photosynthesis in 1804, that finally gave answer to question stated by Van Helmont [1]. Both, uptake of carbon dioxide and incorporation of water are essential for plants growth, moreover next to the production of organic matter, oxygen is released.

In 1818 **Pierre-Joseph Pelletier** and **Joseph B. Caventou** first isolated and named the green-plant pigment "chlorophyll" (derived from the Greek words *chloros* ("green") and *phyllon* ("leaf"). Today it is known that chlorophyll is the most critical biomolecule in photosynthesis, that allows plants to absorb energy from light [4] but it was understood only 20 years after the discovery, by **Henri Dutrochet**, that chlorophyll are required for photosynthesis [4].

Further discoveries by **Hugo von Mohl**, who in 1844 found chloroplasts in plant cells, and **Julius R. von Mayer**, who next to his enormous merits in the field of thermodynamics [11], in 1845 proposed that plants are converting light energy into chemical one [4], lead to the conclusion on the basic factors in photosynthesis and the chemical equation was established

$$\text{carbon dioxide} + \text{water} + \text{light} \xrightarrow{\text{chlorophyll}} \text{organic matter} + \text{oxygen}. \tag{1.1.1}$$

In 1864 **Jean-Baptiste Boussingault** measured the amount of taken up CO_2 and O_2 produced during photosynthesis to conclude that the *photosynthetic quotient* is close to 1. The same year, **Julius von Sachs** found out that by illuminating leaves they accumulate the carbohydrate starch. With the information provided by experiments performed by Boussingault and von Sachs, the simple equation from the beginning of the XIX century (Eq. 1.1.1) could be properly balanced and already written in modern chemical symbols [1]

$$CO_2 + H_2O \longrightarrow \underset{\text{carbohydrate}}{(CH_2O)_n} + O_2 \cdot \tag{1.1.2}$$
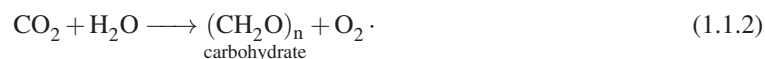
1.1.2 Understanding chemical properties of photosynthesis

Milestone in understanding the chemical properties of the photosynthesis was reached by recognising photosynthesis as a redox system. First hypothesis regarding the redox nature of photosynthesis was proposed by **Torsten Thunberg** in 1923 and was followed by the clearly formulated papers by **Cornelius Van Niel**, who in 1930s discovered redox nature of photosynthesis. By setting his experiments on anoxygenic photosynthetic bacteria, Van Niel found that by adding a reducing compound, carbon dioxide can be assimilated and converted into organic matter, but no molecular oxygen is being produced [1]. Therefore, known so far oxygen-evolving form of photosynthesis could be seen as only a case of more generalised process highlighting the redox nature of photosynthesis, which was formulated by Van Niel as:
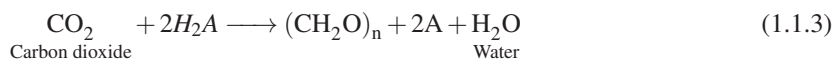
$$\underset{\text{Carbon dioxide}}{CO_2} + 2H_2A \longrightarrow (CH_2O)_n + 2A + \underset{\text{Water}}{H_2O} \tag{1.1.3}$$

This discovery allowed **Robert Hill** to prove in 1939 that the process of water oxidation and carbon dioxide fixation are separated processes and that in order to restore production of oxygen by chloroplast, the reduction of carbon dioxide can be replaced with the reduction of artificial electron acceptors [12].

1.1.3 Identifying mode of operation

The continued research on photosynthesis in the XXth century significantly complemented this now basic understanding of the process of photosynthesis. In '30s and '40s experimentalists **Robert Emerson and William Arnolds** used for the very first time short flashes of light to probe photosynthesis, a technique which in its evolved form is widely used to follow the dynamics of photosynthesis today (see Chapter 2). With numerous experiments they established that photosynthesis consists of light and dark stages (today referred to as photochemical reaction and carbon fixation), proposed the light saturation curve for photosynthesis by measuring oxygen yield per flash, and proposed the concept of photosynthetic unit .

In the '40s and '50s the controversy regarding the quantum requirement of photosynthesis started. Emerson and **Charleton Lewis** in their attempt to measure the quantum requirement for photosynthesis discovered in 1943 the 'red drop' in the maximum quantum yield of photosynthesis while applying long wavelengths of light. This puzzling finding led to another discovery, where by supplementing the ineffective long-wavelength light with short-wavelength light, the photosynthetic efficiency increased. This was named as the *enhancement effect*, due to the enhancing effect of short-wavelength light on photosynthetic efficiency.

The actual explanation for these results was proposed only years later by **Louis Duysens**, who finally

pointed out to the existence of two distinct photosystems, tuned to absorb light of different wavelength. Around the same time, Robert Hill and **Fay Bendall** proposed their concept of photosynthetis structure composed of two systems working in line, where products of the first biochemical reaction are substrates of the second one. This formulation, despite continuous research on photosynthesis remains as a foundation of our understanding of the linear mode of operation of photosynthesis [13] and is commonly known as the Z-scheme of photosynthesis, as it was first drawn in the form of the letter "Z". Currently, many versions the of the Z-scheme are available in the literature but the diagrams are mostly turned 90° counterclockwise to emphasize the energy levels of the components [14]. In Fig. 1.1.1 the Z-scheme incorporating our current understanding of the electron transfer in oxygenic photosynthesis is displayed. The diagram was developed based on several widely available diagrams [15, 16, 17].

Finally, it is impossible to provide a complete summary of the key experiments within section of this Chapter and many of great discoveries and contributors were omitted, including e.g., the whole discovery timeline of carbon fixation. Yet, a good reflection of the importance of the photosynthetic research over the years, and its significance for the society, is the fact that ten Nobel Prizes were granted for work directly related to photosynthesis, ranging from the work on plant pigments to energy transfer (see Table 1.1.1).

1997 — **Paul D. Boyer & John E. Walker***
"for their elucidation of the enzymatic mechanism underlying the synthesis of ATP"

1992 — **Rudolph Marcus**
"for his contributions to the theory of electron transfer reactions in chemical systems"

1988 — **Hartmut Michel, Robert Huber & Johannes Deisenhofer**
"for the determination of the three-dimensional structure of a photosynthetic reaction centre"

1978 — **Peter Mitchell**
"for his contribution to the understanding of biological energy transfer through the formulation of the chemiosmotic theory"

1965 — **Robert Burns Woodward**
"for his outstanding achievements in the art of organic synthesis"

1961 — **Melvin Calvin**
"for his research on the carbon dioxide assimilation in plants"

1938 — **Richard Kuhn**
"for his work on carotenoids and vitamins"

1937 — **Paul Karrer**
"for his investigations on carotenoids, flavins and vitamins A and B2"

1930 — **Hans Fischer**
"for his researches into the constitution of haemin and chlorophyll and especially for his synthesis of haemin"

1915 — **Richard Willstätter**
"for his researches on plant pigments, especially chlorophyll"

Table 1.1.1: Timeline of Nobel Prize winners for their work related to the photosynthetic research. Prize motivation taken from the Official Web Site of the Nobel Prize [18].

Importantly, the research on photosynthesis continues and our knowledge on this process expands with every consecutive year. It is reflected in a number of international congresses on photosynthesis held globally and the amount of money spent on increasing our fundamental knowledge on photosynthesis, optimising its efficiency and even constructing artificial photosynthesis. This work itself is a result of a big collaborative project funded by European Union to join the efforts in understanding one particular aspect of photosynthesis, namely its photoprotective capability [19].
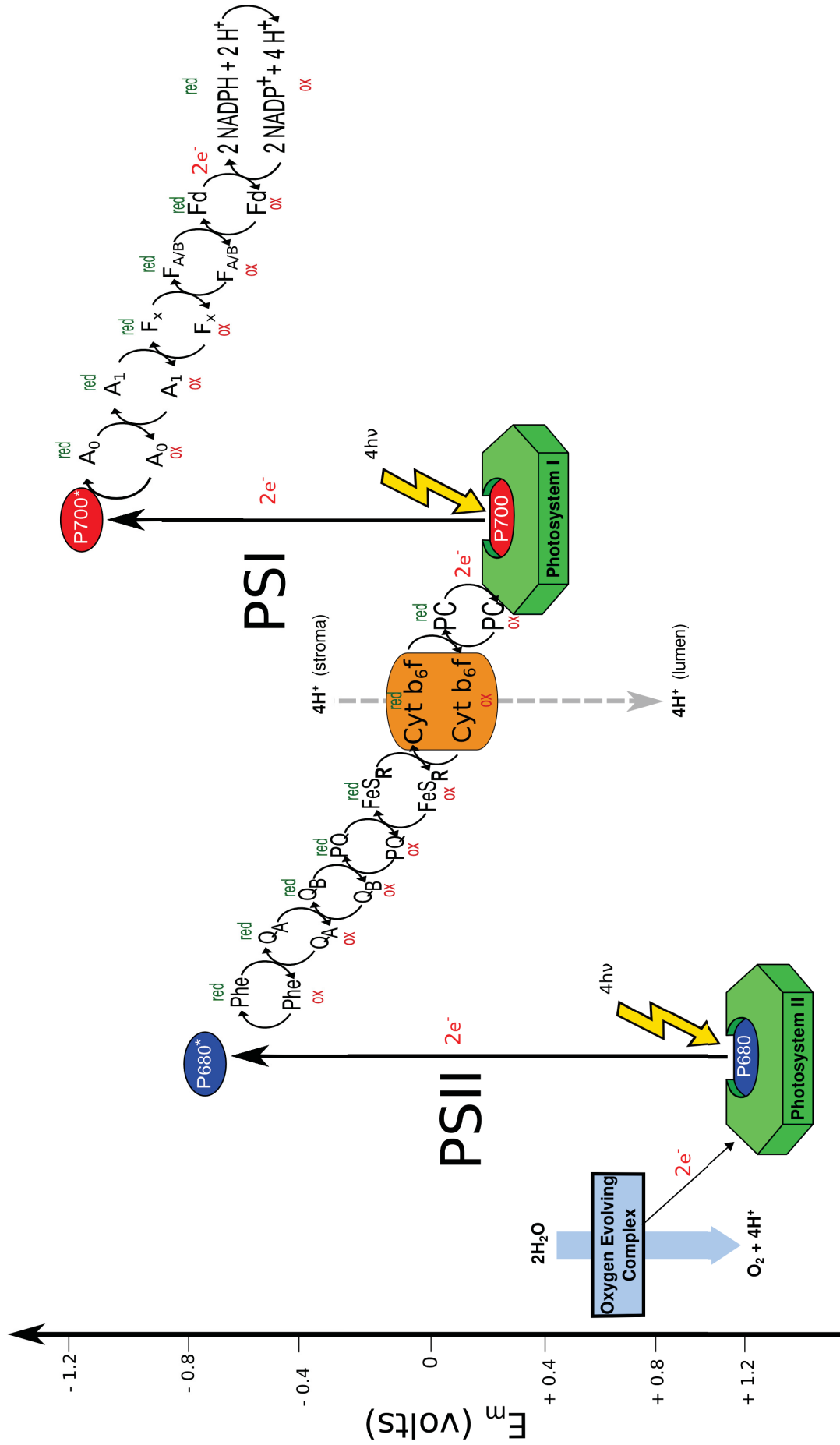
Figure 1.1.1: The Z-scheme for electron transfer in oxygenic photosynthesis. Figure drawn based on several widely available diagrams [15, 16, 17].

1.2   Basic principles

In the process of photosynthesis solar energy is harvested by chlorophyll pigments and by a series of oxidation-reduction (redox) reactions converted into chemical energy. The photosynthetic complexes share fundamental structure in different organisms performing oxygenic photosynthesis, but differ in composition, ratio, and dynamic control of the photosynthetic reactions. Here, a basic description of the common aspects of oxygenic photosynthesis is provided.

1.2.1   Light and dark reactions

Photosynthesis takes place in the chloroplast. Since the Emerson experiment, photosynthetic process is often divided into two stages: the **light reactions**, taking place on the thylakoid membranes, during which the energy from light is used to produce ATP and NADPH with a release of oxygen, and the **dark reactions**, currently referred to as Calvin-Benson-Bassham (CBB) cycle, or Calvin cycle, during which produced ATP and NADPH are used to fixed carbon dioxide, to build sugar molecules.

Light reactions are driven in a sequential mode through a process of **electron transfer** (ET) leading to a net-reaction

$$2\,H_2O + 2\,NADP^+ + 3\,ADP + 3\,Pi \longrightarrow O_2 + 2\,NADPH + 3\,ATP. \tag{1.2.1}$$
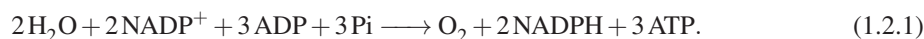
Reactions are catalysed by integral membrane proteins, where the four major protein complexes include photosystem II (PSII) , photosystem I (PSI) , cytochrome b6f and ATP synthase .

1.2.2   Photosynthetic apparatus

The molecular organisation of these complexes inside the chloroplasts indicates spatial separation between photosystem I and photosystem II [20]. The most frequently used model of spatial relationship between granum (closely associated, stacked membranes) and stroma thylakoids [21] assumes that stroma membranes form a structure like 'fork' (originally proposed by Andersson and Anderson [20]). In Fig. 1.2.1 a side view of the well organised membrane planes is presented. The insight into the structural organisation is critical for our understanding of changes that are occurring within the thylakoid membrane during various photoprotective mechanisms.

It was not until late '60s last century when after results of Emerson experiments with the red light, Duysens proposed that there are not one, but two light-driven systems working together and each photochemical complex is sensitive to different light wavelengths. Photosystems II and I are membrane-embedded modular assembly of pigment–protein complexes and are composed of two main parts: the core, containing the reaction centre (RC) and the light-gathering outer antenna [23]. The three-dimensional structure of plant's photosystem II provides a detailed insight into the assembly of the protein.

Antenna complex, also referred to as light harvesting complex (LHC), is a well-defined, three-dimensional structure of pigments responsible for energy collection and transfer to the place where the photochemistry can occur[1] [1]. Size of antenna complex is not fixed and differs significantly among species from 20-30 per RC in some bacteria to even few thousand pigments per RC in some algae [8]. The physical segregation of PSII and PSI in plants and alge (Fig. 1.2.1) imposes the existence of different antenna systems, which excite the two photosystems independently. Therefore antenna are composed of various pigments (for a complete list see Tab. 2 in the review by Antal *et al.* [24]), in different proportions, mainly including chlorophylls and carotenoids and can be primarily associated with either PSII (LHCII) or PSI (LHCI).

---

[1]The energy transfer between antenna molecules occur through the Förster resonance energy transfer (FRET).
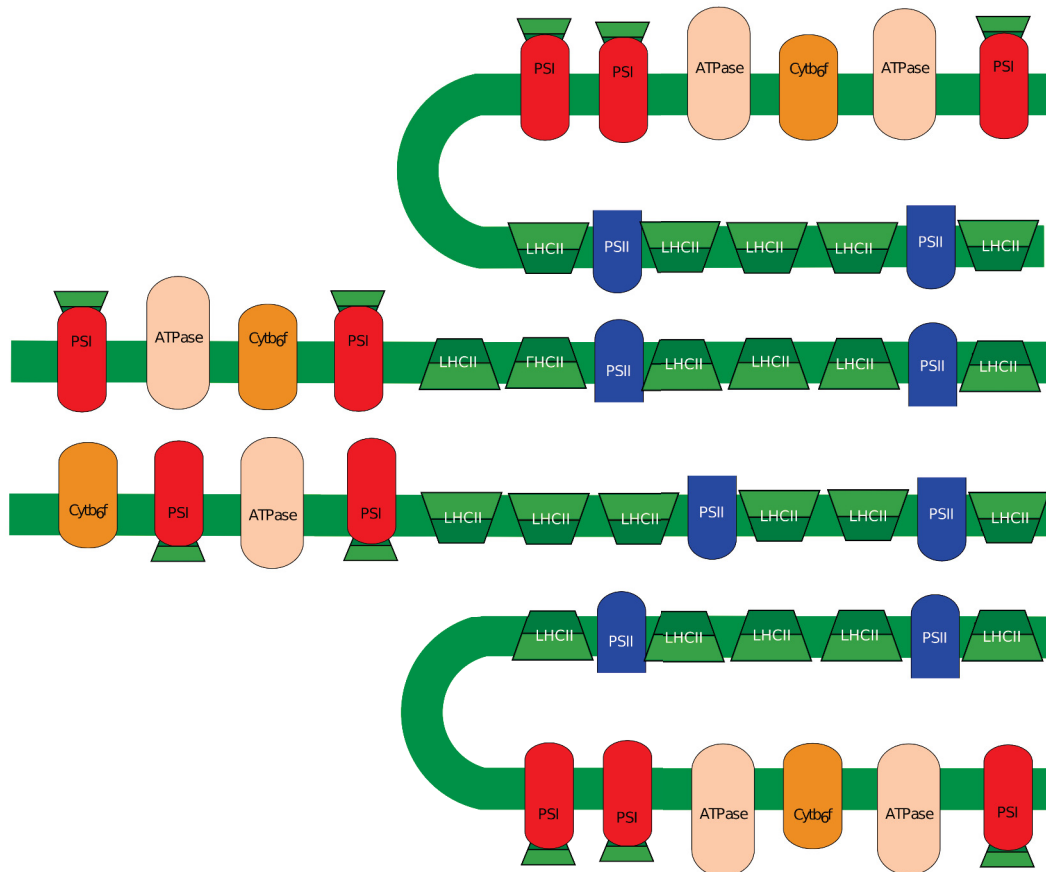
Figure 1.2.1: Side view of the well-ordered membrane planes with the photosystem supercomplex composition inside the chloroplast of green algae *C. reinhardtii*. Figure reproduced from [22].

Reaction centres The conversion of light energy to chemical energy takes place in the reaction centres that contain a special dimer of pigments constituting the primary electron donor. Interestingly, despite years of evolution and high diversity of photosynthetic organisms, the reaction centers are homologous for all species. In photosystem II, a pair of chlorophyll a molecules absorbs light maximally at the wavelength of 680 nm, therefore often referred to as P680, whilst in photosystem I the reaction-center chlorophyll s absorbs light maximally at the wavelength of 700 nm, therefore referred to as P700. The primary electron donor of photosystem I, in its excited state has a potential of approximately 1.2 V, thus making it potentially the most reducing compound found in natural systems [25]. Primary 'stable' electron acceptors of photosystem II and photosystem I are Q_A and A_0 respectively (marked on the Z-scheme, Fig. 1.1.1).

1.2.3 Photosynthetic electron transfer

The **photosynthetic electron transport chain** (ETC) is a series of compounds that transfer electrons from electron donors to electron acceptors via redox reactions, and couples this electron transfer with the transfer of protons (H+ ions) across a membrane. In Fig. 1.2.2 the schematic representation of the electron transport chain with its main components is presented. Photosynthetic flow of electrons starts in the reaction centres where prime, electronically excited dimer rapidly loses his electron to a nearby electron acceptor and that way starts electron transfer cascade. Excitation of this prime, electron donor is promoted mainly by transfer of energy from the antenna systems described above, and less often by direct photon absorption, as majority of chlorophyll molecules acts only as light collectors and transferring units, passing energy into reaction centres.
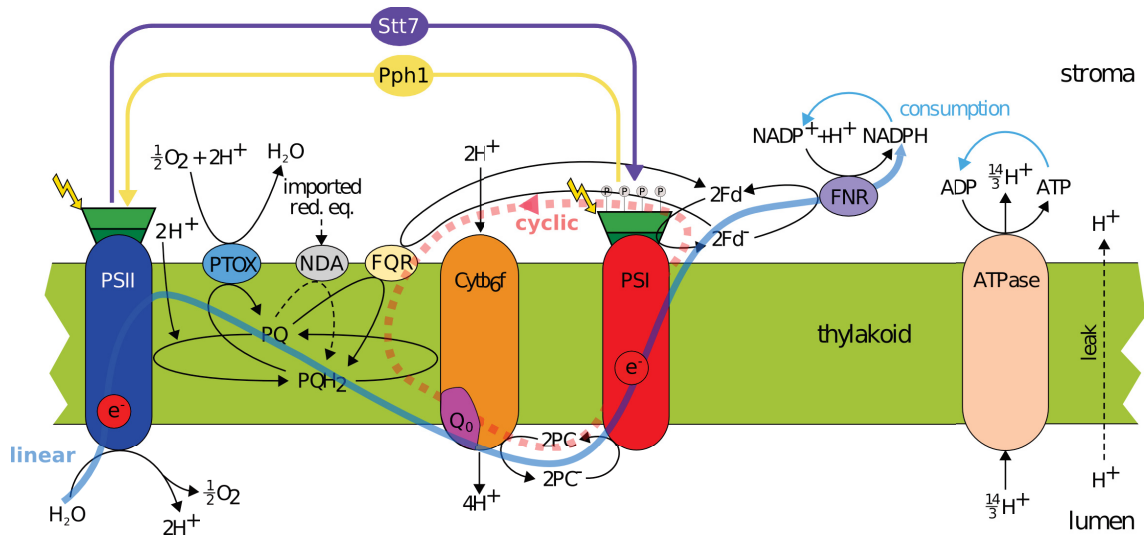
Figure 1.2.2: Schematic representation of the photosynthetic electron transport chain with two modes of electron flow: linear (solid, blue line) and cyclic (dashed, pink line). The electron transfer starts in photosystem II (PSII), where light is absorbed by light-harvesting complex II (LHCII) and the energy is funneled to PSII reaction centre (RC). The oxygen-evolving complex oxidises water, leading to the release of molecular oxygen and protons into the lumen. Electrons derived from this process are further transferred by free electron carriers plastoquinone (PQ) to the cytochrome b6f complex (b_6f). Cytb6f oxidises plastohydroquinone molecules (PQH$_2$) and delivers electrons to photosystem I (PSI) via plastocyanin (PC) at the same time catalysing proton transfer from the thylakoid stroma into lumen. Proton movement generated that way results in pH gradient that powers synthase of ATP. In turn, LHCI associated with PSI drives the transfer of electrons from PSI to ferredoxin (Fd), which is the last electron acceptor in this process (linear electron flow) or re-injects electrons back to the PQ pool (cyclic electron flow). Fd transfers then electrons to the enzyme ferredoxin-NADP reductase (FNR) which reduces NADP to NADPH in the stromal side. Figure reproduced from [26].

Electrochemistry of the electron transfer

Much of our current understanding of the physical principles guiding the photosynthetic energy conversion is based on the electron transfer theory, proposed by Rudolph A. Marcus (awarded for this work with a Nobel Prize in Chemistry in 1992, see Tab. 1.1.1). Photosynthetic electron transfer reactions are the cascade of chemical reactions where electrons are added to species (reduction) and taken away (oxidation). General reduction-oxidation (**redox**) reaction can be written as [26]:

$$A_{ox} + ne^- + mH^+ \rightleftharpoons A_{red} \tag{1.2.2}$$

where A_{ox} and A_{red} represents respectively oxidised and reduced forms of A. Although change in free energy could well describe the properties of those reactions, they are rather quantified in terms of **redox potential changes** and determined using electrical measurements. Therefore, redox potential at the pH=0 is given by the relationship [27]:

$$\Delta E = \Delta E_0 - \frac{RT}{nF} \ln \frac{[A]_{red}}{[A]_{ox}}, \tag{1.2.3}$$

where n is the number of electrons involved in the reaction, F is the Faraday constant and ΔE is the **electrical potential**.

During the photosynthetic reactions electron transport moves electrons toward the equilibrium, except the initial photochemical reaction that takes place at the reaction centre, when a redox couple of donor with higher redox potential than acceptor is generated [28]. Standard redox potentials are called midpoint redox potentials, and are important in the process of understanding photosynthetic electron transport chain, as they

are measurements of the tendency of a compound to accept electrons from other compounds.

Electron flow modes

The schema above (Fig. 1.2.2) includes two modes of the electron flow. The linear and cyclic one. **Linear photosynthetic electron flow** (LEF) is carried out by the four major protein complexes with the participation of the free electron carriers: plastoquinone (PQ), plastocyanin (PC), ferredoxin (Fd), an iron-sulfur protein that mediates electron transfer, and enzyme ferredoxin-NADP reductase (FNR). LEF starts with photoinduced water-splitting process in the photosysystem II, where four photons absorbed by PSII extracts four electrons from two molecules of water, releasing oxygen and four protons into the lumenal side of thylakoid

$$2H_2O + 4h\nu \rightarrow 4e^- + O_2 + 4H^+_{lumen}. \tag{1.2.4}$$
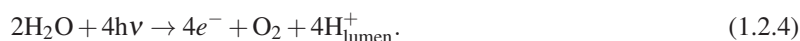
Since $2\,e^-$ are required to reduce one molecule of plastoquinone, further in this work it was decided to refer to net reaction of photosystem II as

$$H_2O + 2h\nu \rightarrow 2e^- + \frac{1}{2}O_2 + 2H^+_{lumen}. \tag{1.2.5}$$

Therefore each further reaction transfers 2 electrons from one electron carrier to another. And such, net reaction mediated by the proton pump cytochrome b_6f, transferring electrons from reduced PQ to PC can be described in chemical terms as

$$PQH_2 + 2PC + 2H^+_{stroma} \rightleftharpoons PQ + 2PC^- + 4H^+_{lumen}. \tag{1.2.6}$$

Reaction mediated by PSI passes electrons to Fd

$$PC^- + Fd \rightarrow PC + Fd^-, \tag{1.2.7}$$

from which they are transferred to NADPH through Ferredoxin—NADP(+) reductase (FNR):

$$2Fd^- + NADP^+ + H^+_{stroma} \rightleftharpoons 2Fd + NADPH. \tag{1.2.8}$$
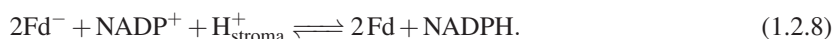
LEF describes therefore an overall process

$$H_2O + h\nu \rightarrow PSII \rightarrow PQ \rightarrow cytb_6f \rightarrow PC \rightarrow PSI \rightarrow NADPH, \tag{1.2.9}$$
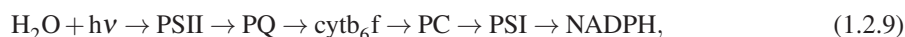
coupled to a proton movement in the lumen that drives ATP synthase, leading to the ultimate coupled production of both NADPH and ATP in a fixed ratio, further used to drive the Calvin cycle.

Second recognised mode of electron flow, the **cyclic electron flow** (CEF) around the PSI [29, 30], though initially considered as physiologically unimportant, recently has gained attention in the photosynthetic community, leading to major developments, such as identification of main pathways [31]. The actual regulation of CEF still remains unknown, and here we follow the assumption that the PQ pool is reduced by direct operation of ferredoxin-plastoquinone reductase (FQR)

$$2Fd^- + PQ + 2H^+_{stroma} \rightarrow {}_2Fd + PQH_2, \tag{1.2.10}$$

contributing to the increase of the proton gradient and therefore leading to the production of ATP.

Proton motive force and photosynthetic productivity

LEF is coupled with a generation of a transthylakoid proton gradient, or proton motive force (pmf) of a pivotal role in balancing photosynthetic productivity [32]. pmf comprises of electric field ($\Delta\Psi$) and pH (ΔpH) gradients [33]. It has an impact on both ATP synthesis and activation of pH-dependent photoprotective mechanisms (described below).

During the linear transport, four protons are released into the lumen during the water split plus eight additional protons can be pumped into the thylakoid lumen through the action of the Q cycle [34]. It is assumed that the ATP synthase with 14 c-subunits requires 14 protons to synthesise three ATP (4.67 H$^+$/ATP) through the CF1-CF0 ATP synthase (ATP synthase). But the LEF alone can generate only 2 NADPH and 2.57 ATP, being not sufficient to meet the predicted demand of the Calvin cycle that consumes three ATP and two NADPH [35]. Therefore five alternative mechanisms of supplying "missing" ATP were proposed, summarised by Krammer *et al.* [36], of which only two are considered in this work: mentioned above cyclic electron flow around PSI, and involvement of plastid terminal oxidase in plastoquinone oxidation.

1.3   Photosynthesis in a variable environment

Photosynthetic organisms face a succession of environmental challenges every day, that may vary from changes in the light intensity and quality, to availability of nutrients, salinity, temperature, irrigation and many others. Although majority of the studies on photosynthesis are performed in the controlled, laboratory conditions, the ultimate goal is to transfer our knowledge outdoors, where the conditions are highly variable. In Fig. 1.3.1 an example of such changes in the field experiment is captured [37]. The fluctuations in temperature, irradiance and precipitations may severely impair plants fitness. For that, a remarkable feature of the photosynthetic apparatus is acquisition of several mechanisms that allow maintaining its normal functionality and adjusting its activity according to such changes in the environmental conditions. On a timescale from seconds to days, plants and algae are able to optimise energy capture, conversion and dissipation efficiency under different light conditions through various **acclimation** responses.
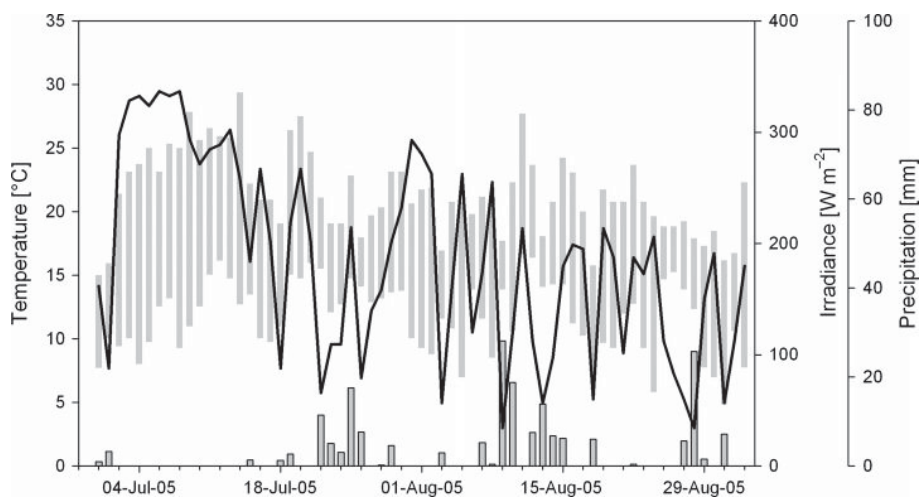

Figure 1.3.1: An example of changes in the weather conditions during the field experiment. Figure taken with permission from [37].

Short-term responses, taking place on a timescale of seconds to minutes, are typically reversible and do

not require extensive changes in either the gene profile expression of the organism, or in the structure of the photosynthetic apparatus. On the other hand, **long-term responses** implies ultrastructural changes in the cell and in most cases *de-novo* synthesis or breakdown of proteins, pigments and redox co-factors. For example, during limiting light conditions, photosynthetic cells tend to increase their light-harvesting capacity to maximize light capture. This requires an increased biosynthesis of photosynthetic pigments [38], as well as the increased expression of the genes encoding for the light harvesting proteins (LHC in plants). Conversely, plants tend to decrease the size of the LHC proteins in high light [39], to avoid absorption of excess light. This leads to a feedback regulation, where the level of irradiance regulate the antenna size of photosystems on the long-term scale of several hours or days [40, 41, 42].

In this work, the focus lies on the mechanisms developed by organisms against rapid changes in light conditions, both to provide a photoprotection against super-optimal light as well as optimisation when the source of light is limited.

1.3.1 Light intensity

The effect of light intensity on photosynthesis is probably one of the most extensively studied one. Light intensity influences among many leaf's anatomy and morphology [43], biomass production [44, 45] and composition [46, 47, 48]. From the photosynthesis-irradiance (PE) curve (Fig. 1.3.2) that provides a convenient way of differentiating between light-saturated and light-limited photosynthesis, we know now that though initially the photosynthetic rate increases linearly with increasing light intensity, at certain intensity it saturates reaching its maximum rate (Pmax)after which phenomenon of photoinhibition occurs. Further analysis of curve's shape, magnitude and initial slope helps to asses various regulatory processes as well as the rate of acclimation [49].
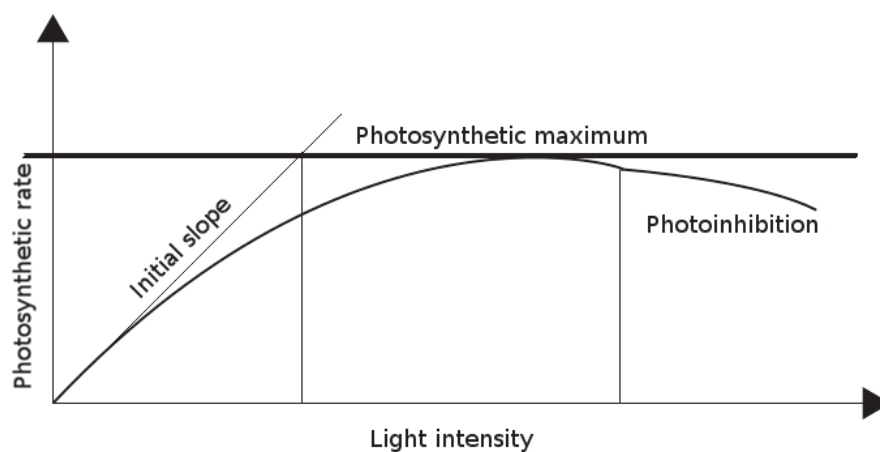
Figure 1.3.2: The PI (photosynthesis-irradiance) curve showing the relationship between the light intensity and net photosynthesis. Photosynthetic rate increases initially linearly with increasing light intensity reaching its maximum rate after which phenomenon of photoinhibition occurs.

1.3.2 Light colour

Out of the sun light reaching Earth, only a narrow electromagnetic spectrum can be used by photosynthetic organisms in the process of photosynthesis. Photosynthetically active radiation (PAR) corresponds to the spectral range of solar radiation between 400 to 700 nanometers, where photosynthesis occurs most

optimally[2].

Due to the diiferent pigment composition of photosystems the spectral absorbance of PSII supercomplex (core and LHCII) and LHCI-PSI supercomplex are different. In Fig. 1.3.3 it is visualised how the distinct absorption spectrum of chlorophyll a, chlorophyll b and carotenoids translates to the overall spectral absorbance of photosystems, demonstrating how important light wavelength is on overall photosynthetic efficiency.
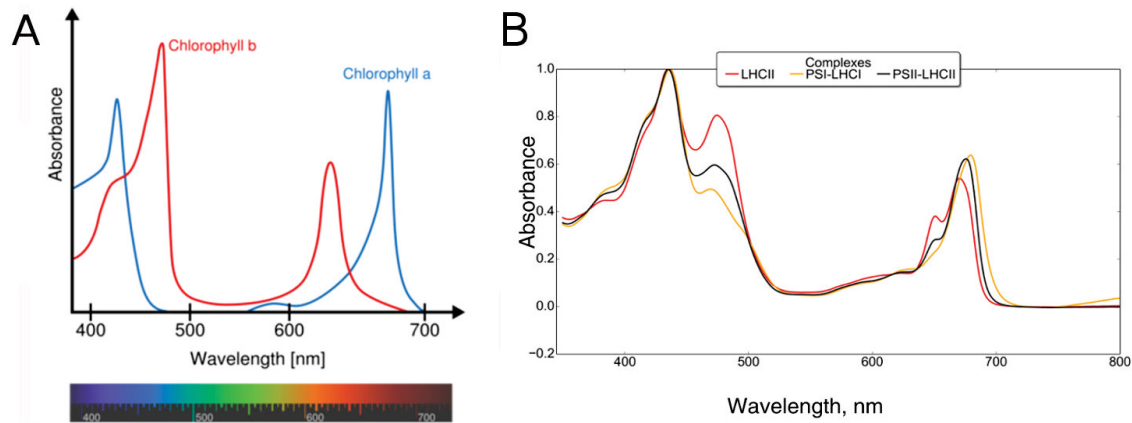
Figure 1.3.3: Difference in pigment composition between two photosystems influences their absorbance. A) Absorption spectrum of chlorophylls a and b. Figure taken with permission from [51]. B) Difference in the spectral absorbance of PSII and PSI supercomplexes. Figure based on the experimental data obtained from Assist. Prof. Ryutaro Tokutsu, National Institute for Basic Biology, Okazaki (Japan).

The role of photosensory proteins (cryptochromes, phototrophins and phytochromes) on the photosynthetic response to changing light conditions becomes more apparent [52, 53]. For instance, in their recent studies Petroutsos *et al.* [54] discussed a specific role of a blue-light receptor in the regulation of qE in the green alga *Chlamydomonas reinhardtii*, whilst Taddei *et al.* [55] studied the transcriptional regulation of LHCX genes in diatoms in response to many signals, including white and blue light. Therefore it is critical that for a complete understanding of light effect on photosynthetic acclimation both intensity and wavelengths are studied.

1.4 Non-photochemical quenching

In their natural conditions, most plants receive more sunlight than they can actually use for photosynthesis [56]. What happens therefore with the excess of absorbed energy? In Fig. 1.4.1 possible fate of energy absorbed by chlorophylls are presented, including pathways leading to its utilisation as well as dissipation. When chlorophyll absorbs a photon of light of v frequency and hv energy[3], it is being excited to its higher energy state, a singlet-state (^{1}Chl*). This can be easily expressed in a simple equation:

$$\text{Chl} + hv \longrightarrow {}^1\text{Chl*} \tag{1.4.1}$$

It can relax back to its ground state through one of several pathways with different consequences for an organism. The most desired fate of excited chlorophyll is to transfer the energy to reaction centres and use it to fuel photochemical reactions resulting in production of ATP and NADPH (k_P, also referred to as photochemical quenching). It may also relax through light re-emission, seen as fluorescence (k_F) or decay via

---

[2]Too much energy (ultraviolet light) breaks the bonds in molecules and can destroy organisms' DNA [50], whilst infrared light does not contain enough energy to excite electrons.

[3]The relation between light frequency and energy of a photon is described through the Plank relation: $E = hv$, where h is the Planck constant and v is the frequency.

the triplet state $^3Chl*$ [57]. Unfortunately, $^3Chl*$ may lead to a generation of $^1O_2*$, a highly damaging reactive oxygen specie (ROS). To avoid the consequences of oxidative stress, photosynthetic organisms developed mechanism that allow to dissipate excitation energy as heat through molecular vibrations (k_H). Such thermal dissipation is a part of several identified fast responses, collectively termed as non-photochemical quenching of chlorophyll fluorescence (NPQ) , as they are detected as a decrease in the chlorophyll fluorescence yield, emitted from fully reduced (photochemically inactive) photosystem II complex (more on fluorescence detection in the next chapter).

Figure 1.4.1: The possible fates of excited singlet-state chlorophyll ($^1Chl*$). Chlorophyll that absorbs light is being promoted to its singlet excited state $^1Chl*$, from which it has several ways to relax back to its ground state: through light re-emission (k_F), through photosynthesis (k_P), by heat dissipation (k_H), or decay via $^3Chl*$ that may have a severe consequences for the system if the energy will get transferred to O_2 to generate singlet oxygen ($^1O_2*$). Figure reproduced from [56].
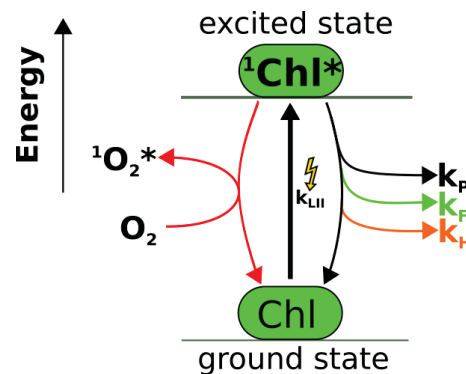
Analyses of the dynamics of Chl fluorescence quenching identified different NPQ components, which in plants have been assigned to three main NPQ mechanisms [58, 59, 60, 61, 62, 63]:

1. the pH-regulated mechanism, qE [64],
2. the state transition mechanism, qT [65],
3. the photoinhibitory quenching, qI [66].

Although a xanthophyll dependent quenching (qZ) is sometimes considered as a separate component of NPQ [59], here we follow the classification where qZ is a process contributing to the maximal activity of high-energy dependent quenching [63]. As a general rule, qE is considered as a major component of NPQ under moderate and high light conditions, whilst the development of qT is supposed to play a role in balancing light quality excitation under low light, where photosynthesis is limited by absorption. Finally, qI becomes predominant when light is oversaturated and exceeds the photosynthetic capacity.

1.4.1 High-energy dependent quenching, qE

The fastest component of NPQ is the energy-dependent component (qE) that in plants relaxes in around one minute and occurs mainly at the level of the LHCII [58]. It is triggered by 1) the acidification of the lumenal space, due to the build-up of transmembrane ΔpH generated by saturated electron flow, 2) changes in pigment composition in the LHCII that are catalyzed by the xanthophyll cycle, and 3) activation of specific qE protein effectors [67]. The exact role of each component is still a matter of debate and it can vary within autotrophs, i.e. number of xanthophyll cycles available in some algae. Several models of actual cooperation of the qE components were proposed [68]. It is currently assumed that both Photosystem II subunit S protein (PsbS) presence and violaxanthin de-epoxidase enzyme (VDE) enzyme are essential to reach a maximal capacity of qE.

Carotenoids and xanthophyll cycle

Carotenoids are key players in acclimation and regulation processes of photosynthesis, as they can directly contribute to both light harvesting (between 350 and 750 nm of the visible spectrum) and photoprotection, through the xanthophyll cycle. Xanthophylls are oxygenated carotenoids that through a cyclic process of

de-epoxidation and epoxidation can facilitate a conformational change in the LHCII, switching the PSII into a quenched state [69].

Three different xanthophyll cycles have been already described [69], though in the context of this research we focus only on the violaxanthin cycle, which operates among all higher plants and some green algae[4]. During NPQ, the VDE activated by a low lumenal pH [70] converts violaxanthin (Vx) into zeaxanthin (Zx) via the intermediate antheraxanthin (Ax) [72]. The conversion of Zx back to Vx is operated by the enzyme zeaxanthin epoxidase (ZEP) [73] (Fig. 1.4.2).
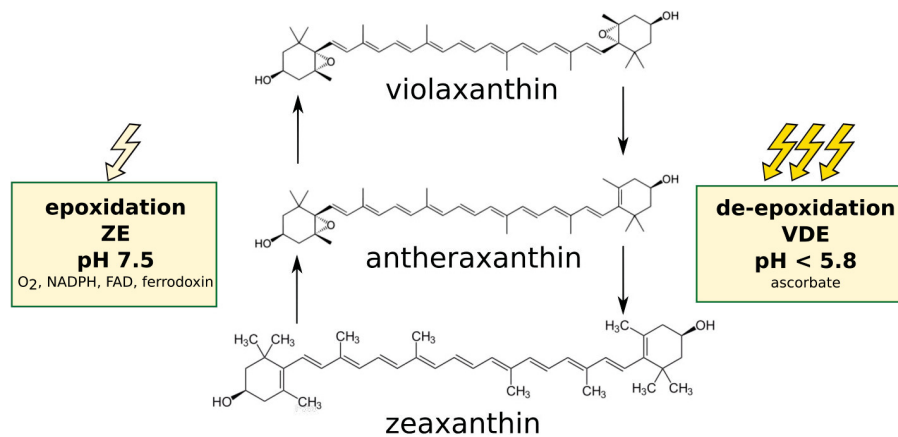
Figure 1.4.2: Xanthophyll cycle. Figure redrawn based on [69].

1.4.2   State transitions, qT

Under limiting light conditions qT plays an important role in a short term chromatic adaptation, as through a process of state transitions the relative cross section of photosystems can be adjusted [74, 75]. The mechanism was discovered independently by two groups nearly 50 years ago [76, 77], yet still the exact mechanism, extent and site of action are under debate [22, 78, 79]. The mechanism involves change between two states (depicted in Fig. 1.4.3).

Molecular mechanisms

State transitions are governed by a kinase-phosphatase pair and since now several homologues in plants and in green algae were identified. In plants, phosphorylation of LHCII is facilitated by protein kinase STN7 (STATE TRANSITION 7), that is activated by the binding of reduced plastoquinone to the Q_o site of cytochrome b6f complex [80, 81]. The reduction of PQ pool is mainly achieved under light conditions that preferentially excite PSII. De-phosphorylation of LHCII by the protein phosphatase PPH1/TAP38 (PROTEIN PHOSPHATASE 1/THYLAKOID ASSOCIATED PHOSPHATASE 38) promotes its association with PSII.

In Tab. 1.4.1 the reported concentration of chlorophyll molecules in PSII core, LHC trimers and monomers and PSI supercomplex is shown. In **State 1**, all light-harvesting complexes primarily associated with PSII are connected to it, leading to a total concentration of 159 Chls connected to PSII and 225 connected to PSI. In **State 2**, all outer antenna of PSII are attached to PSI, so the relative cross section of photosystem I increases to 323 Chls [78, 82].

The mechanism of state transitions is assumed to be absent in diatoms [83] and presents only a moderate

---

[4]Next to Vx-cycle two additional cycles can be found in some classes of algae and plants. Those are diadinoxanthin cycle [70] and lutein-epoxide cycle [71] respectively.

State 1
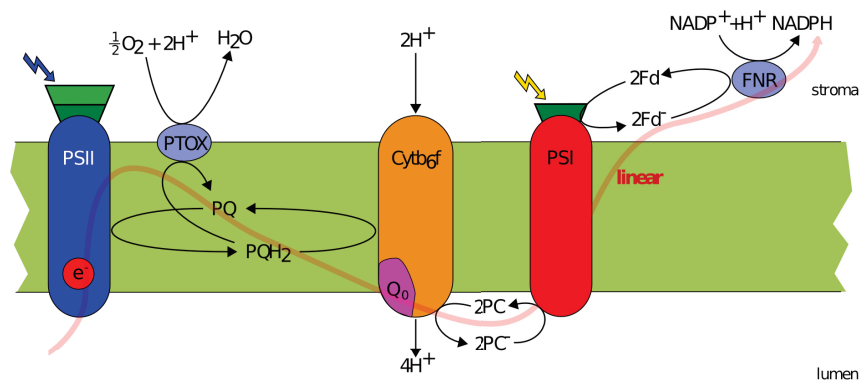
State 2
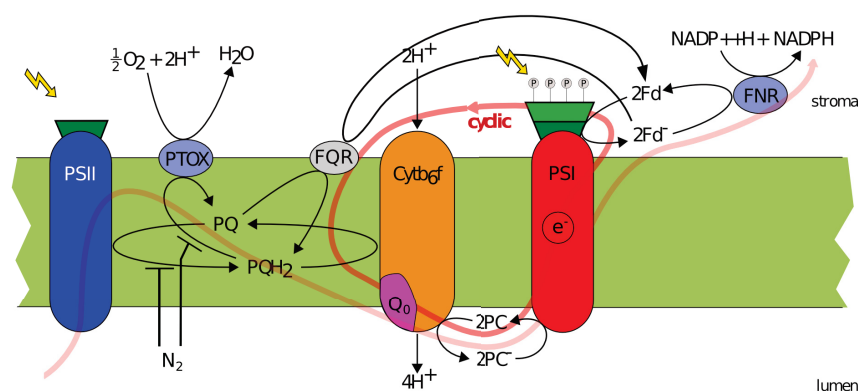
Figure 1.4.3: Scheme of state transitions from state 1 to state 2. The transitions occurs when the redox state of the plastoquinone pool (PQ) is reduced. Docking of plastoquinol (PQH2) to the Q_0 site of Cytb6f leads to the activation of the protein kinase, which phosphorylates LHCII either directly or indirectly. Phosphorylated LHCII dissociates from PSII and binds to PSI.

amplitude in plants [84]. However, it is believed that it plays much more significant role in green algae, as it was demonstrated on the example of *Chlamydomonas renihardtii* that due to qT up to 45% of antennae can be reallocated [85]. The interesting debate goes on for the past few years, whether next to its role in optimising light absorption under low light, qT in *Chamydomonas* can contribute to photoprotection in high light [86] and may actually involve different mechanisms than the simple physical displacement of LHCII between the two photosystems [22, 78, 79].

1.4.3 Photoinhibition, qI

Finally, photoinhibitory quenching (qI) provides the slowest contribution to the NPQ. Photoinhibition targets primarily photosystems II and is mainly achieved by degradation and disassembly of the core subunit of the photosystem II [87]. Photoinhibition causes irreversible damage to reaction centre subunits, and such protein damage and inactivation of PSII can be induced from both acceptor and from donor side of P680 [87]. The process is related with prolonged overexcitation of the photosynthetic machinery and high amount of produced ROS can enhance the degradation of the protein [88], leading to a decrease in photosynthetic quantum yield. The extent of photoinhibition depends on the balance between the rate of such photodamage and the rate of repair of damaged PSII

Chlorophylls	PSII core	Lhcbs	PSI-LHCI
	core	monomer	
Chls a	35	8	183
Chls b	-	6	42
Chls a + Chls b	35	14	225
	CP29	trimer	
Chls a	9	24	
Chls b	4	18	
Chls a + Chls b	13	42	
	CP26		
Chls a	8		
Chls b	6		
Chls a + Chls b	14		
TOTAL	**62**	**97**	**225**

Table 1.4.1: The estimated number of chlorophyll molecules in PSI-LHCI supercomplex, PSII and Lhcbs. It is assumed that the Lhcbs contain 7 antenna: 2 trimeric and 1 monomeric. Based on numbers reported by Croce's Lab [78, 82].

1.5   Remaining Questions

Due to the continuous research on photosynthesis and its dynamics under fluctuating environmental conditions, we acknowledge today the importance of further investigations of the molecular signalling mechanisms guiding acclimation responses. Especially studies on non-photochemical quenching are necessary, as the complete, systems wide understanding of the processes involved is required if one desires to optimise photosynthetic efficiency [89]. A goal, that is more valid today than ever before, considering the expanding global population, aging society and increasing energy demand [90, 91]. Although this research aims at answering only a handful of remaining questions regarding the short-term acclimation responses, it is envisaged that it will contribute to assessing, quantifying and eventually minimising the rate of energy loss due to NPQ, that currently is attributed as one of the largest parts of photosynthetic inefficiency [89].

What is the quantitative contribution of qE components to the quencher?

The exact role of each component of high-energy dependent quenching is still a matter of debate and it can vary within autotrophs. Although many models of interaction between the components was proposed, they are based on *in vitro* measurements and they are lacking an agreement on many molecular aspects, such as the actual side of action [68]. For that reason we first constructed a simple mathematical model of high-energy dependent quenching that incorporates the basic understanding of this process and description of both main components of qE: pH dependent and zeaxanthin dependent. With the theoretical description we aim at quantifying the contribution of each component to the overall quenching capacity under varying light conditions. Moreover, we use an association between qE and the biological phenomenon of short-term illumination memory [92, 93, 94] to verify if the basic mechanisms of quenching and memory are the same among distant species.

How the flexibility of meeting the energy demand is achieved?

The changing environmental conditions and downstream biochemical demand of a cell is well answered by photosynthetic organisms by adjusting the output ratio of ATP:NADPH during the light reactions [95]. A major open question remains how this flexibility is achieved and what is the exact role of the cyclic electron flow? How the cell is actually modulating the ATP to NADPH ratio?

Is reducing the amount of LHCII increasing photosynthetic efficiency?

The idea of reducing the amount of light-harvesting pigments to provide greater rate of absorbed photons to biomass applied to cyanobacteria and algae [96, 97] yields quite promising results. By testing how the reduction of antennas pigments influence the photosynthetic efficiency *in silico* and comparing it to results reported by various groups, the potential of this strategy to optimise biomass productivity is further assessed.

Is our current understanding of state transitions correct?

As high light intensities may severely impair the photosynthetic apparatus and damage the reaction centres, where charge separation occurs, plants and other photosynthetic organisms are capable of switching from a photosynthetic, light-harvesting state to a protective one, in which excess absorbed radiant energy is emitted as heat [56]. But it is still under the debate if such state can be reached during the state transitions, where instead of attaching the phosphorylated antennas to PSI, aggregated antenna will quench inside the thylakoid membrane [22, 78]. Building a model of state transitions in Ch. 5 is an attempt to verify if our current understanding of the mediation by kinase-phosphatase pair is correct and if the aggregation of antennas is possible.

What is the impact of light wavelength on NPQ?

Through the reorganisation of light harvesting complexes plants gain the ability to dynamically react to external stimuli and to keep the redox balance within the thylakoid membrane [98]. However, what is the exact influence of light wavelength is unknown.

Already Bonaventura and Myers in their original paper where state transitions were reported [76] used mathematical model to make a quantitative analysis of the reported observations. Therefore mathematical models developed here are envisaged to provide in many cases not only a qualitative but also a quantitative tool to study photosynthetic acclimation, specifically non-photochemical quenching.

2. Measuring NPQ *in vivo*

„It doesn't matter how beautiful your theory is, it doesn't matter how smart you are. If it doesn't agree with experiment, it's wrong."

*- **Richard P. Feynman**, theoretical physicists, Nobel Prize winner*

Various experimental techniques were developed over the years to allow for a dynamic measurements of changes in photosynthesis. The use of model organisms allows us to get a glimpse into the dynamics of photosynthetic machinery and extrapolate the knowledge gained while studying one specie to the wide range of other organisms, providing more robust overview of photosynthesis in eukaryotes. This Chapter includes a brief introduction to the wet lab techniques used while collecting experimental data for the development, calibration and validation of mathematical models I developed. I start with providing arguments for the selection of model organisms used in both *in vivo*, as well as *in silico* studies. Next, I explain the principles behind fluorescence measurements, powerful and common techniques used in plant physiology. I discuss their applications and limitations and provide short summaries of experimental protocols developed by my collaborators.

2.1 Model organisms

It can be easily claimed that almost everything we know about the fundamental properties of living cells originates from the extensive studies of so called model organisms [99]. Despite their limitations, they still play a key role in contemporary biological and medical research [100]. A model organism is a (non-human) species that has been widely studied to understand a specific biological phenomena with the expectation that investigated processes are shared across other organisms and therefore collected data and theories generated based on model organisms will be applicable to other, ideally, more complex organisms [101]. It is therefore important to distinguish the difference between an experimental and model organism. Experimental organisms are not always becoming a model organism, as they do not necessarily have to be representative of species other than themselves.

Model organisms are characterised by a set of features such as easy breeding and manipulation in a laboratory setting or fast population growth. With time, a wealth of collected biological data makes them even more attractive to study. With the first full genome sequence published in 1995 for a *Haemophilus influenzae*[1] [102], also the amount of available genome data often decides on one organism being more attractive than other.

2.1.1 A dynamic duo

Here, two model organisms are studied, a dynamic duo [103]: a green alga *Chlamydomonas reinhardtii* and higher plant *Arabidopsis thaliana*. As the goal of this doctoral research was to provide a model of short-term light acclimation mechanisms that will be applicable to a number of species, the decision on a selection of these organisms was motivated by their close NPQ characteristics (Fig. 2.1.1) and complementarity [103]. They share the origin of chloroplast, have closely related photosynthetic apparatus with active VAZ cycle and present specific qE protein effectors, but most importantly both *Arabidopsis* and *Chlamydomonas* are widely used in the NPQ studies and therefore a vast amount of data was available for those two organisms.
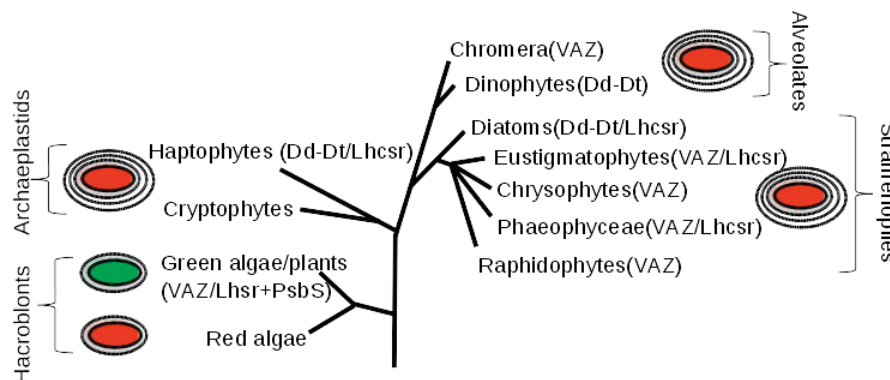
Figure 2.1.1: Phylogenetic tree based on the similarity of NPQ mechanisms in eukaryotes. Figure redrawn from [104]

2.1.2 Arabidopsis thaliana

Arabidopsis thaliana has been the organism of choice for decades now. It is the most popular plant model organism, studied by plant biochemists, physiologists, developmental biologists and geneticists. *Arabidopsis* is a small flowering plant, a member of the mustard or cabbage (*Brassicaceae*) family, which

---

[1]*Haemophilus influenzae* is a Gram-negative, coccobacillary, facultatively anaerobic pathogenic bacterium, residing in the human respiratory tract [102].

includes cultivated species such as broccoli, cabbage, cauliflower and radish. Although itself has mo major agricultural or economical significance, it serves as an important model to study flowering plants, due to its small genome size (125 Mbp)[2], large number of offspring, small size (max. high approximately 20 cm) and short generation time.

Arabidopsis was also the very first plant to have its genome sequenced in 2000 [105] making it even more important model system for identifying genes and determining their functions.

2.1.3 Chlamydomonas reinhardtii

Chlamydomonas reinhardtii is a unicellular flagellate green alga about 10 micrometres long and 3 micrometers wide [106]. *Chlamydomonas* lineage diverged from land plants over 1 billion years ago [107] and currently occupies soil-dwelling. It is widely used in biological research due to its short generation time, being both a heterotroph and a facultative autotroph, it capability of both sexual and asexual reproduction, and availability of genetic information, including the complete nuclear genome sequence [107]. *Chlamydomonas*, often referred to as simply *Chlamy*, is widely studied not only in the context of photosynthetic research but also biomedical studies. Interestingly, the structure of *Chlamydomonas* flagellum and a human airway cilium[3] are virtually indistinguishable [109]. For that, studies in *Chlamy* increased our knowledge about many ciliary and basal body proteins involved in human diseases (including primary ciliary dyskinesia, polycystic kidney disease or epilepsy [109]).

Chlamydomonas is a particularly good organism to study photosynthesis and short-term acclimation mechanisms [110] mainly due to the fact that though its photosynthetic function is very similar to that of vascular plants, it combines the advantage of a unicellular organisms [106] and allows for an easy genetic and molecular manipulation [111]. Moreover, in terms of NPQ, a large collection of acclimation mutants is available, allowing for gene function characteristics [112, 113, 114, 86] and it has been proven to be a well suited organism to study state transitions [74].

The interest in studying *Chlamydmonas*, beside its application to fundamental research, has also a biotechnological and bioeconomical background, extremely important once the possible long-term impact of my research is considered. Since decades micro-algae are constituting a promising source of biofuels [115, 116, 117] and high valuable compounds [118], including food commodities [119], but quite recently their potential as a platform for a production of a recombination proteins was discovered [120].

2.2 Fluorescence emission measurements

There is a great demand for protocols for rapid screening of photosynthetic activity that give information regarding plants' fitness. Fluorescence measurement provides a powerful, minimally-invasive method to monitor photosynthetic dynamics, giving information on the photosynthetic efficiency, protection and energy dissipation. The connection between fluorescence emission and numerous processes taking place during the photosynthetic electron transfer, together with the great advance in spectrometric technique made fluorescence measurements a method of choice while studying oxygenic photosynthesis [121].

---

[2]For a comparison maize has a genome of approximately 2400 Mbp and wheat genome is 16000 Mbp.

[3]Cilium are a membrane-enclosed motile structure extending from the surface of eukaryotic cells that usually occur in groups and beat rhythmically to move a cell or small particles or fluid along the surface [108].
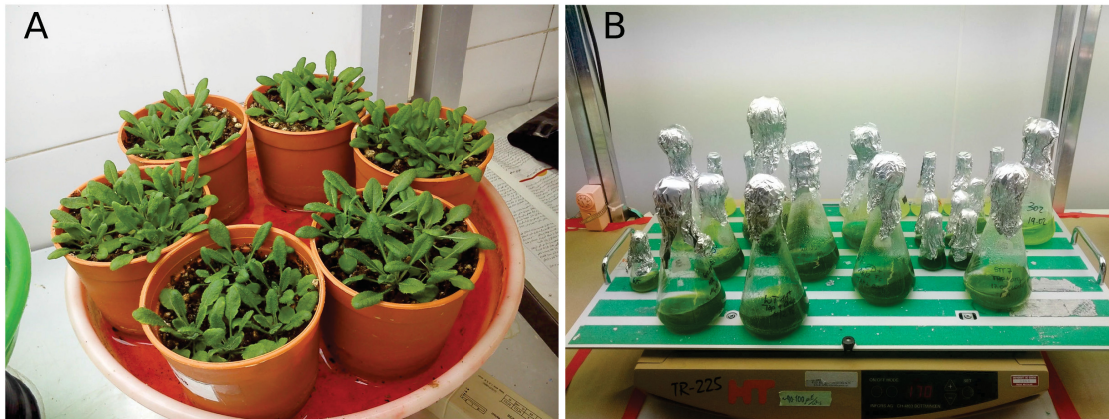
Figure 2.1.2: A dynamic duo grown in the laboratory conditions. A) *Arabidopsis thaliana* grown for the light memory experiment (Ch. 4). Picture taken by Dr S. Heydari. B) Various strains of *Chlamydomonas reinhardtii* grown in the lab of Prof. M. Goldschmidt-Clermont in Geneva for the state transitions experiment (Ch. 5).

2.2.1 Jablonski diagram

In the previous Chapter the possible fates of chlorophyll were described (Ch. 1, Fig. 1.4.1). Pigment can absorb the energy from light and make the transition to the higher energy state only when it is irradiated with light of an energy equal to the energy spacing between two quantum levels. Such transition is called resonance absorption and gives rise to an **absorption spectrum**. A downward transition from the excited state is called fluorescence. Fluorescence spectral data are generally presented as **emission spectra**. The emission rates of fluorescence are typically $10^8 s^{-1}$.

Fluorescence activity, describing both absorption and emission of light, can be schematically illustrated with the classical Jablonski diagram (Fig. 2.2.1 A). Within each column, horizontal lines represent eigenstates for the particular molecule. Bold horizontal lines are representations of the limits of electronic energy states (S_0, S_1, S_2). Within each electronic energy state a multiple vibrational energy states are possible, represented schematically by thin horizontal lines.

In Fig. 2.2.1 B measured absorption (solid line) and fluorescence (dot line) spectra of chlorophyll a are plotted versus the wavelengths. The observed spectrum of fluorescence emission is different to that of absorbed light, with a peak at a longer wavelength. Due to this visible difference, fluorescence yield can be measured by exposing plant's leaf, or algal suspension, to light of defined wavelength and measuring its re-emission at the longer wavelengths [122].

2.2.2 Distinct phases of fluorescence measurement

The first to discover the dynamic changes in chlorophyll *in vivo* were Hans Kautsky and A. Hirsch [124], who noticed that in contrast to fluorescence of Chl a in solution, intensity of Chl a fluorescence *in vivo* changes over the time under constant illumination. The characteristic transitory changes in time became known simply as the Kautsky effect (or chlorophyll transient). During nearly century of followed research, our knowledge on the characteristic changes in Chl a fluorescence of a photosynthetic sample transferred from dark to light significantly increased [125]. We know now that chlorophyll fluorescence represents a sort of signature of photosynthesis, as a variety of photosynthetic events influence different segments of the entire fluorescence transient.

Observed fluorescence transient is often referred to as the **OJIPSMT** transient, where O (the origin) is
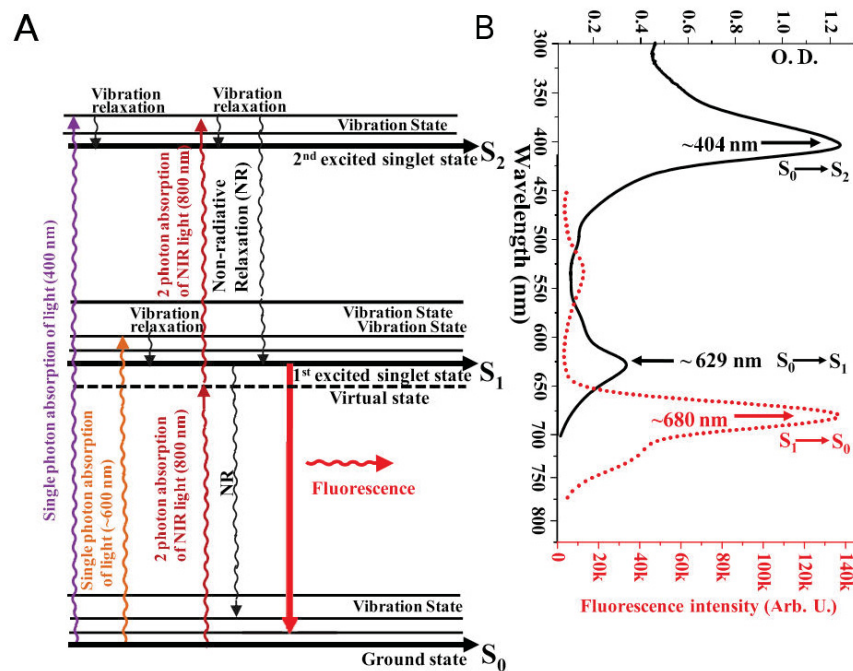
Figure 2.2.1: Basic fluorescence emission principles. A) Jablonski energy level diagram illustrating the transitions between electronic states of a chlorophyll molecule. B) Measured absorption (solid line) and fluorescence (dot line) spectra of chlorophyll a. Figure taken with permission from [123].

for the first measured minimum fluorescence level; J and I for intermediate inflections; P for peak; S for semi-steady state level; M for maximum; and T for terminal steady state level [124]. The **OJIP phase** is the fast phase that is over within a second, whilst the **PSMT phase** lasts for minutes. The PSMT phase is modulated by the redox state of Q_A and NPQ and since the introduction of Pulse Amplitude Modulation (PAM) fluorescence technique, it became a method of choice to measure NPQ level.

2.2.3 PAM measurements

It is assumed that at room temperature the variations in the fluorescence signal arise from PSII only and we ignore emission from PSI. Therefore PAM measurements are interpreted as fluorescence signals emitted only by photosystem II [126]. The PAM technique uses the saturated pulses (SP) of light to promote a photosynthetic state in which photochemistry is blocked due to the rapid and temporary reduction of photosynthetic electron transport. By monitoring the change in the fluorescence yield over the time, the NPQ levels are assessed.

A typical PAM measurement of Chl fluorescence is illustrated in Fig. 2.2.2 with various parameters marked. Fluorescence measurement typically starts with a dark-adapted organism that is during the experiment exposed to various light treatments over the time. A **dark-adapted state** is charasterised by a maximally oxidised Q_A and therefore plants in this state should be capable of performing photochemical reduction of Q_A. It is important that the organism was kept in dark for a time sufficient to reach the maximal oxidation. The relative fluorescence intensity of such dark-adapted plant exposed to a very weak light (*ca.* 0.1 $\mu Em^{-2}s^{-2}$) is designated F_0 and is considered to reflect the rate of photochemistry and the sum of the rates of various basal non-photochemical de-excitations [127]. Upon illumination with the actinic light[4], a maximal fluorescence of a dark-adapted plant is measured after applying a saturating pulse of light (F_M). Comparison of any further fluorescence yield measured after a saturating pulse of light under illumination ($F_{M'}$) to this maximal

---

[4]Actinic light is the light that can be absorbed by photosynthetic apparatus and can drive photochemistry.

fluorescence provides information on the extend of photochemistry and quenching (as marked in Fig. 2.2.2).
As the quantum yield of photochemistry decreases, the quantum yield of NPQ increases. Therefore to
characterise the NPQ we can use the relation:

$$\frac{F_M - F_M'}{F_M'} = NPQ. \tag{2.2.1}$$
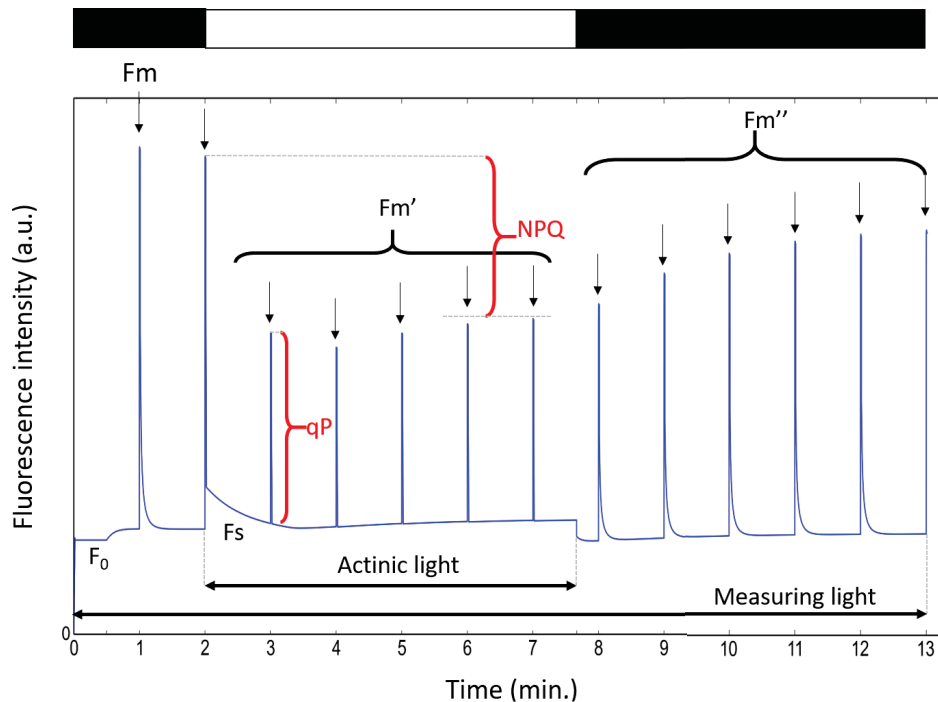
Figure 2.2.2: Example of a typical pulse amplitude modulation trace of *Arabidopsis thaliana* with a marked
fluorescence parameters. A measuring light is switched on at time 0 and the zero fluorescence level is measured (F_0).
First saturating pulse (SP) of applied applied in darkness to a dark adapted plant measures the maximum fluorescence
level (F_M). After this measurement a light capable of driving photochemistry (from latin called actinic light) is
applied. After a fixed period of time another SP is applied to measure the maximum fluorescence in the light (F_M').
The level of fluorescence prior the SP is termed F_S'. Figure reproduced based on [127, 124].

Common fluorescence parameters and relationship

Chlorophyll fluorescence parameters used throughout this work and marked on the Fig. 2.2.2 are summarised
below. For more detailed information please see recent reviews on chlorophyll fluorescence [122, 128, 124].

- F_0: minimal fluorescence. Fluorescence level when all antenna pigment complexes associated with the
  photosystem are assumed to be in the ground energetic state and reaction centres are open. Reflecting
  so called dark adapted state.
- F_M: maximal fluorescence. Fluorescence level measured right after a high intensity flash has been
  applied. All antenna sites are assumed to be closed.
- F_0': Minimal fluorescence (arbitrary units). Fluorescence level of illuminated sample which is lowered
  with respect to F_0 by non-photochemical quenching.
- F_M': Maximal fluorescence (arbitrary units). Fluorescence level of illuminated sample as induced by
  saturating pulses which temporarily close all PSII reaction centers.
- F_v: Variable fluorescence. Difference between maximal fluorescence and minimal fluorescence.
  Demonstrates the ability of PSII to perform photochemistry.
- $\frac{F_v}{F_M}$: Maximum quantum efficiency of PSII photochemistry.

- Φ_F: Quantum yield of fluorescence. Calculated as a probability of relaxing from the higher energy state through fluorescence $\frac{k_f}{k_F + \sigma_{PSI} k_P + k_H}$, where k_i are the rate constants for the decay of excitation energy in PSII in processes as described in Ch. 1, Fig. 1.4.1).
- Φ_{PSII}: Quantum yield of PSII.

2.2.4 Cold fluorescence emission

As fluorescence signal emitted at the room temperature originates mainly from photosystem II, in order to quantitatively analyse differences in PS I/PS II stoichiometries a low-temperature (77 K) fluorescence emission spectra are measured. An example of such spectra is displayed in Fig. 2.2.3.
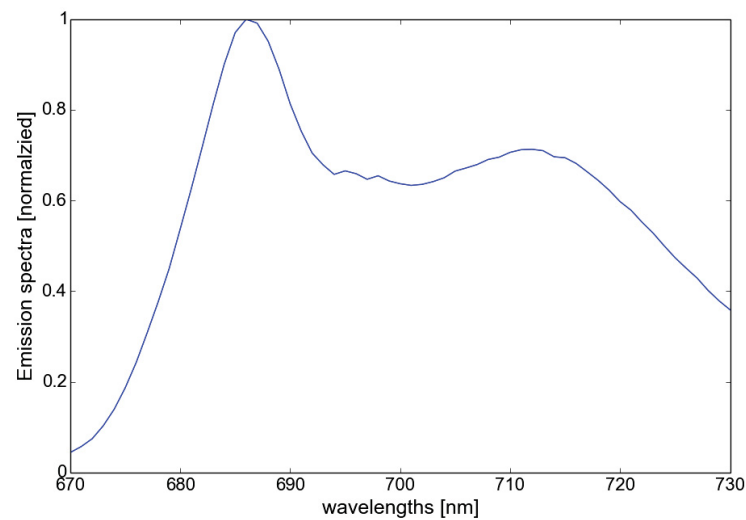
Figure 2.2.3: Example of 77K fluorescence emission spectra collected for WT strain of *Chlamydomonas reinhardtii* in the lab of Prof. Jun Minagawa, Japan.

2.3 Instrumentation

In this work different spectroscopic instruments were used to first measure the absorption of various strains, next to measure the fluorescence emission spectrum and finally to collect PAM measurements under varying stress conditions.

NPQ fluorescence measurements used to develop model in Ch. 4 were performed using Waltz PAM2000 Fluorometer. Fluorescence measurements used to develop model in Ch. 5 were performed using closed FluorCam and PSI Fluorometer. Lastly, cold fluorescence measurements used to develop model in Ch. 6 were performed using Horiba Jobin Ivon.

3. Mathematical modelling of NPQ

"It seems that perfection is attained not when there is nothing more to add, but when there is nothing more to remove."

*- **Antoine de Saint Exupéry**, writer, poet, and pioneering aviator*

Airman's Odyssey (1942)

Well designed mathematical models may provide a good theoretical framework for studying the dynamics of biological networks and allows for further predictions of the behaviour of the system. It is a way of collecting, organising and representing our knowledge in a new, nonchaotic way that allows to verify the accuracy of our assumptions and makes it easier to test new hypotheses. But the construction of mathematical models is often limited by a number of available, measured physiological and kinetic parameters. The possibility of fitting some of the unknowns to the experimental data or simply estimating the values is tempting, and often necessary, but it has to be acknowledged, that with a certain number of free parameters, basically any kind of data can be reproduced. Therefore, it is desired to create models as simple as possible, to reduce the number of free parameters. Here, I provide arguments first for the use of mathematical models in general and next argue that kinetic models, based on systems of ordinary differential equations, are the ideal tool to study the dynamics of photosynthetic acclimation. I moreover provide a selective mini-review of available mathematical models of non-photochemical quenching for higher plants and green algae, explaining the motivation for the development of a new one. Finally, I describe the modular design implemented throughout this work and describe how the numerical computations were performed.

3.1   Introduction

Theoretical approaches are powerful to discover organisational principles governing the design of biological systems. Properly constructed mathematical models verify and complement experimentally obtained results, reflect the current state of knowledge and set theoretical frameworks to derive novel hypotheses and perform investigations which are often experimentally challenging, if not impossible. In other words, building models is "a way of collecting, organizing, and representing knowledge and hypotheses" [129].

Mathematical models can take many forms, depending on the research question they aim to answer [130]. By definition, models are a **simplified representation of reality** and can focus on different timescales and different levels of complexity (Fig. 3.1.1). In photosynthetic research, they may range from detailed models of processes occurring within PSII on the timescale of picoseconds to nanoseconds (reviewed in [131]), over the biochemically structured models of culture growth in bioreactors [132, 133] to models of photosynthethic evolution [134]. Though system-level models of metabolism found a number of applications, due to the intrinsic assumption of a stationary state, their use to study the dynamics of photosynthesis is challenging [135] and other types of models are preferred.
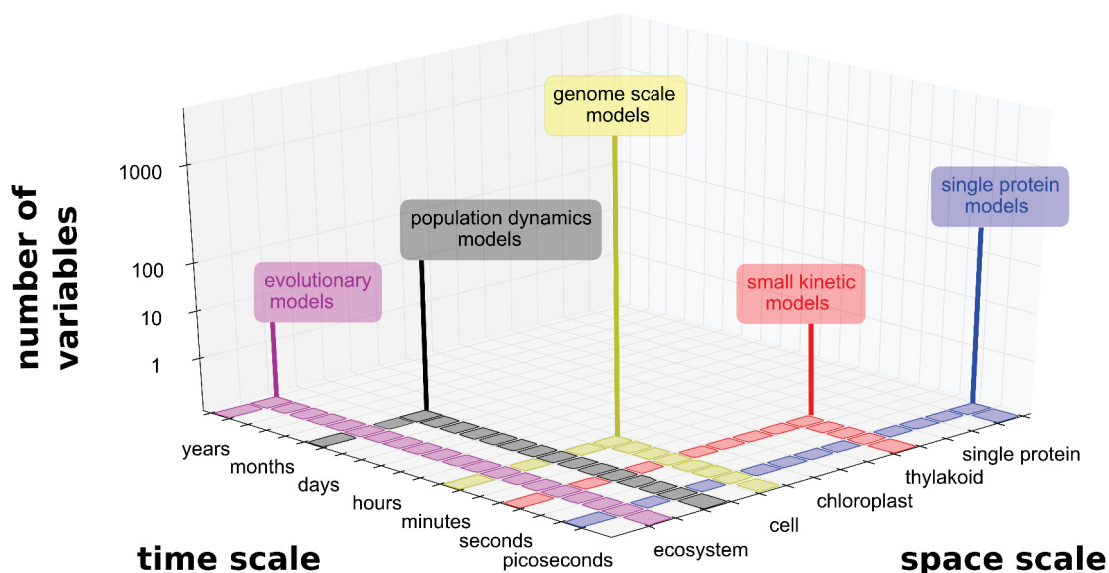
Figure 3.1.1: Three dimensions of reduction. Existing photosynthetic models cover different levels of complexity and details depending on the research questions they aim to answer, ranging from the detailed models of processes occurring within PSII on the timescale of picoseconds to nanoseconds [136], reviewed in [131], over the biochemically structured models of culture growth in bioreactors [132, 133] to models of photosynthethic evolution [134]. Figure taken with permission from [137].

3.1.1   A reductionist approach as a method to model photosynthetic self-regulation

Much of our current knowledge about photosynthesis was brought by reductionist models, dating back to the extremely simplified, but illustrative pioneering model by Thornley [138]. The question is whether this approach is still justified in the era of quantitative biology. The recent rapid advance in experimental techniques, such as mass-spectrometry and high-throughput sequencing, allows obtaining global snapshots of the status of a cell with unprecedented precision [139]. This wealth of information allows for example the reconstruction of genome-scale metabolic networks encompassing the entirety of all known biochemical reactions [140]. One would expect that with this richness of available data, a fundamental biochemical process like photosynthesis would be already well understood. In fact, a few attempts have been made to

apply genome-scale metabolic models to photosynthetic organisms including plants [141], green algae [142] and cyanobacteria [143] (recently reviewed in [135]) and these approaches were successful in providing valuable insight into the dependence of stationary flux distributions to external conditions. However, the inherent steady-state assumptions in the mathematical analysis techniques [144] makes them unsuitable to explore the regulatory mechanisms underlying the dynamic responses, which are so essential for organisms that need to cope with changing environmental conditions [145].

In contrast, small-scale kinetic models are designed for an in-depth investigation of individual biological components and can provide information on the dynamics of the system, far away from the steady state, and predict temporal responses to different perturbations.

3.1.2 Differential Equations based models

Development of systems biology approaches results in a diversity of methods used to model biological networks and pathways, however those are nothing else than differential equations (ODE) that lay in the heart of the analyses and are commonly used to study small systems dynamics. Differential equations itself have a long history of application to biological and physical processes and a number of general laws of nature are expressed using them [146]. Many have contributed to the development of advanced mathematical models based on differential equations, including Newton (law of gravitation), d'Alembert (derivation of the wave equation) or Leibniz (introduced notation of differentials that is used to this day). They provide a good theoretical background for further computational investigations and bring a number of advantages.

3.1.3 Construction procedure

The process of building a kinetic model does not deviate from the general work-flow of constructing any other mathematical model and can be divided into a number of always-occurring steps sumamrised by Almquist *et al.* [129] and illustrated in Fig. 3.1.2. Those steps can be repeated several times, before the completion of work but will always start with a clear definition of the purpose of the model, and scientific questions it aims to answer. Is the model constructed to validate data or make new predictions? What do we need it for? On what time-scale is the system operating? All such questions will lead us to sketch the initial network structure. It will include a set of interconnected reactions that are essential to answer the stated questions and will also set the system boundaries, isolating the external environment from the modelling body.

Rate equations

Once the model's network structure is defined mathematical expressions are used to describe the interaction between the system's elements. The rate of change can be defined as the instantaneous change in the concentration of a designated specie, described by a derivative

$$rate = \frac{dS}{dt} = \mathrm{N}v(S,k), \tag{3.1.1}$$

where S denotes a vector of biochemical reactants, N denotes the stoichiometric matrix and $v(S,k)$ the vector of reaction rates as functions of the substrate concentrations S and parameters k. Kinetic rates can be derived from actual reaction mechanisms or can be simplified by some approximate expressions. The ultimate goal of this work is to determine and to provide the simplest set of equations which realistically describes the photosynthetic system. Therefore, most rate equations are formulated based on the maximum parsinomy principle. If no other evidence is given, the simplest functional form that appears reasonable is employed.
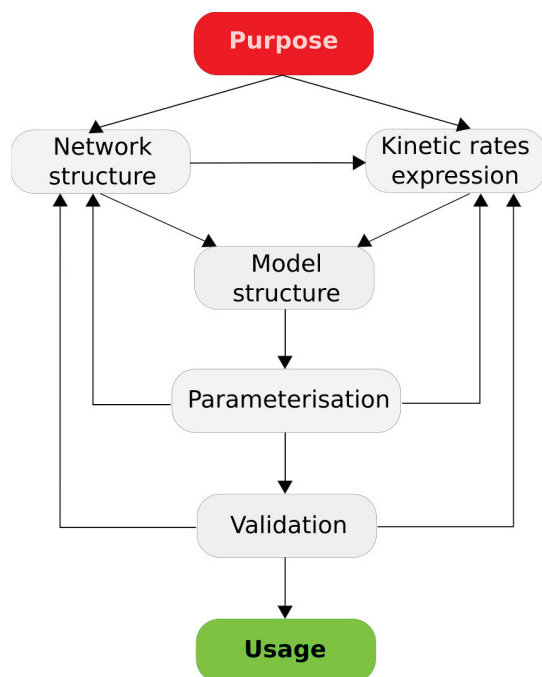
Figure 3.1.2: Schematic representation of the process of constructing a kinetic model, starting from the stating the scientific questions and ending with model usage. Figure reproduced from [129].

As a result the majority of reactions are described by simple mass-action or Michaelis-Menten kinetics.

Parameterisation

Parameterisation constitutes one of the most challenging tasks during model development. In order to provide the numerical values of the parameters used in the mathematical description of the system, either direct measurements are performed or estimation methods are applied. Therefore the parameter space may include:

- parameters measured for the particular organism, under specific conditions,
- parameters measured for a close specie, assumed to be conserved between organisms,
- parameters calculated using chemical or thermodynamics law,
- parameters estimated based on selected constraints (such as parameters resulting in a maximal measured photosynthetic yield),
- parameters fitted to the experimental data.

Validation

Once the parameters are determined, the quality and stability of the model needs to be assessed before model will be used for the purposes it was designed. Various methods of validation can be applied, ranging from the assessment of the qualitative agreement with the experimentally obtained data to a formal statistical testing. It is important to aim at separating the experimental data used for model construction from the data used for model validation. In other case, we may encounter problems with overfitting. A validated model can be used to answer stated research questions, as well as can be further developed to include more processes or their more detailed description.

3.2 Existing mathematical models of non-photochemical quenching

In the past decade a handful of new kinetic models have been published with the aim to help to understand underlying principles governing short-term acclimation mechanisms. Due to the fact that the effect of regulatory acclimation mechanisms can be easily monitored in a minimally invasive way by chlorophyll fluorescence measurements (see Ch. 2), many of the existing models aim at simulating the dynamics of the fluorescence signal [122, 124]. Unfortunately, due to a number of problems (not-reproducible results, lack of particular mechanism, too many free parameters), none of the existing models could be directly used to answer our research questions (Ch. 1, S. 1.5). Even model such as the one proposed by Nikolaou *at el.* [147], though seem to include all mechanisms of interest (the description of the photoproduction, photoinhibition and photoregulation), are not sufficient once we are interested in the actual redox state of an organism, pmf or ATP:NADP production ratio. Therefore available models rather served as a reference and guidance for the construction of the models presented here.

3.2.1 Existing mathematical models of qE

Existing mathematical models of high-energy state quenching are either too simplistic by aiming at reproducing the key biological features of quenching with minimal complexity [148] or too detailed and specialised focusing on quantification of the beneficial effect of qE under extreme light conditions in *Arabidopsis thaliana* [149].

General consensus is that both photochemical and non-photochemical quenching are mainly associated with light harvesting complexes of photosystem II [58] and therefore models investigating qE are commonly reduced to include only the essential reactions around PSII, as proposed by Ebenhöh *et al.* [148]. The complexity of the system is quite substantially reduced, with the boundary drawn at the cytochrome b_6f complex (Fig. 3.2.1). The dynamics of the system is described with only three differential equations where the qE mechanism is simplified to include only the pH dependent component, making this model not eligible to study the interplay between NPQ components. The need to include more detailed description with the precise role of the xanthophyll cycle emerged.
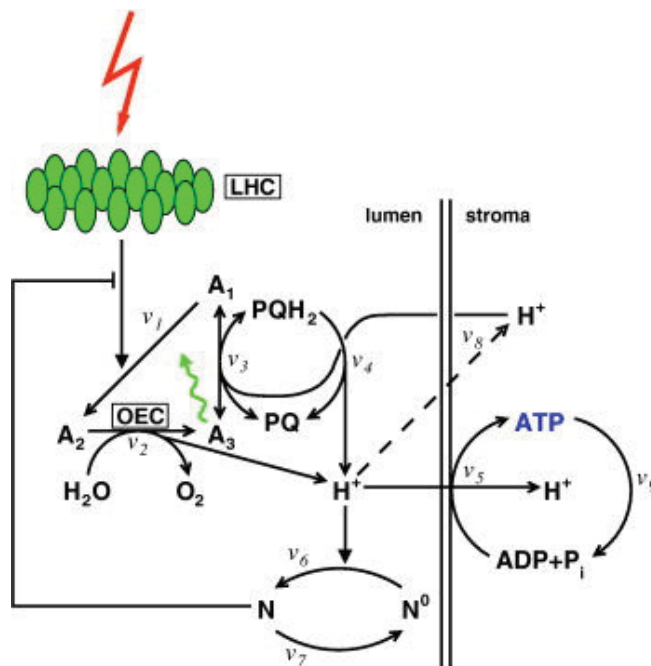
Figure 3.2.1: Schematic representation of the model by Ebenhöh *et al.* [148] where active quencher (N) inhibits energy transfer from open RCs (A1) to charge separation (A2). The oxygen evolving complex (OEC) re-reduces the donor side of the RC, resulting in state A3. The acceptor side is re-oxidised by PQ, which receives protons from the stroma. High proton concentration on the lumenal side triggers activation of a quencher (N). The proton gradient drives the production of ATP that is consumed by external processes. Figure taken with permission from [148].

Though Zaks *et al.* [149] provide a more detailed and accurate mathematical description of non-photocemical
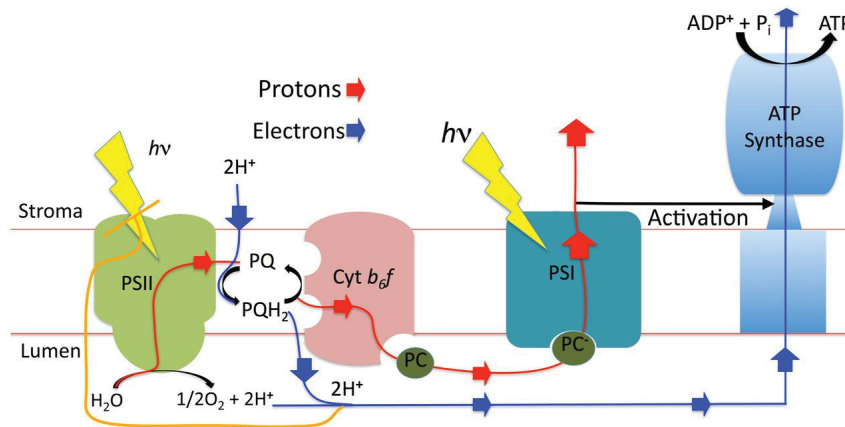
Figure 3.2.2: Schematic of components described in the Zaks model. Not depicted on the scheme are the two components involved in the activation of qE: a protonated PsbS protein and a deepoxodized xanthophyll. Both, triggered by the drop in the lumen pH. Figure taken with permission from [149].

quenching, with the role of xanthophylls included, it is at the cost of drastically increased complexity. Fig. 3.2.2 represents the schematic of components considered in the model, all together represented by a set of 26 non-linear differential equations and 74 parameters. The proposed rate of qE activity depends now on two components, protonation of the PsbS protein and operation of the violaxanthin, antheraxanthin, zeaxanthin (VAZ) cycle but the model is still lacking an explanation for a transiently generated NPQ. Analyses made with this model focused rather on assessing whether qE affects the lumen pH in plants and whether it does regulate the mode of electron flow.

3.2.2 Existing mathematical models of qT

The development of mathematical models of state transitions is challenging due to the limited information regarding the exact molecular mechanisms governing this process. Till now, we are aware of only two available mathematical models of state transitions: one for plants [150] and one for micro algae [26].

The model by Gordienko and Karavaev [150] is the model of light stages of photosynthesis to analyse the slow fluorescence. It includes the regulatory redistribution of antenna between PSs and assesses the impact of State 1 to State 2 transitions on the slow fluorescence. However, the model does not include components beyond the electron acceptors of PSI, such as Fd and NADPH production. The change between the states was modelled as a redistribution of the excitation energy between PSs as a result of LHCII phosphorylation. The activation of LHCII kinase governing the phosphorylation depends on the degree of reduction of the intersystem electron transfer intermediates.

A similar description of the phosphorylation was incorporated into a more complex model of state transitions, proposed by Ebenhöh *et al.* [26]. The model comprised a set of seven coupled ordinary differential equations, implemented in MATLAB programming language for the computation and the schematic representation is captured in Fig. 3.2.3. The system of equations governed the temporal evolution of major protein complexes and electron carriers, including 1) the oxidised fraction of the plastoquinone pool, 2) the oxidised fraction of the plastocyanin pool, 3) the oxidised fraction of the ferredoxin pool, 4) the stromal concentration of ATP, 5) the stromal concentration of NADPH, 6) the lumenal proton concentration and 7) the fraction of mobile antenna associated with photosystem II. Despite the rather heuristic description of some rates and several oversimplifications and omissions (no photoinhibitory effect on photosystem II included, ATP and NADPH demand are considered independent), the model was capable of reproducing the key experimental features of fluorescence measurements and therefore served as an ideal starting point for this work, while constructing a

model of various non-photochemical quenching mechanisms.
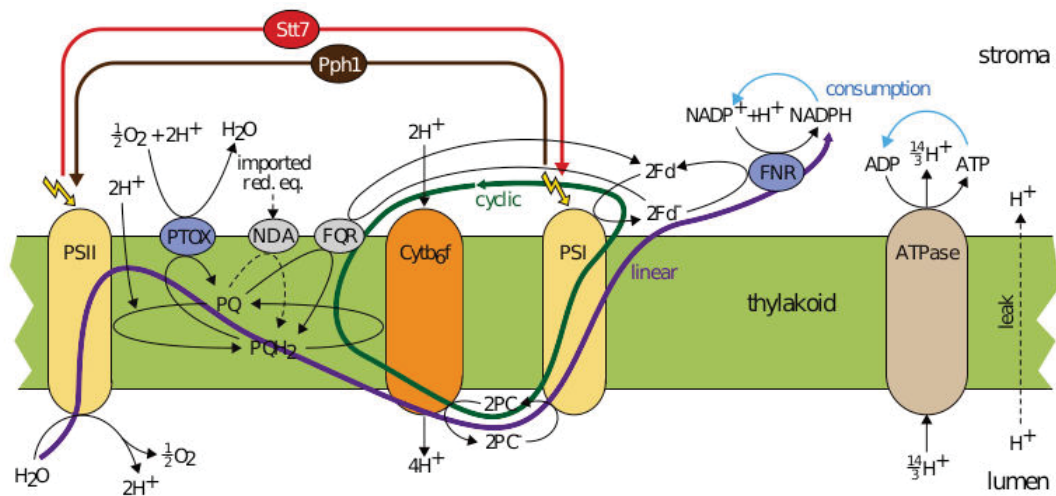
Figure 3.2.3: Schematic of the model of the photosynthetic electron transport chain and state transitions with all processes included in the mathematical model depicted. Figure reproduced from [26].

3.2.3 Existing mathematical models of qI

Comparing the amount of available mathematical models of various NPQ components, photoinhibition definitely gained the highest attention among theoreticians. In the past decade a series of new mechanistic models of photoinhibition that incorporate physiological and molecular mechanisms became available [151, 152, 153]. In Marshall *et al.* [151] photoinhibition is modelled as the decrease in the initial slope of photosynthesis versus irradiance curve. In the work by Han *et al.* [152, 153] photoinhibition is dependent on the cross-section of PSII. With a three-state description of photosystem II (depicted in Fig. 3.2.4), it is assumed that PSII can be either in open, closed or damaged state and the rate of photoinhibition is proportional to the concentration of the damaged unit. Such assumption can be easily transferred to the previously proposed four-state description of the RC, implemented in the Ebenhöh model [26].
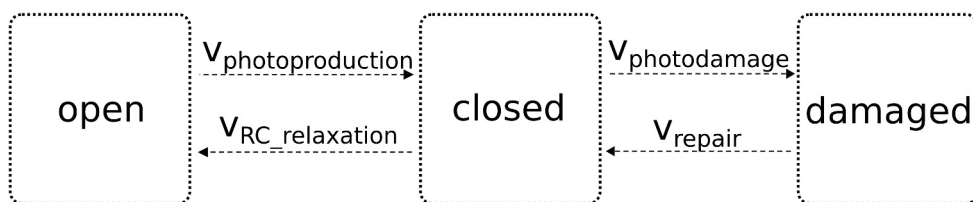
Figure 3.2.4: Schematic representation of the Han model. Figure reproduced from [153].

3.3 Development of a modular model

Our current understanding of the dynamic regulation of photosynthesis to light variations indicates the existence of a complex regulatory network [75]. To fully understand the principles according to which this network operates (Fig. 3.3.1A) and to which degree it is conserved among photosynthetic organisms, we require a model that includes all three main NPQ components. Considerations of only PSII reactions for qE studies (Fig. 3.3.1B) as in Zaks [149] or Ebenhöh [148], or only the PQ balance for qT investigations

(Fig. 3.3.1C) are not sufficient, as none of these mechanisms operate independently and they are likely to affect each other (Fig. 3.3.1D).
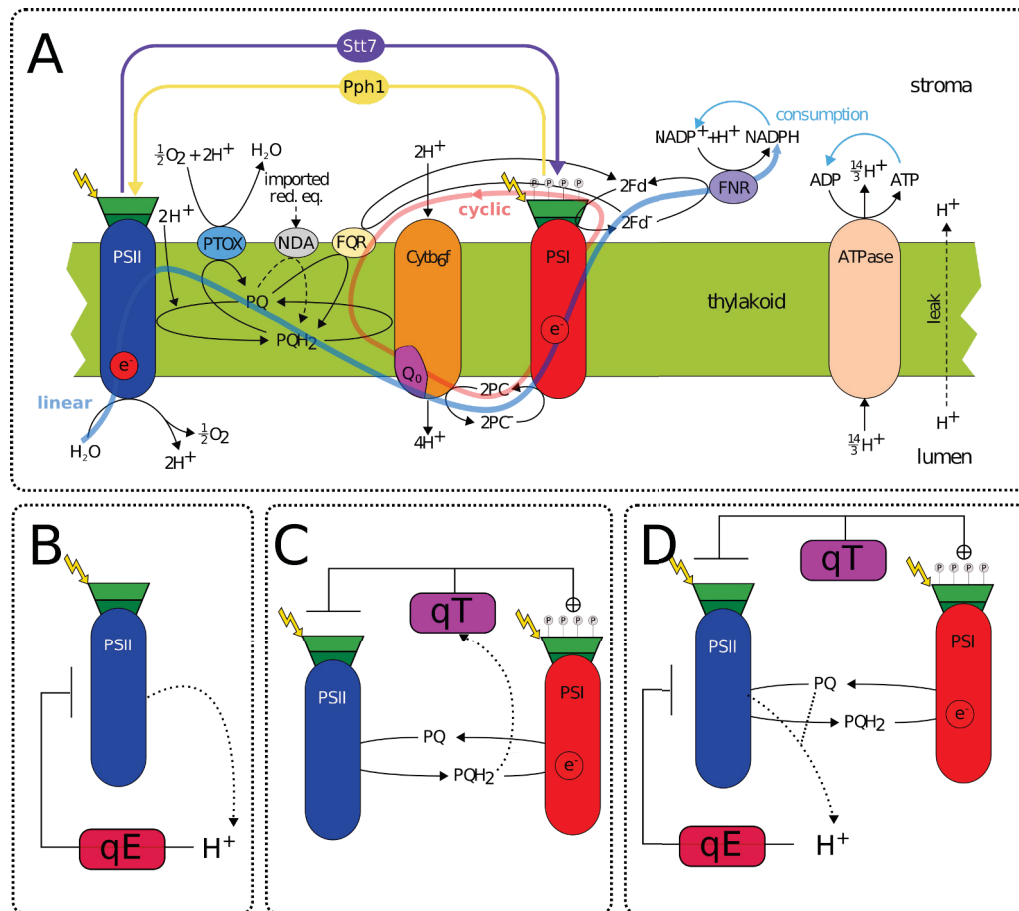
Figure 3.3.1: Illustration of reductionist approaches in modelling photosynthetic acclimation mechanisms. (A) Schematic representation of the photosynthetic electron transfer chain with a high level of complexity including both linear and cyclic electron flow and movement of antennae governed by the kinase-phosphatase pair. (B) Based on our current understanding of qE, we can reduce the system to include only reactions within PSII [148] and simplify the quenching mechanism as a direct consequence of the acidification of the thylakoid lumen. (C) Similarly, to study state transitions we can reduce the system to two photosystems, which antagonistically reduce and oxidise the plastoquinone pool. A reduced pool will activate a kinase, triggering relocation of antennae from PSII to PSI, thus inhibiting PSII activity and inducing the activity of PSI. (D) The two mechanisms are not independent, therefore a model that includes both mechanisms is required to reveal the principles of photosynthetic self-regulation under different light conditions. Figure reproduced from [137].

To the best of our knowledge, so far there is no such unifying model for photosynthetic eukaryotes available. Even the most comprehensive dynamic models of C3 photosynthesis published to date [154, 155] were not designed with such aim. The detailed computer model of C3 photosynthesis by Laisk *et al.* [154], although can correctly reproduce steady state behaviour of photosynthesis and carbon fixation, it cannot reproduce NPQ kinetics. In turn, Zhu et al. [155] do not account for state transitions in their model.

We have therefore applied the reductionist approach to construct a minimal model including state transitions as described in [26], the mechanisms of energy-dependent quenching as described in [149], while aiming for a reduced complexity in the spirit of the minimal model in [148]. Throughout this work, while referring to a mathematical representation of a photosynthetic organism, the description will never include all known biological processes, but rather a subjective set of reactions essential to study light's impact on the short-term photoprotection. The scheme of the concept behind the applied reductionism is presented in Fig. 3.3.2. Here, while describing photosynthesis in microalgae, we focus only on processes inside the chloroplast, and more specifically, inside the thylakoid membranes. Selected biochemical reactions of the electron transfer are

translated into mathematical terms using ordinary differential equations. Next, reactions contributing to the understanding of the same process are clustered together, resulting in a module that can be easily replaced. An integrated structure of all such building blocks is necessary to understand the whole complexity of the photosynthetic system.

$$PQH_2 + 2\,PC + 2\,H^+_{stroma} \rightleftharpoons PQ + 2\,PC^- + 4\,H^+_{lumen}.$$

$$\frac{dP}{dt} = v_{PSII} - v_{b6f} + v_{FQR} - v_{PTOX} + v_{NDH}$$
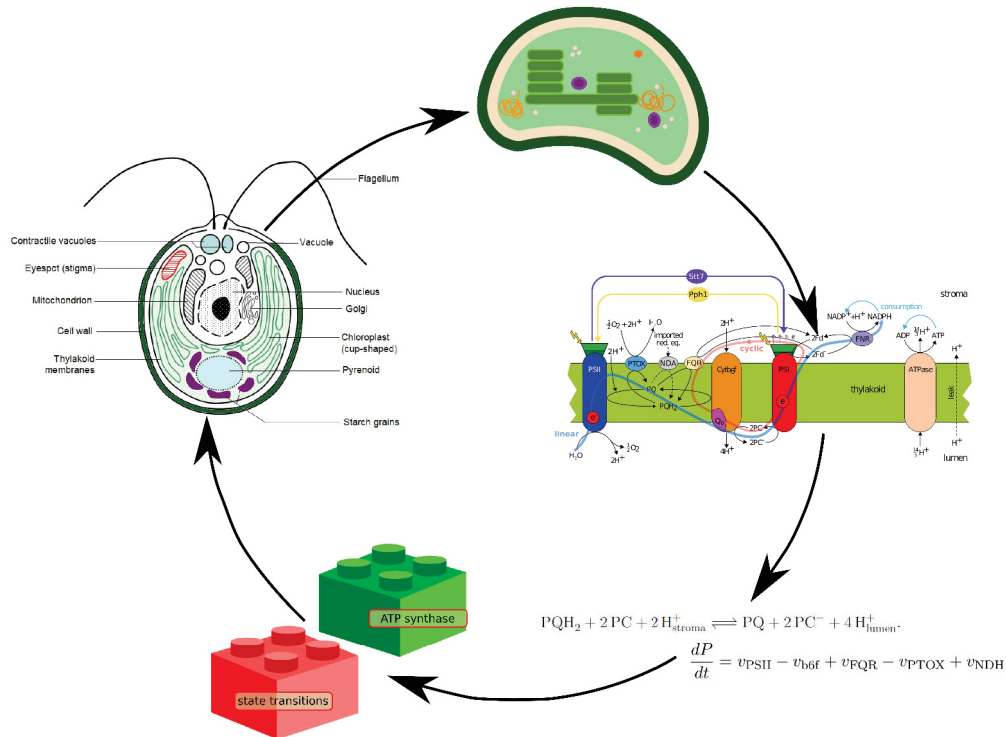
Figure 3.3.2: Scheme of the concept of the reduction applied here to study photosynthesis. Model organisms, represented on the scheme by *Chlamydomonas*, are interpreted as consisting only of chloroplast, precisely the thylakoid membranes, and the reactions taking place inside. Selected biochemical reactions are translated into mathematical terms using ODEs and grouped together in modules to jointly describe bigger processes.

One of the objectives of this work was to develop a mathematical model that will be easy to adapt to various organisms and strains. Such modular construct provides a flexibility in adding, removing or changing its components, simultaneously significantly improving the usability of the model. Instead of building a number of incompatible mathematical models, with the applied modularisation, the model structure resembles now a LEGO® style system, where various components can be easily added or substituted by smaller (simplified, with less parameters or number of reactions) or bigger (more detailed) bricks (modules) (see Fig. 3.3.3). For instance, in order to connect the light intensity with the light absorption rate and production of ATP, a simple model focusing only on linear electron flow is sufficient. Therefore the basic module hereinafter referred to as "ATP module" is constructed. It includes detailed descriptions of photosystem II and ATPase and follows changes in ΔpH, but it simplifies the biochemical reactions around photosystem I by representing them as a lumped reaction. Evidently, such a model is not appropriate to study the mechanism of state transitions. To investigate the mechanism that involves translocation of light harvesting complexes between the two photosystems, a detailed description of photosystem I is also required and therefore a more detailed model needs to be developed. Instead of building a new model, the basic module is complemented with two additional modules: one that includes the description of reactions around photosystem I and a second that includes phosphorylation of antenna by the Stt7 kinase and de-phosphorylation by the Pph1 phosphatase. Together, they describe the dynamics of state transitions.
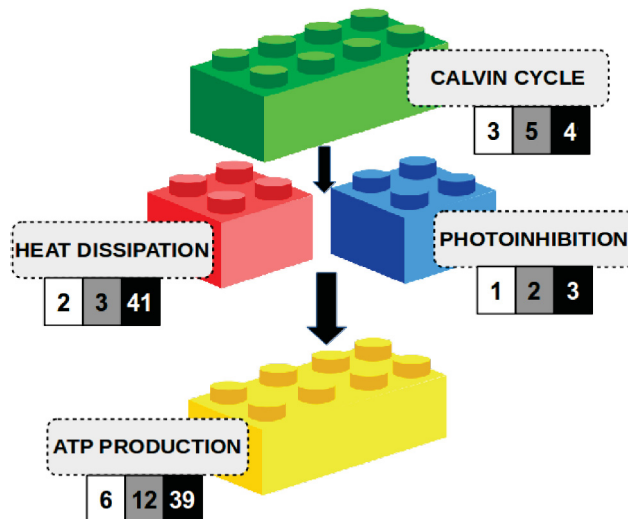
Figure 3.3.3: Due to its modular design, the model resembles a LEGO® style system: various components of the photoprotective mechanisms can be added or removed, thus simulating different strains and organisms. The size of the brick represents the complexity of the module. From the left, the numbers represent exemplary number of ODEs, reaction rates and parameters.

3.3.1 Common assumptions

A set of common assumptions was made before developing the models. Unless stated otherwise, the units used in the models are all given in moles per mole chlorophyll for an organism with a chlorophyll content set to $350 \cdot 10^{-6}$ mol per m^2 thylakoid membrane and the light intensity (photon flux density – PFD) is given in $\mu Em^{-2}s^{-1}$. The volume of thylakoid stroma and lumen are $0.0112 \, l \, m^{-2}$ and $0.0014 \, l \, m^{-2}$, respectively (as in [154, 26]). Thus, 1 mmol(mol Chl)$^{-1}$ corresponds to $2.5 \cdot 10^{-4}$M in the lumen and $3.2 \cdot 10^{-5}$M in the stroma.

Proton gradient

To simulate the lumen pH, relevant for both qE activation and ATP synthesis, the rate of protons entering and leaving the lumen was calculated, under the assumption of a constant buffering of protons in the lumen. For simplicity, we use a constant buffering capacity represented by the fixed parameter b_H like in [149, 26]. Stromal pH is kept constant.

Conserved quantities

Various physiological quantities were assumed to remain unchanged over the time and therefore several constant parameters were introduced to describe the total pool of plastoquinone (PQ^{tot}), plastocyanin (PC^{tot}), ferrodoxin (Fd^{tot}), adenosine phosphates (AP^{tot}), reducing equivalents (NADP^{tot}), xanthophylls (Xanthophylls^{tot}) and antenna (LHCII^{tot}). Moreover, as long as no damage and/or repair is included, both photosystems are assumed to be conserved (PSI^{tot} and PSII^{tot}).

Photosystems and light activation

Photosystems are described as light-activated oxidoreductases. To determine their overall activity, with a minimal complexity, a quasi steady-state approximation is applied as in [148, 26]. QSSA is a common procedure used in the study of chemical reactions kinetics where time-scale separation occurs[1] [156]. Since the model aims at simulating various acclimation mechanisms that take place on a time scale of seconds to minutes and even hours, such fast processes like charge separation and oxygen evolution that occur on time

---

[1]Time-scale separation means that a part of a system is assumed to operate sufficiently faster compared to the rest.

scales of milliseconds and faster can be assumed to be in a stationary state on the time scale that the model operates on (seconds and slower).

The light activation of photosystems is calculated as proposed in [26]. The photon flux density is converted to activation rate through a conversion factor (c_{PFD}), fitted to various experimental data for different species. The activation rates for the two photosystems are multiplied by the relative cross-sections σ_I and σ_{II} for PSI and PSII respectively, giving the activation rates for PSI and PSII equal to

$$k_{LI} \quad = \quad c_{PFD} \cdot \sigma_I \cdot PFD, \tag{3.3.1}$$

$$k_{LII} \quad = \quad c_{PFD} \cdot \sigma_{II} \cdot PFD. \tag{3.3.2}$$

Equilibrium

Some of the reaction rates are calculated from the equilibrium constants. In general, the equilibrium constant of a chemical reaction

$$X + A \rightleftharpoons Y \tag{3.3.3}$$
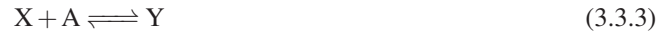
is

$$K_{eq} = \frac{[Y]_{eq}}{[X]_{eq}[A]_{eq}}. \tag{3.3.4}$$

But in case of modelling this reaction assuming that A is kept at a constant value $[A]^*$,

$$X \rightleftharpoons Y, \tag{3.3.5}$$

the equilibrium constant will be equal to

$$\frac{[Y]'_{eq}}{[X]'_{eq}} \frac{1}{[A]^*} = K_{eq}, \tag{3.3.6}$$

leading to an apparent equilibrium constant set to

$$K'_{eq} = [A]^* \cdot K_{eq}. \tag{3.3.7}$$

To calculate equilibrium constants we used standard Gibbs free energies of reaction (ΔG^0) and the relation

$$\Delta G^0 = -RT \ln K_{eq} \implies K_{eq} = e^{-\frac{\Delta G^0}{RT}}, \tag{3.3.8}$$

where R is the universal gas constant and T is the temperature in Kelvin.

3.3.2 Numerical computations

Various programming languages provide tools to solve the systems of ODEs numerically. To ensure open access to the results of this work it was decided to use an open-source language to develop the mathematical models. Therefore, all presented mathematical models were implemented using Python, an object-oriented, general-purpose computer programming language, with a large and comprehensive standard library. The

source code is available from the github repository, together with the experimental data for the light-memory experiments (Chapter 4) [157]. By providing the full documented source code, together with my co-workers we envisage that the models will be further developed by the scientific community.

Integration methods

The initial-value problem for stiff or nonstiff systems of first-order ODEs were numerically solved using the SciPy library, a Python-based ecosystem of open-source software for mathematics, science and engineering. SciPy provides a generic interface class to numeric integrators, named scipy.integrate.ode. The integration method used throughout this work was defined in the file simulation.py. By default the integration method uses the Real-valued Variable-coefficient Ordinary Differential Equation (LSODA) solver. It provides automatic method switching between implicit Adams method (for non-stiff problems) and a method based on backward differentiation formulas (BDF) (for stiff problems).

3.4 Summary

Based on our current understanding of non-photochemical quenching, a reductionist approach was applied to construct a modular, mathematical model of the electron transport chain. Models presented in Part Two of this thesis will use this approach to answer a handful of open questions regarding the dynamics of non-photochemical quenching, formulated in Chapter 1, S. 1.5.

II

Part Two

4. Modelling qE in plants

„Remembering the past gives power to the present."

*- **Fae Myenne Kg**, American novelist*

Bone (1993)

In this Chapter I present a simple model of non-photochemical quenching in higher plants, designed to study how plants can be trained to enhance their photoprotective capabilities and elaborate on the concept of short-term illumination memory. A comprehensive fluorescence measurements to study this phenomena were obtained from a collaborative partner at Ferdowsi University of Mashhad, Iran, Dr Sommayeh Heidari. By monitoring the dynamics of fluorescence emission of a sun-loving crest *Arabidopsis thaliana* Dr Heidari systematically observed the extent of non-photochemical quenching after previous light exposure to recognise the memory effect. The simplified model of photosynthesis includes the key components required for NPQ activation, which allows us to quantify their contribution to photoprotection. Due to model's reduced complexity, it can be easily applied to study similar behavioural changes in other species, here demonstrated by adapting the model to the shadow-tolerant plant *Epipremnum aureum*. By achieving an agreement between our simulations and experimentally observed behaviour, it can be confirmed that our current understanding of non-photochemical quenching molecular mechanisms is accurate. It is remarkable that these findings could be obtained with a very simple model structure and this structure is further used as a module in a more complex model of photoacclimation in the following Chapters.

This Chapter is an extended version of the manuscript:
A. Matuszyńska, S. Heidari, P. Jahns and O. Ebenhöh (2016) A mathematical model of non-photochemical quenching to study short-term light memory in plants, *Biochemica et Biophysica Acta - Bioenergetics*. [In Press] doi: 10.1016/j.bbabio.2016.09.003

4.1   Introduction

Plants require light for photosynthesis, but excessive light may be dangerous, as it can lead to the production of toxic reactive oxygen species [158] and it can inflict irreparable damage to the photosynthetic apparatus. As sessile organisms, plants therefore require adaptive mechanisms to dynamically react to incoming radiation and changes in light conditions. A common photoprotective strategy that has evolved in eukaryotic phototrophs [104] is the dissipation of excess absorbed energy in the form of heat, through processes collectively termed as non-photochemical quenching [56], which can be experimentally assessed by monitoring chlorophyll (Chl) fluorescence dynamics [159]. It is moreover plausible to assume that plants can somehow store information about the illumination history to optimise their photosynthetic performance simultaneously avoiding damaging effects of over-excitation. Such an effect could be termed memory, and indeed numerous recent studies suggest that the photoprotective behaviour in plants can be trained and related information is stored as a cellular light memory [160, 161]. In this study, the association between NPQ and short-term light memory is further investigated, using both experimental and theoretical approach.

4.1.1   High energy quenching

Our knowledge on the molecular mechanisms of NPQ, and in particular high energy quenching, increased significantly over the past 50 years mainly thanks to a Chl fluorescence quenching measurements (described in Ch. 2). The major and most rapid component of NPQ, termed energy-dependent quenching (qE) [56], allows for dissipation of the excess excitation energy of PSII as heat. It is triggered by light-induced formation of trans-thylakoid ΔpH and it is faster than described in the previous chapter state transitions. The discovery of the role of the xanthophyll cycle [162, 163, 69] in NPQ [164] and the identification of xanthophyll cycle mutants [112] provided a significant breakthrough in the understanding of NPQ. Since then, numerous studies supported a critical role of the xanthophyll zeaxanthin (Zx) in energy dissipation. Related to the qE mechanism, a synergistic action of Zx and the thylakoid lumen pH has been proposed [165], explaining why highest qE levels are inducible only in presence of Zx [59, 164, 166, 167].

Based on titration studies under *in vitro* conditions, Horton and co-workers suggested that Zx shifts the pH-dependence of qE by about 1.5 pH units towards higher lumen pH [167, 168]. Furthermore, Zx was shown to modulate the kinetics of NPQ induction (faster in presence of Zx) and relaxation (slower in presence of Zx) [59, 169, 170], and it was proposed to accelerate the reorganisation / aggregation of the PSII antenna [171] that accompanies qE [165, 172, 173, 174, 175]. These characteristics led to the development of the 4 state model of qE [165, 174, 176], which consistently explains the modulation of qE by the lumen pH and Zx, irrespective of the underlying quenching mechanisms and quenching sites involved in qE [173, 92].

Moreover, correlations of the Zx reconversion kinetics with the relaxation of the slower NPQ components qZ and qI indicate a function of Zx also in these processes [59, 177, 178, 179, 180, 181, 182], and Zx reconversion can be considerably down-regulated or inhibited under stress [183, 184] and photoinhibiting [184, 185] conditions. This gradual down-regulation of Zx epoxidation in response to different light stress conditions thus it allows the light stress-specific adjustment of the time of Zx accumulation, and hence the modulation of the NPQ response in dependence of previous light stress, over the full time range from minutes to days or weeks [185]. It should be noted, however, that the accumulation of Zx in parallel with the activation of the different NPQ mechanisms (qE, qZ and qI) does not necessarily imply a direct role of Zx in quenching, but could simply reflect the modulation of the efficiency of quenching or a general photoprotective effect of Zx in the membrane [186]. Plants can thus store information about the illumination history to optimise their photosynthetic performance, simultaneously avoiding damaging effects of over-excitation, and Zx seems to play a crucial role for such a memory effect [92, 93, 94].

4.1.2 Aim of the study

Motivated by this apparent connection between the xanthophyll cycle and NPQ induction [187], we used pulse amplitude modulated chlorophyll fluorescence analysis to systematically investigate whether a memory of light exposure can be detected on the time-scale of minutes to hours (in contrast to other studies that investigated the illumination memory on a longer timescale [160]). Next, we constructed a mathematical model on the basis of our current knowledge, to provide a general description of NPQ dynamics and the associated short-term memory.

We previously argued that a major challenge of theoretical biology is to provide simple, yet robust mathematical models that are not specially tailored for one model organism but describe a variety of species [137], because only such generic cross-species models will allow discovery of common generalised principles while understanding the species-specific features. Mathematical models range in complexity from very simplified and abstract models to extremely detailed ones aiming at including all known interactions. Here, our decision on the level of the model complexity depended strongly on the specific research question that the model is designed to address and a desire to use its component as "NPQ module" in further, more complex work.

Our aim was to find a compromise between an accurate reproduction of experimental observations and a highly reduced complexity. For this, we simplified a number of processes, which are not directly involved in the NPQ mechanism. One particular objective to derive this model is to provide a general framework, that is not specific to one organism, but can be easily adapted to different species and is specifically designed to be convenient to implement and easy to use. The model was therefore initially calibrated for the model organism *Arabidopsis thaliana* (Ch. 2), a sun-tolerant higher plant, and its flexibility is demonstrated by adapting it to the non-model organism *Epipremnum aureum*, a shadow-tolerant, ornamental plant, for which measured kinetic parameters are sparse. Our model is able to realistically reproduce experimentally obtained fluorescence traces and simulate all main features of chlorophyll induction, including transient activation of NPQ [188], the dynamics of fluorescence relaxation in darkness and qualitative differences in the quenching response to different light intensities. Thus, the model serves as a tool in which the role of the main quenching components can be computationally assessed and quantified, allowing simultaneously to test existing hypotheses on short-term light memory.

4.2 Experimental investigation of light memory

The short-term illumination memory in plants was studied by monitoring fluorescence emission dynamics in three-weeks old *Arabidopsis thaliana*. Plants (*Arabidopsis thaliana* ecotype Columbia 0 wild-type) were grown in soil at the temperature of 23°C under light intensity of 90-100 μEm^{-2}s^{-1} with a 16 hours light/8 hours night regime. Three-phases experiment was designed to systematically investigate the behaviour of the sample in each of those phases (see Fig. 4.2.1). The first phase, initial light exposure (also referred to as a training phase) started with two saturating pulses (SP) of light applied in a darkness to a previously dark adapted plant: at time 0 to measure the maximal fluorescence and 30 s later, after which light was switched on for 14 minutes. During this phase eight saturating pulses of light were applied with increasing time intervals between consecutive pulses. In the 15th minute of experiment the light was switched off, marking the beginning of the second phase of the experiment, so called relaxation phase. Seven SPs were applied. This phase was followed by the second light exposure, referred to as a memory phase, as it is the difference in the fluorescence kinetics between the initial and this phase that was mainly investigated to asses the memory phenomena. Two factors affecting the light memory in plants were tested: intensity of incident light (varying from 100 to 900 μEm^{-2}s^{-1}) and the relaxation time between the first and the second light exposure (15, 30 or 60 min). For each combination of light intensity and relaxation time, experiments were

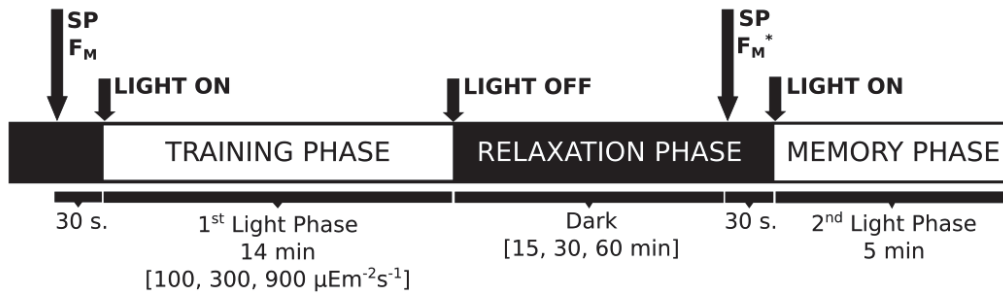repeated three times leading to an overall set of 27 measurements.

Figure 4.2.1: Design of the experiment. Saturating pulses of light (SP) were applied to a previously dark adapted plant from which physiological parameters such as maximal fluorescence (F_M) and photosynthetic yield ($\Phi PSII$) were derived. At time 0 the maximal fluorescence was measured. Immediately after the measurement the light was switched on and 30 s later the first measurement in the light was taken followed by pulses applied with increasing time intervals (50 s, 70 s, 90 s, ..., 170 s). The training period was followed by a dark period, interrupted by six SPs to follow the fluorescence relaxation dynamics. Subsequently, in the second light period (memory phase), the same illumination intensity as in the training period was applied. Each experiment was repeated three times for three light intensities (100, 300 and 900 $\mu Em^{-2}s^{-1}$) and different relaxation times (15, 30 and 60 min).

Using PAM chlorophyll fluorescence analysis we quantitatively investigated the effect of memory on NPQ by monitoring several physiological parameters: maximal fluorescence (F_M), maximal fluorescence in light ($F'_M(t)$), steady fluorescence ($F_s(t)$), photosynthetic yield, apparent electron transport rate and coefficient of non-photochemical fluorescence quenching ($qN = \frac{F - F'_M}{F_M - F_s}$).

4.2.1 Fluorescence results

First, we analysed whether the quenching patterns differ between the two phases of light. We directly analysed the originally measured maximal fluorescence ($F'_M(t)$) data instead of derived NPQ values (presented in Fig. 4.2.2), to avoid mathematical distortion of the kinetics and provide more reliable information on the mechanism [189]. Fluorescence measurements are a non-invasive method for monitoring photosynthetic dynamics, providing information on the photosynthetic efficiency, protection and energy dissipation. However, each measurement can only be relative [122], and therefore at first data is normalised to the maximal fluorescence (measured after the first saturating pulse of light applied to a dark adapted plant, F_M) and then averages and standard deviations of the three replicates are calculated.

In Fig. 4.2.3 the averaged kinetics of all 9 experiments are presented with grey strips marking the periods of darkness. With this representation it is difficult to make any observations regarding the difference in fluorescence kinetics between the light phases. Therefore we decided to improve the readability by plotting only the maximal fluorescence measurements from both phases and overlap them (Fig. 4.2.4). To highlight the key features which we aimed to explain with the mathematical model, only the last two measurements taken in the dark phase (again marked by grey background) and the first five measurements taken in consecutive light phases are displayed.

We observe that for all light intensities the last F'_M in the relaxation phase (denoted $F_M^\star$) is consistently lower than in the training phase (F_M). To visualise how the extent of the incomplete relaxation is influenced by both light intensity and the time spent in darkness we plot the ratio between the second last measurement in the darkness and the first measurement after the dark adaptation (Fig. 4.2.5).
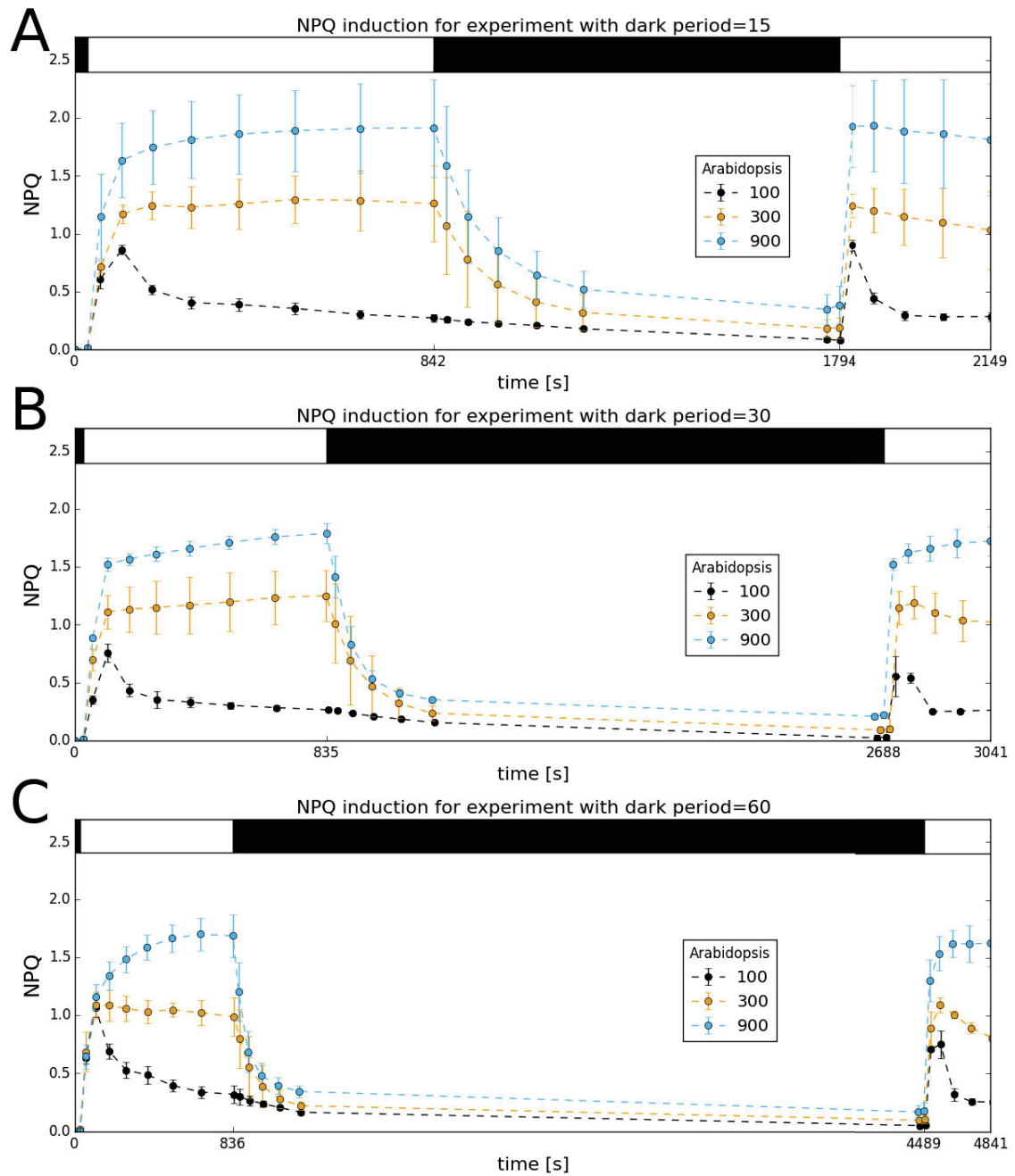
Figure 4.2.2: NPQ traces for all 9 experiments (each repeated 3 times, error bars denote standard deviations), grouped by the duration of the relaxation period: A) 15 min, B) 30 min and C) 1 hour. Transient induction of NPQ in the first 2 minutes of illumination is observed only in *Arabidopsis* exposed to the lowest light intensity (black line). Experiments were performed by Dr Sommayeh Heidari, Ferdowsi University of Masshad, Iran.
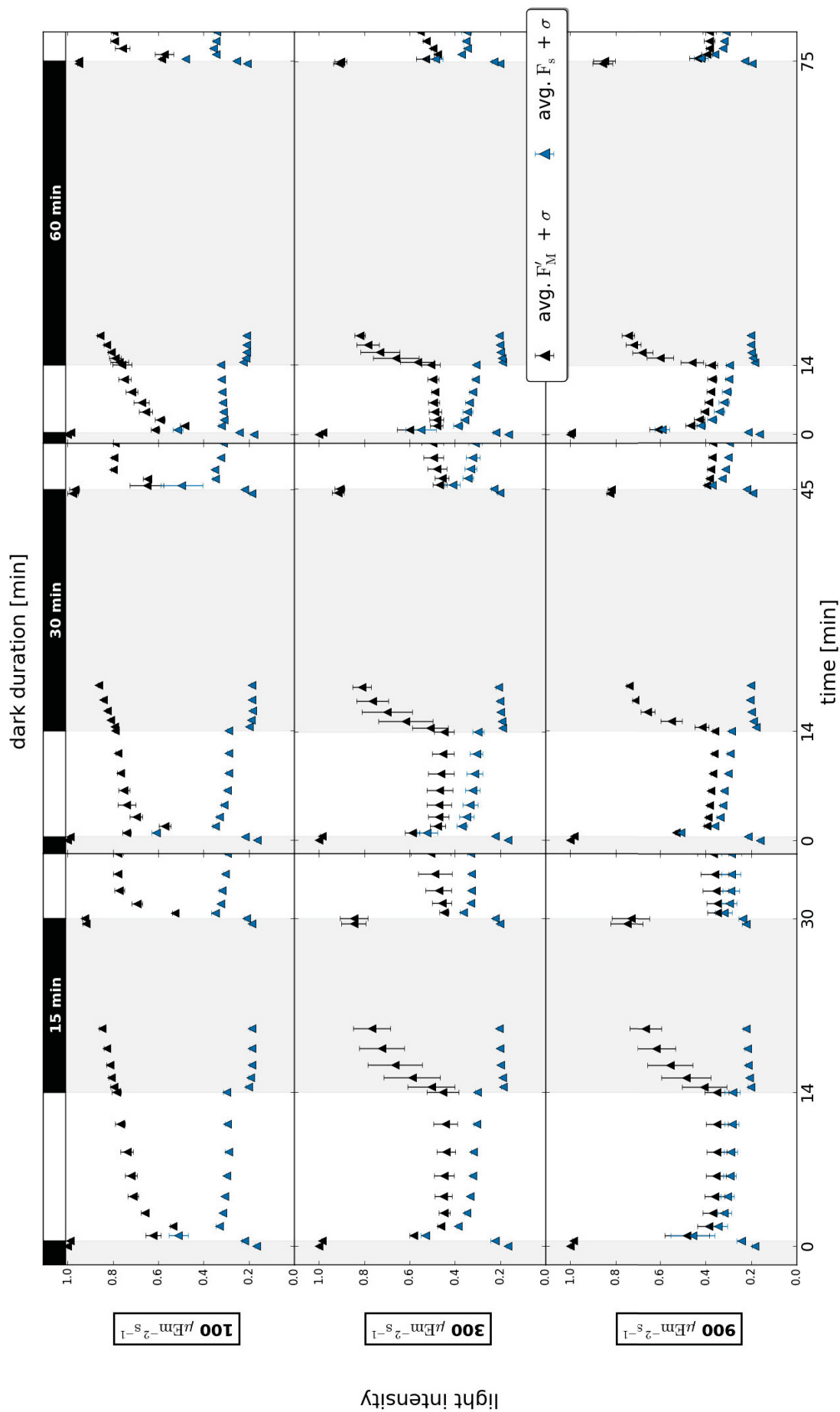
Figure 4.2.3: Experimental results of light memory experiment performed on *Arabidopsis thaliana*, averaged over three replicates. The dark periods are marked with shaded block. Each experiment was repeated three times for three light intensities (100, 300 and 900 μEm^{-2}s^{-1}) and different relaxation times (15, 30 and 60 min).
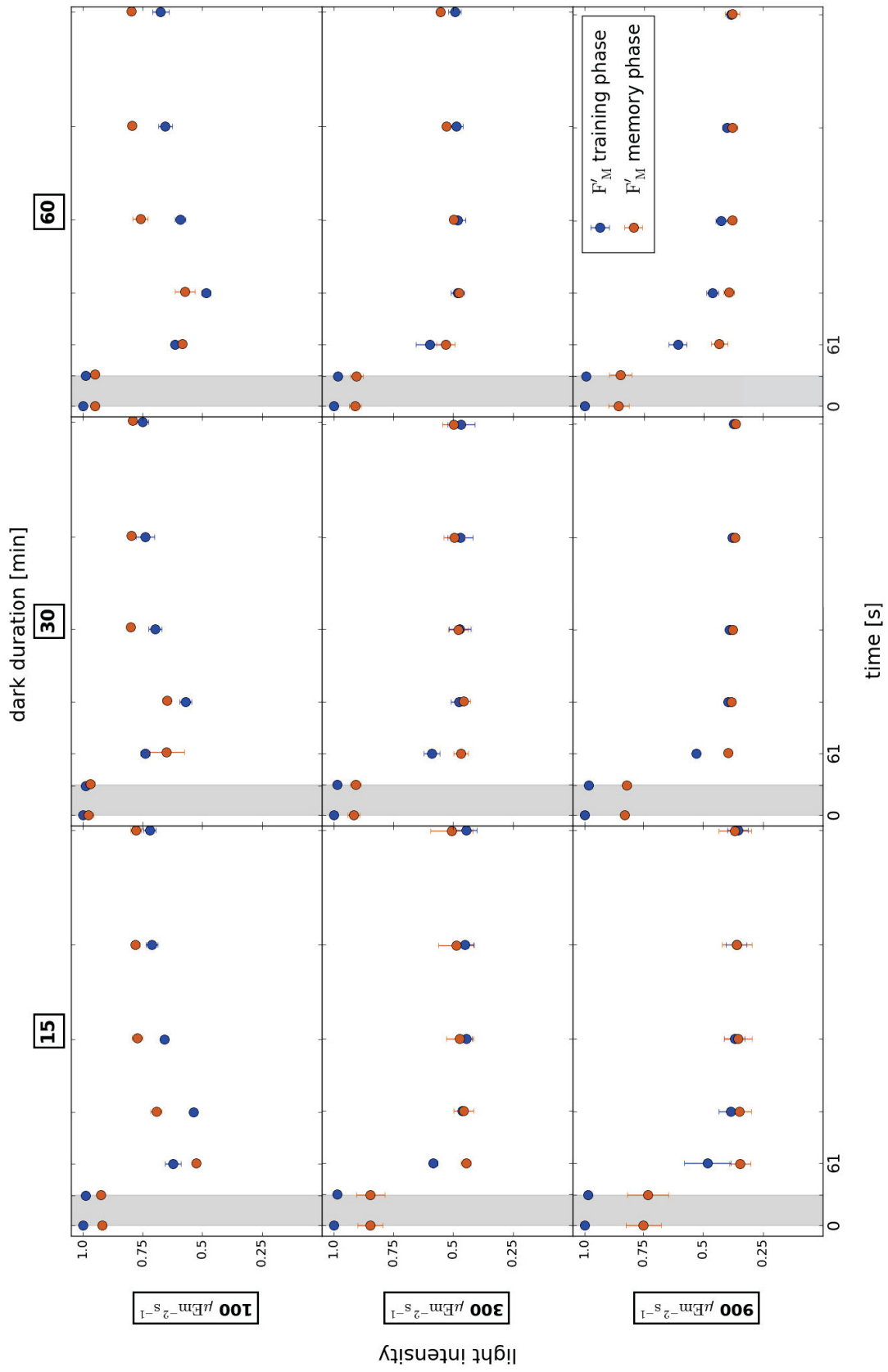
Figure 4.2.4: Comparison of the first two F'_M measurements taken in darkness and first five measurements in training phase (blue points) with the last two measurements taken in the relaxation phase and first five measurements in the second light phase (red points). The first measurement taken in the light (at 61 s) is lower in the memory phase than in the training phase, regardless of light intensity and time of relaxation. Error bars indicate standard deviations for three replicates except for the experiment marked with *, where the experiment was repeated eight times.
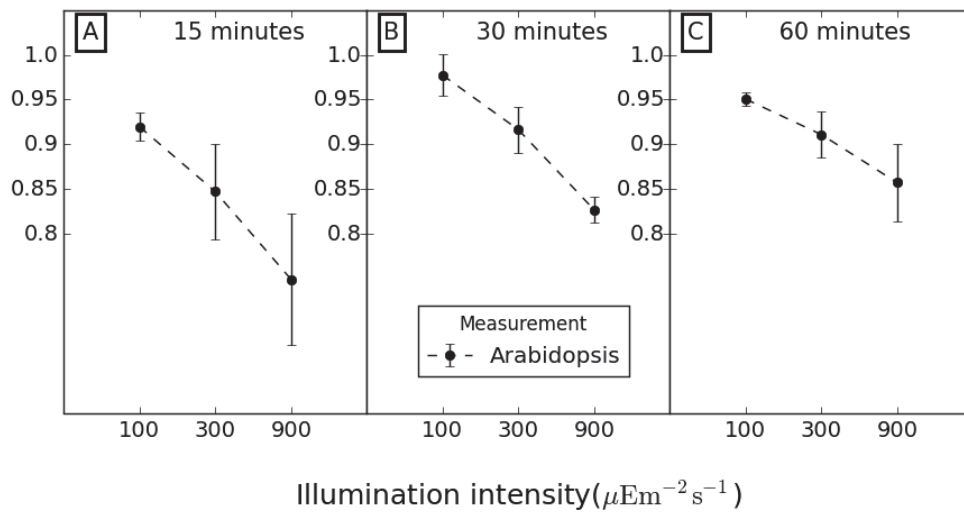
Figure 4.2.5: Relaxation of the fluorescence at the end point of darkness (ratio between the second last measurement in darkness and the first measurement after the dark adaptation), depending on the time spent in the darkness.

Likewise, the first measurement in light at 61 s shows lower fluorescence than the corresponding point in the training phase (Fig. 4.2.3). We have therefore performed two statistical tests to test if there is any statistically significant difference in the extent of quenching and/or its induction rate between the training and memory phase (Tab. 4.2.1).
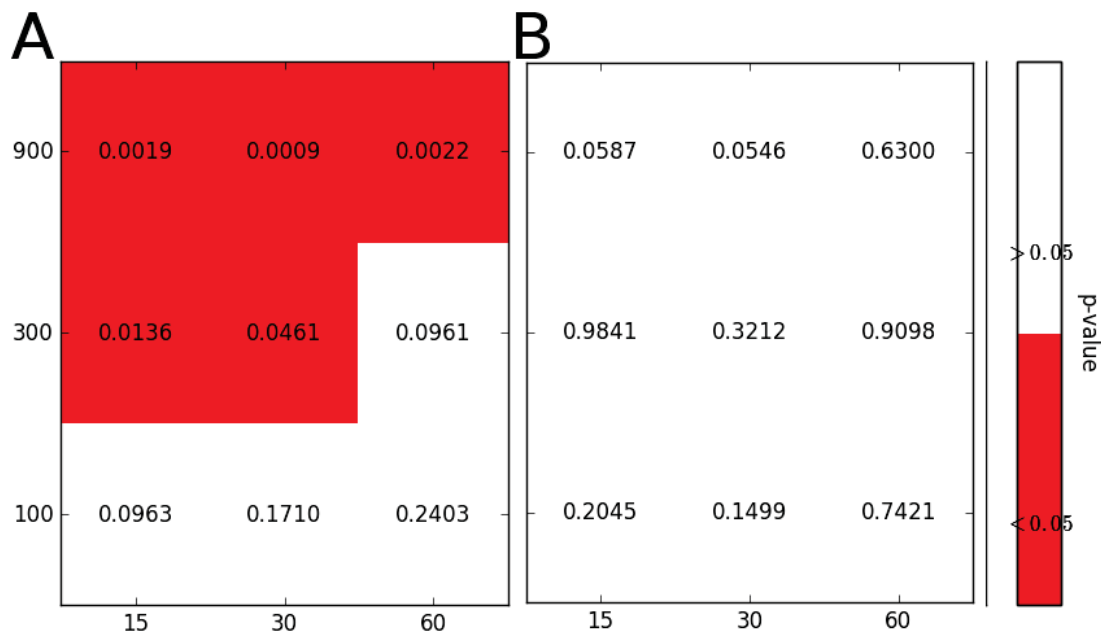
Table 4.2.1: Results of a paired T-test testing. A) The null hypothesis that there is no statistical difference in the first fluorescence measurement in the memory phase (F'_M), compared to the first fluorescence measurement in the training phase. B) The null hypothesis that there is no statistical difference in the slope between last measurement in darkness and the first measurement in the memory phase, compared to last measurement in darkness and the first measurement in the training phase.

We first performed a paired T-test to test the hypothesis that there is no statistical difference between the first F'_M measured in the light in the training phase and the first maximal fluorescence (F'_M) measured in the memory phase. We cannot reject this hypothesis for *Arabidopsis* exposed to low light intensities but we

demonstrate that there is a statistically significant (with a 95% confidence interval) difference in the first fluorescence measurements for plants exposed to higher light intensities, a phenomena associated here with a short-term memory. The results outline that both light intensity and quality have a quantitative effect on the extent of the memory. After one hour of dark relaxation no significant difference in the fluorescence level was observed, unless the plants were previously exposed to high, stressful light of 900 μEm^{-2}s^{-1}. All tests were performed for three biological replicates, except for *Arabidopsis* exposed to 900 μEm^{-2}s^{-1} with a relaxation phase of 15 min (marked by an asterisk in Tab. 4.2.1A), where 8 replicates were measured. Increasing the sample size became necessary, because of the large standard deviation, especially for the points measured in the training phase (see bottom left panel in Fig. 4.2.4). While the variation between the samples is still high, the larger sample size clearly indicated a high statistical significance (which was not observed for only three replicates).

Next, we performed a paired T-test to check if there is a statistically significant difference between the induction rate in the memory phase and training phase (H_0 = no statistically significant difference between phases). For that we compared the slope between the F'_M values from the 18th and 17th pulse (memory phase) with the slope between the 3rd and 2nd pulse (training phase). Due to the high p-value we cannot reject the null hypothesis for all nine cases, therefore concluding that plants with active short-term memory of previously experienced light initiate their photoprotection with some head-start, but at the same speed (Tab. 4.2.1B).

4.2.2 Pigment composition analysis

To investigate if the memory can be therefore explained by the accumulation of zeaxanthin, as proposed by many, the pigment composition at the end of each phase of the experiment was measured. Using the expertise of Peter Jahns' lab at the Heinrich-Heine University Düsseldorf, Germany, pigment analysis was performed.
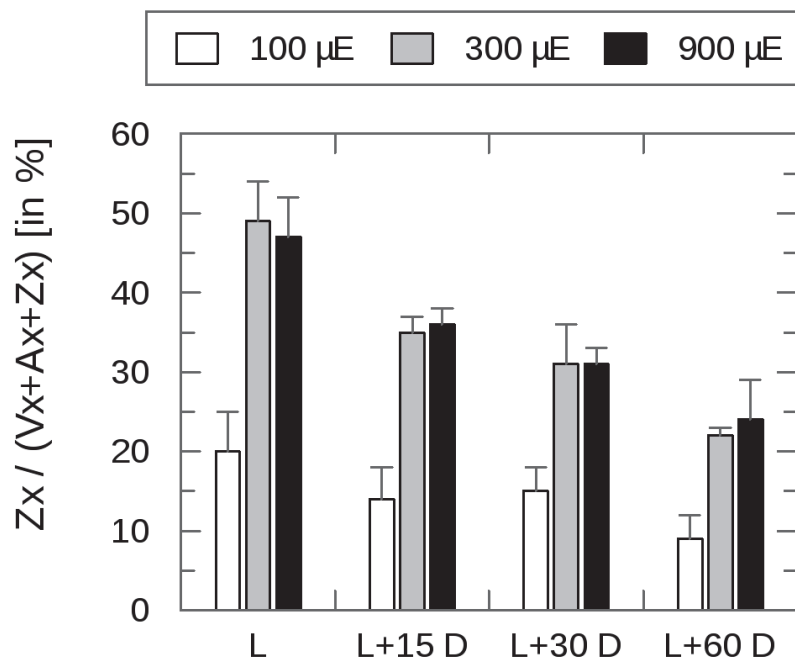
Figure 4.2.6: Pigment composition at the end of each phase (L=light, D=dark) presented as ratios of zeaxanthin (Zx) to total xanthophylls (Vx + Ax + Zx). Experiment performed by Prof. Peter Jahns, Heinrich-Heine University, Düsseldorf, Germany.

Frozen plant material was homogenized in presence of cold acetone. Unsolubilised material was removed by
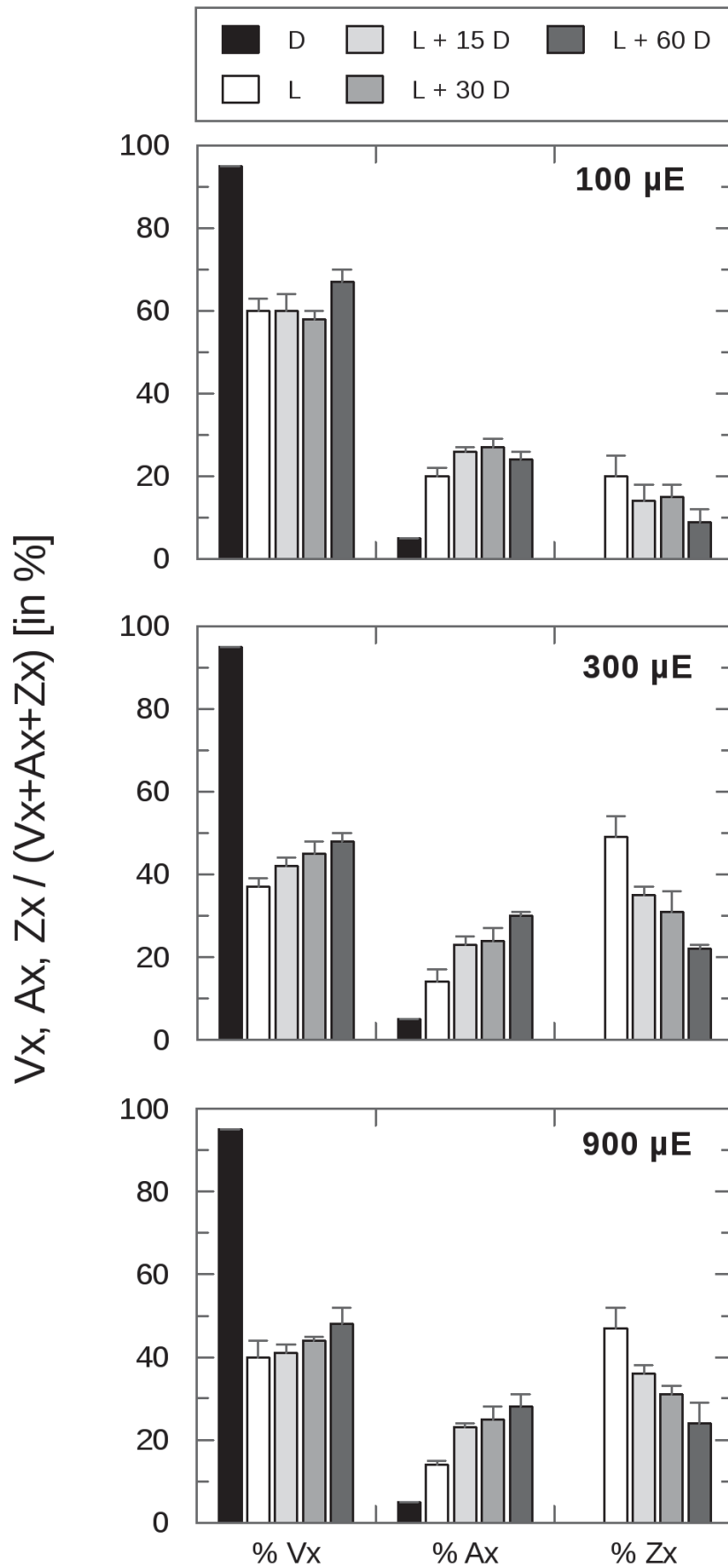
Figure 4.2.7: Pigment composition in *Arabidopsis thaliana* at the end of each experimental phase (D: after dark adaptation, L: after 15 min light exposure, L + D: after relaxation phase). Experiment performed by Prof. Peter Jahns, Heinrich-Heine University, Düsseldorf, Germany.

short centrifugation and the pigment content of the acetone extract was analysed by reversed-phase HPLC according to Färber *et al.* [190]. Figure 4.2.6 shows that after exposing the samples for 15 minutes to high light intensities, Zx levels significantly increased up to 50% of all xanthophyll cycle pigments (sum of violaxanthin (Vx), antheraxanthin (Ax) and zeaxanthin). Simultaneously, one hour in dark was sufficient to reduce this by half, explaining lower quenching effects in samples kept for longer periods in dark. This decrease was not as pronounced under illumination with the lowest light intensity. Moreover, zeaxanthin concentrations alone cannot explain that under 100 μEm^{-2}s^{-1} the fluorescence signal for the later time points is higher in the memory phase compared to the training phase. This indicates that also the relaxation of the transient NPQ depends on the light memory, a conclusion consistent with the previous findings by Johnson *et al.* [169]. The full pigment analysis is summarised in Fig. 4.2.7.

4.3 Model description

Based on the experimental results and our current understanding of NPQ, we developed a small kinetic model of photosynthesis to verify our hypothesis on the induction of light memory and to quantify the contribution of its two molecular effectors. Although photosynthetic electron flow operates in at least two recognised modes in this work we aimed at a maximal reduction of the model complexity and focused solely on the pH regulated non-photochemical processes associated with photosystem II. We included into the model only those processes that are either directly affected by, or are regulating the extent of NPQ. All other processes were described by simplified, 'lumped' reactions or neglected, like the cyclic electron flow. A general schematic of the model of the electron transport chain is shown in Fig. 4.3.1.
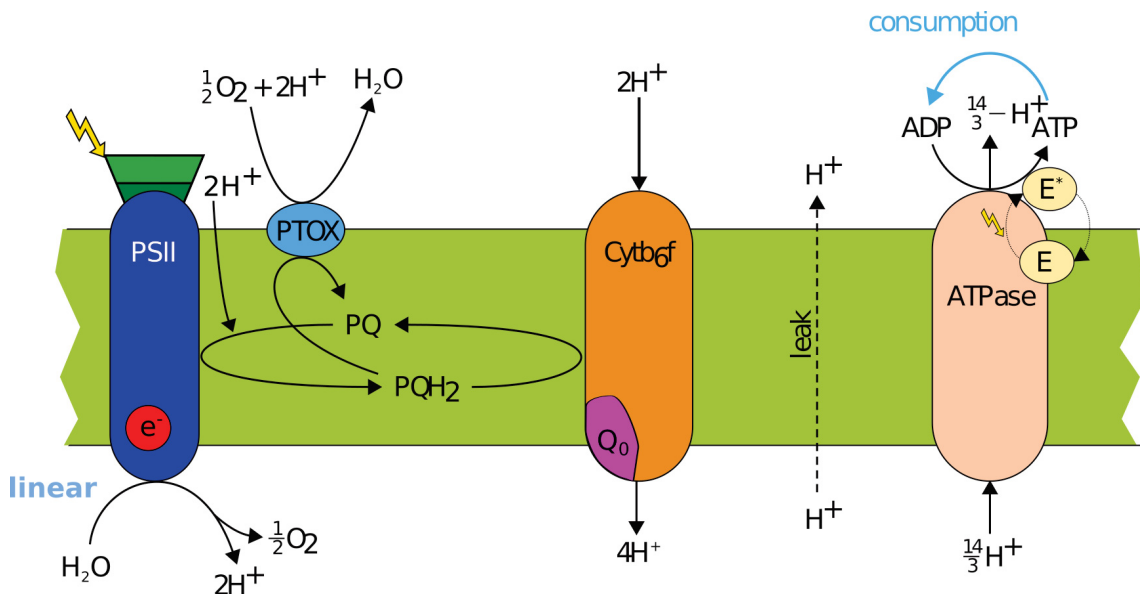
Figure 4.3.1: Scheme of the components included in the simplified mathematical model of photosynthesis. The model contains a detailed description of internal processes occurring inside photosystem II that are directly affected by the quencher. The plastoquinone pool is reduced by PSII, which also releases protons into the lumen by the oxygen evolving complex. PQ can be oxidised by cytochrome b6f and PTOX. Oxidation by cyt b6f is coupled to proton translocation from stroma to lumen. Protonation of the lumen drives the production of ATP through ATPase (E*). ATPase is active in the light and inactive in the dark. Protons can also passively leak out of the thylakoid lumen.

4.3.1 Stoichiometry of the model

Since the variable chlorophyll fluorescence originates from the antennae associated with PSII [191, 124], we limit our model to the photosynthetic reactions around photosystem II, reducing the system to only six

differential equations, 9 reaction rates (Appendix, Tab. A1) and 41 parameters (Appendix, Tab. A2). The system of differential equations reads

$$
\begin{cases}
\dfrac{dP}{dt} = v_{\text{PSII}} - v_{\text{PQ}_{\text{ox}}}, & (4.3.1) \\[2ex]
\dfrac{dH}{dt} = \left(2v_{\text{PSII}} + 4v_{\text{PQ}_{\text{ox}}} - \dfrac{14}{3} v_{\text{ATPsynthase}} - v_{\text{leak}} \right) \dfrac{1}{b_H}, & (4.3.2) \\[2ex]
\dfrac{dE}{dt} = v_{\text{actATPase}} - v_{\text{deactATPase}}, & (4.3.3) \\[2ex]
\dfrac{dA}{dt} = v_{\text{ATPsynthase}} - v_{\text{ATPconsumption}}, & (4.3.4) \\[2ex]
\dfrac{d\text{Pr}}{dt} = -v_{\text{Psbsp}}, & (4.3.5) \\[2ex]
\dfrac{dV}{dt} = -v_{\text{Xcyc}}. & (4.3.6)
\end{cases}
$$

P denotes the reduced fraction of plastoquinone pool (Eq. 4.3.1), H stands for protons concentration in the lumen (Eq. 4.3.2), E for the fraction of active ATPase enzyme (Eq. 4.3.3) and A for stromal concentration of ATP (Eq. 4.3.4). Pr stands for the fraction of non-protonated PsbS protein (Eq. 4.3.5) and V for the fraction of violaxanthin in the total pool of xanthophylls (Eq. 4.3.6).

4.3.2 Reaction rates

Most rate equations are formulated based on the maximum parsimony principle, as reasoned in Ch. 3, except for the photosystem II, which is modelled as an oxidoreductase. In total, nine rates (v_{PSII}, $v_{\text{PQ}_{\text{ox}}}$, $v_{\text{ATPsynthase}}$, $v_{\text{ATPconsumption}}$, $v_{\text{actATPase}}$, $v_{\text{deactATPase}}$, v_{leak}, v_{Psbsp} and v_{Xcyc}) are used to express the dynamics of the system and their functional form is explained below respectively.

Photosystem II

The scheme of internal processes included into the mathematical description of photosystem II is presented in Fig. 4.3.2. Following previous work by Ebenhöh *et al.* [26] it is assumed that photosystem II can be in one out of four possible states (B$_i$, where $i \in (0,1,2,3)$), relating light harvesting capability with the occupation of reaction centres.
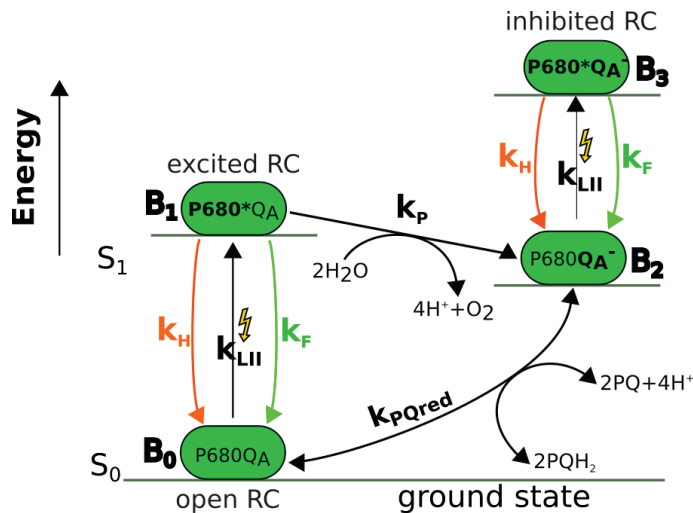
Figure 4.3.2: Schematic representation of internal processes included into the mathematical description of PSII. Radiant energy is absorbed by the light-harvesting complexes (B$_0$) and passed to a reaction centre (RC), resulting with the excited state (B$_1$). In the time scale of nanoseconds chlorophyll may relax back to its ground state through re-emission of light seen as fluorescence (with the rate k_F) or by heat dissipation (with the rate k_H). The energy can be also transfered to the reaction center of photosystem II where charge separation takes place (B$_2$), so called closed state. If the closed state is also excited by light, resulting P680*Q$_A^-$ state can relax back to the unexcited state only by heat or fluorescence emission. Closed RC are re-opened by electron transfer to the PQ pool (k_{PQred}).

State B_0 corresponds to the light harvesting state: reaction centres are open, ready for absorbing light energy to drive the photosynthetic electron transport chain. State B_1 reflects the excited energy state of chlorophyll after absorption of radiant energy. From this state, in a time scale of nanoseconds, the chlorophyll can relax back to its ground state only through one of the three pathways [56], by fluorescence emission (k_F), by heat dissipation (k_H), or by photochemistry (k_P) leading to state B_2, reflecting a 'closed' state, in which charges are separated. State B_3 reflects an inhibited state, in which chlorophyll is excited through absorbed light energy, but the acceptor side of the reaction centre is still occupied. Thus, charge separation and consequently photochemistry cannot occur and the excited chlorophyll can only relax to its ground state through k_F or k_H.

Assuming that the system operates according to the scheme (Fig. 4.3.2) the change in occupation of each state can be described by following differential equations:

$$\frac{dB_0}{dt} = -\left(k_{\mathrm{LII}} + \frac{k_{\mathrm{PQred}}}{K_{\mathrm{eq,QAPQ}}}P\right)B_0 + (k_H + k_F)B_1 + k_{\mathrm{PQred}}(\mathrm{PQ}^{\mathrm{tot}} - P)B_3 \tag{4.3.7}$$

$$\frac{dB_1}{dt} = k_{\mathrm{LII}}B_0 - (k_H + k_F + k_P)B_1 \tag{4.3.8}$$

$$\frac{dB_2}{dt} = k_P B_1 - \frac{k_{\mathrm{PQred}}}{K_{\mathrm{eq,QAPQ}}}(\mathrm{PQ}^{\mathrm{tot}} - P)B_2 + (k_H + k_F)B_3 \tag{4.3.9}$$

$$\frac{dB_3}{dt} = k_{\mathrm{LII}}B_2 - (k_H + k_F)B_3, \tag{4.3.10}$$

where k_{LII} is the light activation rate of PSII.

To determine the fraction of B_1 a quasi steady-state approximation is applied (see Chap. 3). Under a consideration that the protein concentration in a system is constant

$$B_0 + B_1 + B_2 + B_3 = \mathrm{PSII}^{\mathrm{tot}}, \tag{4.3.11}$$

the three differential equations for B_i, where $i \in (0,1,2,3)$, are set to zero, leading to the algebraic linear equation system that is solved numerically by matrix inversion in every integration step:

$$-\left(k_{\mathrm{LII}} + \frac{k_{\mathrm{PQred}}}{K_{\mathrm{eq,QAPQ}}}P\right)B_0 + (k_H + k_F)B_1 + k_{\mathrm{PQred}}(\mathrm{PQ}^{\mathrm{tot}} - P)B_3 = 0 \tag{4.3.12}$$

$$k_{\mathrm{LII}}B_0 - (k_H + k_F + k_P)B_1 = 0 \tag{4.3.13}$$

$$k_{\mathrm{LII}}B_2 - (k_H + k_F)B_3 = 0 \tag{4.3.14}$$

$$B_0 + B_1 + B_2 + B_3 = \mathrm{PSII}^{\mathrm{tot}}, \tag{4.3.15}$$

Finally, the overall rate of the oxidoreductase activity of photosystem II performing the net transformation

$$\mathrm{H_2O} + 2\mathrm{h}\nu \rightarrow 2e^- + \frac{1}{2}\mathrm{O_2} + 2\mathrm{H}^+_{\mathrm{lumen}}, \tag{4.3.16}$$

is therefore proportional to the occupation of the B_1 state and given by the rate

$$v_{\mathrm{PSII}} = \frac{1}{2}k_{\mathrm{LII}}B_1. \tag{4.3.17}$$

The rate of electron transfer through PSII is therefore $2e^-$ per mol Chl per second.

Fluorescence originating from Photosystem II

In the model description, fluorescence is not a system variable, but it can be calculated out of the PSII status, like in previous models proposed by Ebenhöh *et al.* [148, 26]. We therefore calculate it from the rate at which excited chlorophyll will revert to its ground state through fluorescence (k_F), and not quenching (k_H) or photochemistry (k_P). Moreover, we use the fact that the signal is proportional to the occupation of the two ground states of PSII RCs (B_0 and B_2 in Fig. 4.3.2):

$$\Phi_F = \frac{k_F}{k_H \cdot Q + k_F + k_P}[B_0] + \frac{k_F}{k_H \cdot Q + k_F}[B_2], \tag{4.3.18}$$

where $k_H \cdot Q$ is the rate of NPQ, modulated by the quencher activity Q (Eq. 4.3.39).
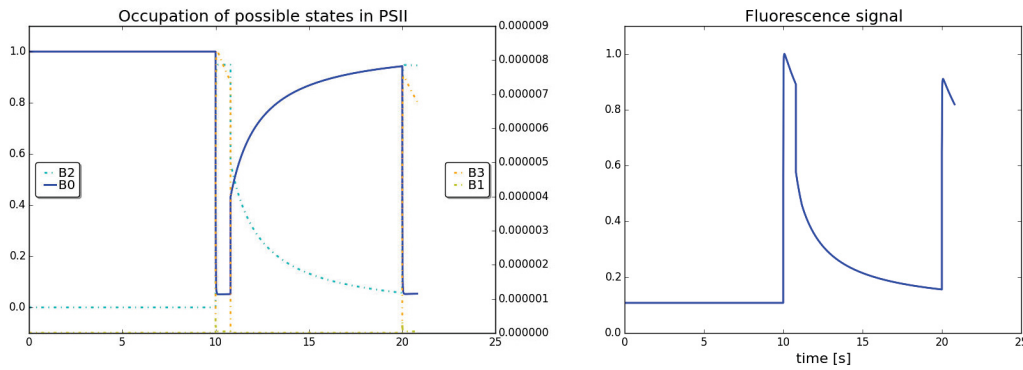
Figure 4.3.3: Visualisation of how occupation of PSII states (left) translates into fluorescence signal (right). After 10 s of darkness a saturating pulse of light was applied after which moderate light was switched on for 10 s and second pulse of light was applied.

In Fig. 4.3.3 we visualise the translation of PSII occupation states to fluorescence signal. After 10 s of darkness (during which base fluorescence F_0 is observed as PSII in mainly in state B_0) a saturating pulse of light was applied for 0.8 s (F_M is observed) and moderate light was switched on for 10 s after which another pulse of light was applied (F'_M). Such calculated fluorescence signal is not normalised and, as argued before, for comparison with other experiments, it is normalised to the first F_M.

Redox state of the PQ pool

Plastoquinones are the key electron carriers in the photosynthetic electron transport chain. Analysis of the redox state of the plastoquinone pool yields valuable information on the photosynthetic activity of an organism. In the simplest form, the pool is reduced by the activity of photosystem II (described above) and oxidised by cytochrome b6f leading to the dynamical description

$$\frac{dP}{dt} = v_{PSII} - v_{PQ_{ox}}, \tag{4.3.19}$$

where $v_{PQ_{ox}}$ includes not only reaction mediated by the Cyt_{b6f} but all downstream steps of the electron flow leading to the production of NADPH

$$v_{PQ_{ox}} = \left(\frac{k_{PFD} K_{eq,cytb6f}(pH)}{K_{eq,cytb6f}(pH) + 1} + k_{PTOX} \right) PQH_2 - \frac{k_{PFD}}{K_{eq,cytb6f}(pH) + 1} PQ. \tag{4.3.20}$$

The equilibrium of the biochemical reaction mediated by the cytochrome is dependent on the stromal and lumenal proton concentration ($K_{\mathrm{eq,cytb6f}}(\mathrm{pH})$) and was calculated exactly as in [26]. Because the rate $v_{\mathrm{PQ_{ox}}}$ is a 'lumped' reaction (see above Eq. 4.3.20) and also includes the process driven by photosystem I, a direct light dependency (k_{PFD}) was implemented

$$k_{\mathrm{PFD}} \quad = \quad k_{\mathrm{Cyt_{b6f}}}\mathrm{PFD}, \tag{4.3.21}$$

where PFD is the photon flux density (expressed in $\mu\mathrm{Em}^{-2}\mathrm{s}^{-1}$). The oxidation of the plastoquinone pool is further included in the presence of oxygen, by the plastoquinol terminal oxidase (PTOX) with a second-order rate constant (k_{PTOX}).

Considering a number of applied simplifications, it may raise a concern whether the system will exhibit a biologically meaningful steady state under extreme conditions. We have therefore investigated the stationary redox state of the plastoquinone pool (PQ) over different light intensities. Under a wide range of light intensities the redox poise is maintained [28], meaning that the plastoquinone pool is neither too oxidised, nor too reduced to limit electron transport (Fig. 4.3.4).
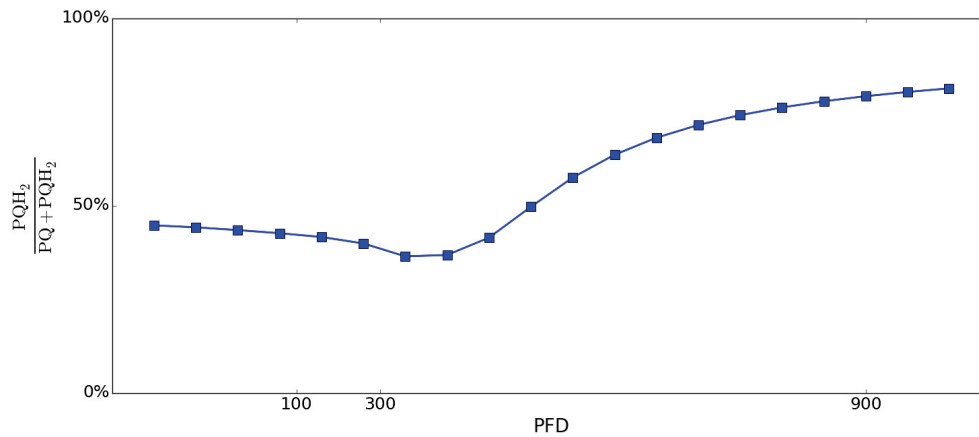
Figure 4.3.4: Steady state plastoquinone redox state for *Arabidopsis thaliana*, simulated for different light intensities. Intensities marked on the x-axis indicate those we used to calibrate the conversion factor translating photon flux density into activation rate.

ATP synthesis

The dynamics of the stromal concentration of ATP is governed by the equation 4.3.4. It was observed that illuminating dark-adapted plants with non-saturating light transiently induces a strong non-photochemical quenching [191, 187], which is explained by the transient generation of a transthylakoid pH gradient [192]. This transient NPQ relaxes within a few minutes when the ΔpH is reduced due to delayed activation of ATP and NADPH consuming reactions, including the $\mathrm{H^+}$-ATPase [193]. It was therefore proposed to included a delayed activation of ATPase, by which the overall dynamics of transient NPQ activation upon dark-light transition can be realistically reproduced. Thus, ATP synthesis is mediated by an active form of ATPase (E), governed by the Eq. 4.3.3. The activation and de-activation rates depend directly on the light availability (see Fig. 4.3.5) and is described in mathematical terms, as

$$v_{\mathrm{actATPase}} \quad = \quad k_{\mathrm{actATPase}}\mathrm{H}(\mathrm{PFD})(1-E) \tag{4.3.22}$$

$$v_{\mathrm{deactATPase}} \quad = \quad k_{\mathrm{deactATPase}}(1-\mathrm{H}(\mathrm{PFD}))\cdot E, \tag{4.3.23}$$

where H(x) is the Heaviside function and PFD is the light intensity.

ATP synthesis was modelled by a simple mass-action kinetic rate law with a dynamic equilibrium constant dependent on the lumen pH, multiplied by a factor describing the amount of available ATPase enzyme

$$v_{\text{ATPsynthase}} = k_{\text{ATPsynthase}} \left(\text{AP}^{\text{tot}} - A - \frac{A}{K_{\text{eq,ATPsynthase}}(H)} \right) \cdot E, \tag{4.3.24}$$

where AP^{tot} is the constant total adenosine phosphate pool.

To calculate the equilibrium constant we used standard Gibbs free energy of reaction ΔG^0 and the relation described in Ch. 3, Sec. 3.3.1. The overall reaction of the hydrolysis of ATP, mediated by the ATPsynthase is:

$$\text{ADP} + \text{P}_i + \frac{14}{3} \text{H}^+_{\text{lumen}} \rightleftharpoons \text{ATP} + \frac{14}{3} \text{H}^+_{\text{stroma}} + \text{H}_2\text{O}. \tag{4.3.25}$$
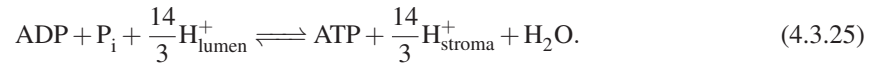
We split this into redox reaction and transport process:

$$\text{ADP} + \text{P}_i \rightleftharpoons \text{ATP} + \text{H}_2\text{O} \tag{4.3.26}$$

$$\text{H}^+_{\text{lumen}} \rightleftharpoons \text{H}^+_{\text{stroma}}. \tag{4.3.27}$$

The overall reaction is the stoichiometric sum

$$1 \cdot (4.3.26) + \frac{14}{3} \cdot (4.3.27), \tag{4.3.28}$$

therefore the contributions to the standard Gibbs free energy change are

$$\Delta G^0_1 = \Delta G^0_{ATP}, \tag{4.3.29}$$

$$\Delta G^0_2 = RT \ln(10)(\text{pH}_{\text{stroma}} - \text{pH}_{\text{lumen}}), \tag{4.3.30}$$

where R and T are consequently the universal gas constant and the temperature. According to the stoichiometry (4.3.28), the overall standard Gibbs free energy change amounts to

$$\Delta G^0 = \Delta G^0_1 + \frac{14}{3} \Delta G^0_2, \tag{4.3.31}$$

and since we do not model the change in external phosphates but instead we keep the pool of phosphates fixed, the overall equation for the equilibrium constant is equal:

$$K_{\text{eq,ATPsynthase}}(\text{pH}) = \text{Pi}_{\text{mol}} \cdot e^{\frac{-\Delta G_{0_{ATP}} - \frac{14}{3}\Delta G^0_2}{RT}}. \tag{4.3.32}$$

Finally, it is important to note that the *standard* redox potentials have to be used for the calculation. These are determined from the mid-point potentials E'^0 (see Ch. 3, p. 61) and provided in the parameters table (Tab. A2).

For the consuming processes the same mass-action kinetics as in the work by Ebenhöh [26] was kept:

$$v_{\text{ATPconsumption}} = k_{\text{ATPconsumption}} \cdot A. \tag{4.3.33}$$
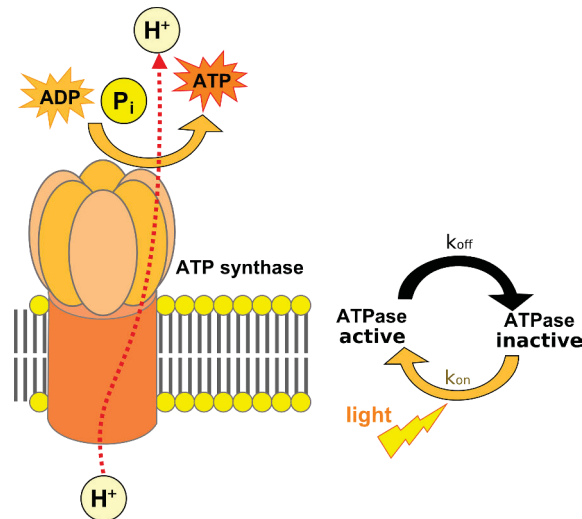
Figure 4.3.5: Scheme of the ATP synthesis with enzyme activated and de-activated by light.

It is acknowledged that such representation is an over-simplification and does not reflect the complex energy demand of a cell, nor it reflects the NADPH requirement for Zx regulated quencher relaxation [194]. Those problems are addressed in the last Chapter, with a search for a better representation of consuming reaction. Here, to overcome difficulties arosen due to this simplification, the conversion factor translating the photon flux density into activation rate was fitted separately for each of the three available experimental data sets ($cpfd$).

Lumenal acidification

As in Ebenhöh model [26] a possible current of protons leaking over the thylakoid membrane is introduced through a simple process linearly dependent on the concentration gradient (v_{leak}):

$$v_{\text{leak}} = k_{\text{leak}} \cdot (H - \text{H}_{\text{stroma}}^+). \tag{4.3.34}$$

Moreover, we assume constant buffering of protons in the lumen (b_{H}, see also [154]). The overall change in the lumenal pH depends therefore on the rate of photosystem II, cytochrome b6f, ATP synthesis and the leak flux, and the dynamics of the proton concentration is described by Eq. 4.3.2.

4.3.3 Quenching mechanism

As described in the introduction (Ch. 1), the high-energy-state quenching represents the main component of NPQ and it is induced on a time-scale of seconds to minutes [93]. Several factors are known to contribute to NPQ induction. A fast one requires the generation of a proton gradient (ΔpH) in the thylakoid membrane and a slow one is activated by low lumen pH and is dependent on xanthophylls cycle. Their active forms were modelled by a Hill kinetics with different saturation and cooperation coefficients to reflect the dependency on the proton gradient.

PsbS is activated by protonation, caused by the lumenal increase of the proton concentration driven by the photosynthetic electron transport. The pH saturation constant was set to 5.8 and moderate cooperativity (Hill coefficient nH_{L}=3) was assumed. The Hill coefficient determines the response rate to the changes of the pH

while converting from inactive (not protonated) to active (protonated) form:

$$v_{\text{Psbs}^{\text{p}}} = k_{\text{ProtonationL}} \frac{H^{\text{nH}_{\text{L}}}}{H^{\text{nH}_{\text{L}}} + \text{pH}_{\text{inv}}(k_{\text{phSatLHC}})^{\text{nH}_{\text{L}}}} (\text{PsbS}^{\text{tot}} - Pr) - k_{\text{Deprotonation}} Pr. \tag{4.3.35}$$

Here, pH_{inv} is a helper function converting pH to proton concentration:

$$\text{pH}_{\text{inv}}(\text{pH}) = 4 \cdot 10^3 \cdot 10^{-\text{pH}} \tag{4.3.36}$$

The Hill coefficient for the forward reaction during the VAZ cycle (de-epoxidation of violaxanthin) is higher (taken from Zaks *et al.* nH$_\text{X}$ is set to 5 [149]). The reaction is catalysed by the enzyme V de-epoxidase (VDE) that is fully active at pH 5.8 (k_{phSat}). The epoxidation from Zx to Vx catalysed by the enzyme Z epoxidase (ZEP) is considered to be a factor of 10 slower than the de-epoxidation [104], resulting in a ratio k_{kDeepoxV}:k_{kEpoxZ} of 10:1

$$v_{\text{Xcyc}} = k_{\text{DeepoxV}} \cdot \frac{H^{\text{nH}_{\text{X}}}}{H^{\text{nH}_{\text{X}}} + pH_{inv}(k_{\text{phSat}})^{\text{nH}_{\text{X}}}} \cdot V - k_{\text{EpoxZ}} \cdot (\text{X}^{\text{tot}} - V). \tag{4.3.37}$$

For simplification, we deliberately omitted the intermediate step of converting violaxanthin to antheraxanthin but the model allows for easy implementation of this step, if required.

Additive model

Identification of these two components lead to a question regarding their role in quenching and possible modes of interaction. Despite proposed models of cooperativity, we started to model the quenching activity under the simplest possible assumption, that both *Pr* and *Z* influence quencher (*Q*) independently. By reaching an agreement with an experimental data with this simple model we would challenge the current understanding of the mechanism of action. Any discrepancies would lead us to implement more complex model, such as proposed in next section 4-state model, where the two players are assumed to work cooperatively. Therefore here, we modelled *Q* as an additive combination of arbitrary functions of *Pr* and *Z*:

$$Q = \alpha[Pr] + \beta \frac{[Z]}{[Z] + k_{\text{ZSat}}}, \tag{4.3.38}$$

where α and β are parameters reflecting the contribution of each component to an overall quencher.
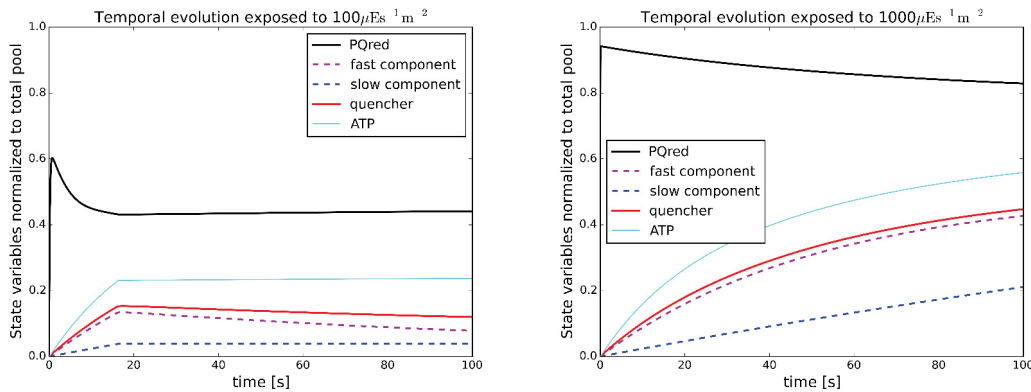

Figure 4.3.6: Results of the simulation for low and high light intensity while applying an additive model of quenching.

Such models were not sufficient to reproduce the dynamics of fluorescence observed during the light memory experiments, as even under the constant light the simulated evolution of state variables is not yielding plausible results (Fig. 4.3.6). Especially under high light conditions it can be observed that simulated concentration of Zx (slow component) has almost linear effect on overall quenching.

4-state 2-site model

The quencher mechanism finally implemented in the model is based on a four state model proposed initially by Horton *et al.* [165, 174, 176, 68]. The scheme of the model is represented in Figure 4.3.7, where the fully relaxed dark state (State a) is characterized by maximal Vx concentration and de-protonated PsbS protein. In high light, a proton gradient is rapidly established, and PsbS acts as a proton sensor thus activates quenching, constituting the fast component of the quencher (State b). Further reduction of the lumen pH (to 5.8) triggers de-epoxidation of Vx to Zx, leading to State c of a fully activated NPQ. From this, a transfer to darkness results in a relaxation of ΔpH, and concomitant de-protonation of PsbS, leading to State d, which still contributes to the overall quencher activity because of the slow relaxation of Zx.
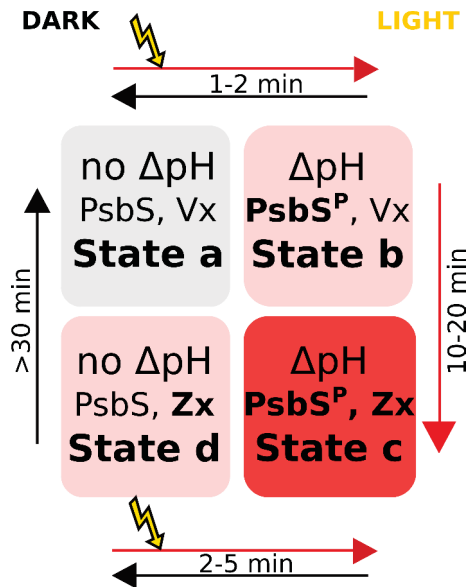
Figure 4.3.7: A four-states description of quenching conditions. Left-top (State a): dark adapted state, right-top (State b): light excited state, right-bottom (State c): fully induced quencher state, left-bottom (State d): slowly relaxing in the darkness state. Figure based on the 4-state 2-site quenching model described in [68].

These considerations lead to the overall equation for the quencher activity:

$$Q = \gamma_0(1 - Z_s)[1 - Pr] + \gamma_1(1 - Z_s)[Pr] + \gamma_2 Z_s[Pr] + \gamma_3 Z_s[1 - Pr], \tag{4.3.39}$$

where $Z_s = \frac{[Z]}{[Z] + k_{ZSat}}$ reflects the contribution of Zx to the quencher and k_{ZSat} is a half-saturation constant. The overall concentration of xanthophylls ($[V] + [Z]$) is assumed to be constant and the temporal changes of violaxanthin and protonated PsbS are determined by appropriate differential equations (Eq. 4.3.5, 4.3.6). The γ parameters were fitted to the fluorescence traces and their effect on the steady state and quencher activity was extensively studied using metabolic control analysis [195], described in next subsection. The parameter γ_0 describes the baseline quenching that does not require activation (and therefore is also active in a dark adapted sample) and was included to account for a small quenching observed in double mutants, where both PsbS and zeaxanthin dependent activation is removed [59]. The parameter was fitted to reproduce the double mutant behaviour. In Fig. 4.3.8 results of the simulation for the 4-state model demonstrate how with this description of the quenching activity we obtain desired behaviour as a response to changes in the concentration of each component.
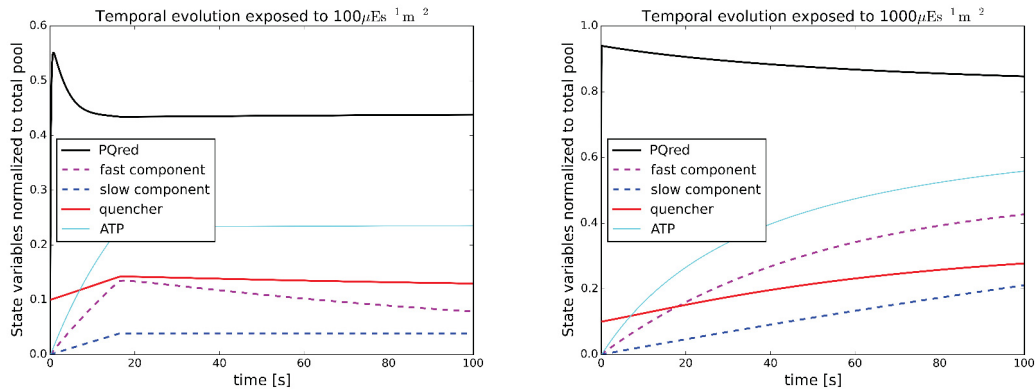
Figure 4.3.8: Results of the simulation for low and high light intensity while applying a 4-state model of quenching. The effect of slow quenching component (Z) does not affect quencher dynamics linearly.

4.3.4 Response coefficients

The effect of each fitted γ parameter on the steady state quenching activity, pH, steady state fluorescence and the PQ redox state was systematically analysed. For quantification response coefficients [195] were calculated, defined as

$$R_i^x = \frac{\gamma_{i,ref}}{x_{ref}} \frac{\partial x}{\partial \gamma_i}. \tag{4.3.40}$$

Here x stands for the steady state values of the dynamic variables and x_{ref} is the corresponding value for the reference parameter $\gamma_{i,ref}$. Fig. 4.4.1 depicts the response coefficients for various light intensities. It confirms the expectations, in particular, that γ_0 has the strongest effect on the overall quencher activity under low light, whereas γ_2 has the strongest impact under high light. Considering that the protonation occurs on a timescale below seconds, the low effect of γ_1 on steady state concentrations is apparent.

4.4 Results

Calculating fluorescence values using Eq. 5.2.42, allows for a reproduction *in silico* of all experimentally obtained fluorescence measurements. We first aimed at reproducing experimental results for *Arabidopsis thaliana* (see Fig. 4.2.3), next analysed the internal variables in a context of short-term illumination memory, performed simple mutant analysis, and finally tried to adapt the model to other organism than *Arabidopsis*.

4.4.1 Fluorescence kinetics

In Fig. 4.4.2 all simulated PAM traces (solid line) are plotted on top of the experimental data (triangles with error bars). The simulation outcomes are in a good agreement with the experiment. First of all, with the introduced ATP synthesis delay we can qualitatively reproduce experimentally observed transient drop in fluorescence in the first minute of light exposure (low light intensity $100~\mu\mathrm{Em}^{-2}\mathrm{s}^{-1}$). Under higher light intensities neither the experiment, nor simulation show this drop. Also, the fluorescence peaks in saturating light ($\mathrm{F_M'}$) are reproduced extremely well, especially the fact that fluorescence does not fully recover after dark relaxation (*cf.* data points in the shaded regions in Fig. 4.2.4).

However, some quantitative discrepancies between the simulation and model can be observed. For instance, the first point in the light in the memory phase is higher in the simulation than in the experiment. Nevertheless, we managed to reproduce the qualitative drop between the corresponding points, as simulated $\mathrm{F_M'}$ in the
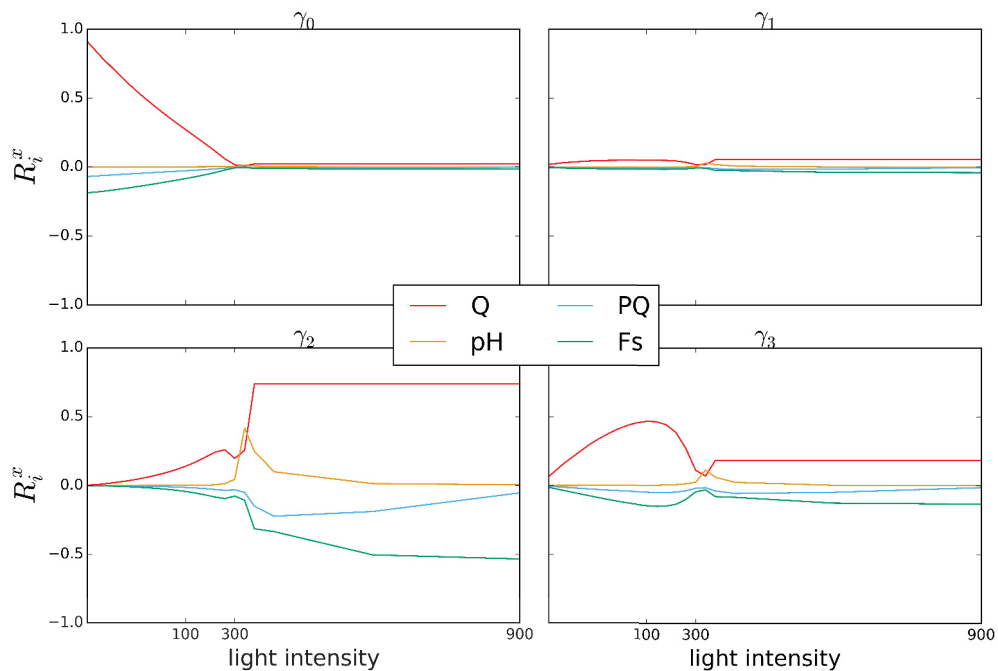
Figure 4.4.1: The effect of γ parameters on steady-state values of the key internal variables Q (quencher), PQ (plastoquinone redox state), pH and F_s (steady fluorescence). Displayed are the corresponding response coefficients R_i^x as functions of light intensity. Response coefficients indicate by how much a steady-state value changes upon a *small* perturbation of a parameter. For example, a coefficient of 1 indicates a 1% increase of the steady-state level as a response of a 1% increase of the parameter, a coefficient of -0.5 indicates a reduction of 0.5%, and a coefficient of zero means no effect.

memory phase is still lower than the corresponding simulated F_M' in the training phase. The steady-state fluorescence values F_s show discrepancies especially in the low and intermediate light intensities, but are very well captured for high light and in dark periods. One possible explanation for the deviations of model results from experimental data is that our model does not include other photoprotective mechanisms that may affect F_s, in particular state transitions [84, 196, 197]. Therefore at this development stage we decided to sacrifice some degree of precision for the sake of a simple model structure. The cross-talk and the interplay between acclimation mechanisms will be discussed further in this work, using more complex model that includes both modes for heat dissipation and state transitions.

4.4.2 Internal variables and light memory

A clear benefit of computer simulations is the possibility of following the dynamics of otherwise hard to measure molecules. In Fig. 4.4.3 we demonstrate how lumenal pH changes in the response to different light intensities and how quenching components saturate under high light and relax in darkness. In Fig. 4.4.3A we plot simulated dynamics of selected internal system variables, with pH shown in the upper panel and quenching components in the bottom panel. We can observe how the transient drop in lumenal pH recovers under low and moderate light conditions but the lumen remains acidic under high light intensity. In the lower panel we can dissect the contribution to the quencher. The fast component (PsbS mediated) is quickly activated and relaxes over time, whereas the slow component continues to increase. In Fig. 4.4.3B we provide the same information in a phase phase plot, where the pH is displayed as a function of quencher activity. This representation clearly indicates the different timescales on which the system operates. Trajectories start in the dark state (low Q, pH close to 8) by rapidly reducing pH (vertical drop), before the quencher is activated (curved trajectories), and eventually the steady-state in constant illumination (red dots) is reached.
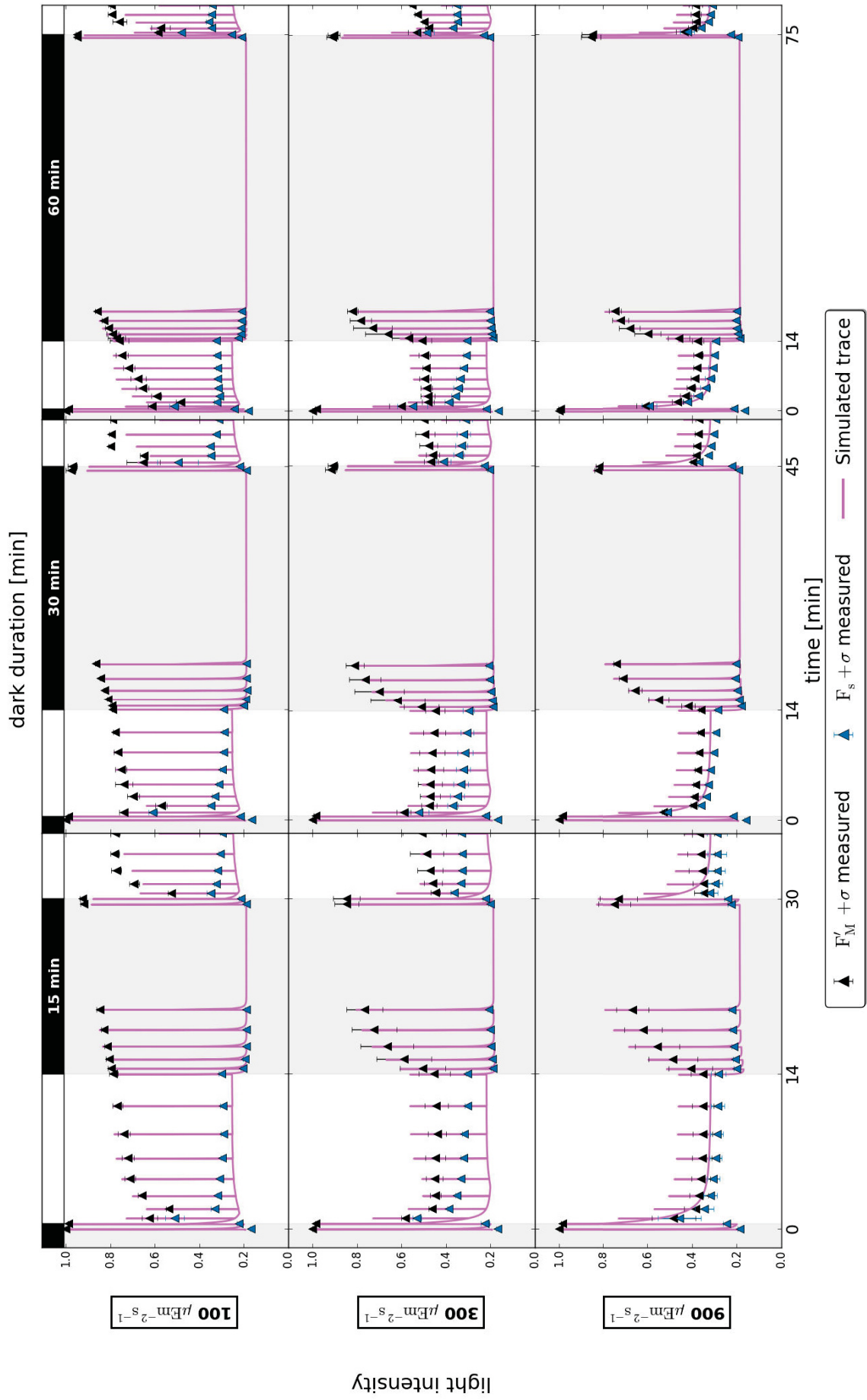
Figure 4.4.2: Pulse amplitude modulation traces of wild type *Arabidopsis* obtained experimentally (triangle points) and simulated by the model (magenta line).

The memory is visualised by the fact that the trajectories do not revert back to the initial dark state after the first dark relaxation phase, and thus the trajectories during the memory phase differ from those of the training phase.
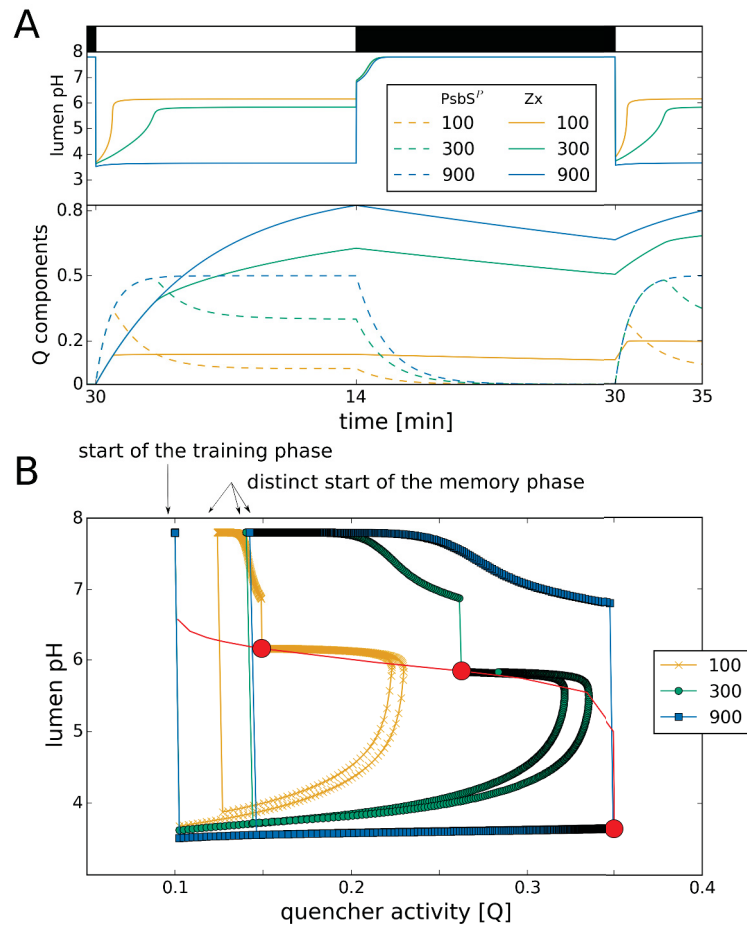
Figure 4.4.3: (A) The phase plane trajectories of the quenching variable (Q) and the lumenal pH during the light memory protocol. The red line depicts stationary states calculated for different light intensities. The markers on the trajectories are set in regular intervals of 1 s to visualise the different time scales on which the system is operating. (B) Internal variables for three different light intensities. The upper panel shows how the ability of relaxing the lumenal pH is lost with increasing light intensity. The bottom panel shows the dynamics of the quenching components (solid line for the relative zeaxanthin concentration, dashed line for the ratio of protonated PsbS).

4.4.3 Mutant analysis

Photosynthetic mutants are widely used to study photoregulatory mechanisms in plants and green algae [112, 86]. Thanks to the detailed description of the NPQ components the model sets the grounds for broad mutant analyses allowing for the simulation of various mutants, including npq4 mutant, which lacks PsbS protein. By setting the rate constant $k_{\text{ProtonationL}}$ to zero and keeping the initial PsbS concentration set to 1 we can create an *in silico* mutant.

Though we can not reproduce quantitative difference in the NPQ dynamics between the wild type and npq4 mutant (compared to already published data by Dall'Osto *et al.* [198]), our simulations for *Arabidopsis* showcase plausible qualitative agreement as we capture the drop of the quenching capacity in the mutant, due to the lack of the PsbS protein (Fig. 4.4.4).
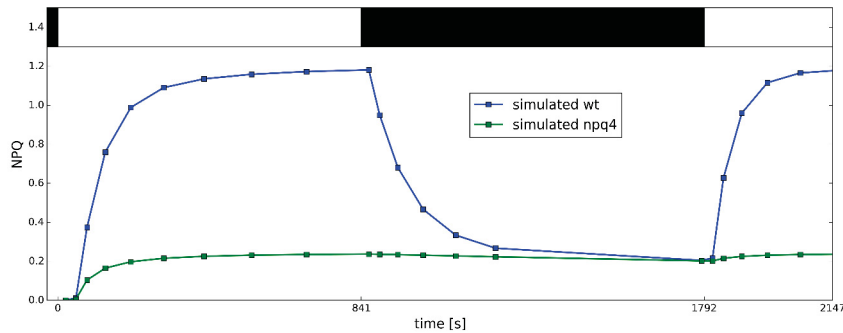
Figure 4.4.4: Simulated NPQ trace for *Arabidopsis* wt (blue line) and npq4 mutant (green line) displays the reported [198] qualitative drop of the quenching capacity of the mutant in the light, due to the lack of the PsbS protein.

Moreover, our simulated traces of WT and npq4 mutants are in better agreement than other well established mathematical models. In our opinion, the model provided by Zaks *et al.* [149] represents the most complete model used to study NPQ (and of a considerable higher complexity, with 26 differential equations) and therefore we compare the results of our highly simplified model to the results of their work. Our simulated traces of WT and npq4 mutants (compare to Fig. S1 from [149]) are in better agreement, both qualitatively and quantitatively. We can reproduce the reduction of the fluorescence in the mutant under high light intensity which was impossible in the compared model, because it did not incorporate slowly reversible components of NPQ (Fig. 4.4.5). Moreover, the relaxation of the fluorescence of the WT in the dark after high light exposure is represented accurately.
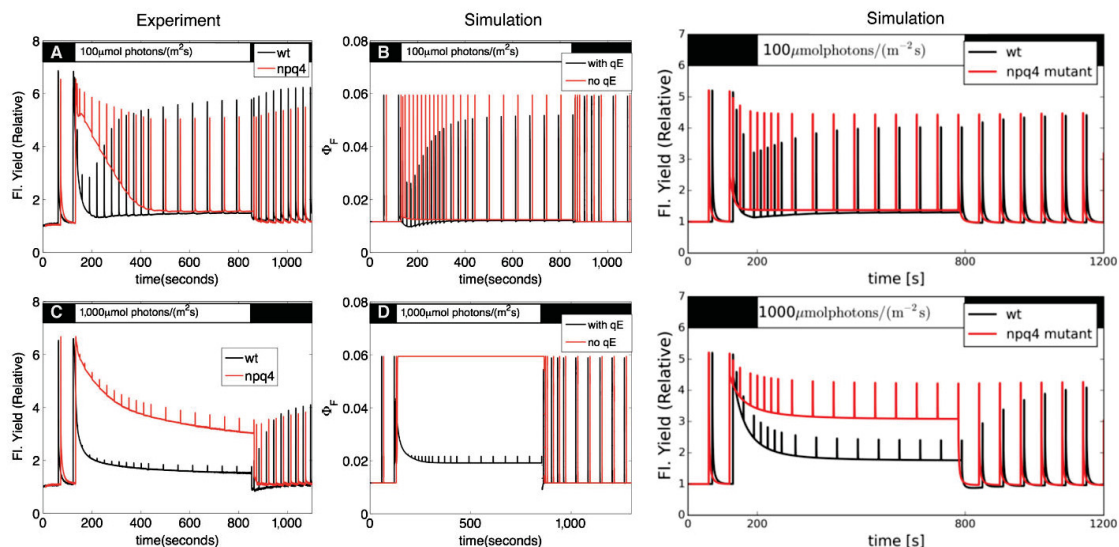
Figure 4.4.5: Simulated traces of WT and npq4 mutants using the same light protocol as in Fig. S1 from [149] (left pannel A-D). Results of the simulation are used to compare our model's performance with the experimental data published in [149] and their theoretical outcomes. We can reproduce the reduction of the fluorescence in the mutant under high light intensity. Moreover, the relaxation of the fluorescence of the WT in the dark after high light exposure is represented accurately.

4.4.4 Application to a non-model organism

It is a well recognised issue in the field of systems biology that modelling biological processes often requires acquiring a number of parameters [199] of which some might have a physical meaning, some may be a rough approximation of measured values, others may be fitted and some may be simply impossible to

measure with current techniques. Much focus was put on developing optimization algorithms that will ease parameter estimation, but the only safe way to reduce the risk of over-fitting is to minimize the dimensions of the parameter space. One of the difficulties of using available and published kinetic models is their often huge parameter space, which makes them hard to adapt to study analogous mechanisms in other species. To demonstrate that our model is of sufficient simplicity to allow for an easy adaptation to a new and not extensively studied organism, we have adapted our model to the ornamental, shadow-tolerant plant *Epipremnum aureum*, also referred to as *Pothos*. This choice was motivated by the finding that shade-tolerant plants are characterised by longer lasting memory for leaf illumination, as compared to plants found in semi-arid climates [200].

Parameter selection

With limited information on essential kinetic parameters for *Pothos* we performed basic measurements to collect data that would allow to change a minimal set of parameters in the model and use it for *Pothos*. We have collected therefore the fluorescence data for *Pothos* using the same experimental setup as described above for *Arabidopsis*. In Fig. 4.4.7 the maximal fluorescence kinetics in the first (training) and second (memory) light phase is visualised in a similar way, as for *Arabidopsis* (Fig. 4.2.4). The fluorescence traces exhibit the same pattern as observed for *Arabidopsis*: under each condition the first fluorescence peak in the second light phase (memory) was lower compared to the first light exposure (training). Once again, to visualise how the extent of the incomplete relaxation is influenced by both light intensity and the time spent in darkness, and to compare it to similar results obtained for *Arabidopsis*, we plot the ratio between the second last measurement in darkness and the first measurement after the dark adaptation (Fig. 4.4.6).
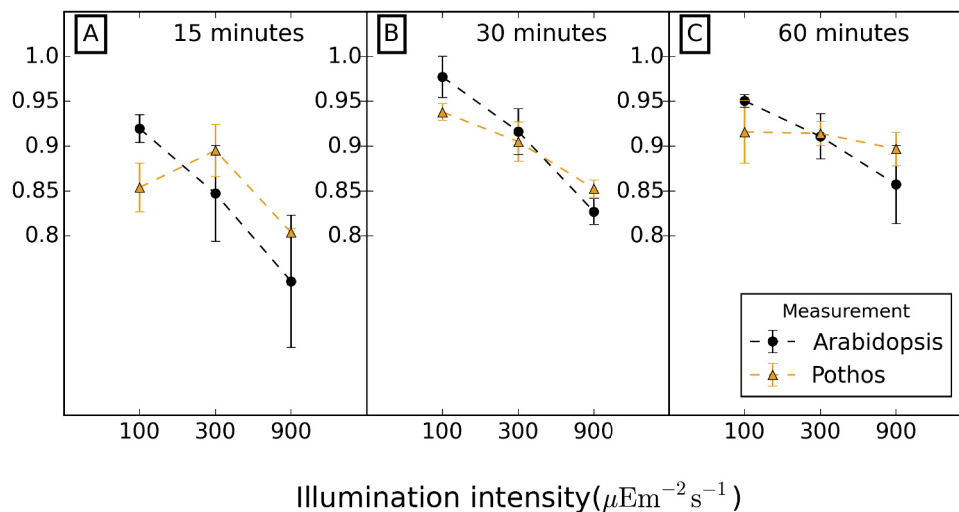
Figure 4.4.6: Relaxation of the fluorescence at the end point of darkness for both species, expressed as ratio between the second last measurement in the darkness and the first measurement after the dark adaptation. For plants kept for more than 15 min in the darkness we observe a linear relationship between light intensity and extent of relaxation.

Next, similar as for *Arabidopsis*, we tested if there is any statistically significant difference in the extent of quenching and/or its induction rate between the training and memory phase (Tab. 4.4.1).
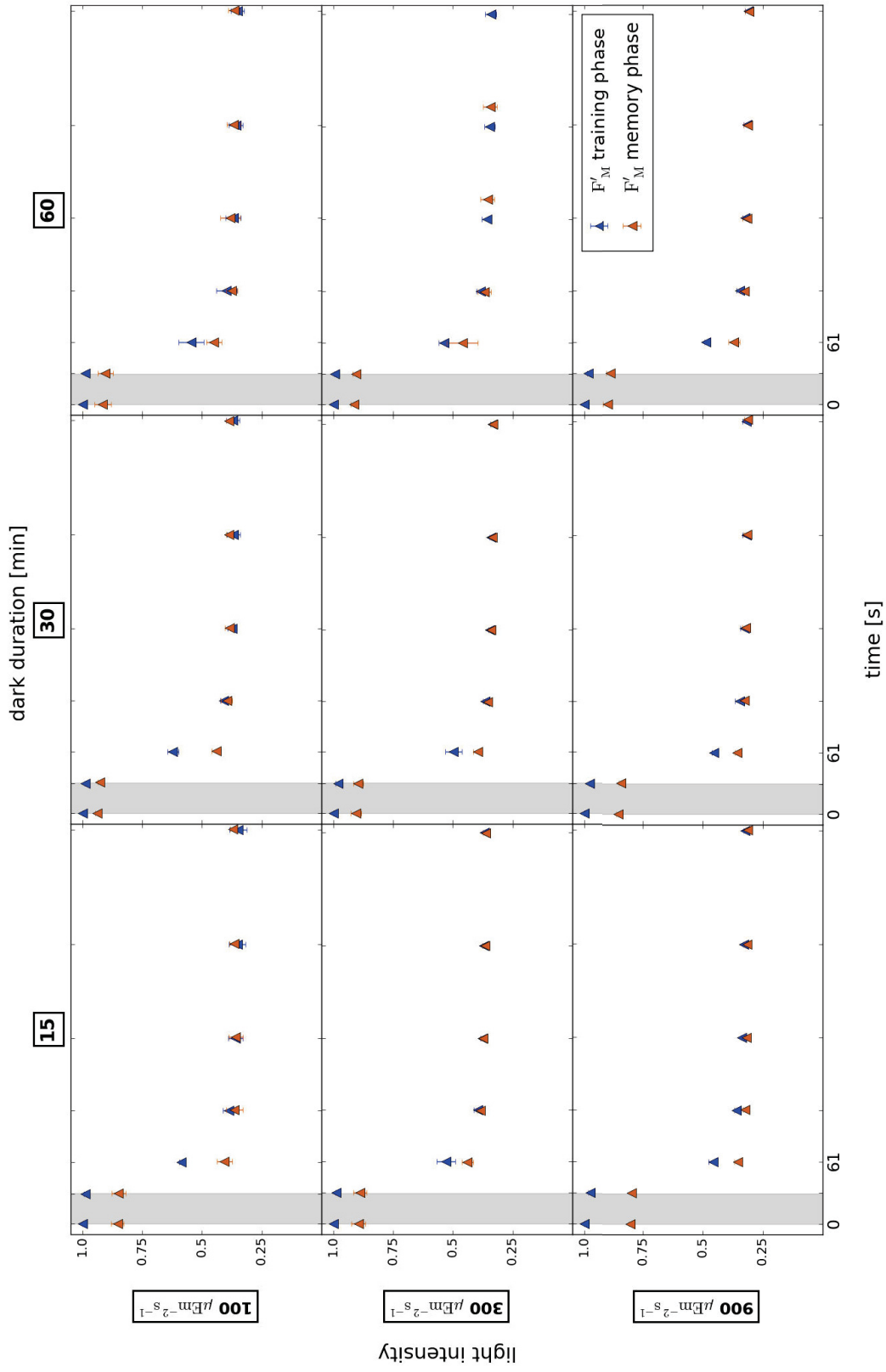
Figure 4.4.7: Comparison of the first two F'_M measurements taken in darkness and first five measurements in training phase (blue points) with the last two measurements taken in the relaxation phase and first five measurements in the second light phase (red points). The first measurement taken in the light (at 61 s) is lower in the memory phase than in the training phase, regardless of light intensity and time of relaxation. Error bars indicate standard deviations for three replicates except for the experiment marked with *, where the experiment was repeated eight times.

We first performed a paired T-test to test the hypothesis that there is no statistical difference between the first F'_M measured in the light in the training phase and the first maximal fluorescence (F'_M) measured in the memory phase, results summarised in Tab. 4.4.1). We cannot reject this hypothesis for *Pothos* exposed to low light intensities and kept for an hour in the darkness, but for other seven cases it has been demonstrated that there is a statistically significant (with a 95% confidence interval) difference in the first fluorescence measurements. We next performed a paired T-test to check if there is a statistically significant difference between the induction rate in the memory phase and training phase (H_0 = no statistically significant difference between phases). For that we again compared the slope between the F'_M values from the 18th and 17th pulse (memory phase) with the slope between the 3rd and 2nd pulse (training phase). We could not explain the fact that for *Pothos* exposed to 100 $\mu Em^{-2}s^{-1}$ and kept in darkness for 15 min, and for exposed to 900 $\mu Em^{-2}s^{-1}$ and left in the darkness for 15 min, the difference in the induction rate is statistically significant. Possibly, a larger number of replicates leads to a more significant result. For all other cases, due to the high p-value we cannot reject the null hypothesis.
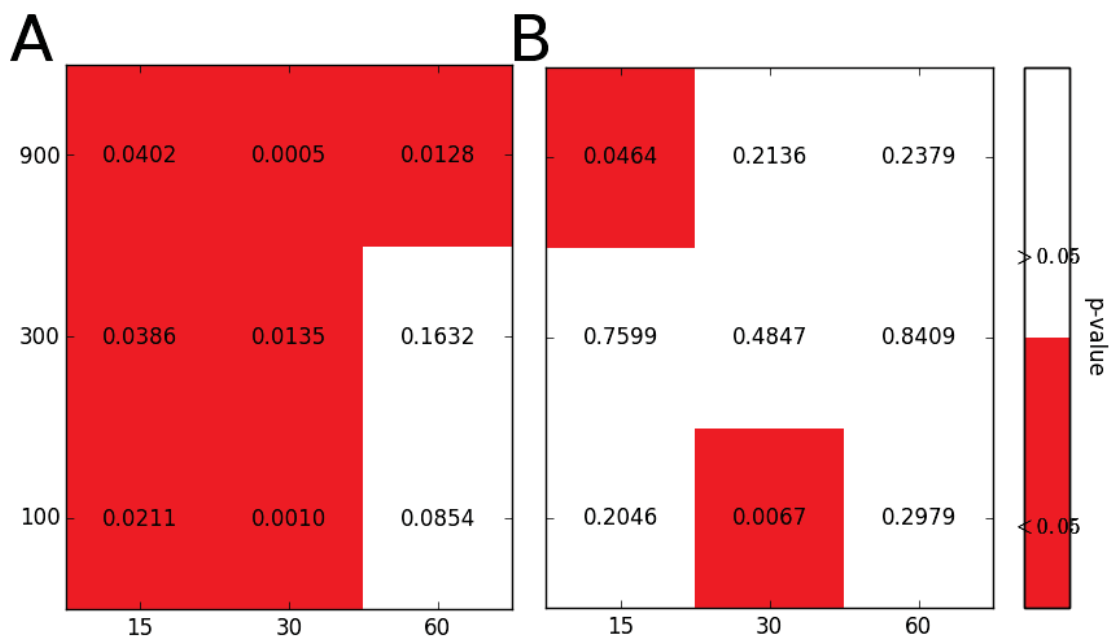
Table 4.4.1: Results of a paired T-test testing (left): there is no statistical difference in the extent of quenching between the light phases (calculated as a ratio between the first F'_M in the light and F_M); (right): there is no statistical difference in the induction rate of quencher in the training phase and memory phase (calculated as a slope between last measurement in darkness and the first measurement in the light phase).

We therefore concluded that *Pothos* with active short-term memory of previously experienced light initiate its photoprotection with some head-start, but at the same speed (as *Arabidopsis*). Considering above, we assumed that the kinetic parameters describing the xanthophyll cycle and the protonation rate might be similar for *Arabidopsis* and *Pothos* and kept them fixed for both species. We next used the NPQ kinetic traces to compare NPQ capacity between the two species. From the traces of the NPQ kinetics in Fig. 4.4.8 we concluded that since under identical conditions *Pothos* plants exceed the quenching capacity of *Arabidopsis* the overall quenching capacity of this plant will be much higher, in agreement with similar observations on other shadow-tolerant plants [200]. In fact, under moderate light *Pothos* already behaves like *Arabidopsis* exposed to high light. We aimed at reflecting this higher quenching capacity by increasing the value of parameter γ_2 from 0.6 to 1.0 (Eq. 4.3.39).

Lastly, we compared the chlorophyll content in both species and found a 70% higher content in *Pothos* than in *Arabidopsis* (Tab. 4.4.2). We assumed that higher chlorophyll content will lead to higher energy conversion and therefore increased the factor converting photon flux density to light activation rate (k_{cpfd}).
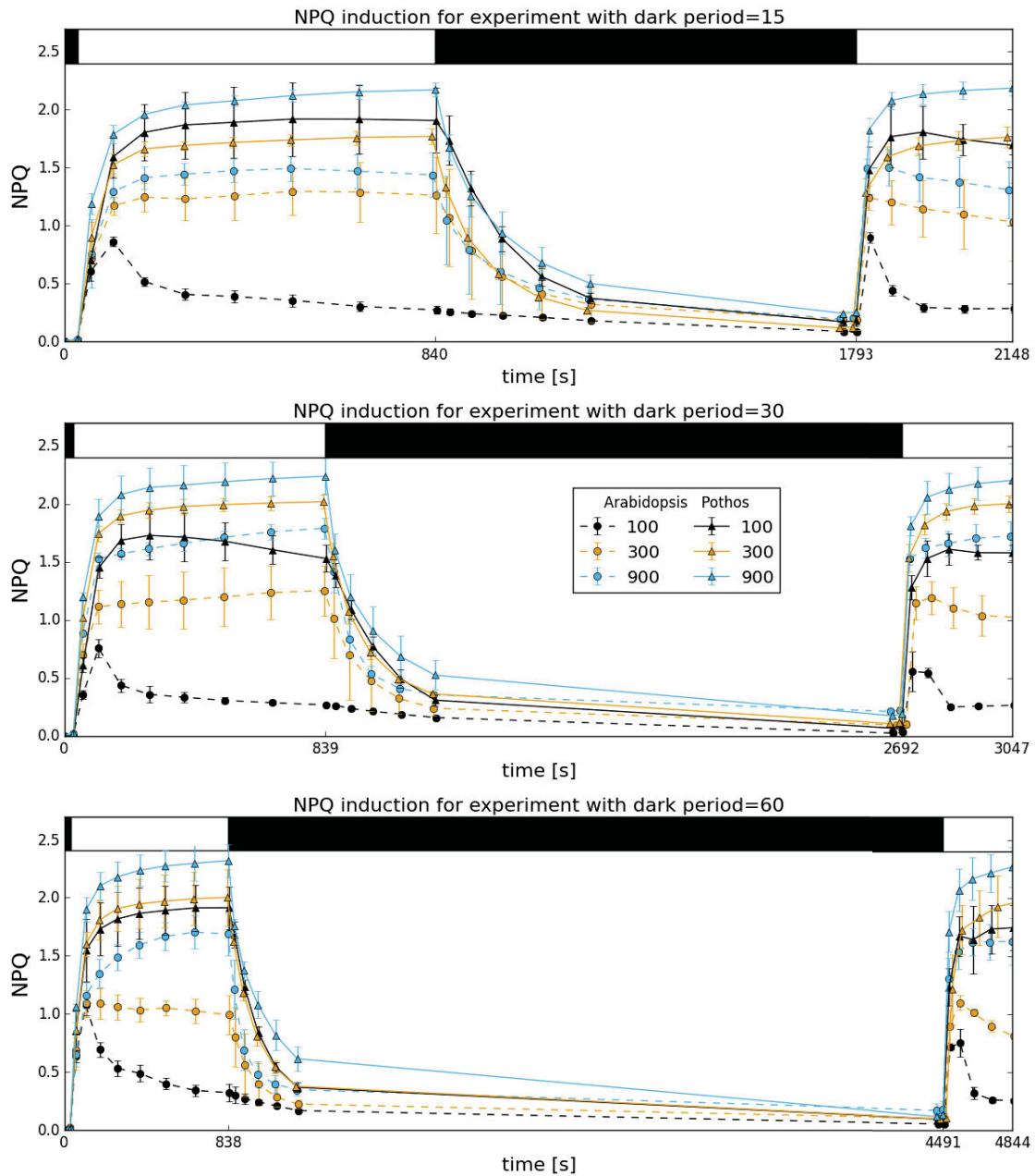
Figure 4.4.8: NPQ traces for all 18 experiments (each repeated 3 times, error bars denote standard deviations), grouped by the duration of the relaxation period. Transient induction of NPQ in the first 2 minutes of illumination is observed only for *Arabidopsis* exposed to the lowest light intensity. NPQ traces for *Pothos* are always higher than for *Arabidopsis*, demonstrating the higher quenching capacity. However, the induction rates for both species are indistinguishable, therefore no evidence is provided that would require us to change related kinetic parameters, such as epoxidation rate constants.

Absorbance						
	Pothos			Arabidopsis		
Replicate	665nm	652nm	470nm	665.2nm	652.4nm	470nm
1	0.578	0.333	0.689	0.444	0.25	0.424
2	0.621	0.359	0.701	0.499	0.285	0.503
3	0.794	0.452	0.9	0.395	0.214	0.401
4	0.744	0.432	0.93	0.356	0.19	0.335
mean	0.684	0.394	0.805	0.424	0.235	0.416

Concentrations (μgram/gram)	Pothos	Arabidopsis
Chls a	783	493
Chls b	298	153
Chls xanthophylls + carotenes	217	112

Table 4.4.2: The quantitative determination of chlorophylls and carotenoids by UV-VIS spectroscopy for methanol extracts [201].

Fluorescence results

With limited information on the electron transport chain, protein abundance and various kinetic parameters, based on the measurements analysed above, we kept the same values of all internal parameters as for *Arabidopsis*, except for γ_2 and k_{cpfd}. With only those two changes in the parameter space we reproduced all features of the fluorescence dynamics observed for *Pothos* (Fig. 4.5.1). Our simulation results allow us to hypothesize that the enhanced quenching capacity can be explained by a more efficient energy transfer from the chlorophylls to the quencher. Possible molecular explanations might be an increased number of quenching sites or a closer spatial arrangement.

4.5 Discussion and Outlook

We have constructed a simplified mathematical model that is based on our current understanding of the quenching mechanisms. By achieving an agreement between our simulations and experimentally observed behaviour, we could confirm that this understanding is basically correct. Moreover, with the mathematical description of the process we could provide a quantitative description of the contribution of the two quenching components to an interesting biological phenomena, short-term light memory. It is remarkable that these findings could be obtained by a very simple model structure.

We realise that very detailed models have the potential advantage that they provide a very specific and accurate representation of experimental observations, but increasing complexity generally implies a higher level of specialisation, e. g. to one particular organism or even a single environmental condition, and moreover systematic model analyses become increasingly difficult. The virtue in model building lies exactly in the process of simplification because this process allows distilling the essential features of the investigated system which give rise to its characteristic emergent properties. Therefore, developing a simple model that can provide the same level of information as the more complex one, built for the same or similar purpose, is in itself a useful scientific exercise, which generates a deeper understanding of the biological system. Moreover, simple models are easier to implement and can be generalised, but often are limited in the quantitative reproduction of the data. For instance, a model of high-energy state quenching of extreme reduced complexity aims at reproducing the key biological features of quenching [148] but is clearly limited in its capability to correctly reproduce the dynamics of quenching induction and relaxation simultaneously. On the other hand, the detailed computer model of C3 photosynthesis by Laisk *et al.* [154] was built to test whether the current understanding of photosynthesis is basically correct. The model is able to correctly

reproduce steady state behaviour of photosynthesis and carbon fixation, but cannot reproduce NPQ kinetics. A recent model that specifically aimed at understanding the transient dynamics of NPQ, was proposed by Zaks *et al.* [149]. Employing a set of 26 nonlinear differential equations, but only considering one quenching state, the model is able to reproduce the quantitative difference in the fluorescence yield between low and high light conditions. The complexity of the latter two models makes it difficult to derive general conclusions that may be valid beyond the boundaries of single species. Further, their size makes a *de novo* implementation a very time-consuming task and the reproduction and verification of the model results is tedious, in particular since they are not provided as open source code.

We have therefore presented here a new, highly simplified mathematical model of NPQ, and employed the model not only to accurately describe the rapidly reversible components of non-photochemical quenching, such as the previously published models [148, 149], but further used it to explain the phenomenon of short-term light memory, and moreover provide a quantitative understanding of the different contributions of the well-known NPQ components.

Our model accurately simulates the changes in the fluorescence yield at low, moderate and high light intensities (Fig. 4.4.2). It further provides an explanation for the higher extent of quenching observed for plants which have previously been illuminated. Furthermore, it supports the notion that the same organisational principles of photoprotective mechanisms are present in plants as different as *Pothos* and *Arabidopsis*.

With a simple experimental setup with two light exposure periods separated by a varying relaxation time, we demonstrate that the extent of quenching does indeed depend on how long ago and how much light a plant has previously experienced – a behaviour which can safely be termed memory. We could demonstrate experimentally and theoretically that this light memory can be attributed to the slow quenching component associated with the de-epoxidation of violaxanthin to zeaxanthin triggered by low lumenal pH, which is in agreement with our current knowledge on NPQ and memory [165, 174, 176]. In the dark, epoxidation of zeaxanthin to violaxanthin is slow, so that even after 30-60 minutes the conversion is not complete. In a second exposure to light, the rapidly protonated antennae PsbS-H further contribute to quenching with an increased efficiency when zeaxanthin is still present. This conclusion is supported experimentally by direct comparison of fluorescence traces, demonstrating that light memory is affected by the length of darkness, which again determines the residual levels of zeaxanthin at the last point of darkness (Fig. 4.2.6).

Essentially, our model captures all key features of the experimental observations. However, due to the applied reduction, we cannot expect that the model will accurately describe every single aspect of NPQ dynamics, especially if processes are involved, that were not included into the model structure. For example, since the CBB Cycle is not explicitly modelled, but only summarised by a downstream consuming reaction, the effect of the redox regulation of CBB Cycle enzymes cannot be accurately reflected. Moreover, the suggested effect of Zx-induced memory on the transient NPQ in low light conditions cannot be quantitatively reproduced, because we do not incorporate any memory-dependent regulation of ATPsynthase activation. Likewise, the observed discrepancies between simulated and observed Fs levels (Fig. 4.4.2) can be explained by the fact that we do not model other acclimation mechanisms, in particular state transitions, which are known to have an effect on the steady state fluorescence [188].

Despite its simplicity, the model structure allows testing various hypotheses on the molecular mechanisms of quenching in mutants impaired in their quenching capabilities. Our simulations for the npq4 mutant, which is lacking the pigment-binding protein associated with photosystem II, but has a normal xanthophyll cycle, are in good qualitative agreement with previously published work on that mutant [198] (Fig. 4.4.4). Although mutant analysis is not in the focus of this research, this again demonstrates the flexible use and adaptability of our model and indicates its value when interpreting experimental results.
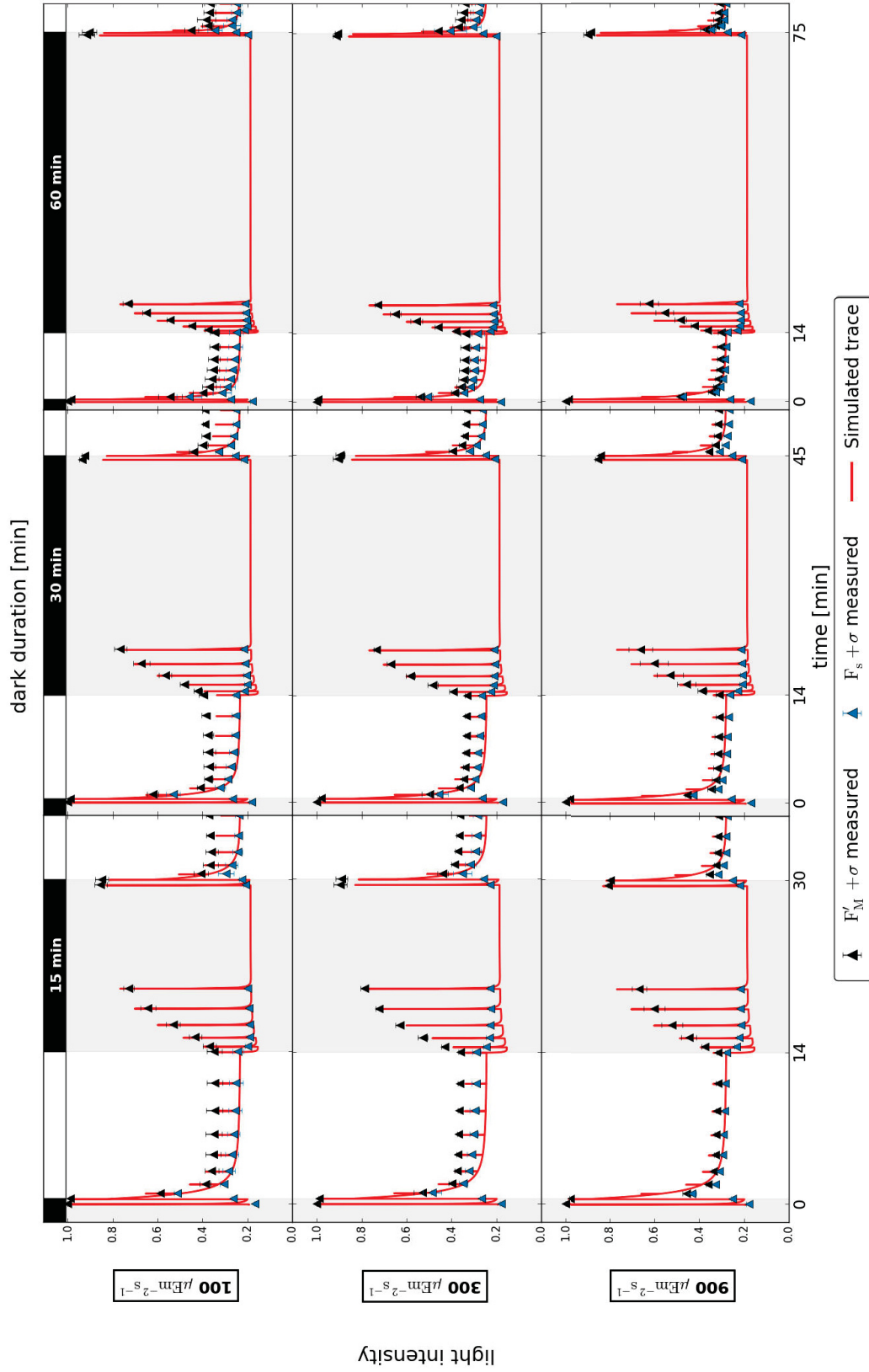
Figure 4.5.1: Pulse amplitude modulation traces of wild type *Pothos* obtained experimentally and simulated by the model with only two changed parameters.

Moreover, our model can be applied to studies that focus on memory in the context of optimisation of photosynthesis (we refer readers to an excellent review covering this topic [94]). For instance, the model can be used to find a theoretical optimum size of the xanthophyll cycle pool, by systematical increasing or decreasing the pool size, in order to find a balance between the benefit of a large pool leading to increased antioxidant, photoprotective activity [202], and the negative effect on the overall photosynthetic efficiency. Additionally, the response of a plant to a wide range of light protocols can be predicted, such as for example repeated light-dark cycles.

The carefully chosen selective model reduction helps to identify common underlying principles of NPQ in different photosynthetic organisms, and we expect that the model should be easily adapted even to as distantly related species as diatoms, where despite a different molecular nature of the xanthophylls, the cycle still operates according to the same principles as in higher plants [104]. For that reason this module was further used to study acclimation mechanisms in green microalga *Chlamydomonas reinhardtii*.

4.6   Concluding remarks

We have demonstrated that our current understanding of quenching processes can be converted into more general, mathematical terms and with the implemented theory we can reproduce the most critical behavioural features of short-term illumination memory. This memory is generated by the interaction of two components of NPQ, that were previously identified by many others. The slower one, accumulation of zeaxanthin, accounts for the amount of memory lasting after relaxation in darkness, while the fast one increases the efficiency of quenching. However, our experiments do not provide evidence for an acceleration of quenching activity by previous light exposure. Rather, we propose to explain the consistently lower F'_M in the first seconds of the second light period by accumulation of Zx only. Therefore, plants with active short-term memory of previously experienced light initiate their photoprotection with some head-start, but at the same speed. Moreover, our computational model supports hypotheses on why shadow-tolerant plants exhibit a higher quenching capacity. Finally, thanks to the modular structure of the model, results of this work are easily merged with the model of state-transitions in *Chlamydomonas reinhardtii* previously published by Ebenhöh *et al.* [26] and further developed in this work (see Ch. 5), making this module a first building block of the final mathematical model of the light acclimation mechanisms.

5. Modelling qT in green algae

„The key to winning is poise under stress."

*- **Paul Brown**, American football coach*

In this Chapter I provide the description of the expanded mathematical model of photosynthesis that includes more details of the photosynthetic electron transport chain than the model constructed to study the light memory effect (Ch. 4). The module of a fast component of non-photochemical quenching described in the previous Chapter was first removed and the focus lied on understanding slower component of NPQ termed state transitions. State transitions mainly occur under low light conditions to maintain the redox poise and energy balance under unfavourable conditions. The model was adapted for the model organism *Chlamydomonas reinhardtii*, as this organism exhibits very large qT capacity [85] and has been extensively used in the past to study this mechanism [75]. The further development was based on the mathematical model of state transitions published by Ebenhöh *et al.* [26]. The module describing state transitions allows to test possible differences in activation mechanisms (triggered by light or upon changes from aerobic to anaerobic conditions) and to test the hypothesis on energy quenching during the transitions. The model outcomes are challenged by experimental data obtained for *Chlamydomonas* cells, which do not express LHCSR3 protein and have therefore little capacity for qE-dependent quenching. After a proper representation has been established, the model was complemented with the equations for qE, as developed in the previous Chapter. This model was then used to assess the potential benefit of reducing antenna size to increase photosynthetic efficiency under high light intensities and to analyse the photosynthetic efficiency of cells grown in a bioreactor and experiencing fluctuating light intensities.

5.1   Introduction

In plants and green algae, the physical separation of PSII and PSI imposes the existence of different antenna systems, which excite the two photosystems independently (see Ch. 1). Natural fluctuations in light quality and quantity can lead not only to an excess excitation energy causing photodamage but may also lead to an imbalance compromising photosynthetic efficiency. As described in the introductory chapter (Ch. 1, S. 1.4.2), acclimation to such fluctuating environments is achieved by balancing the excitation of the two photosystems through a mechanism termed state transitions, during which major light harvesting complexes that are usually associated with PSII separate from the photosystem and move towards PSI. State transitions thus optimise the relative absorption capacity of PSs. Under conditions that preferentially promote excitation of PSII the reduced state of the PQ pool and the Cyt b6/f complex triggers the activation of a protein kinase (Stt7 in *Chlamydomonas* or STN7 in *Arabidopsis*) that phosphorylates the light-harvesting complex of PSII (LHCII). Phosphorylated antenna complexes can migrate laterally towards PSI, balancing the light excitation energy during this so called State 1 to State 2 transition.

While in plants state transitions play a role only in optimising light absorption under low light and involve a rather moderate number of reallocated antenna, in *Chamydomonas* this process also contributes to photo-protection in high light [86]. We decided therefore to construct our state transitions module for micro-alga to incorporate more aspects of this mechanism. We especially focused on the still debated topic whether, in contrary to the previous understanding, not all the detached antennae are moving towards PSI and state transitions actually involve a different mechanism than the simple physical displacement of LHCII between the two photosystems [22, 78, 79].

5.1.1   Aim of the study

Our aim was to develop further the mathematical model of state transitions proposed by Ebenhöh *et al.* [26] to help to answer remaining questions regarding the molecular mechanism of state transitions, analyse the consequences of reduction of relative antenna cross sections and finally, to utilise this module in a broader context of a short-term light acclimation model, where several photoprotective mechanisms will be incorporated.

For this, we first reproduced the work by Ebenhöh *et al.* [26] using our modular approach (see Ch. 3, S. 3.3). Next, we stepwise complemented the description of the model with an additional mechanism of photoinhibition, a more complex description of the mechanism of state transitions to allow for a hypothetical aggregation of antennae quenching complexes within the thylakoid membrane, and coupled the ATP energy demand with the NADPH demand. We also tested how our model can be used to simulate the photosynthetic productivity of a cell grown in a bioreactor where it experiences rapid fluctuations of light due to its movement.

Our model is able to realistically reproduce various experimentally obtained fluorescence traces for wild type and ΔPC mutant, reproduce the light-saturation curve for mutants with truncated light-harvesting chlorophyll antenna and predict the photosynthetic efficiency depending on the molecular mechanism of state transitions assumed.

5.2   Model description

Since the process of state transitions involves a translocation of antenna pigments between two photosystems, the reduced representation of the photosynthetic electron transport chain imposed in the previous model (see

Ch. 4, S. 4.3) could not be used for this work. The model was significantly expanded to include various previously excluded components, treating the work proposed in [26] as a base for further expansion. This model includes a description of both linear and cyclic electron flow and a dynamic adjustment of PSs cross sections through antenna redistribution. The scheme of the model components is depicted in Fig. 5.2.1.

5.2.1 Stoichiometry of the model

Despite removing the quenching module, the system of equations to study the state transitions comprises a set of nine coupled ordinary differential equations, 17 reaction rates (Appendix, Tab. A3) and 54 parameters (Appendix, Tab. A4). Together, they govern the temporal evolution of photosystem II protein concentration (5.2.1), reduced fraction of the plastoquinone pool (5.2.2), reduced fraction of the plastocyanin pool (5.2.3), reduced fraction of the ferredoxin pool (5.2.4), concentration of active ATPase (5.2.5), stromal concentration of ATP (5.2.6) and NADPH (5.2.7), proton concentration in the lumen (5.2.8), and phosphorylated fraction of light harvesting complexes (5.2.9)

$$\frac{dB}{dt} = -v_{\text{degPSII}} + v_{\text{repPSII}}, \tag{5.2.1}$$

$$\frac{dP}{dt} = v_{\text{PSII}} - v_{\text{b6f}} + v_{\text{FQR}} - v_{\text{PTOX}} + v_{\text{NDH}}, \tag{5.2.2}$$

$$\frac{dC}{dt} = 2v_{\text{b6f}} - v_{\text{PSI}}, \tag{5.2.3}$$

$$\frac{dF}{dt} = v_{\text{PSI}} - 2v_{\text{FNR}} - 2v_{\text{FQR}}, \tag{5.2.4}$$

$$\frac{dE}{dt} = v_{\text{actATPase}} - v_{\text{deactATPase}}, \tag{5.2.5}$$

$$\frac{dA}{dt} = v_{\text{ATPsynthase}} - v_{\text{ATPconsumption}}, \tag{5.2.6}$$

$$\frac{dN}{dt} = v_{\text{FNR}} - v_{\text{NADPHconsumption}}, \tag{5.2.7}$$

$$\frac{dH}{dt} = \left(2v_{\text{PSII}} + 4v_{\text{b6f}} - \frac{14}{3}v_{\text{ATPsynthase}} - v_{\text{leak}}\right) \cdot \frac{1}{b_H}, \tag{5.2.8}$$

$$\frac{dL}{dt} = v_{\text{Stt7}} - v_{\text{Pph1}}. \tag{5.2.9}$$

5.2.2 Reaction rates description

Most of the reactions are kept as described in [26], including the photosystems. As described in the section of common assumptions (see Ch. 3, S. 3.3.1), both photosystems were described as a light-activated oxidoreductases and we used the quasi-steady state approximation to calculate their rate of activity. In total, 17 rates (v_{degPSII}, v_{repPSII}, v_{PSII}, v_{PSI}, v_{b6f}, v_{FQR}, v_{PTOX}, v_{NDH}, v_{FNR}, $v_{\text{actATPase}}$, $v_{\text{deactATPase}}$, $v_{\text{ATPsynthase}}$, $v_{\text{ATPconsumption}}$, v_{leak}, $v_{\text{NADPHconsumption}}$, v_{Stt7} and v_{Pph1}) are used to express the dynamics of the system and their functional form is explained below respectively.

Photoinhibition of Photosystem II

Firstly, the Ebenhöh model [26] was complemented with process that reflects the damaging effect of prolonged high light exposure. We applied simple kinetics to reflect protein degradation

$$v_{\text{degPSII}} \quad = \quad k_{deg}(B_1 + B_3), \tag{5.2.10}$$
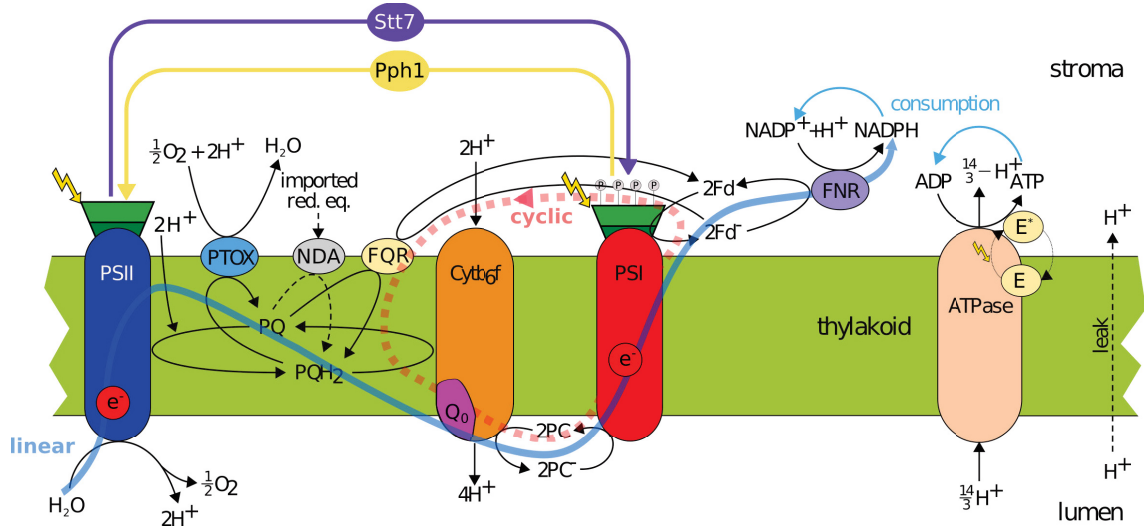
Figure 5.2.1: Scheme of the main components of the photosynthetic electron transport chain included into the mathematical description of the photophosphorylation. The model includes two modes of electron transfer: linear (solid, blue line) and cyclic (red, dashed line). Linear electron flow comprises of photosystem II, cytochrome b6f, photosystem I and ferredoxin-NADPH reductase (FNR), whilst the cyclic electron flow is represented by a single reaction re-injecting electrons back to the plastoquinone pool through the ferredoxin-plastoquinone reductase (FQR). Protonation of the lumen drives the production of ATP through ATPase (E*). ATPase is active in the light and inactive in the dark. Figure adapted from [26].

where k_{deg} is the rate constant $5e7$ slower than charge separation (k_P). We assumed that the damage of photosystem II will be proportional to the occupation of closed states, quite similar to assumptions made in models of photoinhibition by Han *et al.* [152, 153]. For the repair we used the same rate constant (k_{rep}) as in the Nikolaou model [147]

$$v_{\text{repPSII}} \quad = \quad k_{rep}(1 - B/\text{PSII}^{\text{tot}}). \tag{5.2.11}$$

Photosystem II

The rate of photosystem II is derived as described in the previous chapter with the exception that the protein concentration is not constant anymore (PSII^{tot}), and instead it is set to a dynamic variable B:

$$B_0 + B_1 + B_2 + B_3 \quad = \quad B. \tag{5.2.12}$$

It is assumed that reaction centres of photosystem II can be in one of the four defined states and the overall rate of the activity is proportional to the occupation of B_1 and given by the rate:

$$v_{\text{PSII}} = \frac{1}{2}k_{\text{LII}}B_1, \tag{5.2.13}$$

where the light activation (k_{LII}) is now dependent on the total light intensity and the antenna cross-section of PSII.

Photosystem I

The reaction rate of the oxidoreductase activity of PSI is kept as in [26]. The scheme of internal processes included into the mathematical description of the transformation is presented in Fig. 5.2.2, where single steps

are assumed to proceed according to mass-action kinetics.

To determine the overall rate of the oxidoreductase activity of PSI performing the net transformation described by Eq. 1.2.7, p. 33, the fraction of occupation of the ground state (Y_0) needs to be determined, as the rate is proportional to the occupation of the Y_0

$$v_{\text{PSI}} = k_{LI} \cdot Y_0. \tag{5.2.14}$$

A quasi steady-state approximation was applied, where each of the following differential equations

$$\frac{dY_0}{dt} = -\left(k_{\text{LI}} + \frac{k_{\text{PCox}}}{K_{\text{eq,PCP700}}} \cdot (\text{PC}^{\text{tot}} - C)\right) Y_0 + k_{\text{PCox}} \cdot C \cdot Y_2 \tag{5.2.15}$$

$$\frac{dY_1}{d1} = k_{\text{LI}} Y_0 - k_{\text{Fdred}} \cdot (\text{Fd}^{\text{tot}} - F) \cdot Y_1 + \frac{k_{\text{Fdred}}}{K_{\text{eq,P700Fd}}} \cdot F \cdot Y_2 \tag{5.2.16}$$

$$\frac{dY_2}{d1} = \frac{k_{\text{PCox}}}{K_{\text{eq,PCP700}}} \cdot (\text{PC}^{\text{tot}} - C) \cdot Y_0 + k_{\text{Fdred}} \cdot (\text{Fd}^{\text{tot}} - F) \cdot Y_1 - \left(\frac{k_{\text{Fdred}}}{K_{\text{eq,P700Fd}}} \cdot F + k_{\text{PCox}} \cdot C\right) Y_2 \tag{5.2.17}$$

are set to zero. Y_0 is determined from the first two resulting algebraic equations under consideration that the total PSI concentration does not change over time

$$Y_0 + Y_1 + Y_2 = \text{PSI}^{\text{tot}}, \tag{5.2.18}$$

resulting in

$$Y_0 = \frac{\text{PSI}^{\text{tot}}}{1 + \frac{k_{\text{LI}}}{k_{\text{Fdred}} \cdot (\text{Fd}^{\text{tot}} - F)} + \left(1 + \frac{(\text{Fd}^{\text{tot}} - F)}{K_{\text{eq,P700Fd}} F}\right) \cdot \left(\frac{C}{K_{\text{eq,PCP700}}(\text{PC}^{\text{tot}} - C)} + \frac{k_{\text{LI}}}{k_{\text{PCox}} C}\right)}, \tag{5.2.19}$$

where k_{PCox} is the rate constant for oxidation of plastocyanin at P_{700}, k_{Fdred} is the rate for reduction of ferredoxin by PSI and k_{LI} is the light activation rate of PSI (determined by the total light intensity and the relative cross-section of PSI).
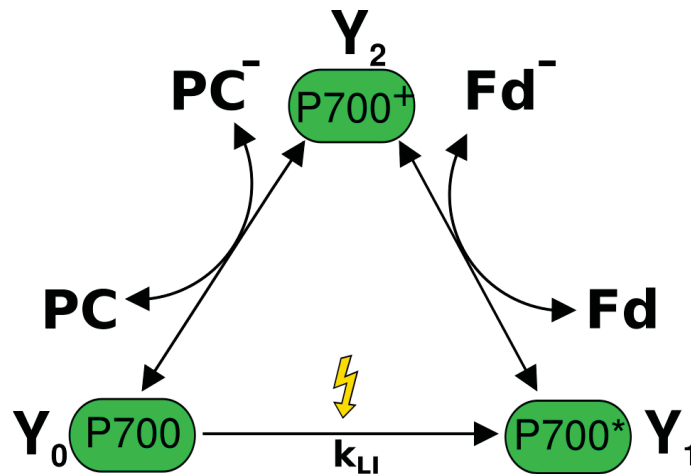
Figure 5.2.2: Schematic representation of internal processes included into the mathematical description of photosystem I. Light energy is absorbed by the light harvesting complexes and passed to a reaction centre (P_{700}) which is excited to the higher energy state $P_{700}^\star$ (Y_1), which reduces ferredoxin (Fd) with its concomitant oxidation to P_{700}^+ (Y_2). Y_2 is reduced by plastocyanin (PC^-) to its ground state (Y_0). Figure reproduced from [26].

Cytochrome b6f

In the previous chapter the equation describing the activity of cytochrome b6f

$$PQH_2 + 2PC + 2H^+_{stroma} \rightleftharpoons PQ + 2PC^- + 4H^+_{lumen}, \tag{5.2.20}$$

was lumped with other reactions leading to the oxidation of PQ pool (Eq. 4.3.20 p. 78). Here, we approximate the rate of the b_6f complex as in [26], by a simple mass-action kinetics:

$$v_{b6f} = \max\left(k_{b6f} \cdot \left(P \cdot (PC^{tot} - C)^2 - \frac{(PQ^{tot} - P) \cdot C^2}{K_{eq,b6f}(H)}\right), v^{min}_{b6f}\right), \tag{5.2.21}$$

with the equilibrium of this reaction dependent on the stromal and lumenal proton concentration. PQ^{tot} and PC^{tot} are constants reflecting the total plastoquinone and plastocyanin pools and as P and C describe the reduced fractions, the $PQ^{tot} - P$ denotes the oxidised fraction of the plastoquinone pool (and likewise for plastocyanin). The minimal rate v^{min}_{b6f} has been introduced in [26] to deal with cases when the extreme drop of lumenal pH leads to the reverse of the direction of the reaction mediated by the cytochrome b_6f and causes rapid export of protons.

ATP synthesis

The rate of ATP synthesis is kept as described in the previous chapter, including the delayed activation of ATPase.

NADPH production

The reaction leading to the reduction of $NADP^+$ to NADPH (mediated by FNR, according to the chemical Eq. 1.2.8, p. 33) is modelled as in [26], using the convenience kinetics developed in [203]. The convenience kinetics is a generalised form of Michaelis-Menten kinetics that covers all possible stoichiometries, describes enzyme regulation by activators and inhibitors, and can be derived from a rapid-equilibrium random-order enzyme mechanism. As K_M-values for FNR were determined, this saturable rate law results in a more realistic rate equation

$$v_{FNR} = V^{max}_{FNR} \cdot \frac{f^{-2} \cdot n^+ - (f^2 \cdot n)/K_{eq,FNR}}{(1 + f^- + f^{-2}) \cdot (1 + n^+) + (1 + f + f^2) \cdot (1 + n^+) - 1}, \tag{5.2.22}$$

where Fd^{tot} and $NADP^{tot}$ are conserved quantities, as described in Ch. 3, S. 3.3.1 and V^{max}_{FNR} is the maximal velocity of FNR enzyme. f, f^-, n^+ and n are the normalised concentrations

$$f = \frac{Fd^{tot} - F}{K_{M,F}}, \ f^- = \frac{F}{K_{M,F}}, \ n^+ = \frac{NADP^{tot} - N}{K_{M,N}}, \ n = \frac{N}{K_{M,N}}, \tag{5.2.23}$$

and $K_{eq,FNR}$ is the equilibrium constant determined by standard potentials (E^0) as described by Eq. 3.3.8

$$K_{eq,FNR} = e^{\frac{2\Delta G^0_1 - \Delta G^0_2 - \Delta G^0_3}{RT}}. \tag{5.2.24}$$

where

$$\Delta G_1^0 = FE^0(\text{Fd}/\text{Fd}^-), \tag{5.2.25}$$

$$\Delta G_2^0 = FE^0(\text{NADP}^+/\text{NADPH}), \tag{5.2.26}$$

$$\Delta G_3^0 = RT\ln(10)\text{pH}_{\text{stroma}}, \tag{5.2.27}$$

and R and T stand consequently for the universal gas constant and the temperature and F is the Faraday constant[1].

Energy demand

For simplicity, the energy demand in the Ebenhöh model [26] was modelled as independent, simple mass-action kinetics

$$v_{\text{ATPconsumption}} = k_{\text{ATPconsumption}} \cdot A, \tag{5.2.28}$$

$$v_{\text{NADPHconsumption}} = k_{\text{NADPHconsumption}} \cdot N. \tag{5.2.29}$$

Since this does not reflect the actual coupled demand through the main energy consumer, Calvin-Benson-Bassham cycle, further in this work we introduce the energy consuming reaction

$$v_{\text{CoupledDemand}} = k_{\text{CalvinDemand}} \cdot A \cdot N \tag{5.2.30}$$

where $k_{\text{CalvinDemand}}$ is the rate constant for simultaneous consumption of ATP and NADPH. The rate was estimated from the steady state concentrations of ATP and NADPH [204] to fit the kinetics of carbon assimilation

$$v_{\text{CO}_2\text{assimilation}} = k_{\text{CalvinDemand}} \cdot [A]_{ss} \cdot [N]_{ss} \tag{5.2.31}$$

$$k_{\text{CalvinDemand}} = \frac{0.82[\frac{mM}{s}]}{1.92[mM] \cdot 0.3[mM]} \tag{5.2.32}$$

$$k_{\text{CalvinDemand}} = 1.42[\frac{1}{mM \cdot s}]. \tag{5.2.33}$$

With such representation of the energy demand we avoid implementation of the whole carbon cycle into the model, yet, we can analyse how changes in the ratio between ATP and NADPH affect the electron transport chain.

Cyclic electron flow, PTOX and NDH

To include the alternative mechanisms of supplying ATP to meet the Calvin energy demand descriptions of cyclic electron flow around PSI, involvement of PTOX in plastoquinone oxidation and NDH in plastoquinone reduction were included. As in [26], we assume FQR catalysing role in reduction of PQ. The rate of cyclic electron flow is described by a simple mass-action kinetics

$$v_{\text{FQR}} = k_{\text{FQR}} \cdot F^2 \cdot (\text{PQ}^{\text{tot}} - P), \tag{5.2.34}$$

that under most conditions should yield a rate of approximately 10% of the linear electron flow. This description is an over simplification, as today we now that there are numerous identified modes of cyclic

---

[1]Please do not confuse with the F state variable for reduced ferrodoxin pool

flow, but as there kinetic properties are not fully understood and they all result at the end in re-injections of electrons back to the PQ pool, we decided to keep only one mechanism as in [26].

The oxidation of the plastoquinol pool catalysed by the plastoquinone terminal oxidase was modelled as a simple mass-action rate law

$$v_{PTOX} = k_{PTOX} \cdot O_2^{ext} \cdot P, \tag{5.2.35}$$

where O_2^{ext} is the external source of oxygen and is a fixed parameter corresponding to 250 μM of oxygen.

In the absence of oxygen, a slow reduction of the plastoquinone pool may be possible due to electrons transferred from external sources, such as glycolysis, which can be mediated by the NADH reductase NDH. The rate of NDH reaction is modelled as in [26] by a simple mass-action rate law

$$v_{NDH} = k_{NDH} \cdot (PQ^{tot} - P). \tag{5.2.36}$$

Lumenal acidification

Again, we assume constant buffering of protons in the lumen and a possible current of protons leaking over the thylakoid membrane. The proton leak is introduced with the same reaction rate as in the qE model (Eq. 4.3.34), where k_{leak} is set to 0.010 s^{-1}. The overall change in the lumenal pH depends therefore on the rate of photosystem II, cytochrome b6f, ATP synthesis and the leak flux, and the dynamics of the proton concentration is described by Eq. 4.3.2.

5.2.3 Kinase-phosphatase activity

It is assumed that state transitions are governed by a kinase-phosphatase pair. The Stt7 kinase is directly responsible for the relocation of antenna from PSII to PSI and is activated by a reduced plastoquinone pool [113]. The activity of the kinase is therefore modeled as in [26] by a Hill kinetics with moderate cooperativity ($n_{ST} = 2$) to describe the rate of phosphorylation of LHCII

$$v_{Stt7} = k_{Stt7} \cdot \left(\frac{1}{1 + \left(\frac{(PQ^{tot} - P)/PQ^{tot}}{K_{M,ST}} \right)^{n_{ST}}} \right) \cdot (1 - L) \tag{5.2.37}$$

with $K_{M,ST}$ setting the half-activity of Stt7 at 20% reduction of PQ and L standing for the fraction of phosphorylated antenna.

The phosphatase Pph1 is performing the de-phosphorylation of phosphorylated antennae and allows for their reconnection to PSII. Due to no further evidence, the enzyme is considered to be constitutively active [2]

$$v_{Pph1} = k_{Pph1} \cdot L. \tag{5.2.38}$$

5.2.4 Relative cross-sections

In their model, Ebenhöh *et al.* [26] assumed that antenna are always either associated with PSI or PSII. Moreover light harvesting complexes could be considered as either fixed or mobile. Fixed antenna (σ_{PS}^0) referred to the fraction of all core pigments that are always associated with specific photosystem, whilst

---

[2]it is assumed that the enzyme works at a constant rate regardless of physiological demand

mobile antenna $(1 - \sigma^0_{\text{PSII}} - \sigma^0_{\text{PSI}})$ referred to the fraction of monomeric and trimeric complexes that were the subject of state transitions and movement between the photosystems. The stoichiometry proposed by Ebenhöh *et al.* [26] allowed for 80% of total chlorophyll pigments to move, fixing 20% of total antenna at PSI and allowing theoretically for none of the antenna to be associated with PSII.

Here, we first changed the amount of fixed antennae. According to the reported data summarised in Ch. 1, Tab. 1.4.1, we assume 10% fixed antenna on PSII and 37% fixed antenna on PSI. Next, we abandoned the assumption that antenna are always either associated with PSI or PSII in favour of a possibility of 'free' antenna formation. In Fig. 5.2.3 the scheme of possible state transitions is presented. With a certain probability $(P(qT))$ a fraction of phosphorylated antenna (L) detached from PSII instead of attaching to photosystem I, can stay in quenched form somewhere within thylakoid membrane, constituting the third pool of antenna referred to as free antenna (σ_{free}). That way the relative cross section of photosystems can be described as

$$\sigma_{\text{PSI}} = \sigma^0_{\text{PSI}} + P(qT)(1 - \sigma^0_{\text{PSII}} - \sigma^0_{\text{PSI}}) \cdot L \qquad (5.2.39)$$

$$\sigma_{\text{PSII}} = \sigma^0_{\text{PSII}} + (1 - \sigma^0_{\text{PSII}} - \sigma^0_{\text{PSI}})(1 - L), \qquad (5.2.40)$$

with the free pool calculated from

$$\sigma_{\text{free}} = (1 - P(qT))(1 - \sigma^0_{\text{PSII}} - \sigma^0_{\text{PSI}}) \cdot L. \qquad (5.2.41)$$
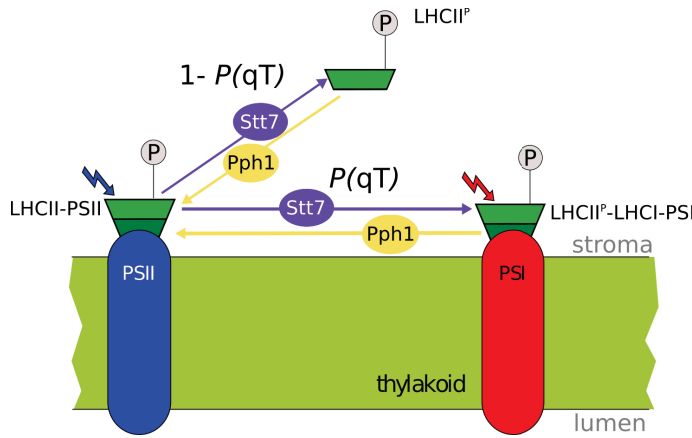
Figure 5.2.3: Scheme of the implemented model of state transitions. Phosphorylated antennae complexes can either detach from photosystem II and move towards photosystem I to form LHCII^P-LHCI-PSI supercomplex or aggregate in thylakoid membrane in a free, probably quenched form (LHCII^P).

5.2.5 Fluorescence signal

As in the previous chapter, the fluorescence can be calculated from the PSII status and depends now on the relative cross section of photosystem II

$$\Phi_F = \sigma_{\text{PSII}} \cdot \left(\frac{k_F}{k_{H_0} + k_F + k_P} [B_0] + \frac{k_F}{k_{H_0} + k_F} [B_2] \right), \qquad (5.2.42)$$

where k_{H_0} stands for a baseline quenching that does not require activation and similar as for the qE model, was included to account for a small quenching observed in double mutants, where both PsbS and zeaxanthin dependent activation is removed [59].

5.2.6 Dark adaptation

If not stated otherwise the PAM experiments were performed on dark adapted cultures. The vector of initial concentrations used in simulations:

```
y0 = np.array([0.4, 4.0, 2.64e-06, 0.5, 0.3, 2.5e-4, 5.1e-02, 2.5, 0]),
```

corresponds to almost completely oxidised PQ and Fd pool, completely reduced PC pool, almost no available ATP and NADPH, lumenal pH of 7.2, almost no phosphorylated antenna, completely undamaged PSII and inactive ATPase.

5.3 Results

To demonstrate that the description of the photosynthetic electron flow and selected photoprotective mechanisms were implemented correctly, and that the model can be used in a similar manner as in [26], we started the analysis with answering the same principle question: "why are state transitions more pronounced in low light and seem to be repressed under high light conditions?" [26]. Obtaining an agreement between our and the Ebenhöh model [26], we used the state transitions module to compare the modes of activation of state transitions (anoxia vs. light induced).

Next, we tested the hypothesis regarding possible aggregation of antenna within the thylakoid membrane and systematically varied the ATP and NADPH demand to observe the influence on the PETC.

5.3.1 A need for state transitions

To understand the need for a mechanism of state transitions, we investigated the bahaviour of the system where such mechanism is not present. As in [26], we set the rate constants for the kinase Stt7 and the phosphatase Pph1 to zero and fixed the relative cross-section of PSII to different values, ranging from 0 (reflecting PSII mutant) to 1 (reflecting PSI mutant). We varied light intensities and analysed the state after two hours of light exposure. In Fig. 5.3.1 the computed A) redox state of the PQ pool, B) stromal ATP concentration and C) lumenal pH are displayed. They are represented as a function of the relative PSII cross-section (σ_{PSII}) and the total light intensity available to the system. As reported by Ebenhöh *et al.* [26], a sharp transition between a strongly oxidised and a highly reduced PQ pool for low light intensities is observed. When the σ_{PSII} is too small, the pool is almost completely oxidised, while for too large cross-sections, it is extremely reduced. Such lack of flexibility illustrates the need for a certain mechanism to adapt the relative antenna cross-section under low light conditions to maintain a redox poise, namely state transitions. Additionally, the observed huge reduction of pH under high light intensities points toward a need for mechanisms such as qE.

By switching on the mechanism of state transitions we could investigate the change in the steady state behaviour of the system and follow the dynamics of each reaction rate (Appendix, Fig. A2).

5.3.2 Light induced vs. anoxia induced qT

Next, we used the model to reproduce the dynamics of state transitions by simulating the exact same experimental set-ups as the one used in [26]. In Fig. 5.3.2 the calculated fluorescence signal (red) is plotted

A reduced PQ pool

B stromal ATP concentration

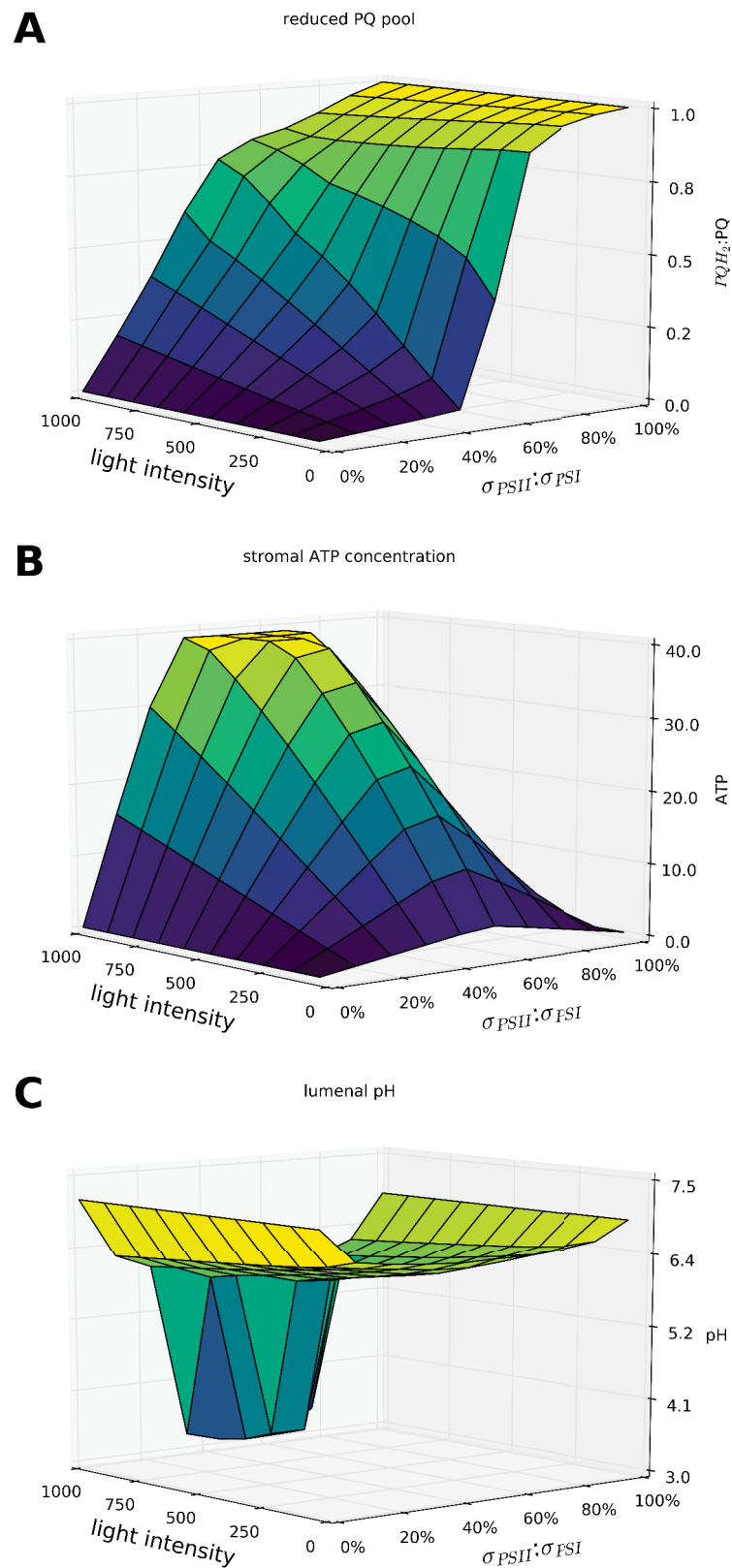**C** lumenal pH

Figure 5.3.1: Simulated state of the system after 2 hours of adaptation to varying light conditions (y-axis) with a fixed relative cross-section of PSII (x-axis). On z-axis (A) the reduced fraction of PQ pool is displayed; (B) stromal concentration of ATP; and (C) lumenal pH. Results of our simulation are in agreement with the predictions reported by Ebenhöh *et al.* [26].
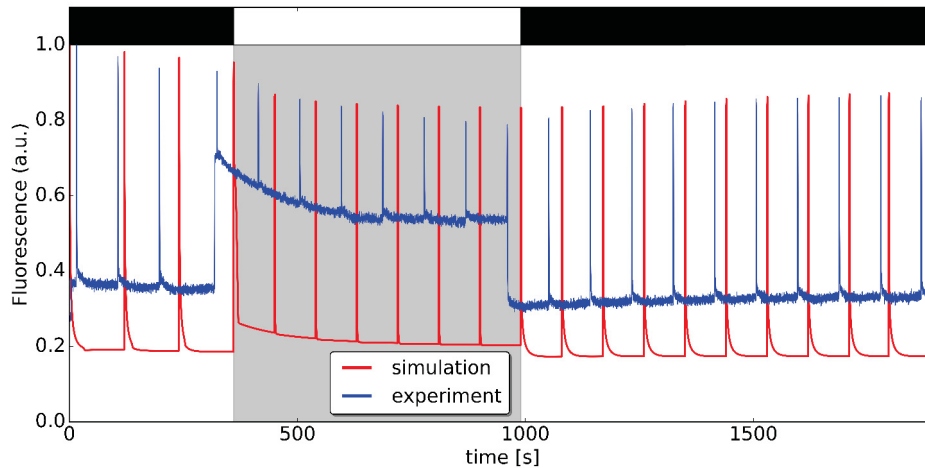
Figure 5.3.2: State transitions induced by a moderate light (100 μEm^{-2}s^{-1}). After three pulses of saturating light applied to a dark adapted cell light was switched on and six additional pulses were applied. The light was switched off after 10 minutes and further measurements reflect the dynamics of de-phosphorylation.

over the experimental results (blue) reported in the manuscript [26].

Dark-adapted *Chlamydomonas* cells were further incubated in the dark for 5 min after which they were exposed for 10 min to a moderate light (100 μEm^{-2}s^{-1}) and then returned to darkness. Saturating light flashes were applied at regular intervals, every 90 s, and the fluorescence signal was recorded. The dynamics of the maximal fluorescence in the light (F$'_M$) reflects the change in antenna cross section of PSII. Our simulations quantitatively reproduce both the transition from State 1 to State 2, as well as the reverse movement in the dark. However, the steady-state fluorescence (F$_s$) is significantly lower in our simulations than in the experiment, similarly to simulations obtained by the Ebenhöh model. On the contrary to their assumption that a more detailed model of the internal processes in PSII may be necessary to refine the calculation of the fluorescence signal, we argue here that the cells used for this particular experiment were not in a healthy condition ($\frac{F_v}{F_M} \approx 0.6$) and therefore we did not aim at fitting our model to this data set. Moreover, the observed increase in the experimental F$_s$ could not be easily reproduced by us while applying the same experimental conditions (see example fluorescence traces in the Appendix, Fig. A1).

Although the role of state transitions under low light intensities is clear, under laboratory conditions it is not trivial to induce the mechanism in *Chlamydomonas* by light. Therefore a common method applied widely in the field is an induction through anoxia. With a removal of oxygen the plastoquinone pool becomes reduced and thus the kinase Stt7 gets activated. In Fig. 5.3.3 A the simulation reproduces the fluorescence dynamics in the experiment where state transitions are induced by anoxia (no oxygen period marked in grey). A dark adapted sample is exposed to three pulses of saturating light after which the culture is sealed and no external source of oxygen is provided. While consuming the available oxygen the PQ pool becomes highly reduced, activating the Stt7 kinase and causing a dynamic reduction of fluorescence emission from photosystem II. After 15 minutes of anoxia air is re-applied by bubbling and the reversed movement of antenna is observed through the relaxation of fluorescence. In the model, anoxic conditions are simulated by switching the v_{PTOX} rate to 0. The calculated fluorescence signal captures well the dynamics of State 1 to State 2 transition, but underestimates the relaxation kinetics, therefore we increased the rate constant of de-phosphorylation (Fig. 5.3.3 B).

Increasing the rate constant of Pph1 activity leads to a faster F$'_M$ relaxation in the last phase of the experiment, but it contributes to an increase of F$'_M$ during the anoxia. A possible explanation is that our assumption of a constitutively active phosphatase is false. We have therefore modelled the activity of Pph1 in a similar
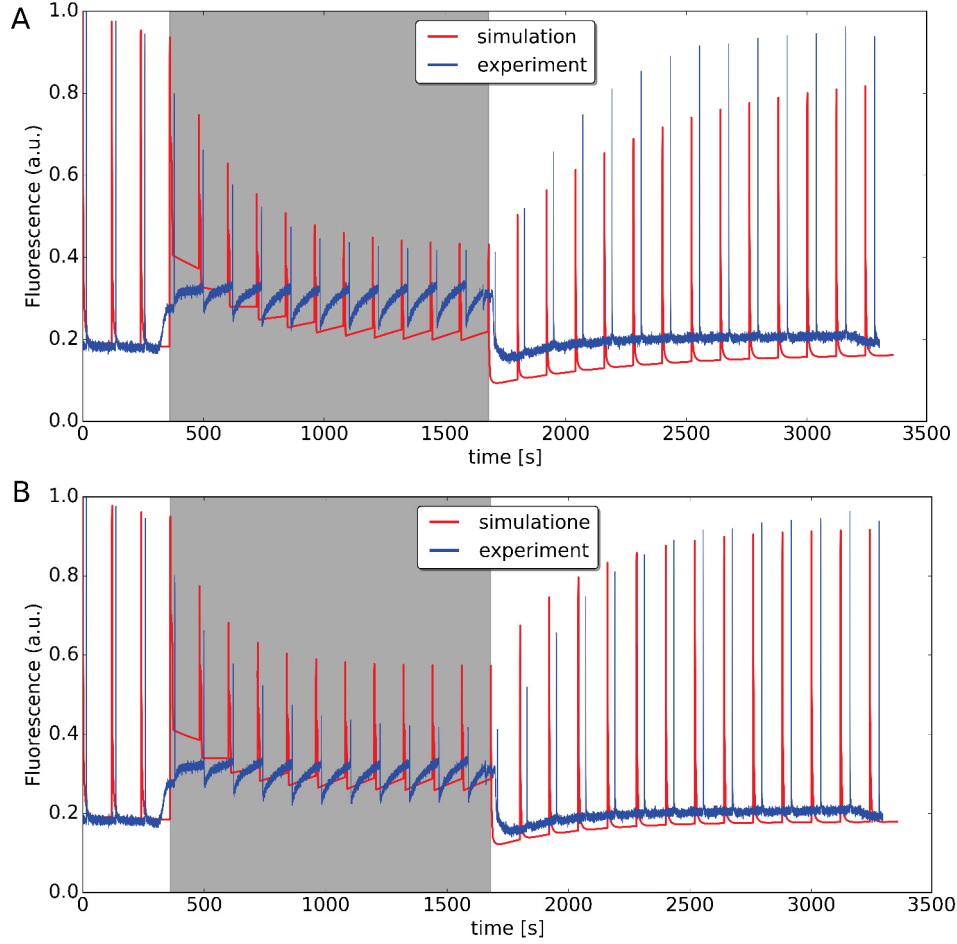
Figure 5.3.3: State transitions induced by anoxia. After three pulses of saturating light applied to a dark adapted cell external source of oxygen is removed and decrease in fluorescence signal is observed due to state transitions. The anoxic phase is marked in grey. B) Experimental and simulated fluorescence traces for increased rate constant of de-phosphorylation ($2k_{\text{Pph1}}$).

manner as the Stt7 kinase using Hill kinetics with moderate cooperativity ($n_{\text{ST}} = 2$)

$$v_{\text{Pph1}} \quad = \quad 2k_{\text{Pph1}} \cdot \left(\frac{1}{1 + \left(\frac{P/\text{PQ}^{\text{tot}}}{K_{\text{M,ST2-1}}} \right)^{n_{\text{ST}}}} \right) \cdot L, \quad (5.3.1)$$

with $K_{\text{M,ST2-1}}$ setting the half-activity of Pph1 at 80% oxidation of PQ. It works antagonistically to the activity of Stt7 kinase, with its maximal rate at completely reduced plastoquinone pool. In Fig. 5.3.4 we plot the calculated change in the rate of phosphorylation and de-phosphorylation, depending on the redox state of the PQ pool, whilst keeping L fixed at 50%.

Under these assumptions the simulated fluorescence trace of anoxia induced state transitions is in a much better agreement, both qualitative and quantitative, with the experimental data than any previously obtained results (Fig. 5.3.5).

5.3.3 Revisiting state transitions: quenching hypothesis

By monitoring fluorescence emission from PSII we can further examine if during state transitions antenna actually transfer the energy between the photosystems or quench the excess of energy after the detachment
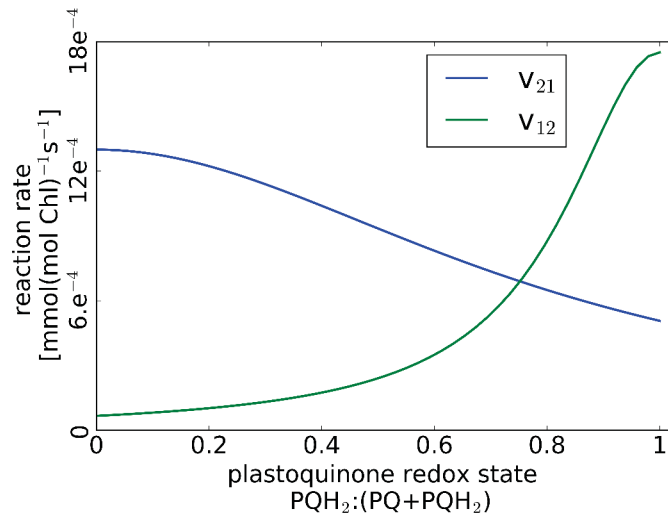
Figure 5.3.4: Reaction rates of kinase (v_{12}) and phosphatase (v_{21}) depending on the redox state of PQ pool. Both enzymes activity is simulated using saturation kinetics with the same, moderate cooperativity.
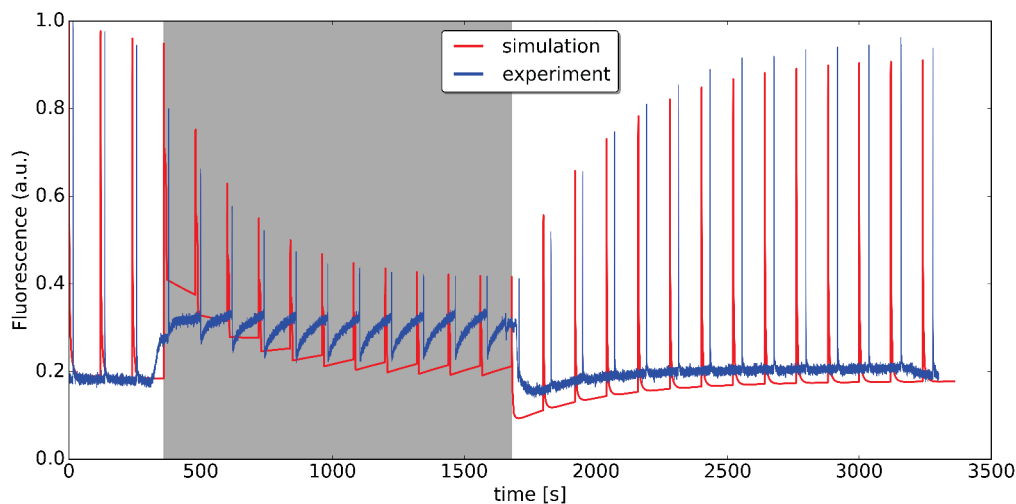
Figure 5.3.5: State transitions induced by anoxia. The simulated fluorescence signal (red) was calculated by a mathematical model where the reaction rate of phosphatase was changed to follow the saturation kinetics (Eq. 5.3.1).

from PSII. We can predict the fluorescence signal under various scenarios by changing the probability of attaching antenna during the transfer ($P(qT)$ in Eq. 5.2.41-5.2.40). $P(qT)=1$ reflects situation where all phosphorylated antenna attach to PSI, whilst $P(qT)=0$ corresponds to a situation where all phosphorylated antenna quench the energy. In Fig. 5.3.6 A simulated fluorescence traces for light induced qT for two extreme situations are plotted (red line for the simulations assuming energy transfer and blue line for the simulations assuming energy dissipation). Despite the fact that the difference between F'_M and F_s under these two conditions are minor, their existence confirms that the model can well capture the feedback loop through the cyclic electron flow. In Fig. 5.3.6 B the change in the relative cross sections is depicted, showing the increase in the pool of free antenna during the light treatment in the energy dissipation mode. In Fig. 5.3.6 D we see how the rate of cyclic electron flow increases during the light phase in the model that assumes complete energy transfer. Assuming such energy transfer to PSI, some energy is used to be re-directed back to the PQ pool through FQR and therefore the PQ is more oxidised (Fig. 5.3.6 C), which correlates with the lower F_s.

To investigate further the redox control over the plastoquinone pool we expanded our studies by simulating the behaviour of the ΔPC mutant. This strain is lacking plastocyanin and by interrupting the electron flow around PSI it prevents the complete oxidation of the plastoquinone pool by illumination [79]. In Fig. 5.3.7 the
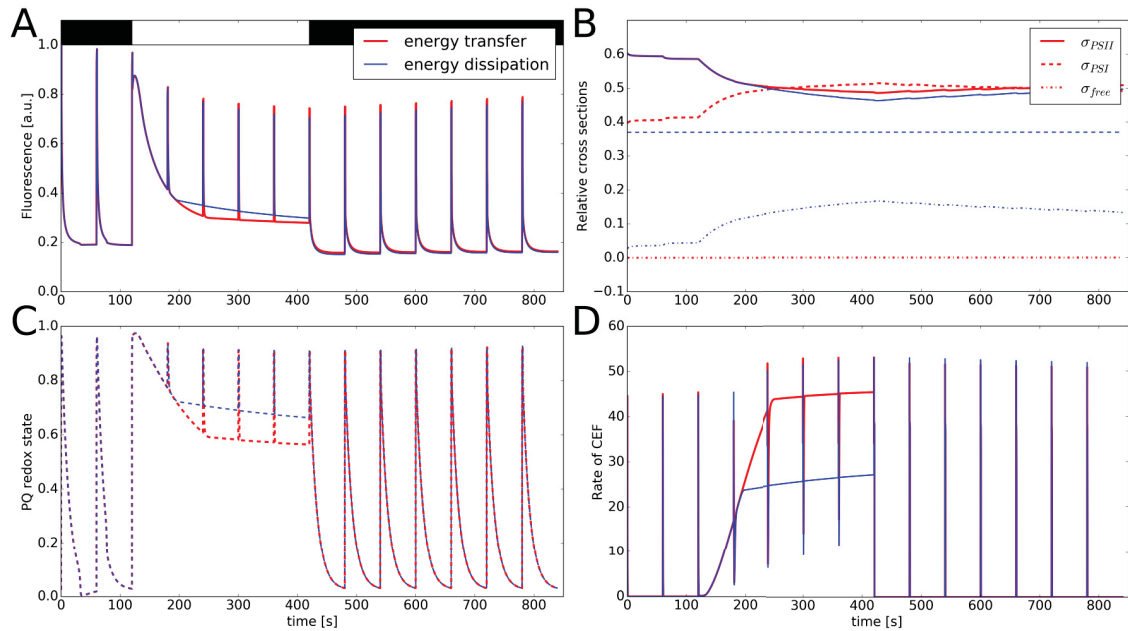
Figure 5.3.6: Light induced state transitions simulated assuming complete energy dissipation (blue) or energy transfer (red). A) The calculated fluorescence signal with an observable decrease of fluorescence due to the State 1 to State 2 transition. B) The relative cross section of PSII (solid line), PSI (dashed line) and pool of free antenna (dotted line) for both cases. Under the complete energy transfer scenario, the pool of free antenna is zero. C) Energy transfer to PSI contributes to faster oxidation of PQ pool in light. D) The PQ oxidation is achieved through increased rate of cyclic electron flow under the energy transfer assumption.

simulated response of ΔPC mutant to light is displayed. Correctly, no difference in the emitted fluorescence or in the PQ redox state is noticed while assuming the energy transfer or quenching mode. Despite changes in the antenna cross-section, no feedback to PQ is possible and PQ pool is completely reduced in light (Fig. 5.3.7 B).
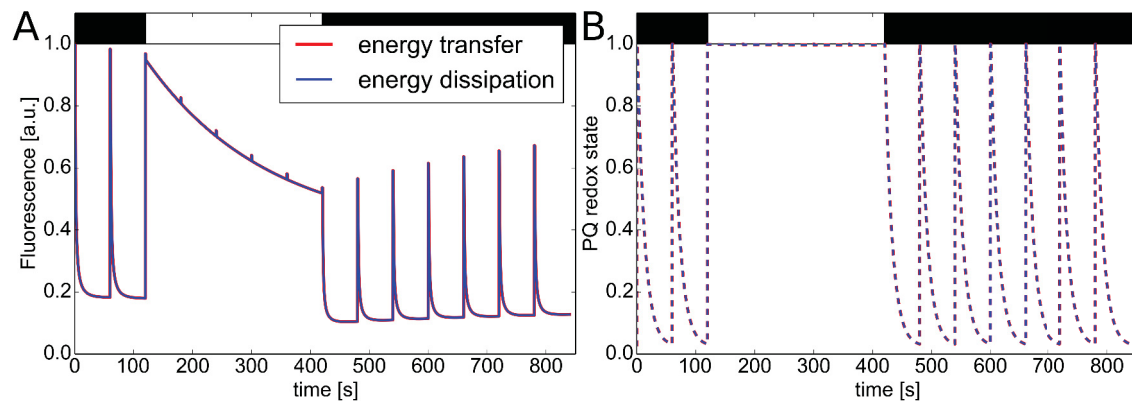
Figure 5.3.7: Light induced state transitions in ΔPC mutant, simulated assuming complete energy dissipation (blue) or energy transfer (red). A) The calculated fluorescence signal with an observable decrease of fluorescence due to the semi-State 1 to State 2 transition. B) Redox state of the PQ pool. Regardless of the scenario, there is no difference in the redox state of the PQ pool, as no redox feedback mechanism is present in this strain.

In order to compare the outcome of our simulation with experimental data, we collected preliminary fluorescence traces using FluorCam, where we could expose several cells simultaneously to the same conditions. In Fig. 5.3.8 we display the fluorescence traces of dark adapted wild type and ΔPC mutant, where state transitions were induced by (A) low light and (B) by adding 0.75 μL of the uncoupling agent FCCP. By transporting hydrogen ions through a cell membrane, FCCP disrupts the synthesis of ATP and the whole electron transfer in a similar manner as removal of oxygen. Although the treatment with an uncoupler

leads to a similar fluorescence emission pattern in both WT and ΔPC mutant, the kinetics of the WT is not consistent with the one simulated by our model (Fig. 5.3.3). Moreover, we observe the difference in the fluorescence relaxation kinetics in the mutant exposed to light and the one treated with an uncoupler. We can not rule our the possibility that the treatment with FCCP actually does not induce state transitions as anoxia, and therefore it would be useful to repeat these experiments under no oxygen conditions.
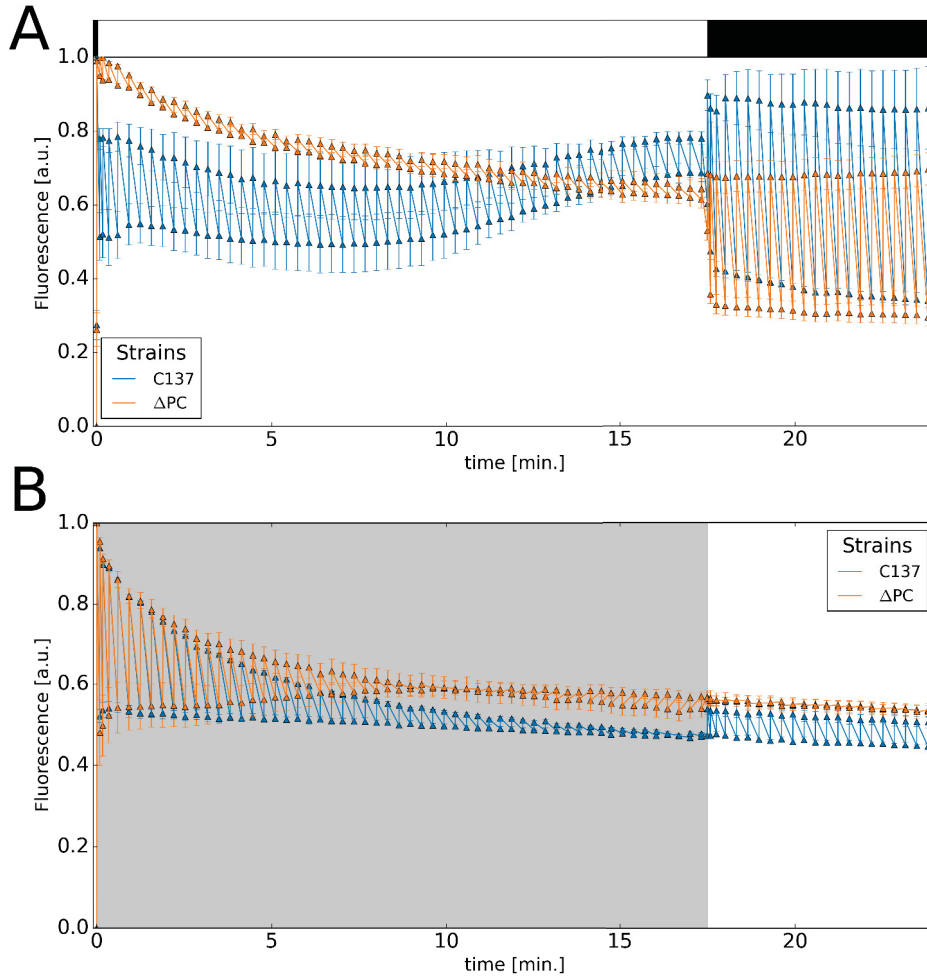
Figure 5.3.8: Fluorescence traces of wild type C137 (blue) and ΔPC mutant (orange) obtained using FluorCam. A) Light induced state transitions. Variable fluorescence of mutant is significantly lower than of the wild type. The rate of relaxation in the darkness is comparable. B) State transitions induced chemically, by adding an uncoupling agent FCCP. Fluorescence kinetics of WT and mutant are qualitatively the same.

5.3.4 ATP and NADPH demand

So far ATP and NADHP consuming reactions are assumed to work independently. In order to reflect the more constrained ATP and NADPH demand by Calvin cycle the new rate is introduced (Eq. 5.2.30). The overall change in ATP and NADPH stromal concentrations are therefore described by following equations

$$\frac{dA}{dt} = v_{\text{ATPsynthase}} - v_{\text{CoupledDemand}}, \tag{5.3.2}$$

$$\frac{dN}{dt} = v_{\text{FNR}} - k_{\text{nrNADPHdemand}} \cdot v_{\text{CoupledDemand}}, \tag{5.3.3}$$

where $k_{\text{nrNADPHdemand}} = \frac{2}{3}$, keeping the ratio between ATP and NADPH fixed. In Fig. 5.3.12 A we plot the time evolution of state variables during the continuous exposure to a high light intensity. The immediate

reduction of the PQ pool inhibits the linear electron flow and it takes 500 s for a system to reach the break point at which pool concentrations are within the range that allow for a system relaxation. By investigating the reaction rates, we envisage that increase of the cyclic electron flow might contribute to faster relaxation of PQ pool. In Fig. 5.3.12 B we plot the time evolution of state variables when the rate constant of cyclic electron flow is increased 10 fold. Indeed, the re-injection of electrons to PQ seems like a reasonable solution for a system to maintain a certain flexibility in response to energy demand with fixed ATP to NADPH ratio. The similar behaviour was obtained after increasing the rate of PTOX 10 fold. This analysis suggests that certain flexibility in the system is needed and therefore for further analysis we keep the separate consuming reactions instead of artificially increasing alternative electron pathways.
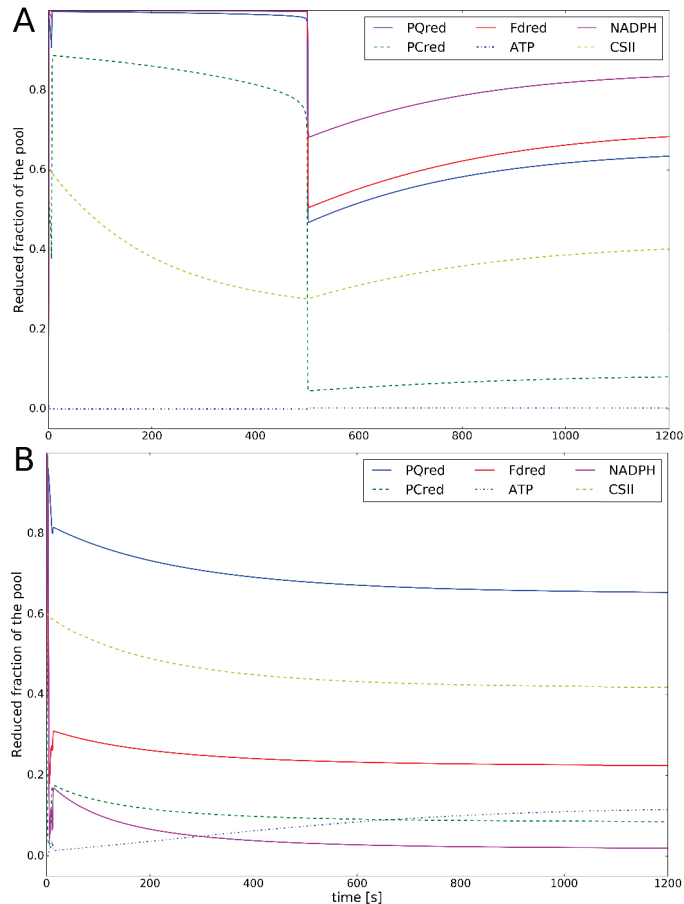
Figure 5.3.9: Results of a simulation of WT *Chlamydomonas* with a coupled energy demand, exposed for 20 minutes to a light of 1000 μEm^{-2}s^{-1}. A) The evolution of state variables showcase that it takes a certain amount of time for the system to balance the redox state of PQ in a response to fixed ATP to NADPH demand. B) A 10 fold increase in the k_{cyc} rate rescues the redox state of the cell.

5.3.5 Adding qE module to the model of qT

With a proper representation of state transitions, the model (Eq. 5.2.1-5.2.9) was complemented with two additional differential equations describing quencher dynamics, exactly as introduced in the previous Chapter (Eq. 4.3.5-4.3.6). In Fig. 5.3.10 we display the value of the quenching variable as a function of the concentration of zeaxanthin and protonated LHCII.

In addition to processes described in [26], our model includes a mechanism of delayed ATP activation, photoinhibition (modelled as a rate of PSII damage and repair), state transitions and high energy dependent quenching with pH and xanthophyll cycle dependent components. With all mechanisms in place, the
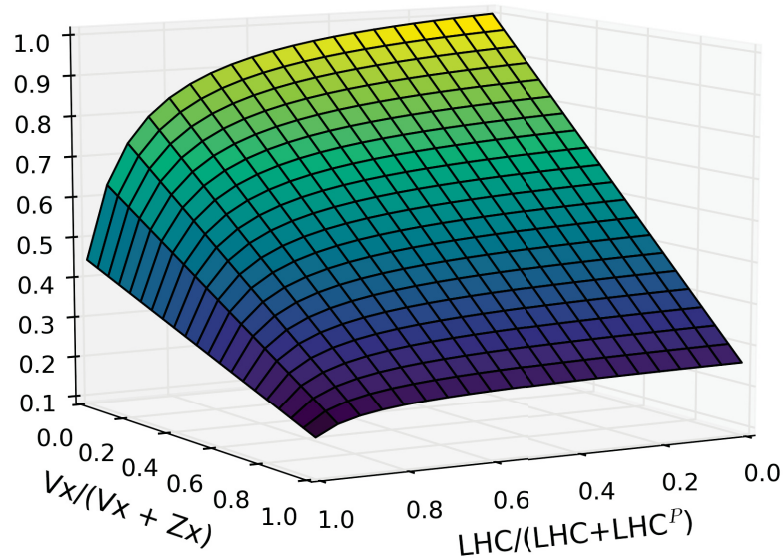
Figure 5.3.10: Normalized quencher value (z-axis) depending on the concentration of violaxanthin (x-axis) and non-protonated LHCII (y-axis). Maximal quencher activity is reached when the pool of xanthophylls consists of only zeaxanthin (Vx=0) and all antennae are protonated (LHC/(LHC + LHC^P)=0).

simulated light-saturation curve of photosynthesis (Fig. 5.3.11) shows a plausible behaviour with initial linear dependency of oxygen evolution and light intensity, maximal efficiency at around $1000\mu\mathrm{Em}^{-2}\mathrm{s}^{-1}$ and slow decrease due to the implemented mechanism of photoinhibition for higher light intensities.
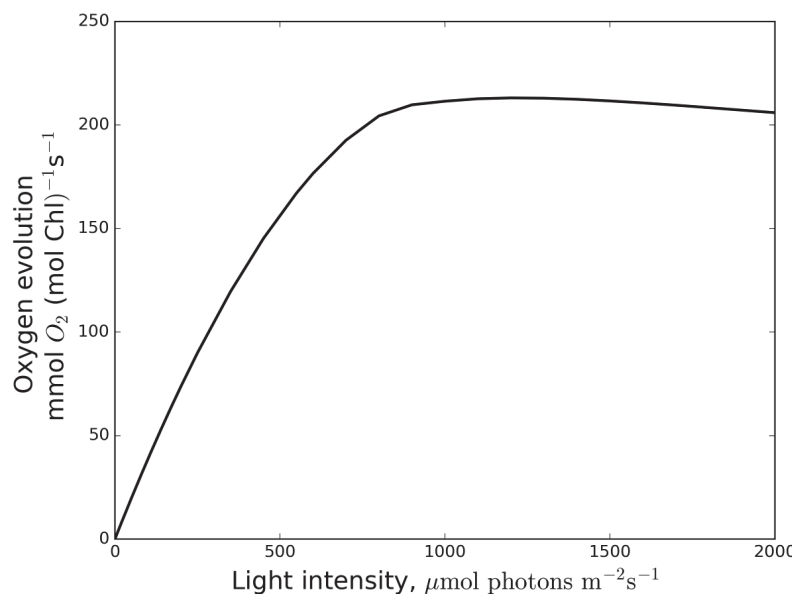
Figure 5.3.11: Simulated light-saturation curve of photosynthesis for a wild type *Chlamydomonas*. Oxygen evolution is equal to a half of the rate of photosystem II, according to Eq. 1.2.5, p. 33.

While investigating the actual interplay between qE and qT under various light intensities (Fig. 5.3.12), we identified a need to change the description of the reaction rate of Stt7 kinase. With a simple dependency on the redox state of the PQ pool (Eq. 5.2.37), the kinase operates even under very high light intensities (Fig. 5.3.12 D) leading to a stronger state transitions than under low light intensities, where the mechanism is believed to be more important. It is assumed that the Stt7/STN7 activity under high light may be regulated via the ferredoxin–thioredoxin system [205]. The kinase is inactivated by reducing equivalents, that by shuttling

from ferredoxin and thioredoxin can reduce the disulphide bond in the lumenal N-terminal domain of Stt7/STN7 [205]. Here, this complex signalling pathway is simplified to directly depend on the concentration of reduced Fd. With no further evidence, we applied heuristic approach by complementing the saturating kinetics of Stt7 activity with inhibitory expression that depends on the redox state of Fd pool

$$v_{\mathrm{Stt7}} \quad = \quad k_{\mathrm{Stt7}} \cdot \left(\frac{1}{1 + \left(\frac{(\mathrm{PQ^{tot}}-P)/\mathrm{PQ^{tot}}}{K_{\mathrm{M,ST}}} + \frac{F/\mathrm{Fd^{tot}}}{K_{\mathrm{M,fdST}}} \right)^{n_{\mathrm{ST}}}} \right) \cdot (1-L) \qquad (5.3.4)$$

with $K_{\mathrm{M,fdST}}$ setting the half-activity of Stt7 at 50% reduction of Fd. With this change, the simulated behaviour of the system yields more plausible results. The model was further used to analyse the photosynthetic activity under continuous and fluctuating light and to predict the photosynthetic efficiency of various antennae mutant.
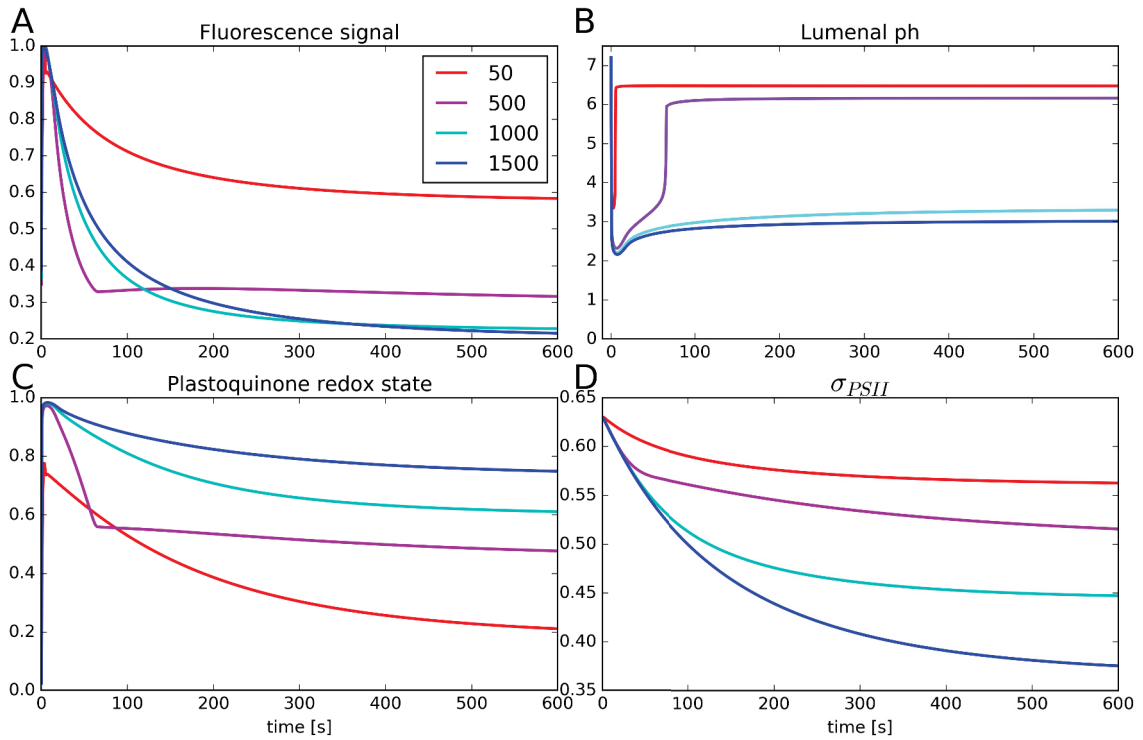
Figure 5.3.12: Results of simulation of WT *Chlamydomonas* exposed for 10 minutes to four different light intensities. A) Steady state fluorescence trace. B) Lumenal pH. C) Redox state of the PQ pool. With the increase in light intensity the fraction of reduced PQ pool increases. D) Relative cross-section of PSII. State transitions are more prolonged under high light intensities suggesting need for a limitation mechanism.

5.3.6 Antenna mutants

The model is used to test the hypothesis that algae with reduced antenna size outperform wild type strains under high light intensities [206, 207]. We directly associated the change in antennae size with change in the chlorophyll content per cell. For that, parameters expressed in regards to the chlorophyll content needed to be changed according to the rate order. First order constants (expressed in s^{-1}) did not require conversion, second rate constants were divided by the conversion factor equal to $\frac{reducedContent}{originalChl}$, third by $\frac{reducedContent}{originalChl}^2$ etc. For instance, the total pool of adenosine is assumed to be equal to 60 mmol(mol Chl)$^{-1}$ for a cell containing 350 mol per m^2 thylakoid membrane. In a 10% antennae mutant we assume a 10% reduction in the chlorophyll content, and so the chlorophyll decreases to 315 mol per m^2 thylakoid membrane. The amount of adenosines per chlorophyll will increase proportionally to 66 mmol(mol Chl)$^{-1}$.

The antenna size of the photosystems influences the light-saturation curve of photosynthesis, therefore we simulated the curve for a wild type and three strains with reduced chlorophyll content (by 20%, 10% and 5%) to compare the solar conversion efficiency and productivity of each strain. Light-saturation curves in Fig. 5.3.13 well capture the reported qualitative difference in the photosynthetic performance between the wild type and antennae mutants. The slope of the initial linear increase in all four strains suggests similar photon use efficiency under low light intensities but under high light intensities the 20% reduced mutant show approximately 2-fold higher maximal photosynthetic efficiency (Pmax) than for the wild type.
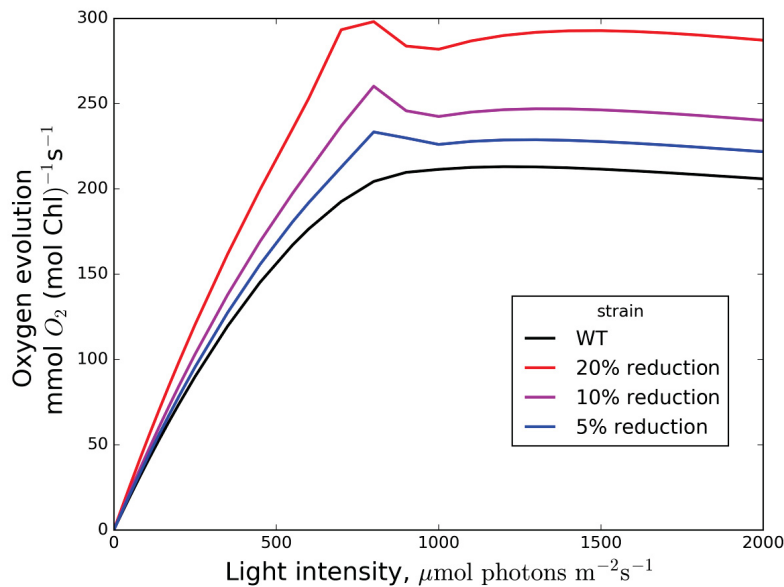
Figure 5.3.13: Oxygen evolution represented as a half of the rate of photosystem II. Initial similar slope for all strains suggests similar photon use efficiency under low light intensities. In agreement with data reported on beneficial performance of antenna truncated mutants, simulated oxygen production rate under high light are higher for all antennae mutants than for the wild type.

5.3.7 Behaviour in the bioreactor

Lastly, the model is applied to study the photosynthetic efficiency of cells grown in a bioreactor. Although the applied light is of a constant intensity, cells grown in bioreactors are exposed to fluctuating light due to their constant movement. We used the data from our collaborators that simulate cells movement in a bioreactor, to model the photosynthetic activity of a single cell grown in bioreactor.

In Fig. 5.3.14 we display the overall results of such simulation for a dark adapted cell. In subfigure A we plot the normalized light intensity that the cell experiences during 100 s. For a simulation we assumed that the maximal light intensity is set to 1000 μEm^{-2}s^{-1}. In subfigure B we plot the calculated fluorescence signal. Interesting behaviour of state variables is captured in subfigure C. Almost no change in cross sections is observed. In Fig. 5.3.14 D we display the photosynthetic reaction rate in terms of oxygen produced.

In order to understand if the history of a cell matters under the given conditions, we run simulations with a constant light of an intensity equal to an average intensity of the light changing variant (here 279 μEm^{-2}s^{-1}). By integrating the area under the curve of oxygen evolution of fluctuating light (5590 mmol O_2 (mol Chl)$^{-1}$) and constant light (5890 mmol O_2 (mol Chl)$^{-1}$) we report that constant light exposure leads to higher photosynthetic efficiency. We used scipy.integrate.trapz method that integrates along the given axis using the composite trapezoidal rule.
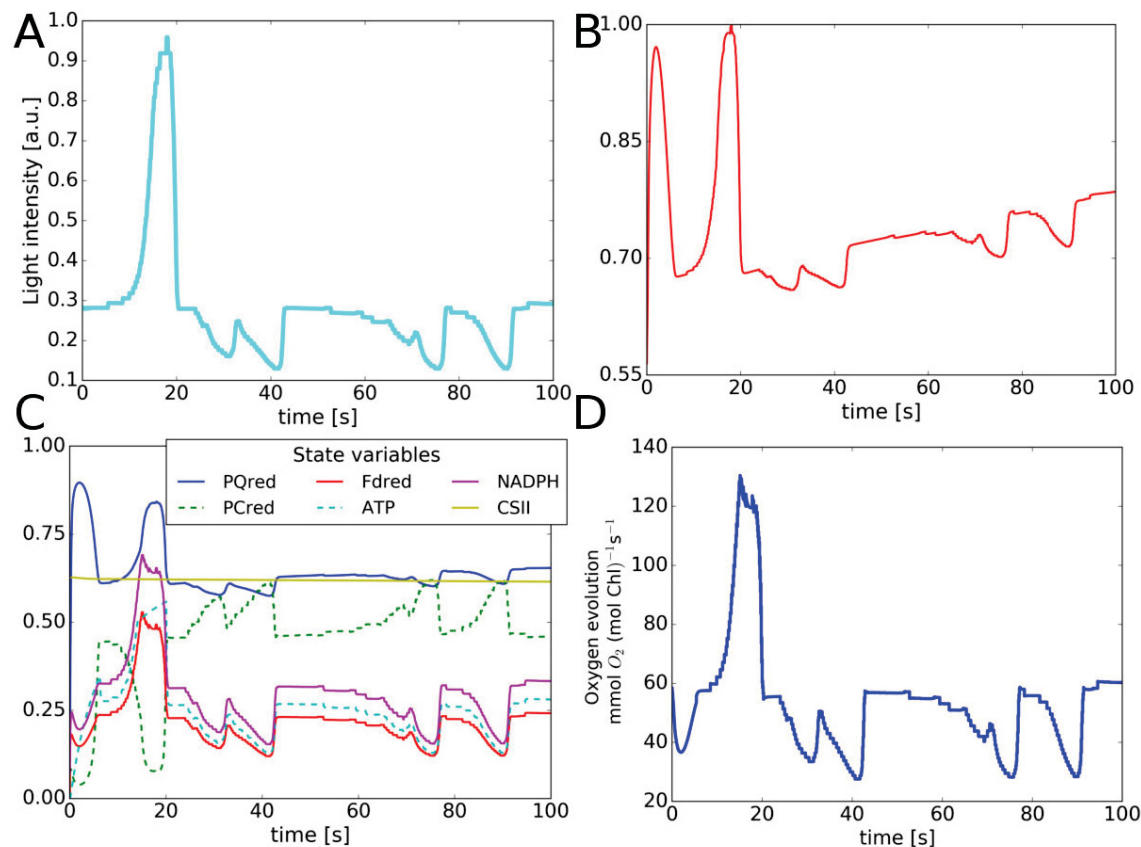
Figure 5.3.14: Simulation of a dark-adapted cell exposed to a fluctuating light. A) Change of the light intensity available to a cell inside the bioreactor. Data obtained from Varun Loomba from Forschunszetrum Jülich. B) Calculated fluorescence emission. C) Change in the state variables of a cell, normalised to total pools. D) Resulting rate of oxygen evolution.

We next checked how sensitive the resulting trajectories are to the initial conditions. We have therefore repeated the simulations with a light adapted cell. In Fig. 5.3.15 we may see that change in the initial conditions influenced the shape of trajectories only in the first seconds of the simulations and they quickly converge to the same trajectory as for a dark adapted cell. The resulting area under the oxygen evolution curve is higher (5877 mmol O_2 (mol Chl)$^{-1}$) than for a dark-adapted cell, probably due to the active ATPase from the first second of simulation.

5.4 Discussion and Outlook

We have developed further a mathematical model that is based on our current understanding of various NPQ mechanisms. By achieving an agreement between our simulations and experimentally observed behaviour, we could confirm that our theoretical implementation is correct. Moreover, with the mathematical description of the processes we could perform interesting analyses of the performance of antenna mutants and cells grown under fluctuating light. It is remarkable that these findings could be obtained still by a very simple model structure, with only 11 differential equations.

Firstly, the analysis of simulated fluorescence traces and comparison to experimental data led to an assumption that phosphatase, so far assumed to be consecutively active, operates according to a saturation kinetics. Despite the fact that after applying Hill kinetics we reached better agreement with experimental data (Fig. 5.3.5), we kept the assumption regarding the unlimited activity in further analysis, as more experimental
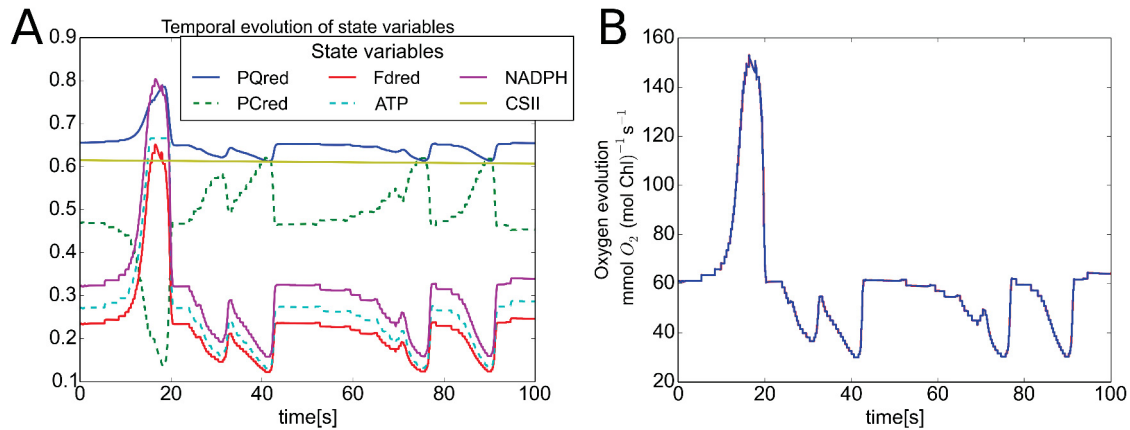
Figure 5.3.15: Simulation of a light-adapted cell exposed to a fluctuating light. A) Change in the state variables of a cell. Due to light adaptation there is no transient reduction of PQ pool observed as in the dark-adapted cell. B) Resulting rate of oxygen evolution. The initial rate in the first 10 seconds is higher than for a dark-adapted cell.

evidence is needed to support this hypothesis.

Next, we used our model to investigate if we can provide a theoretical argument to a vivid debate regarding the possible occurrence of quenching antennae during state transitions. Within the past two years, contradicting observations from European groups were reported, either suggesting possible quenching of phosphorylated antenna [22, 78], and *ipso facto* indicating a need to revisit our current understanding regarding this mechanism, or providing evidence for a complete attachment of phosphorylated antenna [79]. By monitoring fluorescence emission from PSII we simulated two extreme conditions, where antenna transferred the energy between the photosystems and quenched the excess after the detachment from PSII (Fig. 5.3.6). Moreover, we investigated whether the mechanism governing state transitions triggered by anoxia conditions is the same as the mechanism triggered by light. For that we use the PC mutant (ΔPC mutant), where the ETC is blocked and investigated whether there is any difference in the fluorescence traces when there is no feedback on the PQ pool. A preliminary experimental result of state transitions induced by light and anoxia in wild type and ΔPC mutant yield different fluorescence patters (Fig. 5.3.8), a characteristics that cannot be reproduced by our model, as the same mechanism of induction is assumed. A possible explanation is that the actual mechanism triggering the state transitions is different when induced by light or anoxia. Moreover, we acknowledge that the treatment with FCCP could induce different response that anoxia. For those reasons further experimental investigation is required, especially detailed biochemical analyses to compare whether the phosphorylation pattern is the same among strains exposed to different treatments.

A recognised deficiency in the model proposed by Ebenhöh *et al.* [26] was keeping the ATP and NADPH consuming reactions separated. Such representation was believed to be not sufficient to represent the tightly linked energy demand of the main energy consumer, the Calvin-Benson-Bassham cycle. An interesting observation was made here by coupling the rate of ATP and NADPH consumption (Fig. 5.3.12). By fixing the rate of ATP and NADPH consumption to maintain the ratio of 3 ATP consumed per every two NADPH, we observed that under high light intensities, where light is no more a limiting factor and maximal ATP synthesis rate can be obtained, as the system produces one NADPH too much with every linear electron flow, inhibition of the ETC occurs. The immediate reduction of the PQ pool inhibits the linear electron flow and it takes 500 s for the system to reach the break point at which pool concentrations are within the range that allow for the system to relax to a reasonable steady state. By investigating the reaction rates, we envisage that increasing the cyclic electron flow (or rate of PTOX) might contribute to faster relaxation of the PQ pool. Due to missing information about actual energy maintenance, instead of adding other electron sinks, such as Mehler reaction [36], we decided to keep the, apparently necessary, flexibility of the system

by separating the ATP and NADPH consuming reactions. This is of course a temporary solution and we envisage that our modular model can be linked to a more precise description of the Calvin-Benson-Bassham cycle. With a dynamic description of cycle demand, the ratio of ATP and NADPH will change depending on the accumulation strategy (TP vs starch), thus providing certain degree of flexibility, lacking when imposing a fixed ratio.

Lastly, the model was applied to analyse the photosynthetic activity of a cell grown in a bioreactor. Since our model can be integrated for any given light function, we used simulation data from our collaborators interested in cell movement in bioreactors. With a given light function we predicted the state of a cell during the period of 100 s (Fig. 5.3.14). Interestingly, rapid change in the light intensity does not affect PQ sufficiently to activate the Stt7 kinase, therefore the relative cross section of PSII was almost not changed. We were interested in comparing photosynthetic efficiency between a cell exposed to such fluctuating light and the one exposed to constant light of the average intensity and from the preliminary results we conclude that the constant light resulted in a higher photosynthetic efficiency. Understanding potential benefit of growing cells under fluctuating light and finding the precise frequency of light change is of a great economical interest. We envisage that our model in its current state may be used to further investigate the effects of photoacclimation on the productivity of *Chlamydomonas* grown in outdoor reactors and compare our theoretical predictions with available data [208].

5.5 Summary

We have demonstrated that by using more general, mathematical terms, we can study aspects of state transitions that are still poorly understood or under debate. The results of our simulations point towards the hypothesis that Pph1 phosphatase is not consecutively active and actually requires some activation mechanism, here modelled by redox control. Moreover, we could demonstrate that by monitoring fluorescence emission we may distinguish between energy transfer and energy dissipation mode during state transitions. Thanks to the modular structure of the model, we complemented the model of state transitions with the module describing high-energy dependent quenching. The overall model included all three major components of NPQ: qE, qT and qI. Such model was used to study the potential benefit of algae mutants with a truncated antennae size. Our simulations confirm observations in which mutants with 20% reduced chlorophyll content reached 50% higher photosynthetic efficiency. Finally, the model was used to compare photosynthetic dynamics of cells grown under continuous light or fluctuating light in a bioreactor. The results of our simulations indicate that cells grown under continuous light are slightly more efficient. This analysis will be continued in a collaboration with Forschungszetrum Jülich.

6. Including light wavelengths into the model

"If you want to find the secrets of the universe, think in terms of energy, frequency and vibration."

*- **Nikola Tesla**, inventor, electrical and mechanical engineer, physicist a conversation with Ralph Bergstresser (1942)*

In the previous chapters the focus lied on understanding how light intensity affects photosynthesis and triggers acclimation mechanisms, collectively referred to as non-photochemical quenching. In this Chapter I provide arguments for the inclusion of light wavelengths into the model and describe the process of data collection and the development of "spectra module". In order to understand how light wavelengths affect short-term photoprotective mechanisms discussed in previous Chapters, a collaboration between the group of Dr Giovanni Finazzi (CEA-Grenoble, France), Prof. Jun Minagawa (NIBB, Japan) and Dr Oliver Ebenhöh (Heinrich-Heine University Düsseldorf) was established. Firstly, using the Okazaki Large Spectrograph facilities, together with the Assist. Prof. Ryotaro Tokutsu from the NIBB and Dr Oliver Ebenhöh we performed a set of precise spectrometric measurements on four strains of *Chlamydomonas reinhardtii* to collect preliminary data for model construction. Next, I improved the theoretical description of the light function and light absorption, by including light wavelength as a variable and performed a set of simulations to reproduce the experimental data. This is part of an ongoing project and data presented here is preliminary and serves as a proof of concept that the model can be expanded to include precise information about both intensity and wavelength of the light.

6.1   Introduction

Light is critical for photosynthesis. Its excess may cause a photodamage and impairment of the machinery, whilst its deficiency can lead to loss of photosynthetic efficiency. Though a majority of available mathematical models of photosynthesis and non-photochemical quenching are solely focusing on light intensity (as described in Ch. 3), it is known that the light spectra has a great effect on photosynthesis too. First of all, photosystems are composed of various pigments with distinct absorption spectra, therefore they can be preferentially activated by different light wavelengths. Moreover, various photoreceptors are calibrated to perceive light of a specific wavelength, therefore orchestrate the whole photosynthetic machinery. Recently, Petroutsos *et al.* [54] showed that under high light intensities phototropins (blue light sensors) control qE by inducing the expression of the LHCSR3 protein. Dall'Osto *et al.* showed on the other hand the role of red light, as it is less effective than white light in decreasing maximal fluorescence in *Arabidopsis* npq4 mutants [198].

It was therefore desired to include light spectra into the model described in the previous Chapter. In order to change the previous light function to include both intensity and wavelength as variables, a precise set of experiment using sophisticated spectrographic method was used.

6.1.1   The Okazaki Large Spectrograph

The Okazaki Large Spectrograph (OLS) [209] is the largest spectrograph in the world, running on a 30kW Xenon arc lamp and having a compound grating composed of 36 smaller individual gratings. It projects a spectrum of a wavelength range from 250nm (ultraviolet) to 1,000nm (infrared) onto its focal curve of 10m in length (marked with a white arrow in Fig. 6.1.1). The intensity of the monochromatic light at each wavelength is more than twice as much as that of the corresponding monochromatic component of tropical sunlight at noon. It is used for spectroscopical studies of various light-controlled biological processes and here was used to shine simultaneously 22 samples with a monochromatic light of the same light intensity.
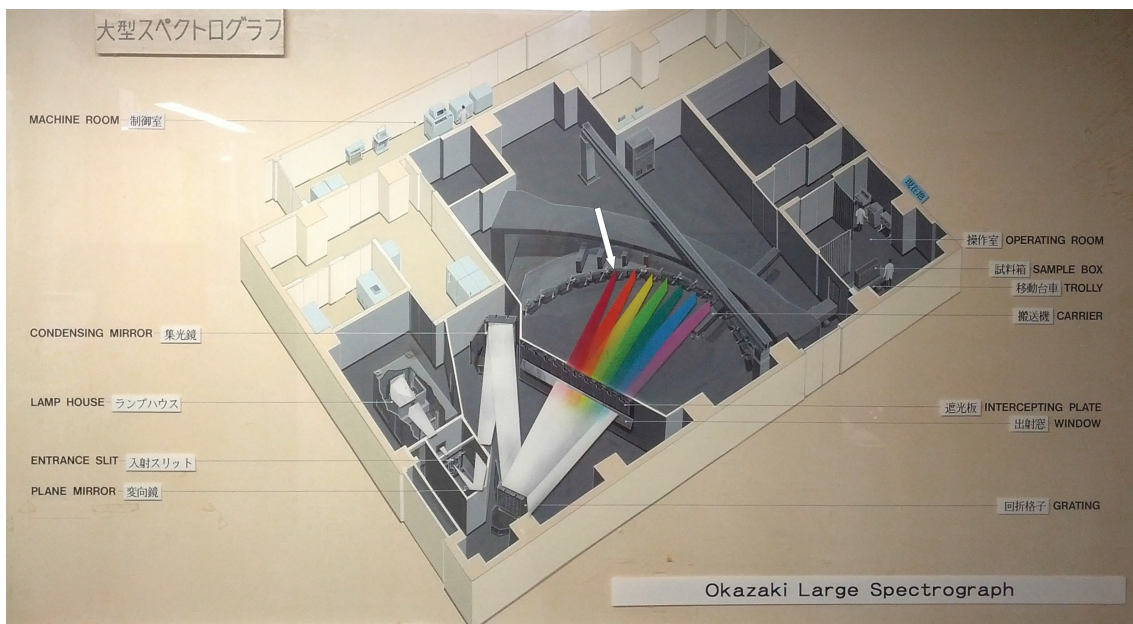
Figure 6.1.1: Scheme of the Okazaki Large Spectrograph. The bench where samples were exposed to light is marked with the white arrow. Picture taken at the entrance to the Operating Room at OLS, Okazaki, Japan.

6.1.2 Aim of the study

Considering that photosystems are composed of distinct pigments that have unique absorption spectra, each photosystem is preferentially activated by different light frequencies. In order to understand how light wavelength affects short term photoprotective mechanisms we combine a dual approach based on precise spectrometric experiments using Okazaki Large Spectrograph facilities and theoretical simulations obtained through mathematical modeling of the photosynthetic electron transport chain **(ETC)**.

Motivated by an apparent role of certain photoreceptors, we used OLS to collect precise photosynthetic data on samples exposed to a monochromatic light. We were interested in understanding how light of a certain wavelength triggers photosythetic activity and acclimatory mechanisms. We have therefore selected four strains of *Chlamydomonas* cultures that differ in their photoacclimatory capacity and exposed them to various light wavelengths and intensities. The exposed samples were immediately frozen and cold fluorescence absorption spectra were collected. From this data information about the relative cross section of photosystem I and photosystem II was drawn. Collected data was used to calibrate the mathematical model of the photosynthetic electron transport chain with new light function that would account for light wavelength. The preliminary results of the experiment allowed to construct the **"spectra module"** and to reproduce the qualitative change in the cross section in the wild type and npq4 mutant. Due to lack of replicates further work on reproducing the quantitative change was withheld until the experiment will be repeated and more data will be collected.

6.2 Experimental Methods

Experimental data was collected using the facilities at the Okazaki Large Spectrograph in Okazaki, Japan (Fig. 6.2.1. We used four strains of *Chlamydomonas reinhardtii* (Tab. 6.2.1) and performed three light experiments, each time changing the intensity of applied light (90 μEm^{-2}s^{-1}, 150 μEm^{-2}s^{-1} or 300 μEm^{-2}s^{-1}).

Name	Characteristis
wt 137c	wild type strain, obtained from the University of Geneva, Switzerland
npq4	lacks two of the three genes encoding LHCSR [114]
stt7-9	state transition–decreased mutant, significantly reduced LHCII phosphorylation
npq4 stt7-9	double mutant [86]

Table 6.2.1: *Chlamydomonas* strains used in the Okazaki experiment.

6.2.1 Strains and conditions

Four strains of *Chlamydomonas reinhardtii* were grown under 150 μEm^{-2}s^{-1} in Tris-acetate-phosphate (TAP) media at 23 °C. Harvested cells were concentrated to $1 \cdot 10^7$ cells/mL and transferred to HSM media prior the experiment. Cell number was determined using BioRad TC20 Automated Cell Counter. Cells were incubated in the darkness for 30 minutes before light exposure.

6.2.2 Light exposure

Having limited number of available set-ups (mirrors and lenses, as shown in Fig. 6.2.1), we selected 21 wavelengths between 370 and 720 nm, that are of a particular interest: 370, 400, 430, 440, 450, 460, 475, 485, 500, 520, 540, 580, 620, 640, 650, 660, 670, 680, 690, 700 and 720 nm. After performing the first
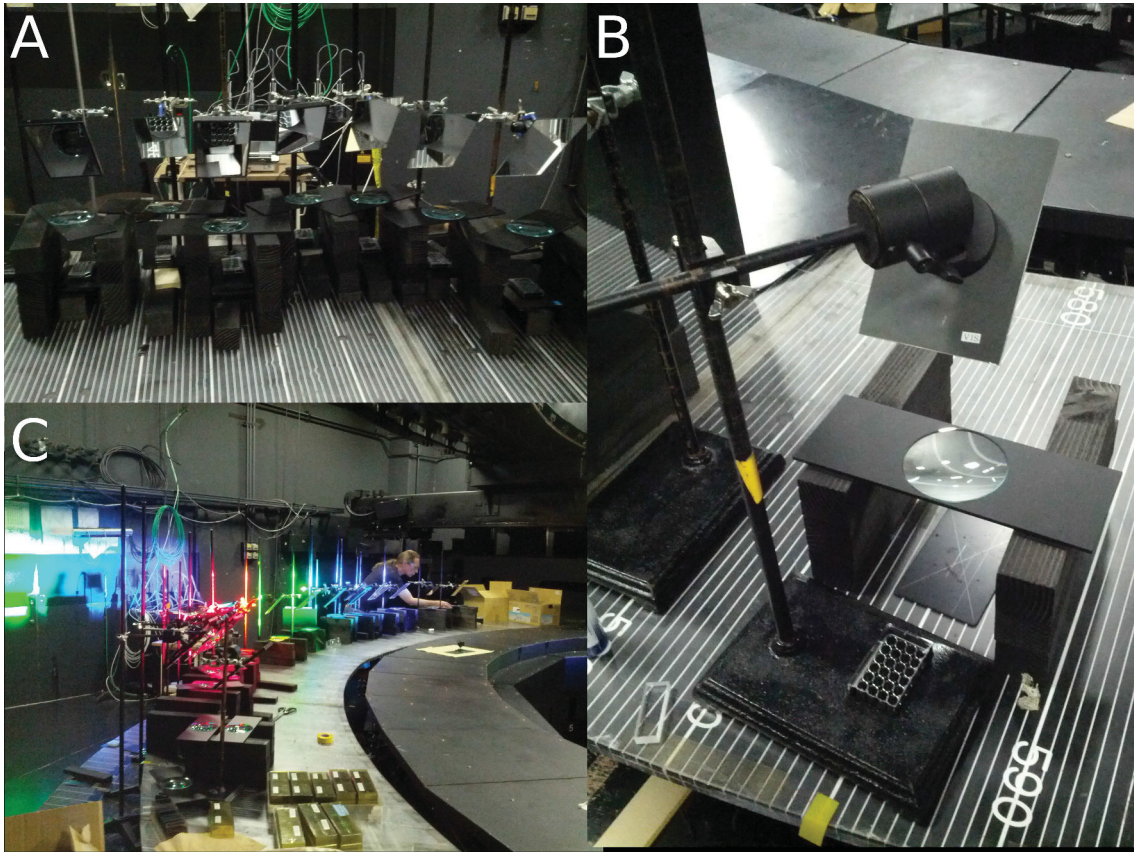
Figure 6.2.1: A) Experimental set up at OLS. B) A single measuring point placed at the 585 nm. C) Ready set-up with the switched-on light, capturing the light spectrum used for this experiment.

experiment with a light intensity of 150 μEm^{-2}s^{-1}, we added measuring station at 560 nm.

We used nine-well-plates to load our samples. We loaded a double replicate of each strain (250 L volume), having 8 samples in every well. As a positive control we exposed all four strains to the white light of the same intensity as the samples exposed to a monochromatic light, and as a negative control we kept samples for the time of experiment in the darkness. With 22 plates (only 21 for 150 μEm^{-2}s^{-1}) and two controls, all together we exposed 192 samples at every run (only 184 for 150 μEm^{-2}s^{-1}). Half of the samples exposed to light were frozen for a possible further biochemical analysis and other half was frozen to perform 77K fluorescence measurements.

6.2.3   77 K fluorescence measurements

The fluorescence spectra were recorded at 77 K using *Horiba Jobin Yvon* spectrometer, with an integration time set to 0.4 s.

6.3   Preliminary Experimental Results

To study the impact of specific light wavelength on photoacclimation we were primarily interested in the change in the relative cross section of PSII and PSI. In Fig. 6.3.1 we plot the ratio between the absorption peak at 715 nm, corresponding to the absorption of PSI, and the peak at 685 nm, corresponding to the absorption of PSII. The raw traces are included in the Appendix Fig. A3.
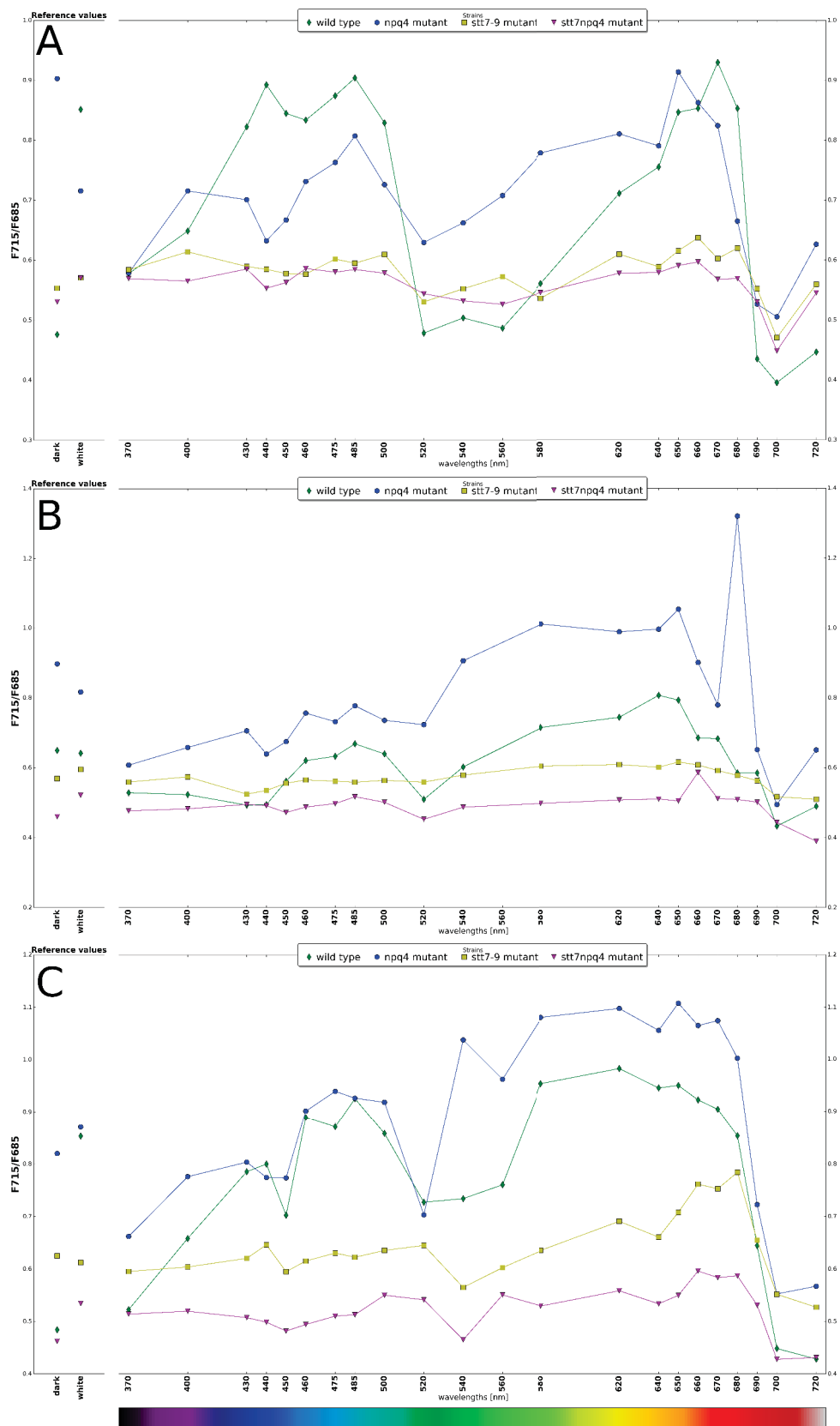
Figure 6.3.1: The results of all three experiments, taken after 3 hours of light exposure to a monochromatic light of A) 90 $\mu Em^{-2}s^{-1}$, B) 150 $\mu Em^{-2}s^{-1}$, and C) 300 $\mu Em^{-2}s^{-1}$ intensity. On the x-axis the wavelength of applied light is displayed. On the y-axis a ratio between the 77 K fluorescence absorption peak at 715 nm (corresponding to PSI) to peak at 685 nm (corresponding to PSII) is displayed.

Although these experiments were performed only one time and therefore no statistics can be done on this data, already some interesting mutant behaviour is observed and we provide here our hypothetical explanations.

For instance, under low light conditions, npq4 mutant should behave in a similar manner as the wild type, as according to our current knowledge, light as low as 90 μEm^{-2}s^{-1} should not activate the high-energy dependent quenching. But as it can be seen in the Fig. 6.3.1 A, both qualitative as well as quantitative behaviour of the WT (marked with green diamonds) and npq-4 mutant (marked with blue circles) differ. Especially at the 440 nm, where for a WT it is a local maximum whilst for a mutant its a local minimum. The behaviour in the green and orange region is qualitatively similar, pointing to higher cross section of PSII. Moreover, we observed that npq4 mutant is characterised with a higher PSI cross section than WT when exposed to longer wavelengths. It may be due to the fact that while LHCSR3 protein is knocked out in this mutant, state transitions overcompensate for the energy balance. We have also observed interesting behaviour in the green region of light, for which we do not find any explanation at this stage and are awaiting for a repetition of this experiment.

The measured behaviour of the stt7 mutant (yellow squares) and the double mutant (magenta triangles) is consistent with our expectations, as in these mutants no mechanism allowing for antenna translocation is available. They exhibit almost no change in the relative cross section across the whole spectra for all three light intensities, except for the longer wavelengths, where the ratio slightly increases, which can be explained by a possible mutant leak.

6.4 Model description

The mathematical model of the electron transport chain used for the simulation of the impact of light wavelength on photosynthesis included all previously developed and described modules. Therefore, the model consists of 11 ODEs, describing the dynamics of linear and cyclic electron flow, photoinhibition, high-energy dependent quenching, state transitions and delayed activation of ATPase. The system of equations reads:

$$\frac{dB}{dt} = -v_{\text{degPSII}} + v_{\text{repPSII}}, \tag{6.4.1}$$

$$\frac{dP}{dt} = v_{\text{PSII}} - v_{\text{b6f}} + v_{\text{FQR}} - v_{\text{PTOX}} + v_{\text{NDH}}, \tag{6.4.2}$$

$$\frac{dC}{dt} = 2v_{\text{b6f}} - v_{\text{PSI}}, \tag{6.4.3}$$

$$\frac{dF}{dt} = v_{\text{PSI}} - 2v_{\text{FNR}} - 2v_{\text{FQR}}, \tag{6.4.4}$$

$$\frac{dE}{dt} = v_{\text{actATPase}} - v_{\text{deactATPase}}, \tag{6.4.5}$$

$$\frac{dA}{dt} = v_{\text{ATPsynthase}} - v_{\text{ATPconsumption}}, \tag{6.4.6}$$

$$\frac{dN}{dt} = v_{\text{FNR}} - v_{\text{NADPHconsumption}}, \tag{6.4.7}$$

$$\frac{dH}{dt} = \left(2v_{\text{PSII}} + 4v_{\text{b6f}} - \frac{14}{3}v_{\text{ATPsynthase}} - v_{\text{leak}}\right) \cdot \frac{1}{b_H}, \tag{6.4.8}$$

$$\frac{dL}{dt} = v_{\text{Stt7}} - v_{\text{Pph1}}. \tag{6.4.9}$$

$$\frac{d\text{Pr}}{dt} = -v_{\text{Psbsp}}, \tag{6.4.10}$$

$$\frac{dV}{dt} = -v_{\text{Xcyc}}, \tag{6.4.11}$$

where each state variable was introduced previously. The various rates are functions of the dynamic variables, external constants and parameters, as derived in previous chapters. The only change made to the model is a new description of the light activation rate.

6.4.1 Activation by light

In order to account for a different absorption capacity of PSI and PSII supercomplexes, as well as change in the absorption during state transitions, a new method of calculating the activation rate for PSI and PSII was derived. The activation rates for the two photosystems are now not only dependent on the relative cross-section of PSI (σ_{PSI}^0) and PSII (σ_{PSII}^0) but also on the specific absorption of the light of certain wavelength ($c_{\mathrm{abs}}(\lambda)$). In Fig. 6.4.1 the change in the absorption of a wild type cell, depending on the light wavelength is presented. The data is normalised to the maximal peak in the blue region.
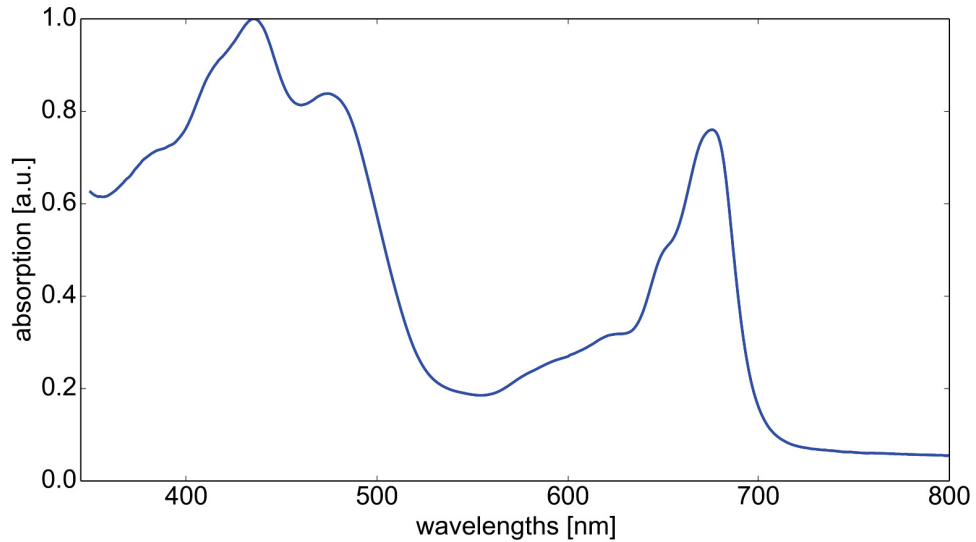
Figure 6.4.1: The absorption spectrum for a wild type *Chlamydomonas reinhardtii*.

We moreover introduced a class of coefficients, $c_{\mathrm{complex}}(\lambda)$, corresponding to how much light is absorbed by a specific protein complex at given wavelength. Coefficients were calculated based on the experimental data obtained from the lab of Prof. Jun Minagwa. The absorption spectra for PSI-LHCI supercomplex, PSII-LHCII and LHCII trimeric of *C. reinhardtii* were normalised to their peak at 475 nm and plotted in Fig. 6.4.2.

With this, the activation rates for PSI (k_{LI}) and PSII (k_{LII}) depend on the relative absorption of each supercomplex and overall absorption of a cell at a specific wavelength ($c_{\mathrm{abs}}(\lambda)$)

$$k_{\mathrm{LI}} = c_{\mathrm{abs}}(\lambda) \cdot \mathrm{PFD} \cdot \left(\sigma_{\mathrm{PSI}}^0 \cdot c_{\mathrm{PSI}}(\lambda) + (1 - \sigma_{\mathrm{PSII}}^0 - \sigma_{\mathrm{PSI}}^0) \cdot L \cdot c_{\mathrm{LHCII}}(\lambda) \right) \tag{6.4.12}$$

$$k_{\mathrm{LII}} = c_{\mathrm{abs}}(\lambda) \cdot \mathrm{PFD} \cdot \left(\sigma_{\mathrm{PSII}}^0 \cdot c_{\mathrm{PSII}}(\lambda) + (1 - \sigma_{\mathrm{PSII}}^0 - \sigma_{\mathrm{PSI}}^0) \cdot (1 - L) \cdot c_{\mathrm{LHCII}}(\lambda), \tag{6.4.13}$$

where L stands consequently for the concentration of phosphorylated antenna, prone to detachment from PSII due to state transitions.
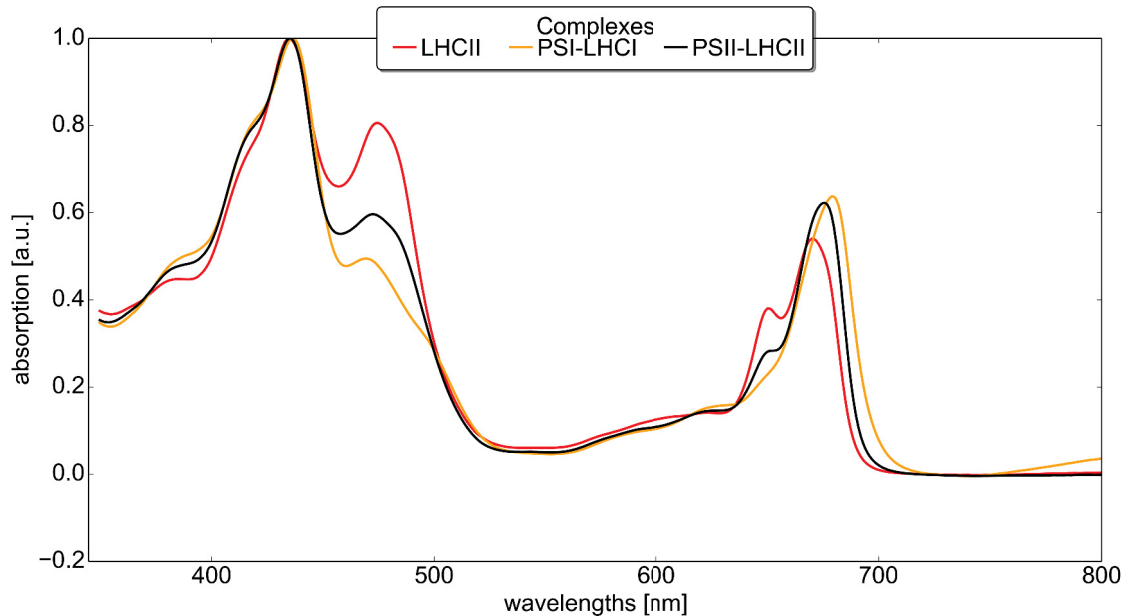
Figure 6.4.2: Absorption spectra of PSI-LHCI supercomplex, PSII-LHCII and LHCII trimeric of *C. reinhardtii*. Data obtained from Asst.-Prof. Ryutaro Tokutsu from the NIBB, Japan.

6.5 Preliminary results

We initially aimed at reproducing the qualitative difference between the light absorption of a wild type and various mutants exposed to the three different light intensities. *In silico* strains were exposed to a constant monochromatic light of the same wavelengths as during the Okazaki experiment and the change in the relative cross section in PSs was read out at the end of simulation.

6.5.1 Wild type

In order to find the conversion factor that converts our internal units into the real incident light we performed the first set of simulations using a wide range of light intensities (10, 100, 150, 300, 1000, 1500, 3000 a.u.). In Fig. 6.5.1 A we plotted the experimentally obtained absorption spectra of the wild type strain, exposed to three light intensities. In subfigure B, the results of our simulations are displayed. The clear benefit of using mathematical model is that we could simulate the behaviour of the cell for any given wavelength, not being limited by any experimental constrains. Therefore, for this simulation we tested 36 different wavelengths.

First of all, our simulations capture well the range in which the ratio between the cross sections changes (0.4 - 1.0 in the experiment and 0.6 - 0.95 in the simulation). Secondly, the qualitative response to different light colours is reflected by the fact that our simulated strains also show local maximum at 485 nm and drop in the blue and yellow region. The peak in the red region is slightly shifted to the left (670 nm in the experiment and 650nm in the simulation), which we can not explain at the moment. We can not reproduce the apparent strong state transitions in the yellow/orange region observed for 300 $\mu Em^{-2}s^{-1}$. We additionally plotted quencher activity in Fig. 6.5.2. The results will require more investigation and information regarding LHCSR protein phosphorylation to confirm if our predictions are correct, but it is suggested that quencher can not reach its maximal capacity for any given light intensity, nor wavelength.

Based on this preliminary results, the light of 10 a.u. (blue line) seems to be too low to reflect the 90 $\mu Em^{-2}s^{-1}$ intensity used in the experiment, as almost no change in the orange and red region is observed.
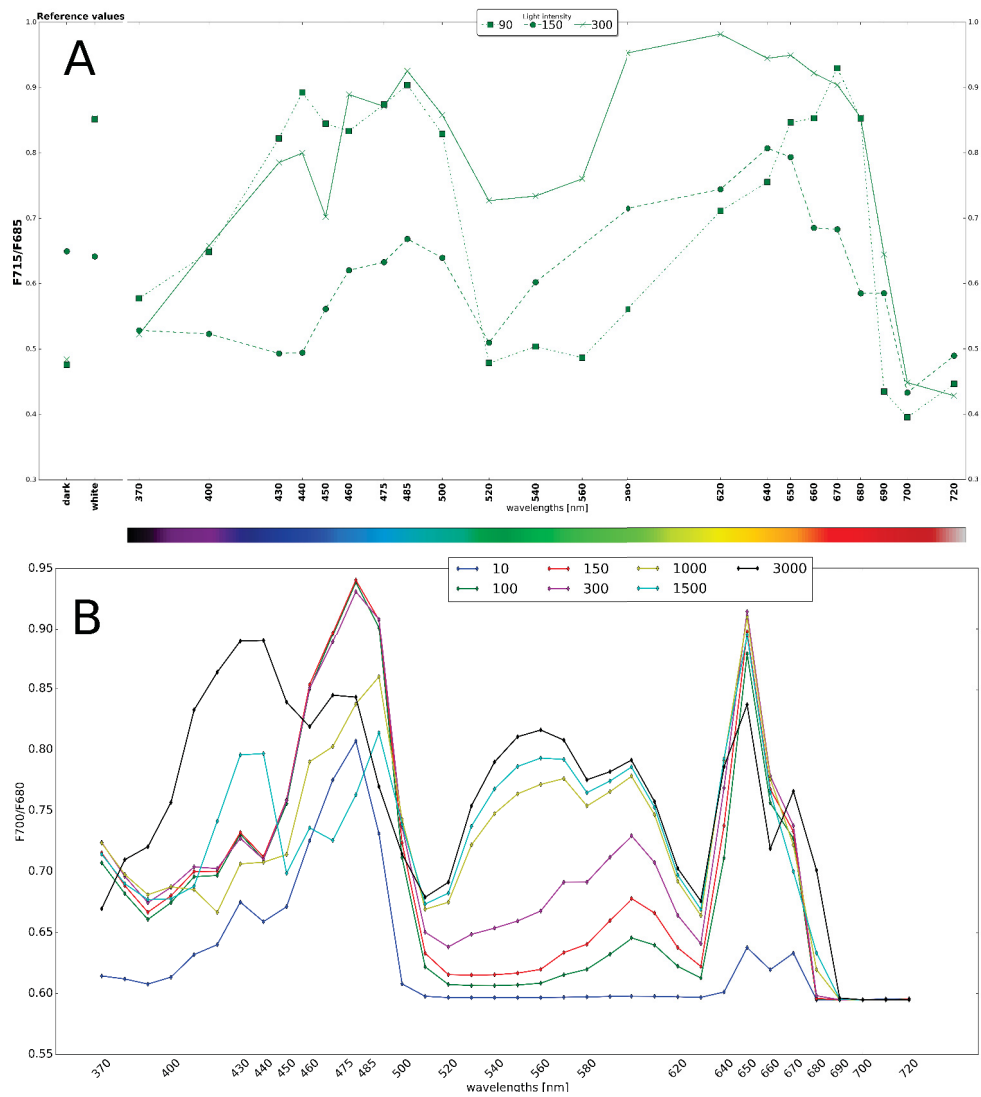
Figure 6.5.1: A) The results of Okazaki experiment for the wild type strain. B) The results of our simulation for various PFDs to compare the qualitative change in the absorption spectra and find the conversion factor. On the x-axis the wavelength of applied light is displayed. On the y-axis a ratio between the 77 K fluorescence absorption peak at 715 nm (corresponding to PSI) to peak at 685 nm (corresponding to PSII) is displayed.
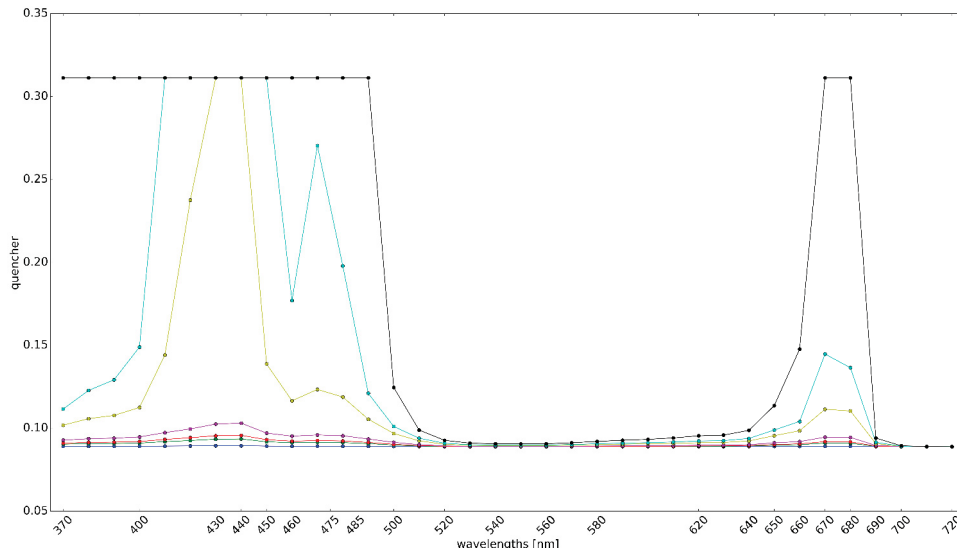
Figure 6.5.2: Calculated quencher activity for various PFDs. On the x-axis the wavelength of applied light is displayed. On the y-axis normalized quencher activity. Qualitative and quantitative change in quencher induction is observed.

On the other hand, simulation with the highest applied intensities (yellow, cyan and black lines) well mimic the behaviour of the wild type exposed to the three selected light intensities. For instance, our simulation with 1000 a.u. well captures the change in the cross sections between blue, green and red region. Excluding the simulation for 620 nm, the simulation also reproduces the increase in the PSI cross section in the green and yellow region. The overall results are plausible and serve as a proof of concept that with the current implementation of light activation function, we are capable of simulating the difference in photosystems cross section upon different light illumination, considering both light intensity and colour (wavelengths).

6.5.2 Mutant analysis

Next we run the simulations for various mutants. We used the absorption coefficients as for the wild type ($c_{\lambda_{abs}}$), which should be improved in future by measuring *in vitro* the actual absorption coefficients for each mutant. Similar as in the Chapter 4, npq4 mutant was simulated by switching off the $k_{protonationL}$ and setting initial concentration of non-protonated antenna to 1. In Fig. 6.5.3, as for the wild type, in the upper panel we plotted the experimental results and in the bottom panel we plotted the results of our simulations. Our simulation can not capture the gradual increase in F700/F680 ratio with the increase of the wavelength of the light, but once again we captured the drop in ratio at 520 nm. An interesting observation is done while simulating with the highest light intensity (3000 a.u., black line), where two peaks are noticed in the red region, at 650 nm and 670 nm. For an npq4 mutant such qualitative behaviour is observed at 650 and 680 nm.

We also verified that our simulated ratio of cross sections for stt7 mutant does not change with light spectrum, therefore some observable increase in the experimental data (see Fig. 6.3.1) may be explained by some leak of this strain.

In addition to predicting behaviour of cells under various other wavelengths, the benefit of applying a theoretical approach is to simulate the behaviour of other mutants for which we did not collect experimental data. For instance, in Fig. 6.5.4 we plot the results of simulation for the npq1-npq4 mutant that is lacking both LHSCR-3 protein, as well as is impaired in the xanthophyll cycle[1]. Basically, this mutant has no capacity of

---

[1]npq1 mutant is unable to convert violaxanthin to zeaxanthin in excessive light [112].
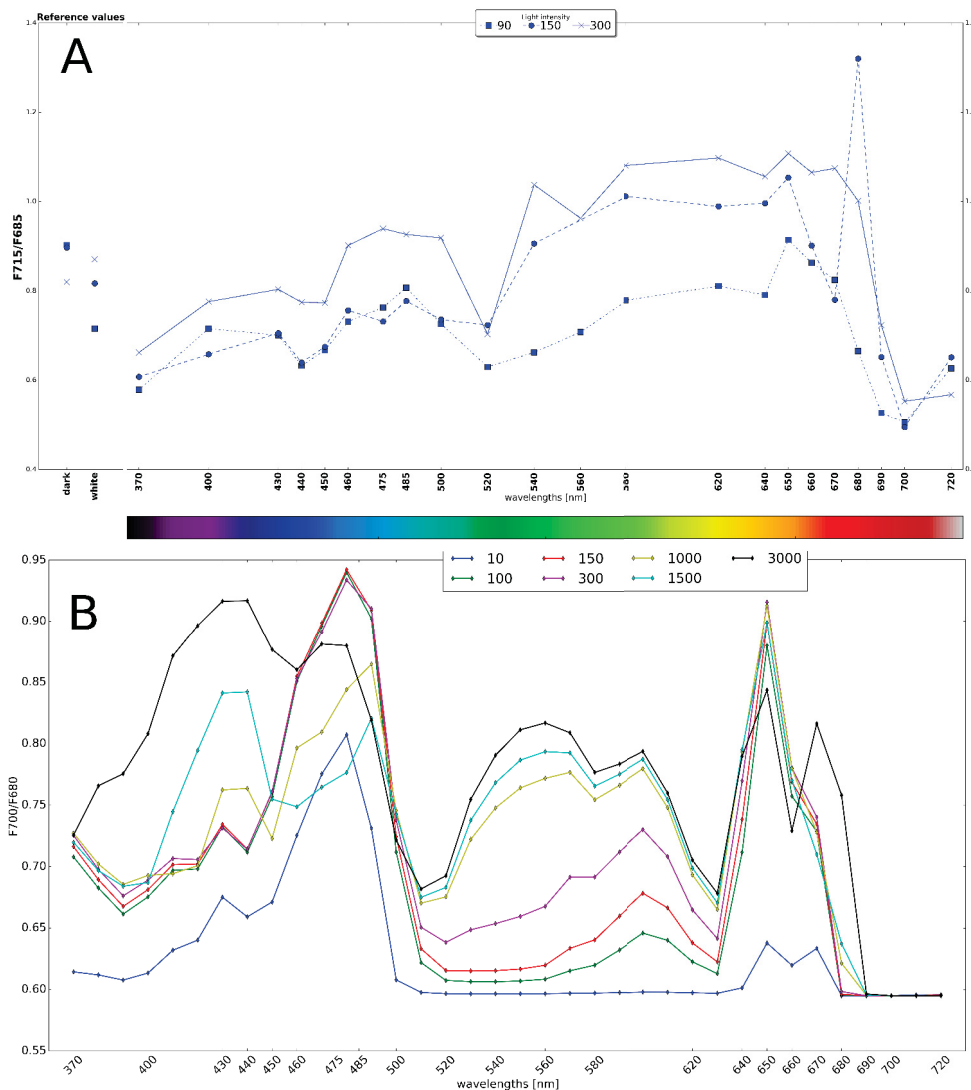
Figure 6.5.3: The results of our simulation for the npq4 mutant. On the x-axis the wavelength of applied light is displayed. On the y-axis a ratio between the 77 K fluorescence absorption peak at 715 nm (corresponding to PSI) to peak at 685 nm (corresponding to PSII) is displayed.

high-energy dependent quenching and therefore we set the k_H rate to zero. The results of these simulation (with high light intensities) resemble more the experimental data that was collected for the npq4 mutant. A possible explanation would be that even high light intensity of a monochromatic light can not induce quenching response and therefore npq4 mutants behaved as complete quenching mutants. A hypothesis that once again can be only confirmed with the biochemical analysis of the samples.

6.6 Discussion and Outlook

Thanks to the implemented mechanisms of high-energy dependent quenching, photoinhibition and state transitions we are capable of simulating various mutants exposed to different light conditions and speculate on the particular role of each mechanism in the absence of others. By changing the method of calculating the light activation rate, we could simulate how relative cross sections change upon illumination with different light colours. Since the experimental data that we used for this analysis originated from only on biological sample, further data are required to calibrate the model. It will be important to increase the number of
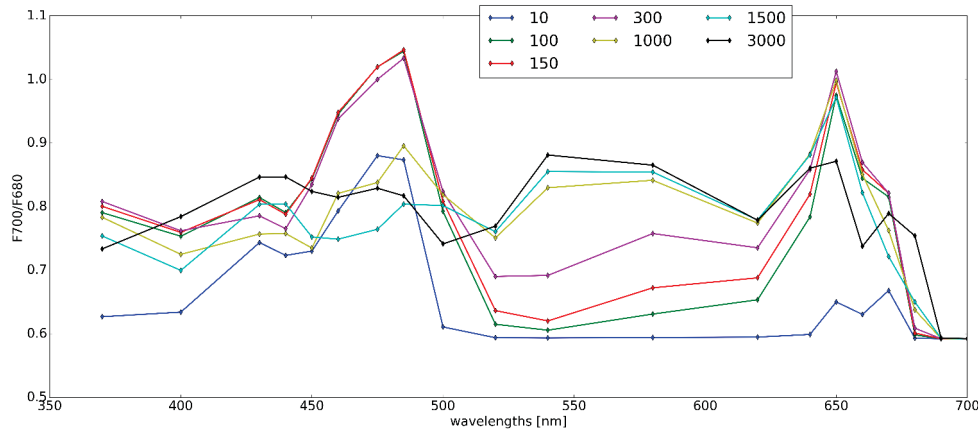
Figure 6.5.4: The results of our simulation for the double mutant npq1-npq4 mutant. On the x-axis the wavelength of applied light is displayed. On the y-axis a ratio between the 77 K fluorescence absorption peak at 715 nm (corresponding to PSI) to peak at 685 nm (corresponding to PSII) is displayed.

biological replicates to collect samples on which statistical analysis can be perform. The model, though finally tuned for a model organism *Chlamydomonas reinhardtii*, is easily adaptable to *Arabidopsis thaliana*, though an absoprtion spectrum of each photocomplex seperately is required to build the organism specific light activation function.

Recent advances in photosynthetic research suggest that we will be more interested in the light wavelength regulation of various non-photochemical quenching mechanisms. Especially, that any information regarding potential benefit of certain light colour on cell growth are being immediately implemented in the industry. For instance, the German company WeGrow, the specialist in setting up plantations of kiri trees[2], during their plant preparation uses red light for roots development and blue light for better leaves growth to obtain faster growing plants [210]. Unfortunately, no systematic light screenings are made and no fundamental research on the cause of such improvement are made. Therefore, it is important for the research such this one to be continued, to increase our understanding of the impact of the colour of the light on photosynthesis.

---

[2]Genus Paulownia, considered as one of the fastest growing trees, may grow up to 5 meter per year.

Conclusions and outlook

„A theory has only the alternative of being right or wrong.
A model has a third possibility: it may be right, but irrelevant."

*- **Manfred Eigen**, biophysical chemist, Nobel Prize winner*
The Physicists's Conception of Nature (1973)

Photosynthesis is a complex process in which photoprotective mechanisms do not operate in isolation, but rather form an interdependent and complex regulatory network. Theoretical approaches are powerful to discover organisational principles governing the design of such biological systems and mathematical models provide a good theoretical framework for studying their dynamics. With this work we delivered a theoretical tool to study the self-regulation of higher plants and green algae in response to changes in light intensity and colour. Our modelling efforts were complemented with an experimental approach. We collected various experimental data for three different species *Arabidopsis thaliana*, *Chlamydomonas reinhartdtii* and *Epipremnum aureum*. Experimental data collected on several mutants, has been useful in identifying distinct molecular mechanisms of non-photochemical quenching. Based on these studies, our current knowledge on NPQ and various other existing models, we build a mathematical model of the electron transport chain that includes all three main components of NPQ: high-energy dependent quenching, state transitions and photoinhibition.

With the high-energy dependent quenching model we provided a qualitative description of the contribution of each qE component to the phenomena of short-term light memory. We confirmed that the current 4 - state model of quencher activity is correct and moreover, suggested that quenching mechanisms operate in a similar manner also in non-model organisms, such as the shadow tolerant plant *Epipremnum aureum* for which available kinetic parameters are sparse. With the state transitions model we challenged the concept of phosphatase being consecutively active and tested the hypothesis that some of the phosphorylated antenna quench instead of attaching to PSI. We are capable of simulating various scenarios, providing new arguments to the discussion on the actual role of state transitions. With the light wavelengths model we

demonstrated how light colour affects photosynthetic efficiency and how *Chlamydomonas* cells change their photoprotective strategy in response to different monochromatic wavelengths. With our model we can calculate the relative cross section of photosystems, photosynthetic activity and redox state of the cell for any given wavelength.

Despite aiming to answer rather fundamental research questions, potential usability of this work can be seen in planning sustainable bioeconomical strategies. Within our lifetime we expect the global population to rise to 9.7 billion. This demographic change will most likely unfold a number of challenges such as increased energy, food and housing demand. Our apparent central task is to make an optimal use of the limited resources, considering various aspects: meeting ever increasing food demand, providing land for energy crops and other alternative sources of energy, while at the same time providing a long term protection of the environment. All of these goals need to be achieved with limited land resources. Sustainable cultivation of microalgae on a commercial scale has the potential to provide a solution to all of the above issues and provide resources to meet expected demand in the future. We demonstrated the potential power of the model in this context, by applying it to study how *Chlamydomonas* performs under fluctuating light in a bioreactor and to assess the potential benefit of growing strains with truncated antenna.

Further, because of its simplicity and easy adaptability, the model has the potential to support knowledge transfer from lab to field. Especially in combination with cheap and easy-to-use devices to measure photosynthetic parameters outdoors (such as MultispeQ designed by the PhotosynQ project [211]), our model provides a theoretical framework in which the multitude of data can be interpreted in a sophisticated way. Thus, it can serve as a bridge to understand to what extent obseravtions obtained under controlled lab conditions can allow us to derive conclusions about the behaviour in real, highly fluctuating, outdoor conditions. Therefore, its real usefulness will depend on the creativity of its users.

Regarding possible future directions, the need for a better description of the cell energy demand emerged from these studies and several approaches were taken in order to solve this problem. Described in this work coupling of ATP and NADPH consuming reactions did not yield plausible results and suggested that a more dynamic description of these processes is needed. The Calvin-Benson-Bassham Cycle is considered as the most energy demanding process and therefore the main consumer of ATP and NADPH. Several already existing mathematical models of CBB cycle were reviewed [155, 212] but for various reasons could not be easily linked to our model of the electron transport. The model by Pettersson and Ryde-Pettersson [212] includes a level of detail that is not necessary for our purpose, on the other hand the Zhu model [155], though highly simplified, does not provide justification for the implemented reduction. With that, we have developing work on a simplified description of the Calvin cycle, constructing an equilibrium module by exploiting entropic principles and applying thermodynamical constraints, following the approach in [213].

When launching this project back in 2013, it was assumed that the apparent difference in the thylakoid structure between plants and diatoms may effect their photosynthesis and therefore those organisms might develop completely different mechanisms of photoprotection. But with the recent findings by Flori *et al.* [214], it seems that photosynthetic complexes in diatoms are structurally segregated and connected in a similar manner as in plants. This lead to an assumption that also several photoprotective mechanisms, so far attributed only to plants or green algae, such as state transitions, can actually be possible in these organisms. Therefore the model has the potential to be applied to diatoms as well.

Finally, due to its modular design and open-access format, the majority of the developed modules are widely available to the scientific community, therefore our models should be easily implemented as a part of more complex models.

Acknowledgements

First and foremost I would like to thank my supervisor, Jun.-Prof. Oliver Ebenhöh for being a great mentor and boss for the past three years. Thank you for giving me an opportunity to become a part of this exciting project and encouraging me to try myself on many grounds. Thank you for listening to all of my ideas and expanding my interest in plant biology (and entropy of life). It was a pleasure to work with you.

I would like to thank Prof. Michel Goldschmidt-Clermont for the first real hands-on lab experience and introduction to the world of state transitions. Big thanks to Federica Cariti for being my guide during the stay at the lab in Geneva and for helping me to perform my very own experiments and making sure I don't leave the lab without data.

I would also like to thank Dr Giovanni Finazzi for great collaboration throughout the project and for the directions given during the time spent in his lab in Grenoble. I would also like to acknowledge Dr Gilles Curien for discussions regarding the Calvin cycle and energy demand that inspired me to work further on the 'dark reactions' of photosynthesis.

I would like to thank Prof. Jun Minagawa for hosting me in his lab in Okazaki and Asst. Prof. Ryotaru Tokutsu for invaluable guidance and support during the OLS experiment. I hope that our ongoing project on light wavelengths will unravel a new exciting information regarding NPQ regulation.

Many thanks to Dr Soma Heidari for approaching us with her biological questions regarding light memory, that we managed to converge into an interesting research paper. I would like to thank Prof. Peter Jahns for jumping on board of the memory project and for his invaluable expertise regarding NPQ.

I would like to thank the Aberdonian Team, with whom I started this journey: Dr Claudia Zabke for your support and good word when there was no one else around, and Dr Ahmad Mannan, for creating together an amazing outreach experience for children, that not only allowed me to share my research passion, but also inspired to continue plant biology studies.

I would like to thank Deutsche Forschungsgemeinschaft Cluster of Excellence on Plant Sciences, CEPLAS Graduate School for connecting me with other students working on plants and therefore broadening my research interest and European Commission for funding my research through the European Project AccliPhot. In this place I want to mention all the fellows from the Project, with whom I shared stress, worries and success over the past few years. It was great to be a part of such diverse group of young researchers.

Many, many thanks to the wonderful QTB Team in Düsseldorf. We are undoubtedly a unique group and the atmosphere created in our Institute is incomparable. Suraj, thanks for sharing the struggles of the only PhD students in the group. Ines, thank you for your help with the Zusammenfassung! Elahe, I am grateful for your ongoing support. Simon, thank you for fixing my computer related dramas. Ovidiu, many thanks for your comments to the biological part of this work. Anto, you were the greatest office-roomie one could imagine and I believe our relationship will go far beyond scientific one. The same goes to Fiona. My dear friend and "partner in crime". Thank you for sharing the most amazing PhD experiences with me and for being your wonderful, supportive self.

And lastly, I would like to acknowledge here all incredible people that are not directly linked to the scientific world, but without a doubt, became an important part of this journey. Without their support and good words I would not be where I am today: Dziękuję Karolko, za stanie na każdym moście, polskim, szkockim czy niemieckim; Magdo i Rafale, za wszystkie słoneczne dni w Aberdeen i oferowanie przyjaźni na całe życie; Magdo, za wszystkie słowa wsparcia i bycia odskocznią od pracy; Miu, za bycie cudowną przyjaciółką.

The quasi-steady state approximation used to calculate the rate of photosystem II

$$-\left(\text{PFD} + \frac{k_{\text{PQred}}}{K_{\text{eq,QAPQ}}}(\text{PQ}^{\text{tot}} - P)\right)B_0 + (k_H Q + k_F)B_1 + k_{\text{PQred}}PB_3 = 0, \tag{1}$$

$$\text{PFD}B_0 - (k_H Q + k_F + k_P)B_1 = 0, \tag{2}$$

$$\text{PFD}B_2 - (k_H Q + k_F)B_3 = 0, \tag{3}$$

$$B_0 + B_1 + B_2 + B_3 = \text{PSII}^{\text{tot}}. \tag{4}$$

Reaction rates used in the dynamic description of the system

$$v_{\text{PSII}} = k_2 \cdot 0.5 \cdot B_1, \tag{5}$$

$$v_{\text{PQ}_{\text{ox}}} = \left(\frac{k_{\text{Cyt}_{\text{b6f}}} \cdot \text{PFD} \cdot K_{\text{eq,cytb6f}}(\text{pH})}{K_{\text{eq,cytb6f}}(\text{pH}) + 1} + k_{\text{PTOX}}\right) \cdot \text{PQH}_2 - \frac{k_{\text{PFD}}}{K_{\text{eq,cytb6f}}(\text{pH}) + 1} \cdot \text{PQ}, \tag{6}$$

$$v_{\text{ATPsynthase}} = \text{ATPase}^* \cdot k_{\text{ATPsynthase}} \cdot \left(\text{AP}^{\text{tot}} - \text{ATP} - \frac{\text{ATP}}{K_{\text{eq,ATPsynthase}}(H)}\right), \tag{7}$$

$$v_{\text{ATPactivity}} = k_{\text{actATPase}} \cdot \text{H}(\text{PFD}) \cdot \text{ATPase} - k_{\text{deactATPase}} \cdot (1 - \text{H}(\text{PFD})) \cdot \text{ATPase}^*, \tag{8}$$

$$v_{\text{Leak}} = k_{\text{leak}} \cdot (H - pH_{\text{inv}}(\text{pH}_{\text{stroma}})), \tag{9}$$

$$v_{\text{ATP}_{\text{consumption}}} = k_{\text{ATPconsumption}} \cdot \text{ATP}, \tag{10}$$

Reaction rates to calculate the quencher activity and the overall rate

$$v_{\text{Xcyc}} = k_{\text{DeepoxV}} \cdot \frac{H^{n_{H_X}}}{H^{n_{H_X}} + pH_{\text{inv}}(K_{\text{phSat}})^{n_{H_X}}} \cdot \text{Vx} - k_{\text{EpoxZ}} \cdot (\text{X}^{\text{tot}} - \text{Vx}), \tag{11}$$

$$v_{\text{Psbs}^p} = k_{\text{ProtonationL}} \cdot \frac{H^{n_{H_L}}}{H^{n_{H_L}} + pH_{\text{inv}}(K_{\text{phSatLHC}})^{n_{H_L}}} \cdot \text{PsbS} - k_{\text{Deprotonation}} \cdot \text{PsbS}^p, \tag{12}$$

$$Q = \gamma_0 \cdot \left(1 - \frac{\text{Zx}}{\text{Zx} + K_{\text{ZSat}}}\right) \cdot \text{PsbS} + \gamma_1 \cdot \left(1 - \frac{\text{Zx}}{\text{Zx} + K_{\text{ZSat}}}\right) \cdot \text{PsbS}^p + \gamma_2 \cdot \frac{\text{Zx}}{\text{Zx} + K_{\text{ZSat}}} \cdot \text{PsbS}^p + \gamma_3 \cdot \frac{\text{Zx}}{\text{Zx} + K_{\text{ZSat}}} \cdot \text{PsbS}, \tag{13}$$

Equilibrium

$$K_{\text{eq,ATPsynthase}}(\text{pH}) = \text{Pi}_{\text{mol}} \cdot e^{\frac{-\Delta G_{0_{ATP}} - log(10) \cdot RT \cdot \text{HPR} \cdot (\text{pH}_{\text{stroma}} - \text{pH})}{RT}}, \tag{14}$$

$$K_{\text{eq,cytb6f}}(\text{pH}) = e^{\frac{-\left(\left(2F \cdot E^0(\text{PQ/PQH}_2) - 2 \cdot \log(10) \cdot RT \cdot \text{pH}\right) - 2 \cdot F \cdot E^0(\text{PC/PC}^-) + 2 \cdot \log(10) \cdot RT \cdot (\text{pH}_{\text{stroma}} - \text{pH})\right)}{RT}}, \tag{15}$$

$$K_{\text{eq,QAPQ}} = e^{\frac{-\left(-2 \cdot E^0(\text{QA/QA}^-) \cdot F - 2 \cdot E^0(\text{PQ/PQH}_2) \cdot F + 2\text{pH}_{\text{stroma}} \cdot \log(10) \cdot RT\right)}{RT}}, \tag{16}$$

Method to calculate the fluorescence signal

$$\Phi = \frac{k_{\text{F}}}{k_{\text{H}} \cdot Q + k_{\text{F}} + k_{\text{P}}}B_0 + \frac{k_{\text{F}}}{k_{\text{H}} \cdot Q + k_{\text{F}}}B_2, \tag{17}$$

Table A1: Complete set of equations used in the qE model.

Parameter	Value	Description and reference
Pool sizes		
$PSII^{tot}$	$2.5\ mmol(mol\ Chl)^{-1}$	PSII reaction centres [215]
PQ^{tot}	$20\ mmol(mol\ Chl)^{-1}$	PQ + PQH$_2$ [216]
AP^{tot}	$50\ mmol(mol\ Chl)^{-1}$	total adenosine phosphate pool (ATP + ADP)[217]
$PsbS^{tot}$	1	LHCII normalized
$Xanthophylls^{tot}$	1	total pool of xanthophylls (V + A + Z) normalized
O_2^{ex}	$8\ mmol(mol\ Chl)^{-1}$	external oxygen pool, corresponds to $250\mu M$, after [26]
Pi_{mol}	0.01	internal pool of phosphates, required to calculate ATP equilibrium
Rate constants and key parameters		
k_{Cytb6f}	$0.104\ mmol^{-2}(mol\ Chl)^2\,s^{-1}$	
$k_{ActATPase}$	$0.01\ s^{-1}$	rate constant of activation of the ATPase in the light
$k_{DeactATPase}$	$0.002\ s^{-1}$	parameter relating the deactivation of the ATPase at night
$k_{ATPsynthase}$	$20\ s^{-1}$	after [26]
$k_{ATPconsumption}$	$10\ s^{-1}$	after [26]
k_{PQred}	$250\ mmol^{-1}(mol\ Chl)\,s^{-1}$	after [26]
k_H	$5\cdot10^9\ s^{-1}$	rate of non-radiative decay, after [26]
k_F	$6.25\cdot10^8\ s^{-1}$	rate of fluorescence
k_P	$5\cdot10^9\ s^{-1}$	rate of photochemistry after [26]
k_{PTOX}	$0.01\ mmol^{-1}(mol\ Chl)\,s^{-1}$	after [26]
pH_{stroma}	7.8	stroma pH of a dark adapted state
k_{leak}	$1000\ s^{-1}$	
b_H	100	proton buffering constant [154]
HPR	$\frac{14}{3}$	ratio of protons to ATP in ATP synthase
Parameters associated with the quencher activity		
Parameters associated with xanthophyll cycle		
$k_{kDeepoxV}$	$0.0024\ s^{-1}$	fitted to keep the ratio of $k_{kDeepoxV}$:k_{kEpoxZ} =1:10 [104]
k_{kEpoxZ}	$0.00024\ s^{-1}$	
K_{phSat}	5.8	half-saturation pH for de-epoxidase activity, highest activity at pH 5.8
nH_X	5	Hill-coefficient for de-epoxidase activity
K_{ZSat}	0.12	half-saturation constant (relative conc. of Zx) for quenching of Zx
Parameters associated with PsbS protonation		
nH_L	3	Hill-coefficient for activity of de-protonation
$k_{Deprotonation}$	$0.0096\ s^{-1}$	rate of PsbS protonation
$k_{ProtonationL}$	$0.0096\ s^{-1}$	rate of PsbS de-protonation
$K_{phSatLHC}$	5.8	pKa of PsbS activation, kept the same as for VDA
Fitted quencher contribution factors		
γ_0	0.1	corresponds to base quenching not associated with protonation or zeaxanthin
γ_1	0.25	fast quenching present due to protonation
γ_2	0.6	fastest possible quenching
γ_3	0.15	slow quenching of Zx present despite lack of protonation
Physical constants		
F	96.485 kJ	Faraday constant
R	$8.3\ JK^{-1}mol^{-1}$	universal gas constant
T	298 K	temperature
Standard potentials		
$E^0(QA/QA^-)$	-0.140 V	[218]
$E^0(PQ/PQH_2)$	0.354 V	[219]
$E^0(PC/PC^-)$	0.380 V	[220]
$\Delta G_{0_{ATP}}$	30.6 kJ/mol/RT	standard Gibbs free energy change of ATP formation (Eq. 4.3.25) [27]

Table A2: Complete summary of parameters used in the qE model.
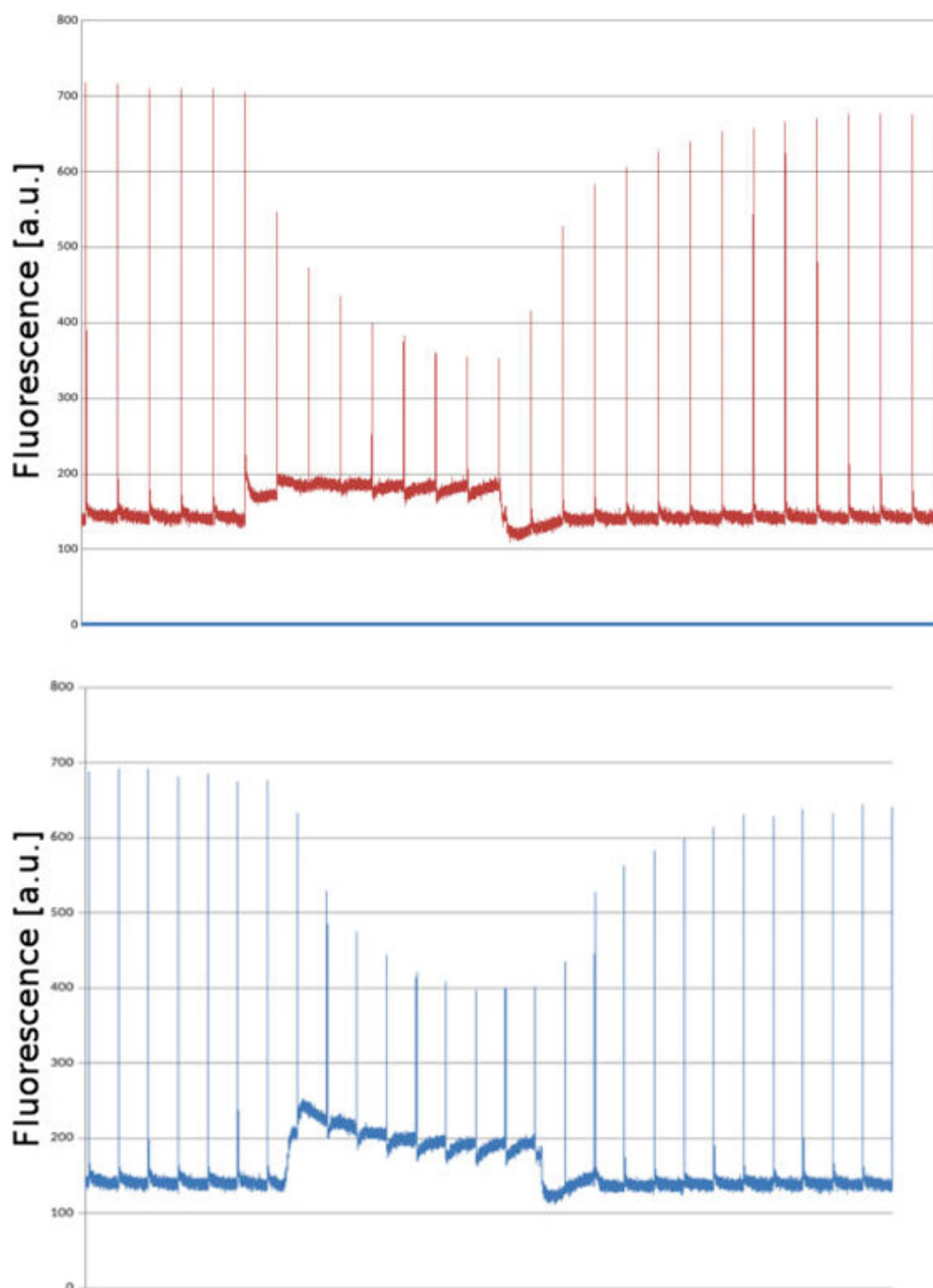
Figure A1: Examples of PAM fluorescence traces for light induced state transitions. The data are not normalised and display a single experiment. Experimental data obtained with a help of Federica Cariti, at the Lab of Michel Goldschmidt-Clermont.

The quasi-steady state approximation used to calculate the rate of photosystems

$$-\left(k_{\text{LI}} + \frac{k_{\text{PCox}}}{K_{\text{eq,PCP700}}} \cdot C\right) Y_0 + k_{\text{PCox}} \cdot (\text{PC}^{\text{tot}} - C) \cdot Y_2 = 0, \tag{18}$$

$$k_{\text{LI}} Y_0 - k_{\text{Fdred}} \cdot F \cdot Y_1 + \frac{k_{\text{Fdred}}}{K_{\text{eq,P700Fd}}} \cdot (\text{Fd}^{\text{tot}} - F) Y_2 = 0, \tag{19}$$

$$Y_0 + Y_1 + Y_2 = \text{PSI}^{\text{tot}} \tag{20}$$

+ Eq. 1 - 4, Tab.A1 to describe photosystem II

Reaction rates used in the dynamic description of the system

$$v_{\text{PSII}} = k_2 \cdot 0.5 \cdot B_1, \tag{21}$$

$$v_{\text{PSI}} = k_{LI} \cdot Y_0, \tag{22}$$

$$v_{\text{b6f}} = \max\left(k_{\text{b6f}} \cdot \left(P \cdot (\text{PC}^{\text{tot}} - C)^2 - \frac{(\text{PQ}^{\text{tot}} - P) \cdot C^2}{K_{\text{eq,b6f}}(H)}\right), v_{\text{b6f}}^{\text{min}}\right), \tag{23}$$

$$v_{\text{ATPsynthase}} = \text{ATPase}^* \cdot k_{\text{ATPsynthase}} \cdot \left(\text{AP}^{\text{tot}} - \text{ATP} - \frac{\text{ATP}}{K_{\text{eq,ATPsynthase}}(H)}\right), \tag{24}$$

$$v_{\text{actATPase}} = k_{\text{actATPase}} \cdot H(\text{PFD}) \cdot \text{ATPase}, \tag{25}$$

$$v_{\text{deactATPase}} = k_{\text{deactATPase}} \cdot (1 - H(\text{PFD})) \cdot \text{ATPase}^*, \tag{26}$$

$$v_{\text{ATP}_{\text{consumption}}} = k_{\text{ATPconsumption}} \cdot \text{ATP}, \tag{27}$$

$$v_{\text{FNR}} = V_{\text{FNR}}^{\text{max}} \cdot \frac{f^{-2} \cdot n^+ - (f^2 \cdot n) / K_{\text{eq,FNR}}}{(1 + f^- + f^{-2}) \cdot (1 + n^+) + (1 + f + f^2) \cdot (1 + n^+) - 1}, \tag{28}$$

$$v_{\text{NADPHconsumption}} = k_{\text{NADPHconsumption}} \cdot N, \tag{29}$$

$$v_{\text{FQR}} = k_{\text{FQR}} \cdot F^2 \cdot (\text{PQ}^{\text{tot}} - P), \tag{30}$$

$$v_{\text{NDH}} = k_{\text{NDH}} \cdot (\text{PQ}^{\text{tot}} - P), \tag{31}$$

$$v_{\text{Leak}} = k_{\text{leak}} \cdot (H - pH_{\text{inv}}(\text{pH}_{\text{stroma}})), \tag{32}$$

$$v_{\text{PTOX}} = k_{\text{PTOX}} \cdot \text{O}_2^{\text{ext}} \cdot P, \tag{33}$$

Reaction rates to calculate the dynamics of state transitions

$$v_{\text{Stt7}} = k_{\text{Stt7}} \cdot \left(\frac{1}{1 + \left(\frac{(\text{PQ}^{\text{tot}} - P)/\text{PQ}^{\text{tot}}}{K_{\text{M,ST}}}\right)^{n_{\text{ST}}}}\right) \cdot (1 - L), \tag{34}$$

$$v_{\text{Pph1}} = k_{\text{Pph1}} \cdot L, \tag{35}$$

Reaction rates to calculate the dynamics of photoinhibition

$$v_{\text{degPSII}} = k_{deg}(B_1 + B_3), \tag{36}$$

$$v_{\text{repPSII}} = k_{rep}(1 - B/\text{PSII}^{\text{tot}}), \tag{37}$$

+ Eq. 14 - 16, Tab.A1 to calculate Equilibrium $\tag{38}$

+ Eq. 17, Tab.A1 to calculate the fluorescence signal $\tag{39}$

Table A3: Complete set of equations used in the qT model.

Parameter	Value	Description and reference
Pool sizes		
$PSII^{tot}$	2.5 mmol(mol Chl)$^{-1}$	PSII reaction centres [215]
PSI^{tot}	2.5 mmol(mol Chl)$^{-1}$	PSI reaction centres [215]
PQ^{tot}	17.5 mmol(mol Chl)$^{-1}$	PQ + PQH$_2$ [216]
PC^{tot}	4 mmol(mol Chl)$^{-1}$	PC$^-$ + PC$^+$ [221]
Fd^{tot}	5 mmol(mol Chl)$^{-1}$	Fd$^-$ + Fd$^+$ [221]
AP^{tot}	60 mmol(mol Chl)$^{-1}$	total adenosine phosphate pool (ATP + ADP)[217]
$NADP^{tot}$	25 mmol(mol Chl)$^{-1}$	NADP + NADPH, corresponds to 0.8mM, [217]
O_2^{ex}	8 mmol(mol Chl)$^{-1}$	external oxygen pool, corresponds to 250μM, after [26]
Pi_{mol}	0.01	internal pool of phosphates, required to calculate ATP equilibrium
Rate constants and key parameters		
k_{PQred}	250 mmol^{-1}(mol Chl) s^{-1}	after [26]
k_{PCox}	2500 mmol^{-1}(mol Chl) s^{-1}	after [26]
k_{Fdred}	$2.5\cdot10^5$ mmol^{-1}(mol Chl) s^{-1}	after [26]
k_{Cytb6f}	2.5 mmol^{-2}(mol Chl)^2 s^{-1}	after [26]
$k_{ActATPase}$	0.05 s^{-1}	rate constant of activation of the ATPase in the light
$k_{DeactATPase}$	0.002 s^{-1}	parameter relating the deactivation of the ATPase at night
$k_{ATPsynthase}$	20 s^{-1}	after [26]
$k_{ATPconsumption}$	10 s^{-1}	after [26]
$k_{NADPHconsumption}$	15 s^{-1}	fitted to yield reasonable NADPH:NADP$^+$ ratios
k_H	$5\cdot10^9$ s^{-1}	rate of non-radiative decay, after [26]
k_F	$6.25\cdot10^8$ s^{-1}	rate of fluorescence
k_P	$5\cdot10^9$ s^{-1}	rate of photochemistry after [26]
k_{PTOX}	0.01 mmol^{-1}(mol Chl) s^{-1}	after [26]
k_{NDH}	0.004 s^{-1}	fitted to inter-flash F$_S$-dynamics in anaerobic conditions (Fig. 2B)
v_{b6f}^{min}	-2.5 mmol(mol Chl)$^{-1}$s^{-1}	ad-hoc estimate to avoid strong reverse currents
V_{FNR}^{max}	1500 mmol(mol Chl)$^{-1}$s^{-1}	[221, 222]
k_{FQR}	1 mmol^{-2}(mol Chl)^2 s^{-1}	ad-hoc value, needs to be refined as model becomes more elaborate
pH_{stroma}	7.8	stroma pH of a dark adapted state
k_{leak}	0.010 s^{-1}	
b_H	100	proton buffering constant [154]
HPR	$\frac{14}{3}$	ratio of protons to ATP in ATP synthase
Michaelis constants		
$K_{M,F}$	1.56 mmol(mol Chl)$^{-1}$	0.05mM, [223]
$K_{M,N}$	0.22 mmol(mol Chl)$^{-1}$	0.007mM, [224, 225]
$K_{M,ST}$	0.2	after [26], to yield a PQ redox poise of $\approx$ 1:1
$K_{M,fdST}$	0.5	estimated to block state transitions under high light intensity
Parameters associated with state transitions		
k_{Stt7}	0.0035 s^{-1}	rate of phosphorylation after [26]
k_{Pph1}	0.0013 s^{-1}	rate of de-phosphorylation after [26]
σ_I^0	0.37	relative cross section of PSI-LHCI supercomplex [78, 226]
σ_{II}^0	0.1	relative cross section of PSII [78, 226]
n_{ST}	2	cooperativity, after [26]
n_{fdST}	2	ad-hoc value to use a reasonable cooperativity
$P(qT)$	1	default probability of attaching phosphorylated antennae to PSI
Parameters associated with photoinhibition		
k_{deg}	100 s^{-1}	rate of protein degradation, estimated to be 5e7 times slower than k_P
k_{rep}	$5.55e-4$s^{-1}	rate of protein repair after [147]
Physical constants		
F	96.485 kJ	Faraday constant
R	8.3 JK^{-1}mol^{-1}	universal gas constant
T	298 K	temperature
Standard potentials		
E^0(QA/QA$^-$)	-0.140 V	[218]
E^0(PQ/PQH$_2$)	0.354 V	[219]
E^0(PC/PC$^-$)	0.380 V	[220]
E^0(P$_{700}^+$/P$_{700}$)	0.480 V	[227]
E^0(FA/FA$^-$)	-0.550 V	[228]
E^0(Fd/Fd$^-$)	-0.430 V	[229]
E^0(NADP$^+$/NADPH)	-0.113 V	[27]
$\Delta G_{0_{ATP}}$	30.6 kJ/mol/RT	standard Gibbs free energy change of ATP formation (Eq. 4.3.25) [27]

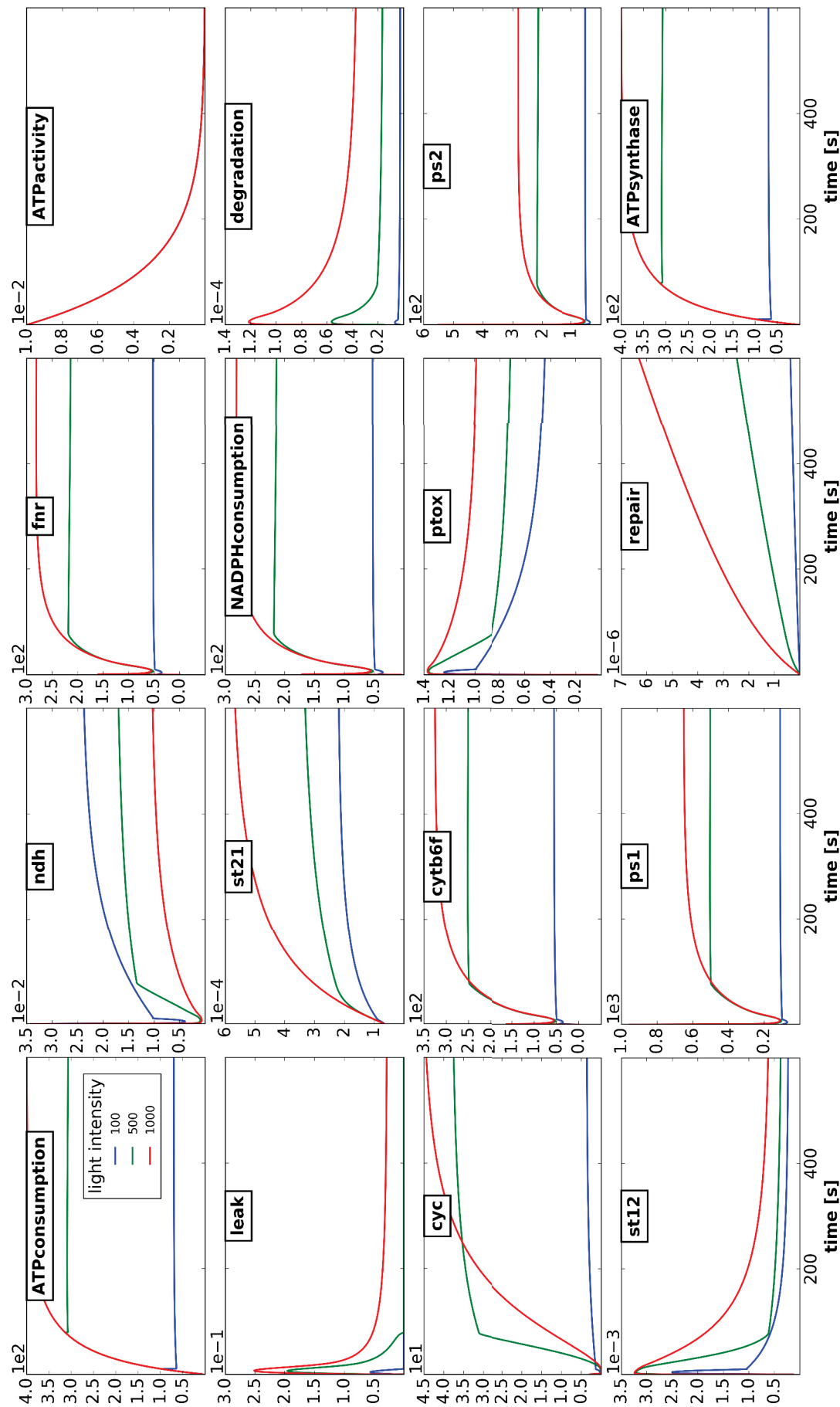**Table A4:** Complete summary of parameters used in the qT model.

Figure A2: Reaction rates of state transition model after 10 min of exposure to three different light intensities. The rates are expressed in $mmol(mol\ Chl)^{-1}s^{-1}$.
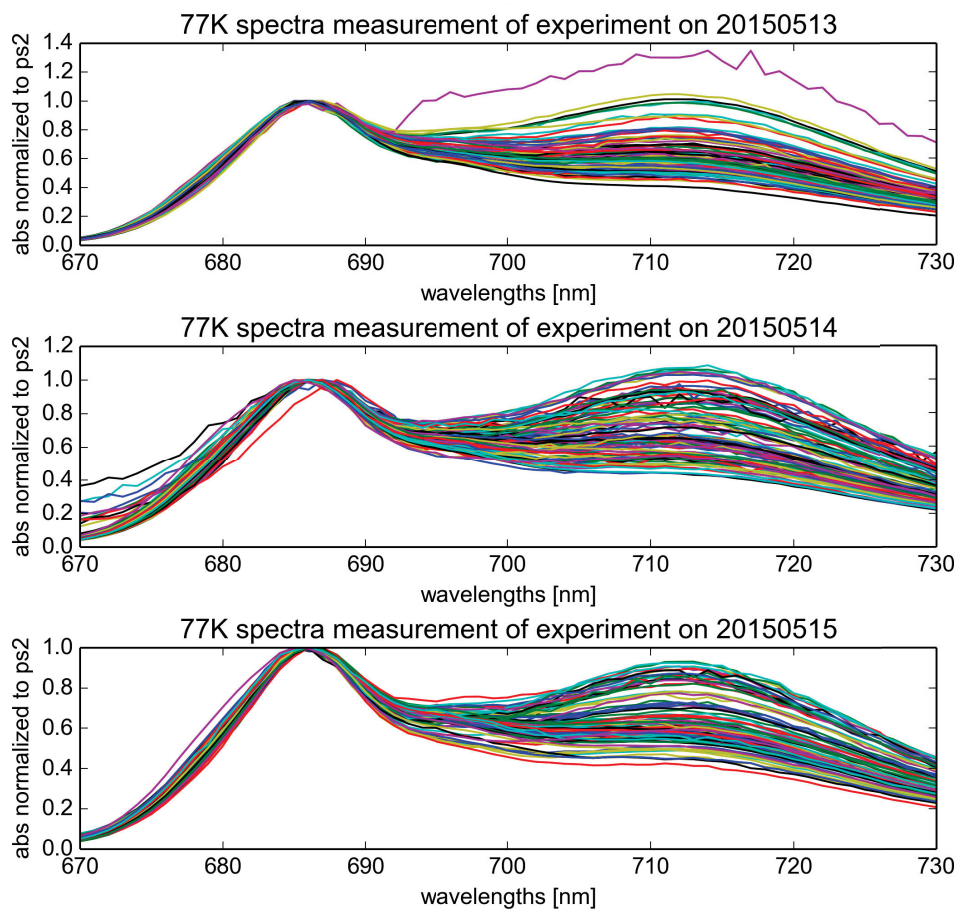
Figure A3: Raw 77K fluorescence absorption spectra for the three experiments performed in Okazaki.

Bibliography

[1] Blankenship, R. E., Molecular mechanisms of photosynthesis, Blackwell Science Ltd, 2008. `doi:10.1002/9780470758472`.

[2] Gest, H., History of the word photosynthesis and evolution of its definition, *Photosynth. Res.* 73 (1-3) (2002) 7–10. `doi:10.1023/A:1020419417954`.

[3] Barnes, C. R., On the Food of Green Plants, *Bot. Gaz.* 18 (11) (1893) 403–411.

[4] Huzisige, H., and Ke, B., Dynamics of the history of photosynthesis research, *Photosynth. Res.* 38 (2) (1993) 185–209. `doi:10.1007/BF00146418`.

[5] Govindjee, and Krogmann, D., Discoveries in oxygenic photosynthesis (1727 – 2003): a perspective, *Photosynth. Res.* 80 (2004) 15–57.

[6] Hershey, D., Misconceptions about Helmont's Willow Experiment, *Plant Science Bulletin* 28 (3).

[7] Hales, S., Vegetable staticks, or, an account of some statical experiments on the sap in vegetation, Printed for W. and J. Innys, 1727. `doi:10.5962/bhl.title.562`.

[8] Taiz, L., and Zeiger, E., Plant Physiology. Fifth Edition, Vol. 24, Sinauer Associates Inc., Publishers, 2010. `doi:10.1104/pp.900074`.

[9] Landmeyer, J. E., Introduction to Phytoremediation of contaminated groundwater. Historical Foundation, Hydrologic Control, and Contaminant Remediation, Springer, 2012.

[10] Priestley, J., and Hey, W., Observations on Different Kinds of Air. By Joseph Priestley, L L. D. F. R. S., *Philos. Trans. R. Soc. London* 62 (0) (1772) 147–264. `doi:10.1098/rstl.1772.0021`.

[11] Cobb, C., and Goldwhite, H., ca. 1848–1914: Thermodynamics- The Heat of the Matter, Springer US, Boston, MA, 1995, Ch. 11, pp. 213–233. `doi:10.1007/978-1-4899-2770-5_11`.

[12] Hill, R., Oxygen Produced by Isolated Chloroplasts, *Proc. R. Soc. B Biol. Sci.* 127 (847) (1939) 192–210. `doi:10.1098/rspb.1939.0017`.

[13] Eberhard, S., Finazzi, G., and Wollman, F.-A., The dynamics of photosynthesis, *Annu. Rev. Genet.* 42 (2008) 463–515. `doi:10.1146/annurev.genet.42.110807.091452`.

[14] Govindjee, and Gest, H., Celebrating the millennium – historical highlights of photosynthesis, *Photosynth. Res.* 73 (2002) 1–6.

[15] Govindjee, R., The Z-Scheme Diagram of Photosynthesis, Website. Accessed on 18.08.2016. URL `http://www.life.illinois.edu/govindjee/ZSchemeG.html`

[16] Lanzi, Lichtreaktion im Detail. Wikimedia Commons, Website. Accessed on 01.08.2016. URL `https://commons.wikimedia.org/wiki/File:Lichtreaktion-z-schema.svg`

[17] Australian Society of Plant Scientists, Online text book. Accessed on 01.08.2016. [link]. URL `http://plantsinaction.science.uq.edu.au`

[18] PhotosynQ Project, Website. Accessed on 15.07.2016. URL `http://www.nobelprize.org/`

[19] Marie Curie Initial Training Network AccliPhot, Website. Accessed on 22.08.2016. URL `http://www.accliphot.eu/`

[20] Andersson, B., and Anderson, J. M., Lateral heterogeneity in the distribution of chlorophyll-protein complexes of the thylakoid membranes of spinach chloroplasts, *Biochim. Biophys. Acta* 593 (2) (1980) 427–440. `doi:10.1016/0005-2728(80)90078-X`.

[21] Mustardy, L., and Garab, G., Granum revisited. A three-dimensional model - Where things fall into place, *Trends Plant Sci.* 8 (3) (2003) 117–122. `doi:10.1016/S1360-1385(03)00015-3`.

[22] Nagy, G., Ünnep, R., Zsiros, O., Tokutsu, R., Takizawa, K., Porcar, L., Moyet, L., Petroutsos, D., Garab, G., Finazzi, G., and Minagawa, J., Chloroplast remodeling during state transitions in Chlamydomonas reinhardtii as revealed by noninvasive techniques in vivo, *Proc. Natl. Acad. Sci. U. S. A.* 111 (13) (2014) 5042–7. `doi:10.1073/pnas.1322494111`.

[23] Wei, X., Su, X., Cao, P., Liu, X., Chang, W., Li, M., Zhang, X., and Liu, Z., Structure of spinach photosystem II–LHCII supercomplex at 3.2 Å resolution, *Nature* 534 (7605) (2016) 69–74. `doi:10.1038/nature18020`.

[24] Antal, T. K., Kovalenko, I. B., Rubin, A. B., and Tyystjärvi, E., Photosynthesis-related quantities for education and modeling, *Photosynth. Res.* 117 (1-3) (2013) 1–30. `doi:10.1007/s11120-013-9945-8`.

[25] Webber, A. N., and Lubitz, W., P700: The primary electron donor of photosystem I, *Biochim. Biophys. Acta* 1507 (1-3) (2001) 61–79. `doi:10.1016/S0005-2728(01)00198-0`.

[26] Ebenhöh, O., Fucile, G., Finazzi, G. G., Rochaix, J.-D., and Goldschmidt-Clermont, M., Short-term acclimation of the photosynthetic electron transfer chain to changing light: a mathematical model, *Philos. Trans. B* 369 (2013) 20130223. `doi:10.1098/rstb.2013.0223`.

[27] Nicholls, D. G., and Ferguson, S. J., Bioenergetics, third edition Edition, Academic Press, London, 2003. `doi:10.1016/B978-012518121-1/50000-2`.

[28] Allen, J. F., Chloroplast Redox Poise and Signaling, no. H 20, Elsevier, 2004, pp. 438–445.

[29] Joët, T., Cournac, L., Peltier, G., and Havaux, M., Cyclic electron flow around photosystem I in C(3) plants. In vivo control by the redox state of chloroplasts and involvement of the NADH-dehydrogenase complex, *Plant physiology* 128 (2) (2002) 760–9. `doi:10.1104/pp.010775`.

[30] Joliot, P., and Joliot, A., Cyclic electron transfer in plant leaf, *Proc. Natl. Acad. Sci. U. S. A.* 99 (15) (2002) 10209–14. `doi:10.1073/pnas.102306999`.

[31] Finazzi, G., and Johnson, G. N., Cyclic electron flow : facts and hypotheses, *Photosynth. Res.* 129 (3) (2016) 227–230. `doi:10.1007/s11120-016-0306-2`.

[32] Avenson, T. J., Cruz, J. A., Kanazawa, A., Kramer, D. M., and Mechanisms, F., Regulating the proton budget of higher plant photosynthesis, *Proc. Natl. Acad. Sci. USA* 102 (27) (2005) 9709–9713.

[33] Cruz, J. A., Sacksteder, C. A., Kanazawa, A., and Kramer, D. M., Contribution of Electric Field ($\Delta\Psi$) to Steady-State Transthylakoid Proton Motive Force (pmf) in Vitro and in Vivo. Control of pmf Parsing into $\Delta\Psi$ and ΔpH by Ionic Strength, *Biochemistry* 40 (2001) 1226–1237. `doi:10.1021/bi0018741`.

[34] Sacksteder, C. A., Kanazawa, A., Jacoby, M. E., and Kramer, D. M., The proton to electron stoichiometry of steady-state photosynthesis in living plants: A proton-pumping Q cycle is continuously engaged, *Proc. Natl. Acad. Sci. USA* 97 (26) (2000) 14283–14288.

[35] Allen, J. F., Photosynthesis of ATP — Electrons, Proton Pumps, Rotors, and Poise, *Cell* 110 (3) (2002) 273–276.

[36] Kramer, D. M., Evans, J. R., State, M., Lansing, E., and Division, P. S., The Importance of Energy Balance in Improving Photosynthetic Productivity, *Plant Physiology* 155 (January) (2011) 70–78. `doi:10.1104/pp.110.166652`.

[37] Frenkel, M., Bellafiore, S., Rochaix, J. D., and Jansson, S., Hierarchy amongst photosynthetic acclimation responses for plant fitness, *Physiol. Plant.* 129 (2) (2007) 455–459. `doi:10.1111/j.1399-3054.2006.00831.x`.

[38] Sukenik, A., Bennett, J., and Falkowski, P., Light-saturated photosynthesis - limitation by electron transport or carbon fixation?, *Biochim. Biophys. Acta* 891 (3) (1987) 205–215.

[39] Anderson, J. M., Chow, W. S., and Park, Y. I., The grand design of photosynthesis: acclimation of the photosynthetic apparatus to environmental cues, *Photosynth. Res.* 46 (1-2) (1995) 129–139.

[40] Smith, B. M., Morrissey, P. J., and Guenther, J. E., Response of the photosynthetic apparatus in Dunaliella salina (green algae) to irradiance stress, *Plant Physiol.* 93 (4) (1990) 1433–1440.

[41] Melis, A., Dynamics of photosynthetic membrane composition and function, *Biochim. Biophys. Acta* 1058 (2) (1991) 87–106.

[42] Ballottari, M., Dall'Osto, L., and Morosinotto, T., Contrasting behavior of higher plant photosystem I and II antenna systems during acclimation, *J. Biol.* 282 (12) (2007) 8947–8958.

[43] Mitchell, K. J., Influence of Light and Temperature on the Growth of Ryegrass (Lolium spp.): I. Pattern of Vegetative Development, *Physiol. Plant.* 6 (1) (1953) 21–46. `doi:10.1111/j.1399-3054.1953.tb08930.x`.

[44] Bonente, G., Pippa, S., Castellano, S., Bassi, R., and Ballottari, M., Acclimation of Chlamydomonas reinhardtii to different growth irradiances, *J. Biol. Chem.* 287 (8) (2012) 5833–5847. `doi:10.1074/jbc.M111.304279`.

[45] Yin, Y., Yu, C., Yu, L., Zhao, J., Sun, C., Ma, Y., and Zhou, G., The influence of light intensity and photoperiod on duckweed biomass and starch accumulation for bioethanol production, *Bioresour. Technol.* 187 (2015) 84–90. `doi:10.1016/j.biortech.2015.03.097`.

[46] Khoeyi, Z. A., Seyfabadi, J., and Ramezanpour, Z., Effect of light intensity and photoperiod on biomass and fatty acid composition of the microalgae, Chlorella vulgaris, *Aquac. Int.* 20 (1) (2012) 41–49. `doi:10.1007/s10499-011-9440-1`.

[47] Brown, M. R., and Hohmann, S., Effects of irradiance and growth phase on the ascorbic acid content of Isochrysis sp. T.ISO (Prymnesiophyta), *J. Appl. Phycol.* 14 (3) (2002) 211–214. `doi:10.1023/A:1019973520381`.

[48] Danesi, E. D. G., Rangel-Yagui, C. O., Carvalho, J. C. M., and Sato, S., Effect of reducing the light intensity on the growth and production of chlorophyll by Spirulina platensis, *Biomass and Bioenergy* 26 (4) (2004) 329–335. `doi:10.1016/S0961-9534(03)00127-2`.

[49] MacIntyre, H. L., Kana, T. M., Anning, T., and Geider, R. J., Photoacclimation of photosynthesis irradiance response curves and photosynthetic pigments in microalgae and cyanobacteria, *J. Phycol.* 38 (1) (2002) 17–38. `doi:10.1046/j.1529-8817.2002.00094.x`.

[50] Müller-Xing, R., Xing, Q., and Goodrich, J., Footprints of the sun: memory of UV and light stress in plants, *Front. Plant Sci.* 5 (September) (2014) 474. `doi:10.3389/fpls.2014.00474`.

[51] Wikimedia Commons. Chlorophyll ab spectra by Daniele Pugliesi, Website. Accessed on 01.09.2016. URL `https://commons.wikimedia.org/wiki/File:Chlorophyll_ab_spectra2.PNG`

[52] Depauw, F. A., Rogato, A., d'Alcala, M. R., and Falciatore, A., Exploring the molecular basis of responses to light in marine diatoms, *J. Exp. Bot.* 63 (4) (2012) 1575–1591. `doi:10.1093/jxb/ers005`.

[53] Rockwell, N. C., Duanmu, D., Martin, S. S., Bachy, C., Price, D. C., Bhattacharya, D., Worden, A. Z., and Lagarias, J. C., Eukaryotic algal phytochromes span the visible spectrum, *Proc. Natl. Acad. Sci. U. S. A.* 111 (10) (2014) 3871–3876. `doi:10.1073/pnas.1401871111`.

[54] Petroutsos, D., Tokutsu, R., Maruyama, S., Flori, S., Greiner, A., Magneschi, L., Cusant, L., Kottke, T., Mittag, M., Hegemann, P., Finazzi, G., and Minagawa, J., A blue-light photoreceptor mediates the feedback regulation of photosynthesis, *Nature* 537 (7621) (2016) 563–566. `doi:10.1038/nature19358`.

[55] Taddei, L., Rogato, A., Bailleul, B., Fortunato, A. E., Annunziata, R., Sanges, R., Thaler, M., Lepetit, B., Lavaud, J., Jaubert, M., Finazzi, G., Bouly, J.-P., and Falciatore, A., Multisignal control of expression of the LHCX protein family in the marine diatom Phaeodactylum tricornutum, *J. Exp. Bot.* 67 (2016) 3939–3951.

[56] Müller, P., Li, X.-p. P., and Niyogi, K. K., Update on Photosynthesis Non-Photochemical Quenching . A Response to Excess Light Energy 1, *Plant Physiol.* 125 (April) (2001) 1558–1566. `doi:10.1104/pp.125.4.1558`.

[57] Vander Meulen, D. L., and Govindjee, Is There a Triplet State in Photosynthesis?, *J. Sci. Ind. Res.* 32 (1973) 62–69.

[58] Horton, P., Ruban, a. V., and Walters, R. G., Regulation of Light Harvesting in Green Plants, *Annu. Rev. Plant Physiol. Plant Mol. Biol.* 47 (1) (1996) 655–684. `doi:10.1146/annurev.arplant.47.1.655`.

[59] Nilkens, M., Kress, E., Lambrev, P., Miloslavina, Y., Müller, M., Holzwarth, A. R., and Jahns, P., Identification of a slowly inducible zeaxanthin-dependent component of non-photochemical quenching of chlorophyll fluorescence generated under steady-state conditions in Arabidopsis, *Biochim. Biophys. Acta* 1797 (4) (2010) 466–475. `doi:10.1016/j.bbabio.2010.01.001`.

[60] Quick, W. P., and Stitt, M., An examination of factors contributing to non-photochemical quenching of chlorophyll fluorescence in barley leaves, *Biochim. Biophys. Acta* 977 (3) (1989) 287–296.

[61] Walters, R. G., and Horton, P., Resolution of components of non-photochemical chlorophyll fluorescence quenching in barley leaves, *Photosynth. Res.* 27 (2) (1991) 121–133.

[62] Joliot, P. A., and Finazzi, G., Proton equilibration in the chloroplast modulates multiphasic kinetics of nonphotochemical quenching of fluorescence in plants, *Proc. Natl. Acad. Sci. U. S. A.* 107 (2010) 12728–12733. `doi:10.1073/pnas.1006399107`.

[63] Dall'Osto, L., Caffarri, S., and Bassi, R., A mechanism of nonphotochemical energy dissipation, independent from PsbS, revealed by a conformational change in the antenna protein CP26, *Plant Cell* 17 (4) (2005) 1217–1232.

[64] Briantais, J.-M., Vernotte, C., Picaud, M., and Krause, G. H., A quantitative study of the slow decline of chlorophyll a fluorescence in isolated chloroplasts, *Biochim. Biophys. Acta* 548 (1) (1979) 128–138.

[65] Allen, J. F., Bennett, J., Steinback, K. E., and Arntzen, C., Chloroplast protein phosphorylation couples plastoquinone redox state to distribution of excitation energy between photosystems, *Nature* 291 (5810) (1981) 25–29.

[66] Krause, G. H., Photoinhibition of photosynthesis. An evaluation of damaging and protective mechanisms, *Physiol. Plant.* 74 (3) (1988) 566–574.

[67] Niyogi, K. K., and Truong, T. B., Evolution of flexible non-photochemical quenching mechanisms that regulate light harvesting in oxygenic photosynthesis, *Curr. Opin. Plant Biol.* 16 (3) (2013) 307–314.

[68] Holzwarth, A., and Jahns, P., Non-photochemical quenching mechanisms in intact organisms as derived from ultrafast-fluorescence kinetic studies, Vol. 40, Springer, 2014, Ch. 5, pp. 129–156. `doi:10.1007/978-94-017-9032-1_5`.

[69] Jahns, P., Latowski, D., and Strzalka, K., Mechanism and regulation of the violaxanthin cycle: The role of antenna proteins and membrane lipids, *Biochim. Biophys. Acta - Bioenerg.* 1787 (1) (2009) 3–14. `doi:10.1016/j.bbabio.2008.09.013`.

[70] Stransky, H., and Hager, A., Das Carotenoidmuster und dieVerbreitung des lichtinduzierten Xanthophyllcyclus in versc-hiedenen Algenklassen, *Arch. Mikrobiol* 73 (1970) 315–323.

[71] Bungard, R. A., Ruban, A. V., Hibberd, J. M., Press, M. C., Horton, P., and Scholes, J. D., Unusual carotenoid composition and a new type of xanthophyll cycle in plants, *Proc. Natl. Acad. Sci. USA* 96 (February) (1999) 1135–1139. `doi:10.1073/pnas.96.3.1135`.

[72] Yamamoto, H. Y., Biochemistry of the violaxanthin cycle in higher plants, *Pure Appl. Chem.* 51 (1979) 639–648.

[73] Hager, A., Untersuchungen üben die Rückreaktionen im Xanthophyll-Cyclus bei Chlorella, Spinacia und Taxus, *Planta* 76 (2) (1967) 138–148. `doi:10.1007/BF00385460`.

[74] Wollman, F. A., State transitions reveal the dynamics and flexibility of the photosynthetic apparatus, *EMBO J.* 20 (14) (2001) 3623–3630. `doi:10.1093/emboj/20.14.3623`.

[75] Minagawa, J., and Tokutsu, R., Dynamic regulation of photosynthesis in Chlamydomonas reinhardtii, *Plant J.* 82 (3) (2015) 413–428. `doi:10.1111/tpj.12805`.

[76] Bonaventura, C., and Myers, J., Fluorescence and oxygen evolution from Chlorella pyrenoidosa, *Biochim. Biophys. Acta* 189 (3) (1969) 366–83. `doi:10.1016/0005-2728(69)90168-6`.

[77] Murata, N., Control of excitation transfer in photosynthesis I. Light-induced change of chlorophyll a fluoresence in Porphyridium cruentum, *Biochim. Biophys. Acta* 172 (3) (1969) 242–251. `doi: 10.1016/0005-2728(70)90104-0`.

[78] Unlü, C., Drop, B., Croce, R., van Amerongen, H., Amerongen, H. V., and Ünlü, C., State transitions in Chlamydomonas reinhardtii strongly modulate the functional size of photosystem II but not of photosystem I, *Proc. Natl. Acad. Sci. U. S. A.* 111 (2014) 3460–5. `doi:10.1073/pnas.1319164111`.

[79] Nawrocki, W. J., Santabarbara, S., Mosebach, L., and Wollman, F.-A., State transitions redistribute rather than dissipate energy between the two photosystems in Chlamydomonas, *Nat. Plants* 2 (4) (2016) 1–7. `doi:10.1038/nplants.2016.31`.

[80] Vener, A. V., van Kan, P. J. M., Rich, P. R., Ohad, I., and Andersson, B., Plastoquinol at the quinol oxidation site of reduced cytochrome bf mediates signal transduction between light and protein phosphorylation: thylakoid protein kinase deactivation by a single-turnover flash, *Proc. Natl. Acad. Sci. USA* 94 (4) (1997) 1585–90. `doi:10.1073/pnas.94.4.1585`.

[81] Zito, F., Finazzi, G., Delosme, R., Nitschke, W., Picot, D., and Wollman, F. A., The Qo site of cytochrome b6f complexes controls the activation of the LHCII kinase, *EMBO J.* 18 (11) (1999) 2961–2969. `doi:10.1093/emboj/18.11.2961`.

[82] Le Quiniou, C., Van Oort, B., Drop, B., Van Stokkum, I. H. M., and Croce, R., The high efficiency of photosystem i in the green Alga Chlamydomonas reinhardtii is maintained after the antenna size is substantially increased by the association of light-harvesting complexes II, *J. Biol. Chem.* 290 (51) (2015) 30587–30595. `doi:10.1074/jbc.M115.687970`.

[83] Owens, T. G., Photosystem II heterogeneity in the marine diatom Phaeodactylum tricornutum, *Photochemistry and Photobiology* 43 (5) (1986) 535–544. `doi:10.1111/j.1751-1097.1986.tb09532.x`.

[84] Bellafiore, S., Barneche, F., Peltier, G., and Rochaix, J.-D., State transitions and light adaptation require chloroplast thylakoid protein kinase STN7, *Nature* 433 (February) (2005) 892–895.

[85] Delosme, R., Olive, J., and Wollman, F. A., Changes in light energy distribution upon state transitions: An in vivo photoacoustic study of the wild type and photosynthesis mutants from Chlamydomonas reinhardtii, *Biochim. Biophys. Acta - Bioenerg.* 1273 (2) (1996) 150–158. `doi: 10.1016/0005-2728(95)00143-3`.

[86] Allorent, G., Tokutsu, R., Roach, T., Peers, G., Cardol, P., Girard-Bascou, J., Seigneurin-Berny, D., Petroutsos, D., Kuntz, M., Breyton, C., Franck, F., Wollman, F.-A., Niyogi, K. K., Krieger-Liszkay, A., Minagawa, J., and Finazzi, G., A dual strategy to cope with high light in Chlamydomonas reinhardtii, *Plant Cell* 25 (2) (2013) 545–57. `doi:10.1105/tpc.112.108274`.

[87] Aro, E.-M., Virgin, I., and Andersson, B., Photoinhibition of photosystem. II. Inactivation, protein damage and turnover, *Biochim. Biophys. Acta - Bioenerg.* 1143 (2) (1993) 113–134. `doi:10.1016/0005-2728(93)90134-2`.

[88] Murata, N., Takahashi, S., Nishiyama, Y., and Allakhverdiev, S. I., Photoinhibition of photosystem II under environmental stress, *Biochim. Biophys. Acta - Bioenerg.* 1767 (6) (2007) 414–421. `doi: 10.1016/j.bbabio.2006.11.019`.

[89] Ort, D. R., Merchant, S. S., Alric, J., Barkan, A., Blankenship, R. E., Bock, R., Croce, R., Hanson, M. R., Hibberd, J. M., Long, S. P., Moore, T. A., Moroney, J., Niyogi, K. K., Parry, M. A. J., Peralta-Yahya, P. P., Prince, R. C., Redding, K. E., Spalding, M. H., van Wijk, K. J., Vermaas, W.

F. J., von Caemmerer, S., Weber, A. P. M., Yeates, T. O., Yuan, J. S., and Zhu, X. G., Redesigning photosynthesis to sustainably meet global food and bioenergy demand, *Proc. Natl. Acad. Sci.* 112 (28) (2015) 201424031. `doi:10.1073/pnas.1424031112`.

[90] Hüner, N. P. A., Dahal, K., Kurepin, L. V., Savitch, L., Singh, J., Ivanov, A. G., Kane, K., and Sarhan, F., Potential for increased photosynthetic performance and crop productivity in response to climate change: role of CBFs and gibberellic acid, *Front. Chem.* 2 (April) (2014) 18. `doi:10.3389/fchem.2014.00018`.

[91] Powell, N., Ji, X., Ravash, R., Edlington, J., and Dolferus, R., Yield stability for cereals in a changing climate, *Funct. Plant Biol.* 39 (7) (2012) 539–552. `doi:10.1071/FP12078`.

[92] Ruban, A. V., Johnson, M. P., and Duffy, C. D., The photoprotective molecular switch in the photosystem II antenna, *Biochim. Biophys. Acta* 1817 (1) (2012) 167–181.

[93] Jahns, P., and Holzwarth, A. R., The role of the xanthophyll cycle and of lutein in photoprotection of photosystem II, *Biochim. Biophys. Acta - Bioenerg.* 1817 (1) (2012) 182–193. `doi:10.1016/j.bbabio.2011.04.012`.

[94] Murchie, E. H., Pinto, M., and Horton, P., Agriculture and the new challenges for photosynthesis research, *New Phytol.* 181 (3) (2009) 532–552. `doi:10.1111/j.1469-8137.2008.02705.x`.

[95] Kramer, D. M., Avenson, T. J., and Edwards, G. E., Dynamic flexibility in the light reactions of photosynthesis governed by both electron and proton transfer reactions, *Trends in Plant Science* 349 (7) (2004) 349–357. `doi:10.1016/j.tplants.2004.05.001`.

[96] Kirst, H., Formighieri, C., and Melis, A., Maximizing photosynthetic efficiency and culture productivity in cyanobacteria upon minimizing the phycobilisome light-harvesting antenna size, *Biochim. Biophys. Acta - Bioenerg.* 1837 (10) (2014) 1653–1664. `doi:10.1016/j.bbabio.2014.07.009`.

[97] De Mooij, T., Janssen, M., Cerezo-Chinarro, O., Mussgnug, J. H., Kruse, O., Ballottari, M., Bassi, R., Bujaldon, S., Wollman, F. A., and Wijffels, R. H., Antenna size reduction as a strategy to increase biomass productivity: a great potential not yet realized, *J. Appl. Phycol.* (2014) 1063–1077`doi:10.1007/s10811-014-0427-y`.

[98] Minagawa, J., Dynamic reorganization of photosynthetic supercomplexes during environmental acclimation of photosynthesis, *Front Plant Sci* 4 (December) (2013) 513. `doi:10.3389/fpls.2013.00513`.

[99] Fields, S., and Johnston, M., Whither Model Organism Research?, *Science* 307 (March) (2005) 1886–1888.

[100] Joyce, A. R., and Palsson, B. Ø., The model organism as a system: integrating 'omics' data sets, *Nat. Rev. Mol. Cell Biol.* 7 (3) (2006) 198–210. `doi:10.1038/nrm1857`.

[101] Leonelli, S., and Ankeny, R. A., What makes a model organism?, *Endeavour* 37 (4) (2013) 209–212. `doi:10.1016/j.endeavour.2013.06.001`.

[102] Fleischmann, R. D., Adams, M. D., White, O., Clayton, R. A., Ewen, F., Kerlavage, A. R., Bult, C. J., Tomb, J.-f., Dougherty, B. A., Merrick, J. M., Mckenney, K., Sutton, G., Fitzhugh, W., Fields, C., Jeannie, D., Scott, J., Shirley, R., Liu, L.-i., Glodek, A., Kelley, J. M., Janice, F., Phillips, C. A., Spriggs, T., Hedblom, E., Cotton, M. D., Fleischmann, R. D., Adams, M. D., White, O., Clayton, R. A., Kirkness, E. F., Kerlavage, A. R., Bult, C. J., Tomb, J.-F., Dougherty, B. A., Merrick, J. M., Mckenney, K., Sutton, G., Fitzhugh, W., Fields, C., Gocayne, J. D., Scott, J., Shirley, R., Liu, L.-i., Glodek, A., Kelley, J. M., Weidman, J. F., Phillips, C. A., Spriggs, T., Hedblom, E., Cotton, M. D.,

Utterback, T. R., Hanna, M. C., Nguyen, D. T., Saudek, D. M., Brandon, R. C., Fine, L. D., Fritchman, J. L., Fuhrmann, J. L., Geoghagen, N. S. M., Gnehm, C. L., Mcdonald, L. A., Small, K. V., Fraser, C. M., Smith, H., and Ventert, J. C., Whole-Genome Random Sequencing and Assembly Haemophilus influenzae of Rd, *Science* 269 (5223) (1995) 496–512. `doi:10.1126/science.7542800`.

[103] Gutman, B. L., and Niyogi, K. K., Chlamydomonas and Arabidopsis. A dynamic duo, *Plant Physiol.* 135 (2) (2004) 607–610. `doi:10.1104/pp.104.041491`.

[104] Goss, R., and Lepetit, B., Biodiversity of NPQ, *J. Plant Physiol.* 172 (2015) 13–32. `doi:10.1016/j.jplph.2014.03.004`.

[105] Arabidopsis Genome Initiative, Analysis of the genome sequence of the flowering plant Arabidopsis thaliana, *Nature* 408 (6814) (2000) 796–815. `doi:10.1038/35048692`.

[106] Rochaix, J.-D., Assembly, Function, and Dynamics of the Photosynthetic Machinery in, *Plant Physiol.* 127 (December) (2001) 1394–1398. `doi:10.1104/pp.010628.1394`.

[107] Merchant, S. S., Prochnik, S. E., Vallon, O., Harris, E. H., Karpowicz, S. J., Witman, G. B., Terry, A., Salamov, A., Fritz-laylin, L. K., Maréchal-drouard, L., Marshall, W. F., Qu, L.-h., Nelson, D. R., Sanderfoot, A. A., Spalding, M. H., Kapitonov, V. V., Ren, Q., Ferris, P., Lindquist, E., Shapiro, H., Lucas, S. M., Grimwood, J., Schmutz, J., Team, C. A., Team, J. A., Grigoriev, I. V., and Rokhsar, A. R., Daniel S. Grossman, The Chlamydomonas Genome Reveals the Evolution of Key Animal and Plant Functions, *Science* 318 (2007) 245–251.

[108] Cilia and Flagella: Structure and Movement, forth edit Edition, W. H. Freeman, New York, 2000.

[109] Pazour, G. J., and Witman, G. B., The Chlamydomonas Flagellum as a Model for Human Ciliary Disease, *Chlamydomonas Sourceb. 3-Vol set* 3 (2009) 445–478. `doi:10.1016/B978-0-12-370873-1.00052-6`.

[110] Rochaix, J. D., Chlamydomonas, a model system for studying the assembly and dynamics of photosynthetic complexes, *FEBS Lett.* 529 (1) (2002) 34–38. `doi:10.1016/S0014-5793(02)03181-2`.

[111] Stauber, E. J., and Hippler, M., Chlamydomonas reinhardtii proteomics, *Plant Physiol. Biochem.* 42 (12) (2004) 989–1001. `doi:10.1016/j.plaphy.2004.09.008`.

[112] Niyogi, K. K., Grossman, A. R., and Björkman, O., Arabidopsis mutants define a central role for the xanthophyll cycle in the regulation of photosynthetic energy conversion, *Plant Cell* 10 (7) (1998) 1121–1134. `doi:10.1105/tpc.10.7.1121`.

[113] Depège, N., Bellafiore, S., and Rochaix, J.-D., Role of chloroplast protein kinase Stt7 in LHCII phosphorylation and state transition in Chlamydomonas, *Science* 299 (5612) (2003) 1572–1575. `doi:10.1126/science.1081397`.

[114] Peers, G., Truong, T. B., Ostendorf, E., Busch, A., and Elrad, D., An ancient light-harvesting protein is critical for the regulation of algal photosynthesis, *Nature* 462 (7272) (2009) 518–521.

[115] Hu, Q., Sommerfeld, M., Jarvis, E., Ghirardi, M., Posewitz, M., Seibert, M., and Darzins, A., Microalgal triacylglycerols as feedstocks for biofuel production: Perspectives and advances, *Plant J.* 54 (2008) 621–639. `doi:10.1111/j.1365-313X.2008.03492.x`.

[116] Griffiths, M. J., and Harrison, S. T. L., Lipid productivity as a key characteristic for choosing algal species for biodiesel production, *J. Appl. Phycol.* 21 (5) (2009) 493–507. `doi:10.1007/s10811-008-9392-7`.

[117] Siaut, M., Cuiné, S., Cagnon, C., Fessler, B., Nguyen, M., Carrier, P., Beyly, A., Beisson, F., Trianta-phylidès, C., Li-Beisson, Y., and Peltier, G., Oil accumulation in the model green alga Chlamydomonas reinhardtii: characterization, variability between common laboratory strains and relationship with starch reserves, *BMC Biotechnol.* 11 (1) (2011) 7. `doi:10.1186/1472-6750-11-7`.

[118] Borowitzka, M. A., High-value products from microalgae-their development and commercialisation, *J. Appl. Phycol.* 25 (3) (2013) 743–756. `doi:10.1007/s10811-013-9983-9`.

[119] Draaisma, R. B., Wijffels, R. H., Slegers, P. M., Brentner, L. B., Roy, A., and Barbosa, M. J., Food commodities from microalgae, *Curr. Opin. Biotechnol.* 24 (2) (2013) 169–177. `doi:10.1016/j.copbio.2012.09.012`.

[120] Braun Galleani, S., Baganz, F., and Purton, S., Improving recombinant protein production in the Chlamydomonas reinhardtii chloroplast using vivid Verde Fluorescent protein as a reporter, *Biotechnol. J.*`doi:10.1002/biot.201400566`.

[121] Stirbet, A., and Govindjee, On the relation between the Kautsky effect (chlorophyll a fluorescence induction) and Photosystem II: Basics and applications of the OJIP fluorescence transient, *J. Photochem. Photobiol. B Biol.* 104 (1-2) (2011) 236–257. `doi:10.1016/j.jphotobiol.2010.12.010`.

[122] Maxwell, K., and Johnson, G., Chlorophyll fluorescence, *J. Exp. Bot.* 51 (345) (2000) 659–668. `doi:10.1093/jexbot/51.345.659`.

[123] Pu, Y., Shi, L., Pratavieira, S., and Alfano, R. R., Two-photon excitation microscopy using the second singlet state of fluorescent agents within the "tissue optical window", *Journal of Applied Physics* 114 (15). `doi:10.1063/1.4825319`.

[124] Stirbet, A., Riznichenko, G. Y., Rubin, A. B., and Govindjee, Modeling chlorophyll a fluorescence transient: relation to photosynthesis, *Biochemistry* 79 (4) (2014) 291–323. `doi:10.1134/S0006297914040014`.

[125] Papageorgiou, G. C., and Govindjee, Photosystem II fluorescence: Slow changes - Scaling from the past, *J. Photochem. Photobiol. B Biol.* 104 (1-2) (2011) 258–270. `doi:10.1016/j.jphotobiol.2011.03.008`.

[126] Murchie, E. H., and Lawson, T., Chlorophyll fluorescence analysis : a guide to good practice and understanding some new applications, *Journal of Experimental Botany*`doi:10.1093/jxb/ert208`.

[127] Kasajima, I., Takahara, K., Kawai-Yamada, M., and Uchimiya, H., Estimation of the relative sizes of rate constants for chlorophyll de-excitation processes through comparison of inverse fluorescence intensities, *Plant & cell physiology* 50 (9) (2009) 1600–1616. `doi:10.1093/pcp/pcp102`.

[128] Baker, N. R., Chlorophyll fluorescence: a probe of photosynthesis in vivo, *Annu. Rev. Plant Biol.* 59 (2008) 89–113. `doi:10.1146/annurev.arplant.59.032607.092759`.

[129] Almquist, J., Cvijovic, M., Hatzimanikatis, V., Nielsen, J., and Jirstrand, M., Kinetic models in industrial biotechnology - Improving cell factory performance, *Metab. Eng.* 24 (2014) 38–60. `doi:10.1016/j.ymben.2014.03.007`.

[130] Pfau, T., Christian, N., and Ebenhöh, O., Systems approaches to modelling pathways and networks, *Brief. Funct. Genomics* 10 (5) (2011) 266–279. `doi:10.1093/bfgp/elr022`.

[131] Lazár, D., and Jablonský, J., On the approaches applied in formulation of a kinetic model of photosystem II: Different approaches lead to different simulations of the chlorophyll a fluorescence transients, *J. Theor. Biol.* 257 (2) (2009) 260–269. `doi:10.1016/j.jtbi.2008.11.018`.

[132] Cornet, J.-F., Dussap, C. G., and Gros, J.-B., Kinetics and energetics of photosynthetic micro-organisms in photobioreactors, in: Bioprocess Algae React. Technol. Apoptosis, Vol. 59 of *Advances in Biochemical Engineering Biotechnology*, Springer Berlin Heidelberg, 1998, pp. 153–224. `doi: 10.1007/BFb0102299`.

[133] Cogne, G., Rügen, M., Bockmayr, A., Titica, M., Dussap, C. G., Cornet, J. F., and Legrand, J., A model-based method for investigating bioenergetic processes in autotrophically growing eukaryotic microalgae: Application to the green algae Chlamydomonas reinhardtii, *Biotechnol. Prog.* 27 (3) (2011) 631–640. `doi:10.1002/btpr.596`.

[134] Heckmann, D., Schulze, S., Denton, A., Gowik, U., Westhoff, P., Weber, A. P. M., and Lercher, M. J., XPredicting C4 photosynthesis evolution: Modular, individually adaptive steps on a mount fuji fitness landscape, *Cell* 153 (7). `doi:10.1016/j.cell.2013.04.058`.

[135] Baroukh, C., Muñoz-Tamayo, R., Steyer, J.-P., and Bernard, O., A state of the art of metabolic networks of unicellular microalgae and cyanobacteria for biofuel production, *Metab. Eng.* 30 (2015) 49–60. `doi:10.1016/j.ymben.2015.03.019`.

[136] Zhu, X. G., Govindjee, Baker, N. R., DeSturler, E., Ort, D. R., and Long, S. P., Chlorophyll a fluorescence induction kinetics in leaves predicted from a model describing each discrete step of excitation energy and electron transfer associated with Photosystem II, *Planta* 223 (1) (2005) 114–133. `doi:10.1007/s00425-005-0064-4`.

[137] Matuszyńska, A., and Ebenhöh, O., A reductionist approach to model photosynthetic self-regulation in eukaryotes in response to light, *Biochem. Soc. Trans.* 43 (6) (2015) 1133–1139. `doi:10.1042/BST20150136`.

[138] Thornley, J. H. M., Light Fluctuations and Photosynthesis, *Ann. Bot.* 38 (1974) 363–373.

[139] Mast, F. D., Ratushny, A. V., and Aitchison, J. D., Systems cell biology, *J Cell Biol* 206 (6) (2014) 695–706. `doi:10.1083/jcb.201405027`.

[140] Fell, D. a., Poolman, M. G., and Gevorgyan, A., Building and analysing genome-scale metabolic models, *Biochem. Soc. Trans.* 38 (5) (2010) 1197–201. `doi:10.1042/BST0381197`.

[141] Poolman, M. G., Poolman, M. G., Miguet, L., Miguet, L., Sweetlove, L. J., Sweetlove, L. J., Fell, D. A., and Fell, D. A., A Genome-scale Metabolic Model of Arabidopsis thaliana and Some of its Properties, *Plant Physiol.* 151 (November) (2009) 1570–1581. `doi:10.1104/pp.109.141267`.

[142] Chang, R. L., Ghamsari, L., Manichaikul, A., Hom, E. F. Y., Balaji, S., Fu, W., Shen, Y., Hao, T., Palsson, B. Ø., Salehi-Ashtiani, K., and Papin, J. A., Metabolic network reconstruction of Chlamydomonas offers insight into light-driven algal metabolism, *Mol Syst Biol* 7 (2011) 518. `doi:10.1038/msb.2011.52`.

[143] Knoop, H., Zilliges, Y., Lockau, W., and Steuer, R., The metabolic network of Synechocystis sp. PCC 6803: systemic properties of autotrophic growth, *Plant Physiol.* 154 (1) (2010) 410–422. `doi:10.1104/pp.110.157198`.

[144] Kauffman, K. J., Prakash, P., and Edwards, J. S., Advances in flux balance analysis, *Curr Opin Biotechnol* 14 (5) (2003) 491–496.

[145] Collakova, E., Yen, J. Y., and Senger, R. S., Are we ready for genome-scale modeling in plants?, *Plant Sci.* 191-192 (2012) 53–70. `doi:10.1016/j.plantsci.2012.04.010`.

[146] Simmons, G. F., Differential equations with applications and historical notes, McGraw-Hill, 1972.

[147] Nikolaou, A., Bernardi, A., Meneghesso, A., Bezzo, F., Morosinotto, T., and Chachuat, B., A model of chlorophyll fluorescence in microalgae integrating photoproduction, photoinhibition and photoregulation, *J. Biotechnol.* 194 (2015) 91–99. `doi:10.1016/j.jbiotec.2014.12.001`.

[148] Ebenhöh, O., Houwaart, T., Lokstein, H., Schlede, S., and Tirok, K., A minimal mathematical model of nonphotochemical quenching of chlorophyll fluorescence, *Biosystems* 103 (2) (2011) 196–204. `doi:10.1016/j.biosystems.2010.10.011`.

[149] Zaks, J., Amarnath, K., Kramer, D. M., Niyogi, K. K., and Fleming, G. R., A kinetic model of rapidly reversible nonphotochemical quenching, *Proc. Natl. Acad. Sci. U. S. A.* 109 (39) (2012) 15757–15762. `doi:10.1073/pnas.1211017109`.

[150] Gordienko, T. V., and Karavaev, V. A., Theoretical analysis of inductive effects in higher plant photosynthesis, *Translated from Izv Akad Nauk Ser Biol* 30 (1) (2003) 41–47.

[151] Marshall, H. L., Geider, R. J., and Flynn, K. J., A mechanistic model of photoinhibition, *New Phytol.* 145 (2) (2000) 347–359. `doi:10.1046/j.1469-8137.2000.00575.x`.

[152] Han, B., Virtanen, M., Koponen, J., and Straskraba, M., Effect of photoinhibition on algal photosynthesis: a dynamic model, *J. Plankton Res.* 22 (5) (2000) 865–885. `doi:10.1093/plankt/22.5.865`.

[153] Han, B.-P., A mechanistic model of algal photoinhibition induced by photodamage to photosystem-II, *J. Theor. Biol.* 214 (4) (2002) 519–527. `doi:10.1006/jtbi.2001.2468`.

[154] Laisk, A., Eichelmann, H., and Oja, V., C3 photosynthesis in silico, *Photosynth. Res.* 90 (1) (2006) 45–66. `doi:10.1007/s11120-006-9109-1`.

[155] Zhu, X.-G., Wang, Y., Ort, D. R., and Long, S. P., e-photosynthesis: a comprehensive dynamic mechanistic model of C3 photosynthesis: from light capture to sucrose synthesis, *Plant. Cell Environ.* 36 (9) (2013) 1711–1727. `doi:10.1111/pce.12025`.

[156] Bisi, M., Conforto, F., and Desvillettes, L., Quasi-steady-state approximation for reaction - diffusion equations, *Bulletin of the Institute of Mathematics Academia Sinica (New Series)* 2 (4) (2007) 823–850.

[157] GitHub Repository. NPQ Model., Website. Accessed on 02.08.2016.
URL `https://github.com/QTB-HHU/npqmodel/`

[158] Ballottari, M., Mozzo, M., Girardon, J., Hienerwadel, R., and Bassi, R., Chlorophyll triplet quenching and photoprotection in the higher plant monomeric antenna protein Lhcb5, *J. Phys. Chem. B* 117 (38) (2013) 11337–11348. `doi:10.1021/jp402977y`.

[159] Krause, G. H., and Jahns, P., Non-photochemical energy dissipation determined by chlorophyll fluorescence quenching: characterization and function, in: Papageorgiou, G. C., and Govindje (Eds.), Chlorophyll a Fluoresc. a Signat. Photosynth., Springer, 2004, Ch. 18, pp. 465–495. `doi:10.1016/j.neuroscience.2004.06.066`.

[160] Szechyńska-Hebda, M., Kruk, J., Górecka, M., Karpińska, B., and Karpiński, S., Evidence for light wavelength-specific photoelectrophysiological signaling and memory of excess light episodes in Arabidopsis, *Plant Cell* 22 (7) (2010) 2201–2218. `doi:10.1105/tpc.109.069302`.

[161] Karpiński, S., and Szechyńska-Hebda, M., Secret life of plants: from memory to intelligence, *Plant Signal. Behav.* 5 (11) (2010) 1391–1394. `doi:10.4161/psb.5.11.13243`.

[162] Yamamoto, H. Y., Nakayama, T. O., and Chichester, C. O., Studies on the light and dark interconversions of leaf xanthophylls, *Arch. Biochem. Biophys.* 97 (1962) 168–173. `doi:10.1016/0003-9861(62)90060-7`.

[163] Pfündel, E., and Bilger, W., Regulation and possible function of the violaxanthin cycle, *Photosynth. Res.* 42 (2) (1994) 89–109.

[164] Demmig-Adams, B., Winter, K., Krüger, A., and Czygan, F. C., Zeaxanthin and the Induction and Relaxation Kinetics of the Dissipation of Excess Excitation Energy in Leaves in 2{%} O(2), 0{%} CO(2), *Plant Physiol.* 90 (3) (1989) 887–893.

[165] Horton, P., Ruban, A. V., Rees, D., Pascal, A. A., Noctor, G., and Young, A. J., Control of the light-harvesting function of chloroplast membranes by aggregation of the LHCII chlorophyll-protein complex, *FEBS Lett.* 292 (1-2) (1991) 1–4. `doi:10.1016/0014-5793(91)80819-0`.

[166] Demmig-Adams, B., Winter, K., Kruger, A., and Czygan, F.-C., Light stress and photoprotection related to the carotenoid zeaxanthin in higher plants, in: Briggs, W. R. (Ed.), Photosynthesis, A.R. Liss, New York, 1989, pp. 375–391.

[167] Noctor, G., Rees, D., and Horton, P., The relationship between zeaxanthin, energy-dependent quenching of chlorophyll fluorescence, and trans-thylakoid pH gradient in isolated chloroplasts, *Biochim.Biophys.Acta* 1057 (1991) 320–330.

[168] Rees, D., Noctor, G., Ruban, A. V., Crofts, J., Young, A., and Horton, P., pH dependent chlorophyll fluorescence quenching in spinach thylakoids from light treated or dark adapted leaves, *Photosynth. Res.* 31 (1) (1992) 11–19. `doi:10.1007/bf00049532`.

[169] Johnson, M. P., Davison, P. A., Ruban, A. V., and Horton, P., The xanthophyll cycle pool size controls the kinetics of non-photochemical quenching in Arabidopsis thaliana, *Febs Lett.* 582 (2) (2008) 259–263.

[170] Ruban, A. V., and Horton, P., The xanthophyll cycle modulates the kinetics of nonphotochemical energy dissipation in isolated light-harvesting complexes, intact chloroplasts, and leaves of spinach, *Plant Physiol.* 119 (2) (1999) 531–542.

[171] Johnson, M. P., Goral, T. K., Duffy, C. D. P., Brain, A. P. R., Mullineaux, C. W., and Ruban, A. V., Photoprotective Energy Dissipation Involves the Reorganization of Photosystem II Light-Harvesting Complexes in the Grana Membranes of Spinach Chloroplasts, *Plant Cell* 23 (4) (2011) 1468–1479. `doi:10.1105/tpc.110.081646`.

[172] Betterle, N., Ballottari, M., Zorzan, S., de Bianchi, S., Cazzaniga, S., Dall'Osto, L., Morosinotto, T., and Bassi, R., Light-induced Dissociation of an Antenna Hetero-oligomer Is Needed for Non-photochemical Quenching Induction, *J. Biol. Chem.* 284 (22) (2009) 15255–15266.

[173] Holzwarth, A. R., Miloslavina, Y., Nilkens, M., and Jahns, P., Identification of two quenching sites active in the regulation of photosynthetic light-harvesting studied by time-resolved fluorescence, *Chem. Phys. Lett.* 483 (4-6) (2009) 262–267.

[174] Horton, P., Wentworth, M., and Ruban, A., Control of the light harvesting function of chloroplast membranes: The LHCII-aggregation model for non-photochemical quenching, *Febs Lett.* 579 (20) (2005) 4201–4206.

[175] Johnson, M. P., Zia, A., Horton, P., and Ruban, A. V., Effect of xanthophyll composition on the chlorophyll excited state lifetime in plant leaves and isolated LHCII, *Chem. Phys.* 373 (1-2) (2010) 23–32.

[176] Horton, P., Johnson, M. P., Perez-Bueno, M. L., Kiss, A. Z., and Ruban, A. V., Photosynthetic acclimation: does the dynamic structure and macro-organisation of photosystem II in higher plant grana membranes regulate light harvesting states?, *FEBS J.* 275 (6) (2008) 1069–1079. `doi:10.1111/j.1742-4658.2008.06263.x`.

[177] Adams, W. W. I., Demmig-Adams, B., Verhoeven, A. S., and Barker, D. H., 'Photoinhibition'during winter stress: involvement of sustained xanthophyll cycle-dependent energy dissipation, *Funct. Plant Biol.* 22 (2) (1995) 261–276.

[178] Jahns, P., and Miehe, B., Kinetic correlation of recovery from photoinhibition and zeaxanthin epoxidation, *Planta* 198 (1996) 202–210.

[179] Oquist, G., and Huner, N. P. A., Photosynthesis of overwintering evergreen plants, *Annu. Rev. Plant Biol.* 54 (2003) 329–355.

[180] Thiele, A., Schirwitz, K., Winter, K., and Krause, G. H., Increased xanthophyll cycle activity and reduced D1 protein inactivation related to photoinhibition in two plant systems acclimated to excess light, *Plant Sci.* 115 (1996) 237–250.

[181] Verhoeven, A., Sustained energy dissipation in winter evergreens, *New Phytol.* 201 (1) (2014) 57–65. `doi:10.1111/nph.12466.`

[182] Verhoeven, A. S., Adams III, W. W., and Demmig-Adams, B., Two forms of sustained xanthophyll cycle-dependent energy dissipation in overwintering Euonymus kiautschovicus, *Plant Cell Envir.* 21 (1998) 893–903.

[183] Adams, W. W. I., Demmig-Adams, B., Rosenstiel, T. N., Brightwell, A. K., and Ebbert, V., Photosynthesis and photoprotection in overwintering plants, *Plant Biol.* 4 (05) (2002) 545–557.

[184] Reinhold, C., Niczyporuk, S., Beran, K. C., and Jahns, P., Short-term down-regulation of zeaxanthin epoxidation in Arabidopsis thaliana in response to photo-oxidative stress conditions, *Biochim. Biophys. Acta - Bioenerg.* 1777 (2008) 462–469.

[185] Demmig-Adams, B., Cohu, C. M., Muller, O., and Adams William W., I. I. I., Modulation of photosynthetic energy conversion efficiency in nature: from seconds to seasons, *Photosynth. Res.* 113 (1-3) (2012) 75–88. `doi:10.1007/s11120-012-9761-6.`

[186] Havaux, M., and Niyogi, K. K., The violaxanthin cycle protects plants from photooxidative damage by more than one mechanism, *Proc.Natl.Acad.Sci.USA* 96 (15) (1999) 8762–8767.

[187] Kalituho, L., Beran, K. C., and Jahns, P., The transiently generated nonphotochemical quenching of excitation energy in Arabidopsis leaves is modulated by zeaxanthin, *Plant Physiol.* 143 (4) (2007) 1861–1870. `doi:10.1104/pp.106.095562.`

[188] Finazzi, G., Rappaport, F., Furia, A., Fleischmann, M., Rochaix, J.-D., Zito, F., and Forti, G., Involvement of state transitions in the switch between linear and cyclic electron flow in Chlamydomonas reinhardtii, *EMBO Rep.* 3 (3) (2002) 280–285. `doi:10.1093/embo-reports/kvf047.`

[189] Holzwarth, A. R., Lenk, D., and Jahns, P., On the analysis of non-photochemical chlorophyll fluorescence quenching curves: I. Theoretical considerations, *Biochim. Biophys. Acta* 1827 (6) (2013) 786–92. `doi:10.1016/j.bbabio.2013.02.011.`

[190] Färber, A., Young, A. J., Ruban, A. V., Horton, P., Jahns, P., Farber, A., Young, A. J., Ruban, A. V., Horton, P., and Jahns, P., Dynamics of Xanthophyll-Cycle Activity in Different Antenna Subcomplexes in the Photosynthetic Membranes of Higher Plants: The Relationship between Zeaxanthin Conversion and Nonphotochemical Fluorescence Quenching, *Plant Physiol.* 115 (4) (1997) 1609–1618. `doi: 10.1104/pp.115.4.1609.`

[191] Finazzi, G., Johnson, G. N., Dall'Osto, L., Joliot, P., Wollman, F.-A., and Bassi, R., A zeaxanthin-independent nonphotochemical quenching mechanism localized in the photosystem II core complex, *Proc. Natl. Acad. Sci. U. S. A.* 101 (33) (2004) 12375–12380. `doi:10.1073/pnas.0404798101.`

[192] Horton, P., Effects of changes in the capacity for photosynthetic electron transfer and photophosphorylation on the kinetics of fluorescence induction in isolated chloroplasts, *Biochim. etBiophysicaActa,* 724 (1983) 404–410.

[193] Mills, J. D., and Mitchell, P., Modulation of coupling factor ATPase activity in intact chloroplasts. Reversal of thiol modulation in the dark, *Biochim. Biophys. Acta* 679 (1) (1982) 75–83. `doi: 10.1016/0005-2728(82)90257-2`.

[194] Büch, K., Stransky, H., and Hager, A., FAD is a further essential cofactor of the NAD (P) H and O 2-dependent zeaxanthin-epoxidase, *FEBS Lett.* 376 (1) (1995) 45–48.

[195] Heinrich, R., and Schuster, S., The regulation of cellular systems, Chapman and Hall, 1996. `doi: 10.1007/978-1-4613-1161-4`.

[196] Ruban, A. V., and Johnson, M. P., Dynamics of higher plant photosystem cross-section associated with state transitions, *Photosynth. Res.* (2009) 173–183`doi:10.1007/s11120-008-9387-x`.

[197] Minagawa, J., State transitions–the molecular remodeling of photosynthetic supercomplexes that controls energy flow in the chloroplast, *Biochim. Biophys. Acta* 1807 (8) (2011) 897–905. `doi: 10.1016/j.bbabio.2010.11.005`.

[198] Dall'Osto, L., Cazzaniga, S., Wada, M., and Bassi, R., On the origin of a slowly reversible fluorescence decay component in the Arabidopsis npq4 mutant, *Philos. Trans. R. Soc. Lond. B. Biol. Sci.* 369 (1640) (2014) 20130221. `doi:10.1098/rstb.2013.0221`.

[199] Lillacci, G., and Khammash, M., Parameter estimation and model selection in computational biology, *PLoS Comput. Biol.* 6 (3). `doi:10.1371/journal.pcbi.1000696`.

[200] Samoilova, O. P., Ptushenko, V. V., Kuvykin, I. V., Kiselev, S. A., Ptushenko, O. S., and Tikhonov, A. N., Effects of light environment on the induction of chlorophyll fluorescence in leaves: A comparative study of Tradescantia species of different ecotypes, *BioSystems* 105 (1) (2011) 41–48. `doi:10.1016/j.biosystems.2011.03.003`.

[201] Chlorophylls and Carotenoids: Measurement and Characterization by UV-VIS Spectroscopy, John Wiley & Sons, Inc., 2001. `doi:10.1002/0471142913.faf0403s01`.

[202] Johnson, M. P., Havaux, M., Triantaphylide, C., Ksas, B., Pascal, A. A., Robert, B., Davison, P. A., Ruban, A. V., and Horton, P., Elevated Zeaxanthin Bound to Oligomeric LHCII Enhances the Resistance of Arabidopsis to Photooxidative Stress by a Lipid-protective , Antioxidant Mechanism *, *Journal of Biological Chemistry* 282 (31) (2007) 22605–22618. `doi:10.1074/jbc.M702831200`.

[203] Liebermeister, W., and Klipp, E., Bringing metabolic networks to life: convenience rate law and thermodynamic constraints, *Theor Biol Med Model* 3 (2006) 41. `doi:10.1186/1742-4682-3-41`.

[204] Curien, G., Bastien, O., Robert-Genthon, M., Cornish-Bowden, A., Cárdenas, M. L., and Dumas, R., Understanding the regulation of aspartate metabolism using a model based on measured kinetic parameters, *Mol. Syst. Biol.* 5 (271). `doi:10.1038/msb.2009.29`.

[205] Lemeille, S., and Rochaix, J.-D., State transitions at the crossroad of thylakoid signalling pathways, *Photosynth. Res.* 106 (2010) 33–46. `doi:10.1007/s11120-010-9538-8`.

[206] Polle, J. E. W., Kanakagiri, S.-D., and Melis, A., tla1, a DNA insertional transformant of the green alga Chlamydomonas reinhardtii with a truncated light-harvesting chlorophyll antenna size, *Planta* 217 (1) (2003) 49–59. `doi:10.1007/s00425-002-0968-1`.

[207] Kirst, H., Garcia-Cerdan, J. G., Zurbriggen, A., Ruehle, T., and Melis, A., Truncated photosystem chlorophyll antenna size in the green microalga Chlamydomonas reinhardtii upon deletion of the TLA3-CpSRP43 gene, *Plant Physiol.* 160 (4) (2012) 2251–60. `doi:10.1104/pp.112.206672.`

[208] Yarnold, J., Ross, I. L., and Hankamer, B., Photoacclimation and productivity of Chlamydomonas reinhardtii grown in fluctuating light regimes which simulate outdoor algal culture conditions, *Algal Res.* (2015) 1–13`doi:10.1016/j.algal.2015.11.001.`

[209] Watanabe, M., Furuya, M., Miyoshi, Y., Yasunori, I., Iwahashi, I., and Matsumoto, K., Design and performance of the Okazaki Large Spectrograph for photobiological research, *Photochem. Photobiol.* 36 (1982) 491–498.

[210] WeGrow, Website. Accessed on 22.09.2016.
URL `http://www.wegrow.de/kirinews.html`

[211] Official Web Site of the Nobel Prize, Website. Accessed on 10.11.2013.
URL `https://www.photosynq.org/`

[212] Pettersson, G., and Ryde-Pettersson, U., A mathematical model of the Calvin photosynthesis cycle, *Eur. J. Biochem.* 175 (3) (1988) 661–672. `doi:10.1111/j.1432-1033.1988.tb14242.x.`

[213] Kartal, , Mahlow, S., Skupin, A., and Ebenhöh, O., Carbohydrate-active enzymes exemplify entropic principles in metabolism, *Mol. Syst. Biol.* 7 (542) (2011) 1–11. `doi:10.1038/msb.2011.76.`

[214] Flori, S., Petroutsos, D., Falconet, D., and Finazzi, G., Chloroplast tomography allows revisiting diatoms photosynthesis, *Biochim. Biophys. Acta* 1857 (2016) e12–e13. `doi:10.1016/j.bbabio.2016.04.375.`

[215] Schöttler, M. A., Kirchhoff, H., and Weis, E., The role of plastocyanin in the adjustment of the photosynthetic electron transport to the carbon metabolism in tobacco, *Plant Physiol.* 136 (4) (2004) 4265–4274. `doi:10.1104/pp.104.052324.`

[216] Kirchhoff, H., Mukherjee, U., and Galla, H.-J. J., Molecular architecture of the thylakoid membrane: Lipid diffusion space for plastoquinone, *Biochemistry* 41 (15) (2002) 4872–4882. `doi:10.1021/bi011650y.`

[217] Heineke, D., Riens, B., Grosse, H., Hoferichter, P., Peter, U., Flügge, U. I., and Heldt, H. W., Redox Transfer across the Inner Chloroplast Envelope Membrane, *Plant Physiol* 95 (4) (1991) 1131–1137.

[218] Allakhverdiev, S. I., Tsuchiya, T., Watabe, K., Kojima, A., Los, D. A., Tomo, T., Klimov, V. V., and Mimuro, M., Redox potentials of primary electron acceptor quinone molecule (QA)- and conserved energetics of photosystem II in cyanobacteria with chlorophyll a and chlorophyll d, *Proc. Natl. Acad. Sci. USA* 108 (19) (2011) 8054–8058. `doi:10.1073/pnas.1100173108.`

[219] Okayama, S., Redox potential of plastoquinone A in spinach chloroplasts, *Biochim. Biophys. Acta* 440 (2) (1976) 331–336.

[220] Suzuki, S., Sakurai, T., and Nakajima, T., Characterization of Plastocyanin Isolated From Brazilian Elodea, *Plant Cell Physiol.* 28 (5) (1987) 825–831.

[221] Böhme, H., Quantitative Determination of Ferredoxin, Ferredoxin-NADP+ Reductase and Plastocyanin in Spinach Chloroplasts, *Eur. J. Biochem.* 83 (1) (1978) 137–141. `doi:10.1111/j.1432-1033.1978.tb12077.x.`

[222] Carrillo, N., and Ceccarelli, E. A., Open questions in ferredoxin-NADP+ reductase catalytic mechanism, *Eur. J. Biochem.* 270 (9) (2003) 1900–1915.

[223] Aliverti, A., Jansen, T., Zanetti, G., Ronchi, S., Herrmann, R. G., and Curti, B., Expression in Escherichia coli of ferredoxin:NADP+ reductase from spinach. Bacterial synthesis of the holoflavo-protein and of an active enzyme form lacking the first 28 amino acid residues of the sequence, *Eur. J. Biochem.* 191 (3) (1990) 551–555.

[224] Shin, M., Ferredoxin-NADP reductase from spinach, in: Pietro, A. S. (Ed.), Photosynth. Nitrogen Part A, Vol. 23 of *Methods in Enzymology*, Academic Press, 1971, pp. 440–447. `doi:10.1016/S0076-6879(71)23116-5`.

[225] Aliverti, A., Pandini, V., and Zanetti, G., Domain exchange between isoforms of ferredoxin-NADP+ reductase produces a functional enzyme, *Biochim. Biophys. Acta* 1696 (1) (2004) 93–101.

[226] Drop, B., Yadav K N, S., Boekema, E. J., and Croce, R., Consequences of state transitions on the structural and functional organization of Photosystem I in the green alga Chlamydomonas reinhardtii, *Plant J.* 78 (2014) 181–191. `doi:10.1111/tpj.12459`.

[227] Witt, H., Bordignon, E., Carbonera, D., Dekker, J. P., Karapetyan, N., Teutloff, C., Webber, A., Lubitz, W., and Schlodder, E., Species-specific differences of the spectroscopic properties of P700: analysis of the influence of non-conserved amino acid residues by site-directed mutagenesis of photosystem I from Chlamydomonas reinhardtii, *J. Biol. Chem* 278 (47) (2003) 46760–46771. `doi:10.1074/jbc.M304776200`.

[228] Evans, M. C., and Heathcote, P., Effects of glycerol on the redox properties of the electron acceptor complex in spinach photosystem I particles, *Biochim. Biophys. Acta* 590 (1) (1980) 89–96.

[229] Cammack, R., Rao, K. K., Bargeron, C. P., Hutson, K. G., Andrew, P. W., and Rogers, L. J., Midpoint redox potentials of plant and algal ferredoxins, *Biochem. J* 168 (2) (1977) 205–209.